Novel Low Cost Ceramic and Zeolite-Ceramic Composite Tubular Membranes for Liquid Phase Separation Applications

Thesis submitted in partial fulfillment of the requirements for the degree of

DOCTOR OF PHILOSOPHY

by

VINOTH KUMAR R

Department of Chemical Engineering

Indian Institute Technology, Guwahati

Guwahati - 781039, India

June 2016

Novel Low Cost Ceramic and Zeolite-Ceramic Composite Tubular Membranes for Liquid Phase Separation Applications

-Vinoth Kumar Raja

Novel Low Cost Ceramic and Zeolite-Ceramic Composite Tubular Membranes for Liquid Phase Separation Applications

Thesis submitted in partial fulfillment of the requirements for the degree of

DOCTOR OF PHILOSOPHY

by

VINOTH KUMAR R

Roll No.: 136107022

Department of Chemical Engineering

Indian Institute Technology, Guwahati

Guwahati - 781039, India

June 2016

Department of Chemical Engineering
Indian Institute of Technology Guwahati
Guwahati - 781039, India

CERTIFICATE

This is to certify that the thesis entitled "**Novel Low Cost Ceramic and Zeolite-Ceramic Composite Tubular Membranes for Liquid Phase Separation Applications**" being submitted by **Mr. Vinoth Kumar R** for the award of PhD degree has been carried out under my guidance and supervision. The work documented in this thesis has not been submitted to any other University or Institute for the award of any degree or diploma.

Date:

(Signature of Thesis Supervisor)
Dr. G. Pugazhenthi
Professor
Department of Chemical Engineering
Indian Institute of Technology Guwahati
Guwahati-781039, Assam, India

DEDICATION

This Thesis is Dedicated to My Father Mr. A.M. Raja and My Mother Mrs. Nagavalli Raja

--- Without Them I am Nothing ---

Acknowledgements

At foremost, I would like to express my sincere and heartfelt gratitude to my supervisor **Prof. G. Pugazhenthi** for his invaluable guidance, continuous support, motivation, kindness, and patience with me. His guidance helped me in all the ways of doing research and writing this thesis. His preplanning nature in completion of the experiments, data analyses, writing manuscripts and thesis within the stipulated time period helped me a lot in completing my research work in shorter span of time. He definitely provided me enough facilities that I needed for my research works towards successful completion of my thesis work. He trained me greatly to handle any kind of critical situations in my life. I could not imagine having a better person than him for my stay at IIT Guwahati.

I am grateful to **Prof. Pakshirajan** for providing me various general needs of my research work. He helped me a lot in improving the quality of journal papers with several aspects. I thank **Prof. Mihir Kumar Purkait** for his valuable suggestions towards improving the quality of my research work. I would also thank **Prof. Sasidhar Gumma** for constantly reviewing the progress of my research work with valuable suggestions.

I wish to express my sincere thanks to all the faculty members and technical staffs in the Department of Chemical engineering and Central Instruments Facility for their help to carry out the experiments throughout the work.

I would like to acknowledge my friends, Mr. Randeep Singh, Dr. T. Kannan, Dr. C. Shyam Anand, Dr. Padam Priyal, Dr. R. Anantharaj, Dr. Shanmuga Priya, Dr. V. Satheeshkumar, Dr. S. Arun, Mr. R. Someswaran, Mr. Sivaramakrishnan, Mr. Thyagarajan, Mr. Anil Kumar, Mr. Arun, Mr. Krishna Kumar, Mr. Arun Pandian, Mr. Muthuvel, Mr. Narendren and Mr. Srinivasan for their help at different stages of my work.

I would like to thank my lab mates Dr. Monash, Dr. Vasanth, Dr. Ashim Kumar Basumatary, Dr. Ganesh Moorthy, Mr. Kelothu Suresh, Mr. Manish Kamal, Mr. Lalit Goswami, Mr. Kanchapogu Suresh and Mr. Mohan Kumar for their friendly support and timely assistance whenever needed.

Last but not the least, I would like to thank my family: my beloved parents Mr. Raja and Mrs. Nagavalli, my sisters Dr. Sangeetha and Mrs. Rathipriya Darsini, my brothers Mr. Vignesh Kumar and Mr. Hari Kumar, and my brother-in-law Mr. Ananda Prabu for supporting me spiritually throughout writing my thesis and my life in general. My family has been my strength throughout these years. I especially thank my father, as my role model and as my best friend, Mr. Raja for inspiring and encouraging me to do hard work. He taught me about life by his examples, through his courage, and his strength taught me to have faith in myself. I do not have words to express thank my mother, Mrs. Nagavalli, without her, I might not be the person I am today.

Finally, I express my sincere thanks to all who helped me in all the forms during my stay at IIT Guwahati and successful completion of this thesis.

Sincerely,

Vinoth Kumar Raja

Abstract

A novel tubular configured ceramic membrane fabricated using locally available inexpensive raw materials by extrusion technique. Detailed characterization of the raw materials used and the fabricated membrane were carried out following standard techniques, such as particle size distribution (PSD), scanning electron microscopy (SEM), energy dispersive X-ray spectroscopy (EDX), X-ray diffraction (XRD), thermogravimetric (TG) and field emission scanning electron microscopy (FESEM) analyses. The properties of the prepared membrane were porosity 53%, water permeability 5.93×10^{-7} m^3/m^2s kPa, average pore size 0.309 µm and mechanical strength 12 MPa. In addition to these excellent properties, the membrane was found to be highly resistant to corrosion under both acidic and basic condition. Furthermore, the manufacturing cost of the acquired membrane is estimated to be \$0.5 (or 69 \$/m^2). In order to explore the potential application of this novel tubular membrane, treatment of two different type of wastewater, viz. synthetic oily and local dairy wastewater was studied using the tubular membrane. The effect of various process conditions, namely applied pressure, feed concentration and cross flow rate was examined on the wastewater treatment efficiency. In order to analyze the membrane fouling mechanism associated with the wastewater treatment process, four different pore blocking models (complete, standard, intermediate pore blocking and cake filtration) were employed. An increase in both applied pressure and cross flow rate on the treatment process reduced the percentage rejection of oil in the oily wastewater and chemical oxygen demand (COD) removal from the dairy wastewater. An applied pressure of 69 kPa was found to be the best for achieving the highest rejection (99.98%) of oily wastewater with a permeate flux of 3.16×10^{-5} m^3/m^2s. A maximum COD reduction of up to 91% in the membrane permeate stream with a flux of 2.59×10^{-6} m^3/m^2s was achieved for treating the dairy wastewater.

The novel low cost tubular ceramic membrane was further used as a support for preparing Faujasite (FAU) and Mordenite framework inverted (MFI) type zeolite membranes following the hydrothermal treatment method. Solution containing a mixture of silicate and aluminate with molar composition of

$70Na_2O:Al_2O_3:20SiO_2:2000H_2O$ was used to create a FAU zeolite separation layer on the support under hydrothermal condition in Teflon made autoclave reactor operated at 75^0C for 12 h. For MFI zeolite layer formation on the porous support, hydrothermal solution prepared using silicate solution with a gel composition of $100SiO_2:5(TPA)_2O:5.3Na_2O:1420H_2O$, was subjected to hydrothermal treatment at 185°C for 4 h. To eliminate the template (TPAOH) from the zeolite channels, the membrane was calcined at 400°C for 5 h in an air atmosphere. The synthesized zeolite powders (FAU & MFI) as well as the prepared composite membranes were characterized for their XRD, PSD, Fourier transform infrared spectroscopy (FTIR), TGA, zeta potential, FESEM, porosity, pore size and water permeability analyses. XRD analysis of the FAU zeolite membrane revealed a peak at 2θ value of 12.40 confirming the highly pure and crystal nature of the material. Similarly, the distinctive peaks obtained at the 2θ value of 7.5 and 23.5 for MFI zeolite powder revealed its high purity. The reduction in the porosity, pore size and water permeability, and an increase in weight of the membranes as compared to those in the support confirmed the incorporation of the zeolite layers on the ceramic support by hydrothermal treatment.

The separation efficiency of FAU and MFI type zeolite membranes supported on the low cost tubular ceramic support was evaluated for chromium removal from aqueous solution. The effect of various process parameters, such as applied pressure, initial feed concentration and cross flow rate on permeate flux and chromium removal efficiency by the composite membrane was studied. Results showed that chromium removal efficiency increased with an increase in the applied pressure and feed concentration. On the other hand, chromium removal reduced slightly with an increase in the cross flow rate for both the zeolite membranes. A maximum chromium removal of 82% and 78% is obtained with FAU and MFI membrane, respectively, at 345 kPa applied pressure, 1000 ppm initial feed concentration and unadjusted solution pH 2.35. These novel membranes showed excellent performance in the removal of chromium with 1 to 6 order higher fluxes than other membranes reported in the literature for chromium removal. The FAU and MFI type zeolite membranes were further tested for the separation of bovine serum albumin (BSA)

protein from aqueous solution followed by optimization of critical parameters of the microfiltration system. The levels of three operating parameters, namely BSA concentration, pH and applied pressure were optimized for a maximum separation efficiency by the membranes employing response surface methodology (RSM) and bi-objective genetic algorithm (GA) approaches. The optimum levels of these variables are: 100 ppm BSA concentration, solution pH 2 and applied pressure 276 kPa. At these optimum conditions of the process parameters, a higher permeate flux and BSA rejection of 2.66×10^{-5} m^3/m^2s and 88% respectively, were obtained for the FAU membrane. In case using the MFI membrane, these values were 4.63×10^{-5} m^3/m^2s and 82%, respectively. These research findings strongly suggest that membrane separation is a highly cost effective and environmentally sound method for the separation of proteins, thereby, proving that microfiltration is a promising alternate technique to the conventional protein separation methods. Besides, this work would offer advantages in terms of the reduction in purification cost and improved recovery of BSA for the large scale operation.

Compared with the MFI zeolite membrane, FAU zeolite membrane is found to be better for chromium removal as well as BSA separation application. Owing to its high removal efficiency and low synthesis temperature, and no requirement of calcinations step for its preparation. In addition to the excellent properties and performance of the novel low cost tubular membrane, the use of simple fabrication method, reduced sintering temperature and inexpensive raw materials used for its fabrication clearly establish its potential large scale liquid phase separation applications as compared with high cost commercial α-alumina, zirconia and titania based microfiltration membranes. Overall, the obtained results serve as the useful guide for further development of membrane research.

Contents

	Page no.
Certificate	iv
Dedication	vi
Acknowledgements	xi
Abstract	xii
Contents	xvii
List of Tables	xxi
List of Figures	xxiii
Nomenclatures	xxix
Chapter 1: Introduction, Literature review and Objectives	**1-57**
1.1 Background of present research work	1
1.2 Introduction to Membrane Processes	3
1.2.1 Definition of Membrane	3
1.2.2 Types of membranes	4
1.2.3 Classifications of membrane processes	6
1.2.4 Separation mechanism of membrane processes	7
1.2.5 Modes of operation in a membrane separation process	7
1.2.6 Industrial applications of membranes	9
1.2.7 Membrane Modules	10
1.3 Membrane materials	12
1.3.1 Polymeric membranes	12
1.3.2 Ceramic membranes	13
1.3.3 Types of ceramic membranes	13
1.3.4 Applications of ceramic membranes in various industries	15
1.3.5 Polymer vs. Ceramic membranes	16
1.4 General methods for preparation of ceramic membrane	17
1.4.1 Support fabrication	17
1.4.2. Top layer formation	24
1.5 Zeolite Membranes	27
1.5.1 Zeolite membrane synthesis methods	27
1.6 State of the art	30
1.6.1 Fabrication of ceramic supports/membranes with tubular configuration	30
1.6.2 Fabrication of zeolite-ceramic composite membranes	37
1.6.3 Application of ceramic membranes for liquid phase separations	44
1.6.3.1 Treatment of oily wastewater	44
1.6.3.2 Treatment of dairy wastewater	47

1.6.3.3 Removal of chromium from aqueous solution 50
1.6.3.4 Separation of bovine serum albumin (BSA) from aqueous solution 52
1.7 Objectives of the thesis 55
1.8 Organization of the thesis 56

Chapter 2: Elaboration and characterization of novel tubular ceramic membrane from locally available low cost raw materials by extrusion method 59-83

2.1 Experimental 59
2.1.1 Raw materials 59
2.1.2 Elaboration of tubular ceramic membrane 60
2.1.3 Characterization techniques 62
2.2 Results and discussion 64
2.2.1 Characterization of raw materials 64
2.2.1.1 PSD analysis 64
2.2.1.2 SEM and EDX analysis 67
2.2.1.3 XRD analysis 67
2.2.1.4 TGA and DTG analysis 70
2.2.2 Characterization of tubular ceramic membrane 72
2.2.2.1 XRD analysis 72
2.2.2.2 Morphological analysis 73
2.2.2.3 Porosity, mechanical strength and corrosion resistance 75
2.2.2.4 Experimental setup and measurement of water flux 76
2.2.3 Estimation of manufacturing cost of the membrane 80
2.3. Summary 83

Chapter 3: Treatment of oily and dairy wastewater using novel low cost tubular ceramic membrane and analysis of fouling mechanism using pore blocking models 85-111

3.1 Treatment of oily wastewater 85
3.1.1 Experimental 85
3.1.1.1 Microfiltration of synthetic oily wastewater 86
3.1.1.2 Analytical method 86
3.1.1.3 Membrane regeneration 87
3.1.1.4 Analysis of fouling mechanism 88
3.1.2 Results and discussion 90
3.1.2.1 Performance in synthetic oily wastewater treatment 90
3.1.2.1.1 Effect of applied pressure 90
3.1.2.1.2 Effect of feed concentration 92
3.1.2.1.3 Effect of cross flow rate 92

3.1.2.2 Fouling analysis 94
3.1.2.3 Potential evaluation of the elaborated membrane with other membranes 100
3.2 Treatment of dairy wastewater 101
3.2.1 Experimental 101
3.2.2 Results and discussion 102
3.2.2.1 Potential application of low cost membrane in dairy wastewater treatment 102
3.2.2.1.1 Effect of applied pressure on treatment process 103
3.2.2.1.2 Effect of crossflow rate on treatment process 105
3.2.2.2 Fouling analysis 105
3.2.2.3 Potential evaluation of the elaborated membrane with other membranes 110
3.3 Summary 111

Chapter 4: Fabrication and characterization of tubular configured FAU and MFI type zeolite composite membranes on low cost tubular ceramic support **113-132**

4.1 Experimental 113
4.1.1 Materials 113
4.1.2 Preparation of FAU and MFI zeolite composite membranes 113
4.1.3 Characterization 117
4.2 Results and discussion 118
4.2.1 Characterization of FAU and MFI zeolite powder 118
4.2.1.1 XRD analysis 118
4.2.1.2 FTIR analysis 120
4.2.1.3 TGA and DTG analysis 121
4.2.1.4 Zeta potential measurements 123
4.2.1.5 Particle size distribution 125
4.2.2 Characterization of FAU and MFI zeolite composite membranes 126
4.3 Summary 131

Chapter 5: Removal of chromium from aqueous solution using FAU and MFI type zeolite membranes supported on low cost tubular ceramic substrate **133-147**

5.1 Experimental 133
5.2 Results and discussion 134
5.2.1 Potential of FAU and MFI zeolite in chromium removal 134

5.2.1.1 Influence of applied pressure on zeolite composite membranes 135
5.2.1.2 Influence of initial feed concentration on zeolite composite membranes 139
5.2.1.3 Influence of cross flow rate on zeolite composite membranes 142
5.2.1.4 Potential assessment of the prepared membrane with other membranes 144
5.3 Summary 146

Chapter 6: Separation of BSA using zeolite membranes and optimization of microfiltration process through hybrid RSM-GA approach 149-177

6.1 Experimental 149
6.1.1 Materials 149
6.1.2 Microfiltration of BSA using FAU and MFI zeolite membranes 149
6.1.3 Response surface methodological approach 151
6.1.4 Genetic algorithm based optimization 153
6.1.5 Validation of optimum conditions predicted by hybrid RSM-GA 155
6.2. Results and discussion 155
6.2.1 Microfiltration of bovine serum albumin 155
6.2.2 Response surface methodological approach 156
6.2.3 Model adequacy checking 158
6.2.3.1 Statistical parameters for model adequacy 158
6.2.3.2 Diagnostic and influence plots for model adequacy 163
6.2.1 Effects of process variables on separation efficiency 168
6.2.1.1 Effect of concentration of BSA 168
6.2.1.2 Effect of pH 169
6.2.1.3 Effect of applied pressure 170
6.2.2 Prediction of optimum conditions through hybrid RSM-GA 173
6.2.3 Validation of the predicted model 175
6.3 Summary 176

Chapter 7: Conclusions and Scope of Future works 179-183

7.1 Conclusions 179
7.2 Future scopes 182

References 185-202

List of Publications 203-205

List of Tables

Table No.	Table Caption	Page No.
Table 1.1	Summary of literature survey on tubular ceramic support/membrane preparation	36
Table 1.2	State of the art on zeolite-ceramic composite membranes	43
Table 2.1	Summary of identified raw material compositions for tubular membrane fabrication	60
Table 2.2	Particle size distribution of various clay powders used in the preparation of membrane	66
Table 2.3	Properties of the tubular ceramic membrane	81
Table 2.4	Estimation of manufacturing cost of the membrane	82
Table 3.1	Summary of parameters associated with various pore blocking models for different applied pressures	98
Table 3.2	Summary of parameters associated with various pore blocking models for different feed concentrations	98
Table 3.3	Summary of parameters associated with various pore blocking models for different cross flow rates	99
Table 3.4	Potential evaluation of other membranes with prepared membrane	99
Table 3.5	Composition of the raw dairy wastewater	102
Table 3.6	Summary of parameters associated with various pore blocking models for different applied pressures	109
Table 3.7	Summary of parameters associated with various pore blocking models for different cross flow rates	109
Table 3.8	Potential evaluation of other membranes with the prepared membrane	110
Table 4.1	Characterization results of ceramic support, FAU and MFI zeolite composite membrane	131
Table 5.1	Potential assessment of FAU and MFI zeolite composite membranes with other membranes on chromium(VI) removal	145
Table 6.1	Variables and its levels for RSM-FCCCD experimental design	153

Table No.	Table Caption	Page No.
Table 6.2	Coded and actual levels of the independent variables according to the RSM-FCCCD experimental design and experimental results of FAU and MFI membranes separation efficiency	157
Table 6.3	Analysis of variance of the developed second-order polynomial models for FAU membrane separation efficiency as per the RSM-FCCD experimental design	161
Table 6.4	Analysis of variance of the developed second-order polynomial models for MFI membrane separation efficiency as per the RSM-FCCD experimental design	162
Table 6.5	Comparison of separation efficiency of FAU and MFI zeolite membrane with other membranes	176

List of Figures

Figure No.	Figure Caption	Page No.
Figure 1.1	Diagram of membrane process	3
Figure 1.2	General classification of synthetic membranes	5
Figure 1.3	Pictorial depiction of various mode of operation in membrane separation process	8
Figure 1.4	(a) Flat sheet, (b) Tubular, (c) Hollow fiber, (d) Spiral-wound membrane modules	11
Figure 1.5	Typical cross-section of ceramic membrane structure	18
Figure 1.6	Classification of membrane supports production methods based on the precursor aggregate stage	20
Figure 1.7	Schematic of an extrusion apparatus: (1) paste, (2) piston, (3) endless screw (4) die	23
Figure 1.8	Steps involving in dip coating process	25
Figure 1.9	Pictorial representation of inorganic membrane preparation by sol-gel method	26
Figure 1.10	Illustration of the experimental procedure of in-situ and secondary growth methods.	29
Figure 2.1	Schematic representation of tubular ceramic membrane fabrication	61
Figure 2.2	(a) Table top mechanized extruder, and (b and c) fabricated membrane at different views	61
Figure 2.3	Particle size distribution of the raw materials used for preparation of membrane	65
Figure 2.4	(a-f) SEM and EDX analysis of the raw materials used in membrane fabrication (a) Kaolin, (b) Ball clay, (c) Quartz, (d) Pyrophyllite, (e) Feldspar and (f) $CaCO_3$	68
Figure 2.5	XRD patterns of the raw materials used for the preparation of membrane	69
Figure 2.6	TGA profiles of the raw materials used for the preparation of membrane	71

Figure No.	Figure Caption	Page No.
Figure 2.7	TGA and DTG curves of mixed raw materials	71
Figure 2.8	XRD patterns of the membrane (a) before sintering and (b) after sintering (1- Kaolin, 2- Quartz, 3-Anorthite, 4- Calcium oxide, 5-Mullite, 6-Wollastonite)	72
Figure 2.9	Photograph of the sintered membrane (a) Microscope image of cross sectional view of the membrane, (b) FESEM images of inner (c) and outer surfaces of the membrane (d)	73
Figure 2.10	SEM mapping analysis of the sintered membrane. (a) Zone at which EDX and mapping analysis done, (b), (c), (d) and (e) represents the mapping results of Si, Al, O and Ca, respectively	74
Figure 2.11	Schematic and optical representation of experimental system (V_1-by-pass valve, V_2- inlet valve, V_3- retentate valve)	77
Figure 2.12	Tubular membrane before fixing and after fixing into module	77
Figure 2.13	(a) Water flux as a function of time for five applied pressures and (b) water flux as a function of applied pressure	
Figure 3.1	Droplet size distribution of oil-water emulsions	79
Figure 3.2	Fouling mechanism due to: (a) complete pore blocking, (b) intermediate blocking, (c) standard blocking, and (d) cake layer formation models	89
Figure 3.3	Influence of applied pressure on (a) permeate flux and (b) oil rejection	91
Figure 3.4	Effect of feed concentration on (a) permeate flux and (b) oil rejection	93
Figure 3.5	Effect of cross flow rate on (a) permeate flux and (b) oil rejection	94
Figure 3.6	Linearized plots of permeate flux versus time for various pore blocking models (applied pressures: 69-345 kPa; feed concentration: 100 ppm; cross flow rate: 1.11×10^{-6} m^3/s)	96
Figure 3.7	Linearized plots of permeate flux versus time for various pore blocking models (feed concentration: 50 - 200 ppm; applied pressure: 207 kPa; cross flow rate: 1.11×10^{-6} m^3/s)	96

Figure No.	Figure Caption	Page No.
Figure 3.8	Linearized plots of permeate flux versus time for various pore blocking models (cross flow rates: 1.66×10^{-6} - 5.55×10^{-7} m^3/s; feed concentration: 100 ppm; applied pressure: 207 kPa)	96
Figure 3.9	Effect of applied pressure on (a) permeate flux and (b) COD removal	104
Figure 3.10	Effect of cross flow rate on (a) permeate flux and (b) COD removal	106
Figure 3.11	Linearized plots of permeate flux versus time for various pore blocking models (applied pressures = 207 - 414 kPa; cross flow rate = 1.11×10^{-6} m^3/s)	108
Figure 3.12	Linearized plots of permeate flux versus time for various pore blocking models (cross flow rates = 5.55×10^{-7} - 2.22×10^{-6} m^3/s; applied pressure = 278 kPa)	108
Figure 4.1	Preparation of FAU type zeolite composite membrane	114
Figure 4.2	Preparation of MFI type zeolite composite membrane	116
Figure 4.3	XRD pattern of FAU zeolite	118
Figure 4.4	XRD pattern of MFI zeolite	119
Figure 4.5	FTIR spectrum of FAU zeolite	120
Figure 4.6	FTIR spectra of MFI zeolite	121
Figure 4.7	TG analysis of FAU	122
Figure 4.8	TGA and DTG curves of MFI zeolite	123
Figure 4.9	Zeta potential measurement of FAU zeolite	124
Figure 4.10	PSD of FAU zeolite	125
Figure 4.11	PSD of MFI zeolite	126
Figure 4.12	FESEM images of (a) inner and (b) outer surfaces of ceramic support, (c) inner and (d) outer surfaces of FAU and inner (e) and outer (f) surfaces MFI zeolite composite membranes	127
Figure 4.13	FESEM images of FAU (a) and MFI (b) zeolite crystals, as well as cross sectional views of FAU (c) and MFI (d) zeolite composite membranes	128
Figure 4.14	Water flux as a function of time for (a) ceramic substrate, (b) FAU membrane, (c) MFI membrane and (d) pure water flux as a function of applied pressure for substrate and zeolite membranes	130

Figure No.	Figure Caption	Page No.
Figure 5.1	Influence of applied pressure on permeate flux with time for (a) FAU zeolite membrane, (b) MFI zeolite membrane and (c) permeate flux as a function of applied pressure for zeolite membranes (feed concentration = 1000 ppm, natural pH~ 2.35)	136
Figure 5.2	Influence of applied pressure on removal (%) with time for (a) FAU zeolite membrane, (b) MFI zeolite membrane and (c) removal as a function of applied pressure (feed concentration = 1000 ppm, natural pH~ 2.35)	137
Figure 5.3	Schematic representation of chromium separation by zeolite membranes	139
Figure 5.4	Influence of initial feed concentration on permeate flux with time for (a) FAU zeolite membrane, (b) MFI zeolite membrane and (c) permeate flux as a function of feed concentration for zeolite membranes (Applied pressure = 69 kPa, cross flow rate: 1.11×10^{-6} m^3/s)	140
Figure 5.5	Influence of of initial feed concentration on removal (%) with time for (a) FAU zeolite membrane, (b) MFI zeolite membrane and (c) removal as a function of feed concentration (Applied pressure = 69 kPa, cross flow rate: 1.11×10^{-6} m^3/s)	141
Figure 5.6	Influence of cross flow rate on permeate flux with time for (a) FAU zeolite membrane (b) MFI zeolite membrane and (c) permeate flux as a function of cross flow rate for zeolite membranes (Applied pressure = 69 kPa, Concentration = 1000 ppm)	143
Figure 5.7	Influence of cross flow rate on removal (%) with time for (a) FAU zeolite membrane, (b) MFI zeolite membrane and (c) removal as a function of feed concentration (Applied pressure = 69 kPa Concentration = 1000 ppm)	144
Figure 6.1	Diagnostic plots for the adequacy of predictive models obtained for FAU membrane	164
Figure 6.2	Diagnostic plots for the adequacy of predictive models obtained for MFI membrane	165

Figure No.	Figure Caption	Page No.
Figure 6.3	Influence plots of MFI membrane for the adequacy of predictive models	166
Figure 6.4	Influence plots of MFI membrane for the adequacy of predictive models	167
Figure 6.5	Contour plots representing relative effects on the responses for FAU membrane	171
Figure 6.6	Contour plots representing relative effects on the responses for MFI membrane	172
Figure 6.7	Pareto front plot of optimal solution set obtained from multi-response genetic algorithm technique (a) FAU membrane (b) MFI membrane	174

Nomenclature

Abbreviations

AAD	absolute average deviations
ANOVA	analysis of variance
APHA	American public health association
BOD	biological oxygen demand
BSA	bovine serum albumin
CA	cellulose acetate
CHA	chabazite
CIP	cold isostatic pressing
COD	chemical oxygen demand
CTAB	cetyltrimethylammonium bromide
DTG	derivative thermogravimetric analysis
DTG	differential thermogravimetric
EDX	energy dispersive X-ray spectroscope
ELISA	enzyme-linked-immunosorbent assay
FAU	faujasite
FCCCD	face centred central composite design
FESEM	field emission scanning electron microscope
FTIR	Fourier transforms infrared spectroscopy
GA	genetic algorithm
IEP	isoelectric point
IOCL	Indian oil Corporation limited
JCPD	joint committee on powder diffraction standards
LTA	linde Type A
MCM	mobile crystalline matter
MF	microfiltration
MFI	mordenite framework inverted
PA	polyamide
PAN	polyacrylonitrile

PEI	polyetherimide
PES	polyethersulphone
PP	polypropylene
PRESS	predicted error sum square
PSD	particle size distribution
PSU	polysulphone
PTFE	polytetrafloroethylene
PV	pervaporation
PVA	polyvinyl alcohol
PVDF	polyvinylidene fluoride
PZC	point of zero charge
RO	reverse osmosis
RSM	response surface methodology
SDS	sodium dodecyl sulfate
SEM	scanning electron microscopy
SGM	secondary growth method
TEOS	tetraethyl orthosilicate
TFC	thin film composite
TGA	thermogravimetric analysis
TGA	thermogravimetric analysis
TKN	total Kjeldahl nitrogen
TMP	transmembrane pressure
TSS	total suspended solid
UF	ultrafiltration
XRD	x-ray diffraction
ZSM	zeolite socony mobil

Notations

X_3	applied pressure (kPa)
X_1	concentration of BSA (ppm)
x	input decision variable vector

$f(x)$	non-linear quadratic model equations
ε	random error
y_i	responses of RSM predictive models
x_2	solution pH
$\vec{x}^*$	vector
r	weight factor
$	United States dollar
A	effective membrane area (m^2)
C_f	concentration in the feed stream (ppm)
C_p	concentration in the permeate stream (ppm)
D	overall desirability
d_{in}	inner diameter of the tube (mm)
d_{out}	outer diameter of the tube (mm)
F	applied force (N)
J_o	initial permeate flux ($m^3m^{-2}s$)
J_w	pure water flux ($m^3m^{-2}s^{-1}$)
k_b	complete pore blocking model constant (s^{-1})
k_c	cake filtration model constant ($s\ m^{-2}$)
k_i	intermediate pore blocking model constant (m^{-1})
k_s	standard pore blocking model constant ($m^{-0.5}s^{-0.5}$)
L	distance between the sample support points (mm)
L	lower response
l	pore length of the membrane (m)
L_h	water permeability of the membrane ($m^3m^{-2}s^{-1}$ kPa)
n	number of response
n	number of variables
Q	permeated water in volume (m^3)
R	observed rejection (%)
r	pore radius of the membrane (µm)
R^2	square of correlation coefficient (dimension less)
t	measured time (s)

U	higher response
$V_{membrane}$	total volume of the membrane (cm^3)
W_{dry}	dry weight of the membrane (g)
W_{wet}	wet weight of the membrane (g)
X_i & X_j	level of the independent variables
Y	response (permeate flux and rejection)
β_i	liner effect term
β_{ii}	square effect term
β_{ij} -	interaction effect term
β_o	model intercept term
ΔP	applied pressure across the membrane (kPa)

Greek Letters

ε	porosity of the membrane (%)
Θ	diffraction angle (degree)
λ	CuKα radiation wavelength (Å)
μ	viscosity of water (Pa s)
ρ_{water}	density of the water (kg m^{-3})
σ	mechanical strength of the membrane (MPa)
τ	tortuosity factor (dimension less)

Chapter 1

Introduction, Literature review and Objectives

Introduction, Literature review and Objectives

This chapter presents a brief summary of the basic fundamentals, classifications and applications involved in membrane technology along with the basis of problem chosen in this work. State of the art on preparation of tubular ceramic as well as zeolite-ceramic composite membranes and their applications have been elaborately discussed. Based on the membrane preparations and their applications for the treatment of oily and dairy wastewater, removal of chromium and separation of bovine serum albumin from aqueous solutions, the objectives of the thesis have been highlighted. Finally, the organization of the present work has been summarized.

1.1 Background of present research work

In recent years, the potential utilization of ceramic membranes has greatly improved, especially in a broad range of industrial processes and pollution treatment technologies. Ceramic membranes can be applied in extreme harsh environments due to their distinct advantages, including good thermal stability, mechanical strength, chemical resistance, long lifetime and defouling properties. While organic polymer membranes cannot be applied owing to their restricted stability. In general, most of the commercialized ceramic membranes available in the market are produced from alumina, silica, zirconia and titania materials. However, these ceramic membranes are severely restricted in large scale application due to their higher cost of starting materials (Al_2O_3: \$53/kg, SiO_2: \$208/kg, ZrO_2: \$74/kg, TiO_2: \$43/kg) and sintering processes (1000-1600 °C). Therefore, the preparation of ceramic membranes with lower cost and excellent characteristics are the challenging tasks for the upcoming development of ceramic membranes for the treatment of a large volume of feed. Tubular configured ceramic membranes are especially suitable in applications where the feed stream contains a relatively high

proportion of large particles, and where the membranes are exposed to extreme pH and temperature conditions. The fabrication of porous ceramic membrane with the tubular configuration needs the expertise on choosing appropriate starting materials and methods. Shaping by extrusion is achievable only if the paste created from starting materials has rheological characteristics similar to those of clays.

Generally, ceramic membranes are made up of a composite formation with an active top layer, which typically decides its separation characteristics. Mostly, the active top layers are fabricated using inorganic oxides such as γ-alumina, zeolites, zirconia, titania, etc. Among these, zeolites provide well-defined pore structures, better chemical and thermal stability and exhibit excellent applications in various separation processes. This charged membrane facilitates to attain good separation even utilizing a realistically larger pore sized zeolite membrane. Most of the research groups revealed the utilization of ceramic support for the fabrication of zeolite membranes. The membrane support can be produced by various techniques, including isostatic pressing, extrusion, slip casting, etc. It is noteworthy to point out that many of the researchers have used α-alumina as a support material to fabricate the zeolite membranes. However, the cost of α-alumina supports is very expensive (approximately $500/m^2$) and also requires higher temperature (>1200 °C) for the fabrication. Therefore, identification of alternative low cost materials that provide ceramic membrane support with excellent characteristics is necessary. Various techniques, including dip coating, electroless plating, chemical vapor deposition, in-situ hydrothermal synthesis and microwave assisted hydrothermal methods are used for the fabrication of zeolite membranes. Among these techniques, zeolite composite membranes are mainly synthesized by in-situ hydrothermal method. Mesoporous MCM-48, Silicate-1, CHA, MFI, NaY and FAU type zeolite membranes were fabricated on α-alumina support and the prepared zeolite membranes were applied for gas phase separation applications. Therefore, the

parametric study targeting for the fabrication of zeolite membrane on low cost ceramic support using hydrothermal synthesis for liquid phase separation would be beneficial for industrial applications.

1.2 Introduction to Membrane Processes

1.2.1 Definition of Membrane

'A region of discontinuity interposed between two phases'

Based on the above definition, the membrane can be solid/liquid/gas/combination of these phases.

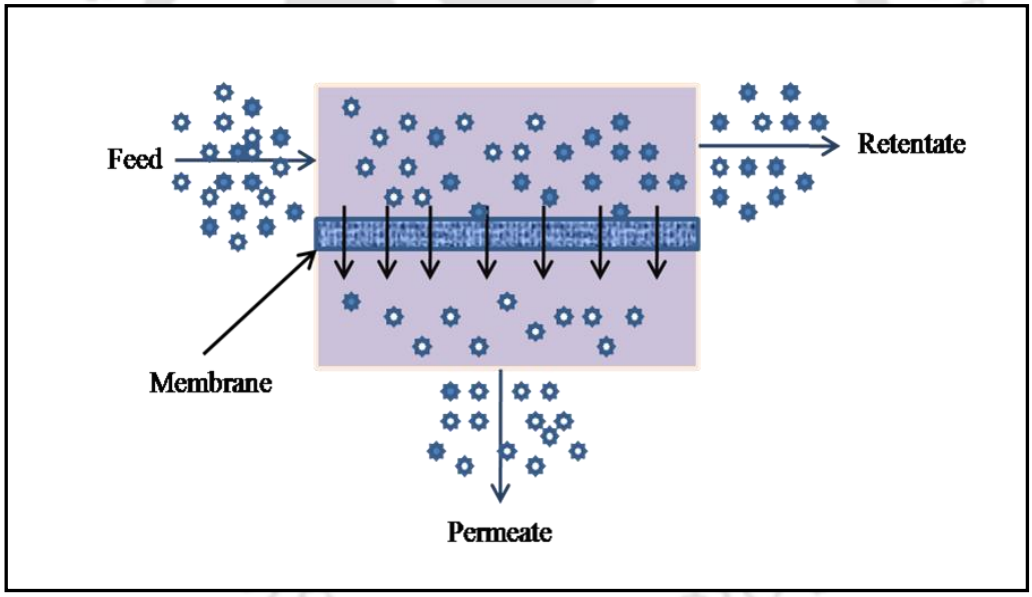

Figure 1.1: Diagram of membrane process

The above illustration (Figure 1.1) describes that a membrane is positioned in a container so that two compartments, i.e. upper and lower compartments, are formed. As a feed stream of a feed mixture consisting constituents flows on the membrane in the upper compartment, one of the constituents permeates selectively and is enriched in the permeate stream (Wang and Kammermeyer 1975).

1.2.2 Types of membranes

In general, membranes can be classified into two major types, namely biological and synthetic membrane (Cheryan 1998; Mulder 1991; Nunes and Peinemann 2001). While biological membranes refer to those that are present in living cells and aid in cellular functional separations, synthetic membranes are those that are prepared using various materials such as solids and liquids. A conventional example for biological membrane is nephrons present in human kidney, which facilitate separation of waste compounds (urea and excess sugars) from the blood in living beings. The classification of membranes is presented in Figure 1.2. Synthetic membranes are classified into two types, namely solid and liquid membranes. Solid membranes are further classified into dense, porous and electrically charged membranes. Porous membranes possess highly void structures with random distribution of inter-connected pores in a mechanically rigid morphology. The separation occurs in these membranes due to the size difference of the particles and membrane pores.

However, dense membranes consist of dominating non-porous structures and hence separation occurs due to diffusion and activation phenomena. Electrically charged membranes being porous or dense membranes carry fixed positive or negative charge that aid in the separation of solutions with ions. A further structural classification of various membranes indicates symmetric and asymmetric membranes. Symmetric membranes consist of a single layer with homogenous porous structures. On the other hand, asymmetric membranes posses heterogeneous membrane structure that is accomplished using two or more porous structures or layers. Typically, asymmetric membranes consist of a thin permeable layer with narrow pores on the top of a porous structure with wide pores (support). In an asymmetric membrane, while the thin film provides higher separation and permeation characteristics of the membrane, the support provides higher mechanical strength to the membrane with minimum resistance to

permeation. Therefore asymmetric membranes are always regarded to be advantageous than symmetric membranes. A pore size distribution based classification indicates symmetric membranes to be either isotropic or anisotropic. While uniform membrane pore sizes throughout the membrane structure are present in isotropic membranes, varied pore sizes throughout the membrane structure are present in anisotropic membranes. Solid phase symmetric and asymmetric membranes are primarily used for pressure driven membrane separation processes.

Based on the different types of materials with which these membranes are fabricated, the membranes are classified as polymeric and ceramic symmetric membranes and polymer-polymer, polymer-ceramic, ceramic-ceramic asymmetric membranes. Symmetric membranes are typically fabricated using single functional materials and asymmetric multilayered membranes are typically fabricated by depositing a thin film of polymeric, inorganic or any other suitable materials over a porous support.

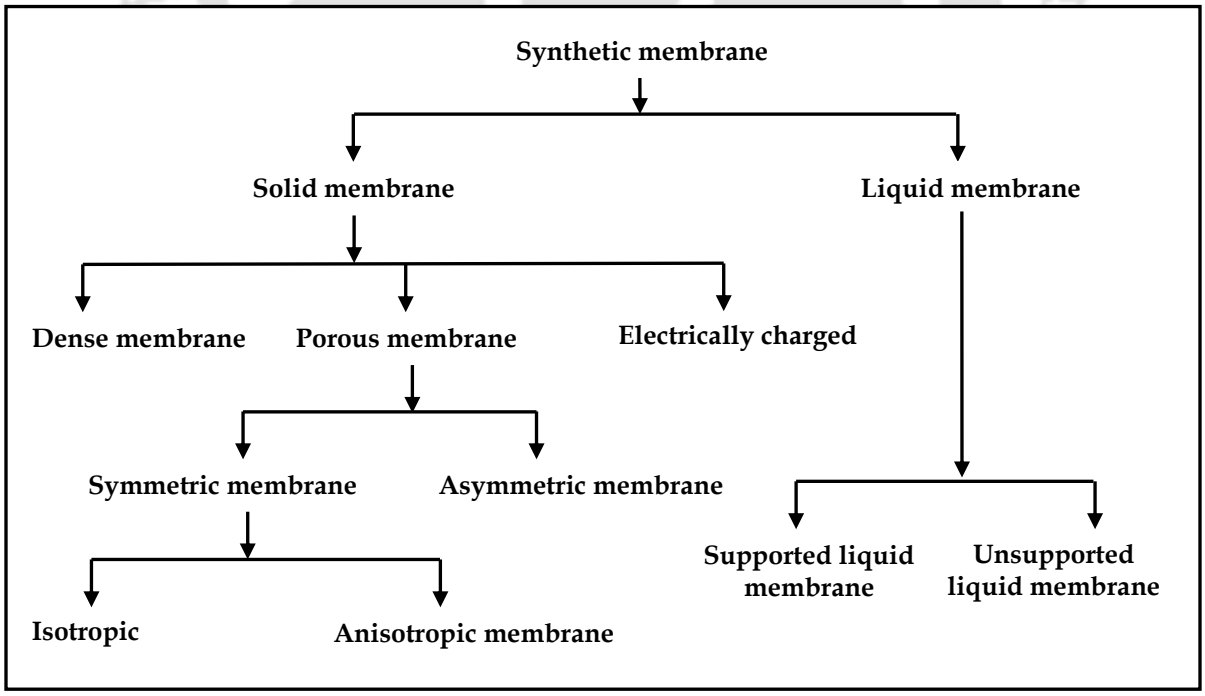

Figure 1.2: General classification of synthetic membranes

1.2.3 Classifications of membrane processes

Various types of membrane processes have been mentioned in almost all of the literature. The membrane processes are can be classified based on the driving force developed in the process. The most technical and commercial related processes are pressure driven processes namely microfiltration, ultrafiltration and reverse osmosis, gas separation or pervaporation; concentration gradient process such as dialysis; and electrical potential driven process, for instance electrodialysis. In industries application, membranes can be broadly categorized into following four classes based on the driving force, which leads to obtain permeates by passing through the membranes (Mulder 1991).

a. Pressure driven membrane process:

- Microfiltration (MF)
- Ultrafiltration (UF)
- Nanofiltration (NF)
- Reverse osmosis (RO)

b. Concentration gradient driven membrane processes:

- Pervaporation (PV)
- gas separation
- Dialysis
- Membrane extraction

c. Temperature driven processes:

- Membrane distillation
- Thermo-osmosis

d. Electrical potential driven membrane processes:

- Electrodialysis

- Electrofiltration
- Electrochemical ion exchange

1.2.4 Separation mechanism of membrane processes

Basically, there are three types of mechanism can be occurred during separation (Manohar 2012):

- ***Separation by size-the sieve effect:*** This needs porous membranes with relatively larger pores. The microporous, mesoporous and macroporous terms are used to represent pore size in membrane nanofiltration, ultrafiltration and microfiltration.
- ***Separation by variation in diffusivity and solubility of material:*** This mechanism can be occurred in the reverse osmosis processes and it needs nonporous (dense) membrane.
- ***Separation by charge:*** An ion-exchange membranes can separates constituents of different charges. Ion-exchange membranes are utilized in electrodialysis process and are usually nonporous.

1.2.5 Modes of operation in a membrane separation process

There are several modes of operation in the membrane separation process. The schematic representation of the various operations of membrane separation process is shown in Figure 1.3.

- ***Dead-end Filtration:*** The primary mode operation of membrane process is dead-end filtration. The entire feed flow is forced to pass through the membrane and filtered matter is accumulated on the membrane surface. It is a batch process, as accumulated stuff on the membrane surface leads to decrease the efficiency of the membrane owing

to clogging. Dead-end filtration needs a step to removal of accumulated matter on the membrane surface and it is highly useful technique for concentrating compounds.

- ***Cross-flow Filtration:*** In this mode of operation, a fixed turbulent flow along the membrane surface restrains the accumulation of matter on the membrane surface. Generally tubular shaped membranes are employed in this mode of operation. The feed flow through the membrane tube has a higher pressure as driving force for the filtration process and a higher flow rate to create turbulent conditions. The method is called as "cross-flow", because the feed flow and filtration flow direction is perpendicular. Cross-flow mode of operation is a greatest route to filter liquids with a high concentration of filterable matter.

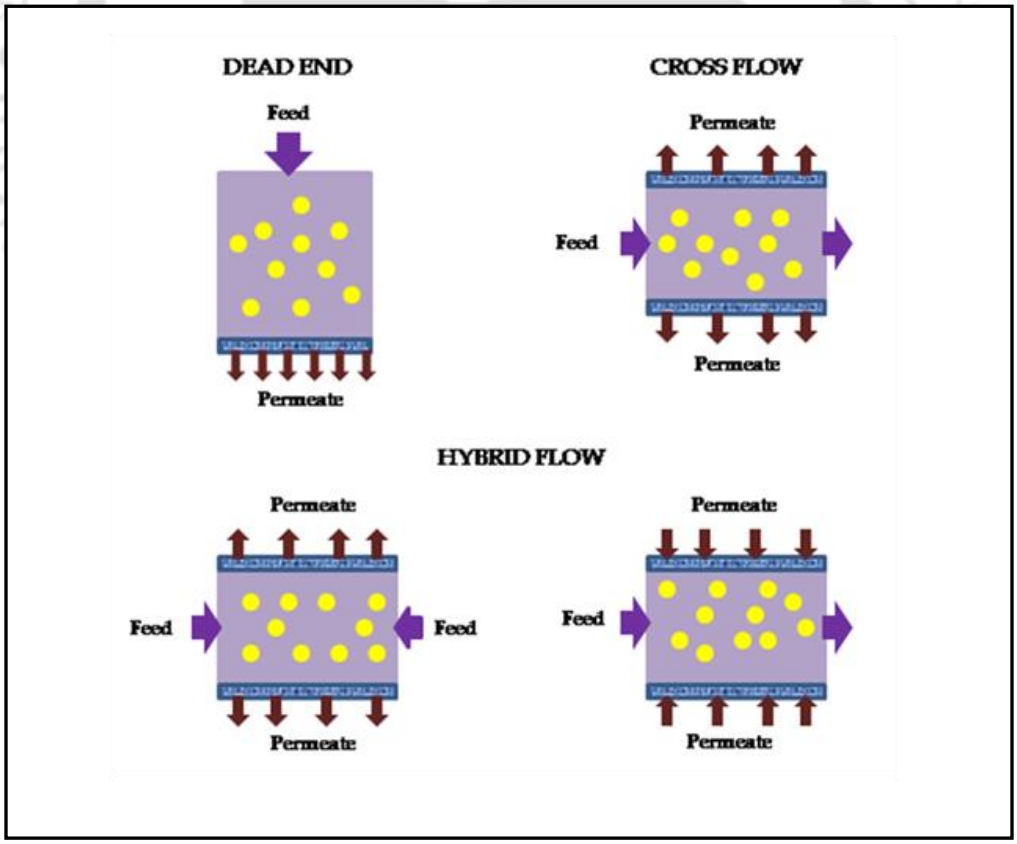

Figure 1.3: Pictorial depiction of various mode of operation in membrane separation process

- ***Hybrid-flow Filtration:*** It works with combination of dead-end as well as cross-flow concept. The tubular membranes are made with inner filtration layer is used in the cross-flow filtration system. This filtration system consists two phases, namely production and flushing phase. The one end of tubes is blocked and dead-end principle is applied in the production phase. Using cross-flow pattern, the both end of the tube sides are open and the fraction that did not passed through the membrane is eliminated with the aim of cleaning the membrane surface. This filtration method is particularly appropriate for treatment of liquids holding low concentrated suspended solids (polishing).

1.2.6 Industrial applications of membranes

Numerous industrial applications of synthetic solid symmetric and asymmetric membranes exist for *MF and UF*.

- Production of drinking water from different sources to remove various particles as well as bacteria.
- Biotechnological applications such as protein recovery, milk concentration and separation of fat from milk.
- Treatment of industrial waste streams such as oily wastewater, pulp and paper wastewater, leather wastewater, etc., for the removal of various suspended solids in the wastewater streams.
- Production of clarified fruit juices which posses long term storage characteristics and thereby enable the reduction of transportation costs of food products.

The industrial applications of other membrane separation processes such as NF, RO, pervaporation, dialysis, electrodialysis and gas separation are presented as follows:

- ***NF and RO:*** Desalination of sea water to generate drinking water, treatment of various industrial wastewater, removal of nitrates, fluorides, heavy metals etc.,
- ***Pervaporation:*** Separation of organic and azeotropic mixtures (such as ethanol-water), which are difficult to separate using conventional methods such as distillation.
- ***Dialysis and electrodialysis:*** Removal of different harmful components from human blood during kidney failure.
- ***Gas permeation:*** For the production of oxygen enriched air, nitrogen enriched air and hydrogen recovery using porous as well as dense membranes. In addition, dense membranes are used to accomplish carrier facilitated separations.

1.2.7 Membrane Modules

Membrane module is the way the membrane is incorporated into devices and hardware to separate the feed stream into permeate and retentate streams. The following four modules are extensively utilized in the industries.

- Flat sheet modules
- Tubular modules
- Hollow fiber modules
- Spiral-wound modules

In order to attain various properties on the filtration conditions, filtration areas and energy consumptions, these are the membrane modules are designed and developed by industrial manufacturers. The flat sheet circular or rectangular shaped membranes are resembles to filter paper (see Figure 1.4(a)). The most general form of tubular membrane is bearing a resemblance to a single hollow tube of circular cross-section, the wall of the tube working as the membrane.

Other types of cross-sections also exist in the form of tubular membranes. The monolith tubular membranes look like cylindrical blocks with larger number of parallel tubes within them. These tubes are holding diameter in the range of 0.5 - 2 cm. The pictorial representation of tubular membrane is shown in Figure 1.4(b). Hollow fibres also look similar to tubular in form. However, the hollow fibre membranes are having very small diameters compared to tubular membranes. The hollow fibre membranes typical fibre diameter is of the order or 1 mm. Figure 1.4(c) demonstrates the pictorial representation of hollow fibre membrane. The design of spiral-wound modules resembles to that of flat sheet modules (see Figure 1.4(d)). The two membrane sheets are divorced by a mesh-like spacer with the active membrane sides facing away in the spiral-wound modules. Three edges of the two membrane sheets are glued jointly with the fourth edge open to a perforated center tube for the permeate collection. On the other two sides of "the envelope," another two mesh-like spacers with thicknesses in the range of 0.56 - 3 mm are positioned as the feed path spacers. The entire assembly is rolled around the perforated centre tube in a spiral configuration (Cui and Muralidhara 2010).

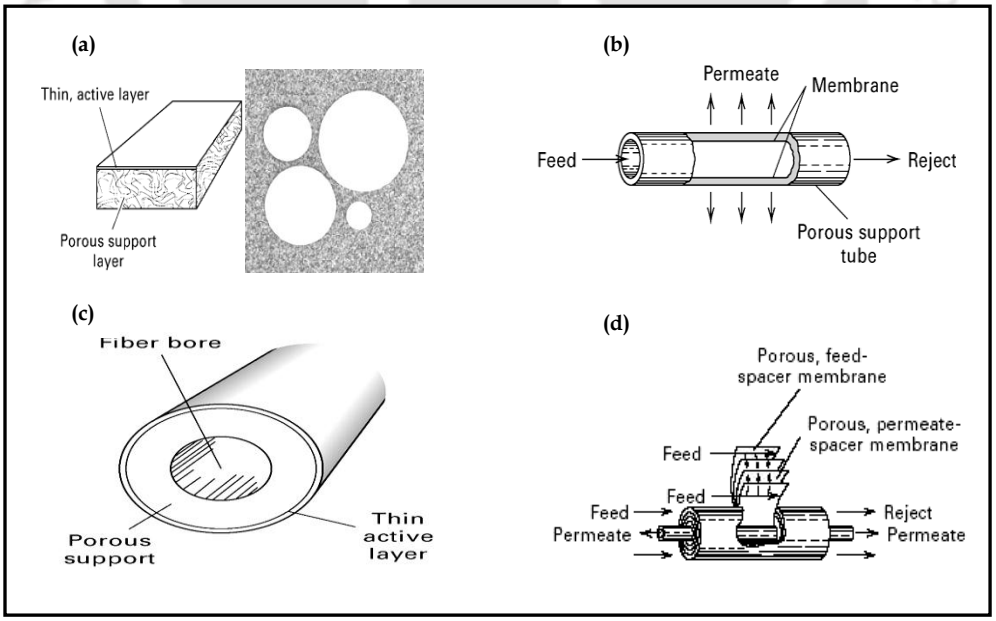

Figure: 1.4: (a) Flat sheet, (b) Tubular, (c) Hollow fiber, (d) Spiral-wound membrane modules

1.3 Membrane materials

Polymeric materials and ceramic are the most widely used functional membrane material to prepare symmetric membranes for industrial scale applications. The asymmetric membranes are usually prepared form symmetric polymeric or ceramic membrane materials or both. In an asymmetric membrane, usually the support layer provides desired mechanical strength and the thin skin layer constituting either polymeric or ceramic materials caters towards the desired separation characteristics.

1.3.1 Polymeric membranes

Polymeric membranes are thin films of 10-100 μm thickness. Different types of polymers such as polysulphone (PSU), cellulose acetate (CA), polyamide (PA), polyethersulphone (PES), Polyvinylidene fluoride (PVDF), polyacrylonitrile (PAN), polytetrafloroethylene (PTFE), polyetherimide (PEI), polypropylene (PP) are used widely to fabricate the polymeric membranes.

- ***Advantages of polymeric membranes:***
  - Wider ranges of pore sizes varying from MF to RO are available.
  - Comparatively low cost than ceramic membrane
  - Easy to fabricate
  - Ease to scale up
- ***Disadvantages of polymeric membrane:***
  - Low solvent resistance
  - Lower applicable range of pH and hence, low corrosion resistance
  - Applicable to low temperature ranges
  - Lower life span (12-18 months)

1.3.2 Ceramic membranes

Ceramic membranes are type of artificial membranes made from various inorganic materials such alumina, zirconia, silica, titania, kaolin etc. Ceramic membranes possess superior chemical, thermal and mechanical stability. The thickness of ceramic membrane is in the range of 2-5 mm and some times higher depending on the specific applications. Asymmetric ceramic membranes constitute thin film (10-100 μm) of ceramic coating over a thick porous symmetric support.

- ***Advantages of ceramic membranes:***
  - Very high corrosion resistance
  - Applicability to wider pH ranges (0.5-14)
  - Applicability of wider temperature ranges (350-500 ^{o}C). As a result they are used in industrial scale separations without any feed pre-conditioning steps.
  - Less fouling tendency
  - Inertness to common chemicals and solvents
  - Higher mechanical strength
- ***Disadvantages of ceramic membranes:***
  - Most ceramic membranes are available in pore diameters within the MF and UF range (0.010 – 10 μm)
  - Comparatively higher cost
  - Brittle in nature

1.3.3 Types of ceramic membranes

In general, ceramic membranes are broadly classified into two categories, i.e. dense and porous membranes, based on the absence or presence of the pores in the membrane structure. However, the actual classification is based on the transport mechanism of the species through

the membrane. If the separation mechanism is mainly controlled by sieving the species (molecules, ions etc.,) then it is called as porous membranes. If the membrane follows general solution diffusion type mechanism of the transport of species, then the membranes are referred as dense membranes. The separation mechanism is attributed to the affinity (selective adsorption and diffusion) of molecules with membrane materials and it plays an important and dominant role when the pore size is relatively small.

Dense membranes

Two major types of dense ceramic membranes, metal and solid electrolyte, have been studied and developed extensively for gas separation. Dense metal membranes made of palladium and its alloys have been suggested for hydrogen separation and purification applications (Hsieh 1996). Other metals membranes fabricated using tantalum; vanadium and niobium possess better selectivity for hydrogen. Solid electrolyte membranes are made of mixed conducting oxides (doped zirconia and thoria) that are selective to certain ionic species.

Porous membranes

Porous ceramic membranes are prepared with several layers of porous materials. These layers have gradations of pore diameters and each layer is applied and stabilized so as to acts as the support for the next finer layer. In general, microfiltration, ultrafiltration and nanofiltration membranes are porous in nature and employed in various industrial liquid phase applications to concentrate or purify dilute (aqueous) solutions (Noble and Stern 1995). The microstructure of the membranes (shape, size, porosity, tortuosity etc.,) will strongly depend on the method of fabrication (Burggraaf and Cot 1996).

1.3.4 Applications of ceramic membranes in various industries

In earlier, the ceramic membranes are used in wastewater treatment applications. Later, its effective and potential usages cover the entire industries where media are filtered.

- ***Ceramic membranes in chemical industries:***
  - Catalysts separation.
  - Product separation and cleaning.
  - Recycling and cleaning of organic solvents.
  - Desalination of products.
  - Recovery of pigments and dyes.
  - Concentration of metal hydroxide solutions.
  - Concentration of polymer suspensions.
- ***Ceramic membranes in metal industries:***
  - Oil-in-water emulsions treatment
  - Heavy metals recovery.
  - Treating of wastewater from grinding processes.
  - Recycling and disposal of degreasing and rinsing wastewater.
  - Treatment of wastewater from glass and glass fiber production.
- ***Ceramic membrane in food and beverage industries:***
  - Purification of drinking water.
  - Dewatering of products.
  - Desalination of whey.
  - Clarification/Concentration of fruit juices and beers.
  - Sterilization of milk and whey.

- ***Ceramic membrane in biochemical industries :***
    - Separation, concentration and dewatering of biomass and algae.
    - Concentration fractionation, isolation and sterilization for antibiotics, enzymes, proteins, amino acids and vitamins.
    - Separation of yeast.
    - Disposal of fat emulsions.
    - Desalination.
- ***Ceramic membrane in environment and recycling:***
    - Chemical oxygen demand (COD) / Biological oxygen demand (BOD) removal.
    - Removal of heavy metals and radioactive substances.
    - Oil/water separation.
    - Retention of microorganism.
    - Recovery of pharmaceuticals and pesticides.
    - Purification of the drain of sewage plants.
    - Recycling of water from swimming pools.

1.3.5 Polymer vs. Ceramic membranes

Considering the advantages and disadvantages of both membranes; it can be observed that polymeric membranes are much useful for laboratory scale use. For laboratory scale use, applicability of the membrane technology towards any particular separation is the main aim but not their life span and cost. However, for industrial scale applications, cost and life span are the most relevant matters along with the separation efficiency. For most of the applications, the life span is evaluated as 12 – 18 months (extendable to 36 months by adopting cleaning schemes)

and 10 years for polymeric and ceramic membranes, respectively (Mulder 1991). Therefore, though ceramic membranes involve higher initial costs, their ability to prove higher flux and applicability to wide range of temperature, chemical processing conditions could favor them to be the choice in contrary to the polymeric membranes. Though the separation characteristics of ceramic membrane processes are similar to polymeric membranes, they are not yet widely applied in industrial scale applications owing to its higher cost. Under these circumstances, the development and usage of comparatively low cost membranes with longer life span is anticipated to drive the economic competitiveness of ceramic membranes in the industry.

1.4 General methods for the preparation of ceramic membrane

The fabrication of ceramic membrane primarily consists of two phases, namely the fabrication of ceramic support that provides mechanical resistance to the filtered medium and achieving a selective skin or top layer. Depending upon the pore size, the skin layers play an active role in ultrafiltration (UF) and nanofiltration (NF) processes. Figure 1.5 illustrates the typical cross-section morphology of a ceramic membrane. This includes a macroporous support layer, mesoporous intermediate layer and a microporous membrane/skin layer. Further details with respect to the fabrication of these layers are presented as follows.

1.4.1 Support fabrication

A ceramic support is fabricated by casting inorganic powder into desired shape and subsequent consolidation of the green substrate by sintering. The fabrication process for the ceramic support consists of four sequential steps, namely:

a. Choice of appropriate inorganic raw materials

b. Preparation of ceramic powder/paste

c. Fabrication of ceramic support

d. Consolidating or firing (heat treatment)

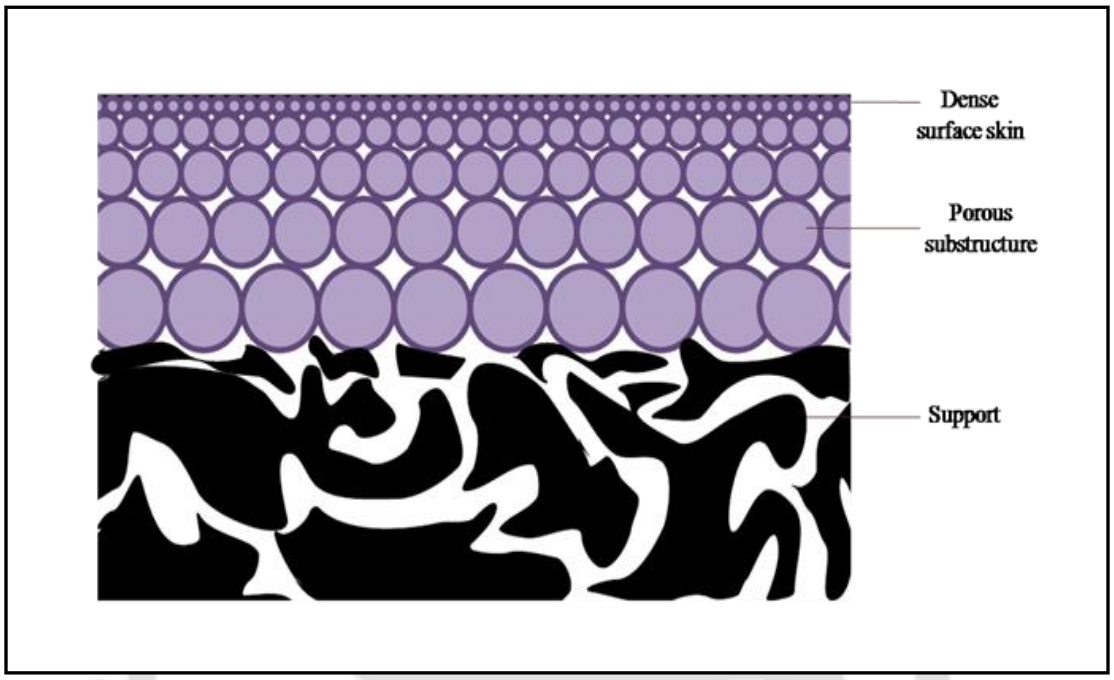

Figure 1.5: Typical cross-section of ceramic membrane structure

a. Choice of appropriate inorganic raw materials:

The morphological property of various raw materials influences the porosity (or structural density) and pore size of the ceramic support and is therefore an important parameter to achieve membranes with desired attributes. The structural density of the support increases with decreasing grain size of the raw materials. Typically, the ratio of grain to pore size is strongly dependent on shape of the particles and is about 2.5. In order to facilitate the coating of a homogeneous thin layer on the support, the pore size of the thin layer must be adaptable with the grain size of the layer on which it is to be deposited. The presence of large pores on the internal surface of the channels cloud leads to penetration of the skin layer grains into the support which will give raise to defects such as pinholes and cracks in the membrane

morphology. The structural density of the membrane must be sufficient enough to ensure excellent mechanical resistance. On the other hand, lower structural density offers higher transport resistance for fluid through the support. Therefore, tradeoffs exits for the optimization of grain size to achieve acceptable combinations of raw materials can be used to target the variation in grain size. Thereby, additional variations in pore size distributions can be achieved after sintering.

b. Preparation of ceramic powder/paste

During the paste preparation step, the ceramic powder is usually mixed with the solvent (water) and organic additives (Burggraaf and Cot 1996) to induce plastic properties to the prepared paste. The plasticity of the paste enables flexibility to shape the ceramic structure without cohesion. Another desired effect of the organic additives is to increase the unfired material strength during the shaping and dying steps which enables the elimination of defects such as cracks. Typical organic additives used during the paste preparation include binder, plasticizers, lubricants and deflocculants. Plasticizers include plastic properties to the paste. Generally, viscous and wetting polymers are used as plasticizers. Lubricants such as glycerin assist the paste to slide in the extrusion apparatus. By controlling the surface charge of the particles, deflocculants avoid powder agglomeration by steric effect. Moreover, mixing and pugging are also important steps in paste preparation. Mixing is an essential to obtain good dispersion and perfect homogeneity by the even distribution of constituents. Similarly, pugging is necessary to obtain paste. During pugging, the progressive addition of water to the powder mixture leads to achieving a high viscous paste. The powder preparation procedure is very simple in comparison to that of the paste preparation. During the powder preparation step, the

powder is usually mixed in a mixer or ball mill with suitable binders. Subsequently, the powders are sieved with the suitable screen (30 - 40 mesh).

c. Ceramic support fabrication

There are several methods are adopted to fabricate the ceramic support by researchers. Most of the ceramic supports are prepared by powder pressing, colloidal processing and paste processing routes. The detailed classification methods for fabrication of ceramic membrane supports are presented in Figure 1.6.

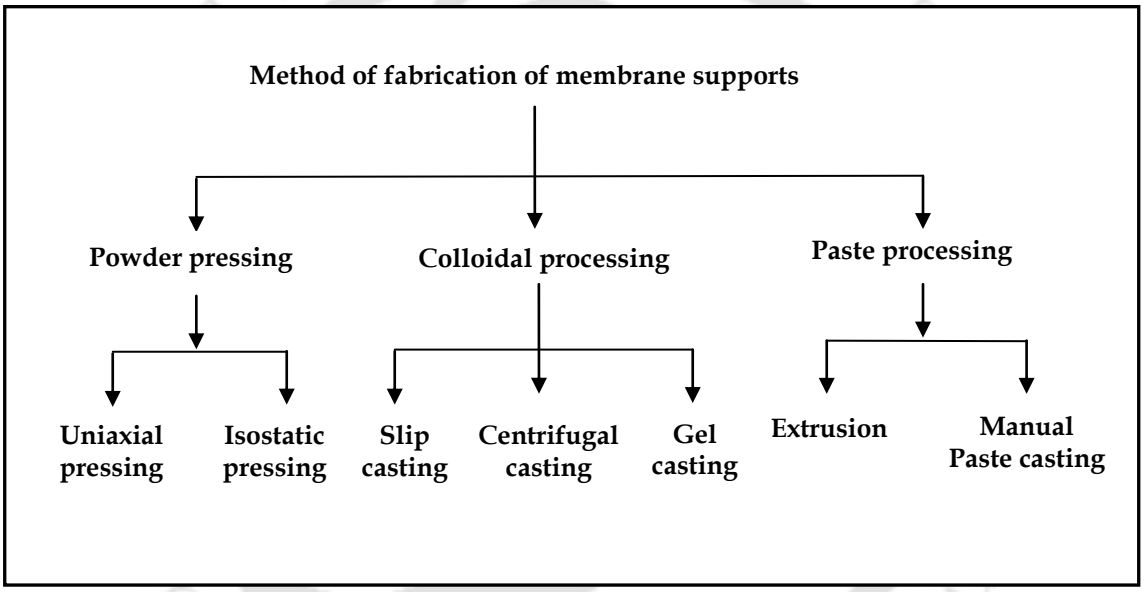

Figure 1.6: Classification of membrane supports production methods based on the precursor aggregate stage

(i) Powder pressing method

The powder pressing method has been used for the preparation of ceramic tiles and high-density products in the earlier stages. Later on, because of the characteristics of the ceramic materials, there were attempts to use this method for the fabrication of membrane supports. Typically, two types of pressing methods, axial pressing and isostatic pressing, have been used

for the fabrication of membrane supports. The axial pressing (uniaxial and biaxial) technique is economical and appropriate for high volume creation of simple geometrical forms like flat and circular supports. Axial pressing is classified into two types, namely, dry pressing and wet pressing. In order to shape the ceramic raw materials, the wet pressing requires the addition of water, whereas dry pressing can be performed without addition of water to the raw materials. In isostatic pressing, pressure is applied from various directions to achieve better homogeny of compaction and enhance shape capability compared with uni-axial pressing. Isostatic pressing methods are classified into cold and hot isostatic pressing. In cold isostatic pressing (CIP), the isostatic pressure is created by applying external pressure onto the fluid, normally water or oil. This pressure is uniformly applied to ceramic powder to form the required shape of the membrane support. In the case of hot isostatic pressing, the isostatic pressure is created by heating the encapsulated fluid (mostly argon gas) to the working temperature. This isostatic pressure forms the ceramic support of desired shape.

(ii) Colloidal processing method

In general, colloidal processing involves a sequence of steps such as powder synthesis and purification, colloidal/suspension preparation, consolidation into the chosen component form, elimination of the solvent phase, and heat treatment (sintering temperature) to produce the membrane support for optimal performance. Based on the consolidation mechanism, the colloidal processing methods are classified in to three major classifications, namely slip, centrifugal, and gel casting. In slip casting, ceramic membranes have been fabricated by pouring a stable slip (suspension of clay or ceramic material in water) in a porous mold, especially gypsum mold, or in nonporous surfaces, such as Petri dishes or glass plates. The centrifugal casting method is used to prepare tubular membrane supports from the slip solution subjected

to a higher centrifugal force. The biggest particles present in the suspension move first to the mold wall followed by the smaller particles. The quality of the outer surface of the tubular support depends on the surface quality of the mold, whereas the inner surface of the support depends on the suspension quality, especially the quantity of the smallest particles present in the suspension (Burggraaf and Cot 1996). The speed of the centrifuge and the particle size distribution of the slip solution are the main parameters that influence the mean pore size of the membrane supports. Gel casting forms a strong and cross-linked polymer-solvent gel after being poured into a mold. According to this process, ceramic powders are dissolved in water based monomer solution to form consistent slurry. Subsequently, the catalyst and initiator are added to the slurry and poured in the mold of desired shape. Before filling the mold, the slurry must be deaerated, and it must be poured carefully to the mold to avoid the introduction of defects, which may affect the characteristics of the membrane support. The chemical cross-linking reactions form a strong hydrogel that permanently immobilizes the ceramic particle. The support is demolded, dried, and sintered to get the required membrane support.

(iii) Paste processing method

One of the most classical method for the preparation of ceramic membrane is paste processing. Extrusion and manual pasting techniques are used for the fabrication of membrane supports, however; extruded supports are mostly suitable for industrial applications. Moreover, the majority of the ceramic supports are prepared by extrusion using clay materials. This is accredited to the plastic properties of the clay materials. With clay materials, the paste can be formed instantly and extruded simply to the desirable shape with lower pressure in extrusion process. The mixing of inorganic materials with additives (binders/plasticizers/lubricants) provides the necessary plasticity to the materials that gives exceptional shape forming abilities

without lost of its cohesion. Generally, cellulose derivatives (hydroxyethyl cellulose, carboxymethyl cellulose, methyl cellulose, etc.) are used as binders, organic polymers (polyvinyl alcohol, polyacrylic acid, polyethylene glycol, etc.) are utilized as plasticizers or lubricants, and a starch derivative, principally corn starch, is used as the pore-forming agent.

In the extrusion method, the homogeneous paste is forced through the opening of a die with the help of an endless screw, especially auger or extruder (in industry) or a piston (in the laboratory) (see Figure 1.7). Ceramic membranes are fabricated with various specifications (e.g., inner and outer diameter of the tubes and number of channels) by changing the geometry of the die. Tubular and multichannel membrane supports have been widely prepared by this method. The high surface-to-volume ratio of the modules provides good opportunity to process large feed rates. Due to this reason, the membranes have enhanced implementation in industries. The most important parameters that determine the membrane properties (mean pore size and porosity) are particle size of the ceramic or clay powder, nature and proportion of organic additives, pugging and ageing of the paste, extrusion pressure, and velocity.

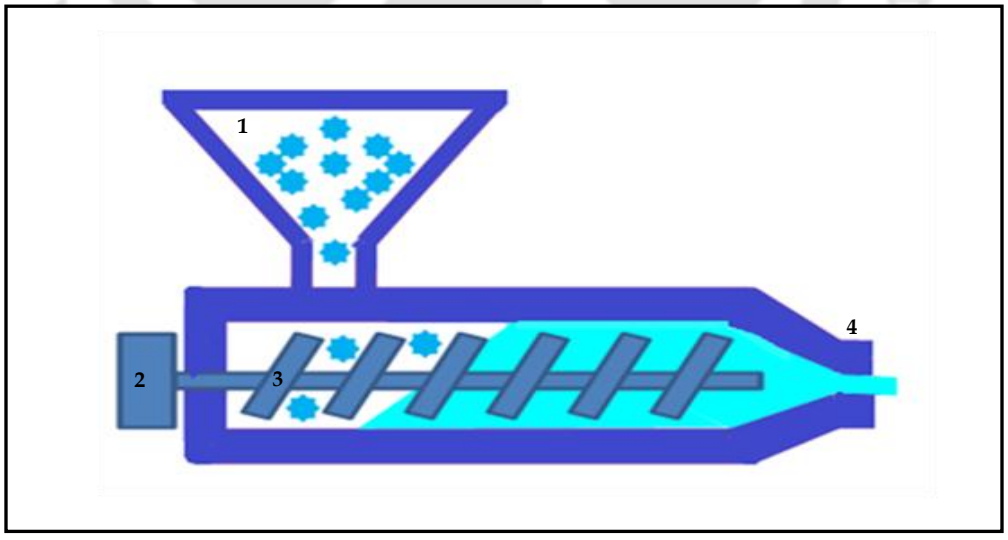

Figure 1.7: Schematic of an extrusion apparatus: (1) paste, (2) piston, (3) endless screw (4) die

In the manual pasting method, the membrane supports are fabricated manually on a flat porous (gypsum) or nonporous surface. The pressure is applied manually to form the required shape. It is the simplest and the oldest technique compared with other fabrication methods and does not require any instrument for fabrication. However, controlling the microstructure (to produce optimum reproducible results) is a hard challenge and requires skills to achieve membrane supports without defects.

d. Consolidation or firing (heat treatment)

The firing treatment strengthens the green membrane support. Heat treatment enables the elimination of bonded water and organic additives to finally achieve the temperature of allotropic transitions. Therefore, to visualize upon the completion of the firing step, thermogravimetric analysis is necessary. The firing treatment can be described in two stages in which the first corresponds to the densification and grain growth. During sintering, membrane properties such as pore diameters, density and mechanical resistance depend on the temperature and time of sintering.

1.4.2. Top layer formation

Several coating techniques exits for the fabrication of the top layer over a membrane support. Among these, dip coating and sol gel methods are the most versatile methods due to simplicity and ease of operation.

Dip coating

The dip coating method is mostly used in the preparation of composite membranes. In this technique, support is prepared from a homogeneous precursor solution and the dip coated

solution is permitted to drain to a desired thickness. The thickness of the layer is mainly calculated by the rate of evaporation of the solvent and the viscosity of the solution. Figure 1.8 displays the dip coating process.

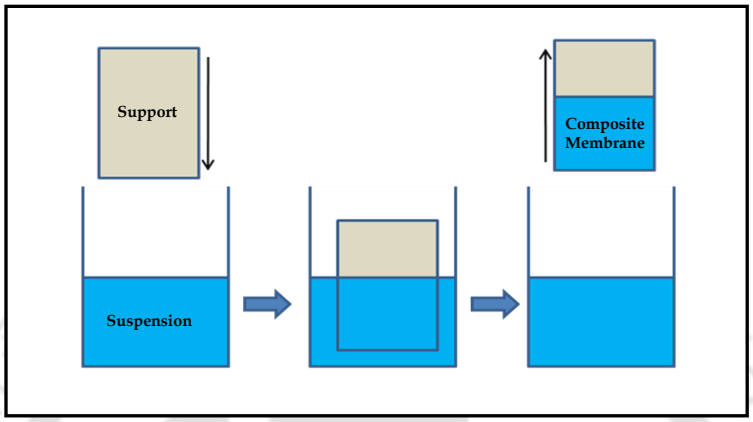

Figure 1.8: Steps involving in dip coating process

Sol-gel method

The sol-gel process is most suitable technique to acquire a functional active top layer on a membrane support. It has several advantages; it produces tremendously active products with higher surface area, controllable and facile amalgamation of other compounds such as promoters or stabilizers, alteration of well pore structure and direct casting of the selective layer over the membrane support (Agrafiotis and Tsetsekou 2002). Further, it generates high purity products with narrow pore size distribution and needs low sintering temperature. Being the less energy, it is widely used due to its facile method and does not require sophisticated instrumentation. A sol is a steady dispersion of colloidal very fine particles or polymer in a liquid. The particles may be amorphous or crystalline. A gel consists of three dimensional continuous networks, which enclosed a liquid phase where the network is built from agglomeration of colloidal particles. For the fabrication of composite membrane, two sol-gel routes are used. The first one corresponds to colloidal route that explores colloidal chemistry in aqueous media and the other corresponds to the polymeric route, which searches the chemistry

of metal organic precursors with organic solvents. Figure 1.9 demonstrates the sol-gel method for both colloidal and polymeric routes. In the sol-gel process, the first stage refers to the preparation of a sol using molecular precursors either with metal salts or metal organics. The condensation reactions occurred at the sol stage for both cases with the formation of colloids or clusters that coalesce finally to form gel. For the fabrication of active layer, the coating must be carried out with the sol whose rheological behavior is adaptable for the porous membrane support or substrate. Drying and sintering steps subsequently followed, which determine the chemical characteristics of the membrane. In the drying process of coated sol, gelation takes place and cross linking of the gel particles are formed to produce desired product due to the thermal treatment. Usually, thin and crack-free membrane layers are acquired with this technique.

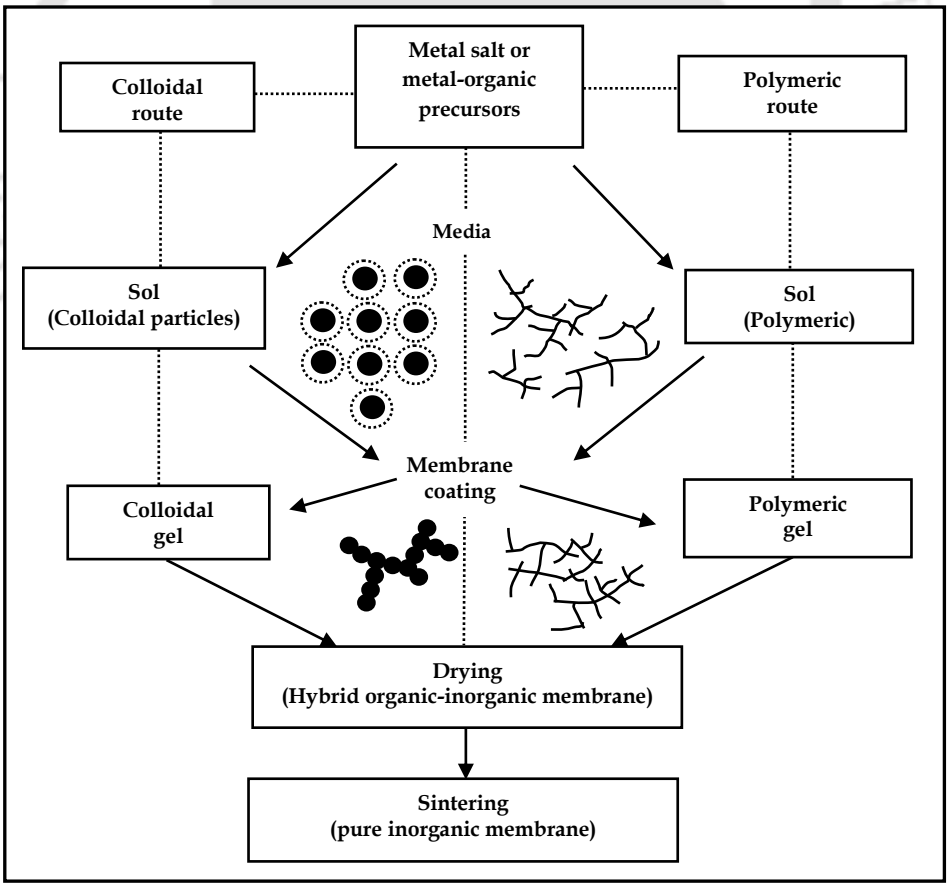

Figure 1.9: Pictorial representation of inorganic membrane preparation by sol-gel method

1.5 Zeolite Membranes

Zeolites are crystalline inorganic oxides built up by connected TO_4 (T=Siliconor Aluminum) tetrahedral resulting in unique pore sizes and structures. These inorganic materials are easily tailored along with activities and stabilities. Zeolites are utilized in numerous applications such as catalysts in the field petrochemical and chemical industries, ionic-exchangers for water purification and softening, and detergents. Zeolites have unique and molecular-sized pore structures so that close-sized molecules can be separated through membranes. Zeolite membranes are physical barriers that can separate molecules based on even slight variations in molecular shape and/or size (Dyer et al. 1988). Therefore, the utilization of zeolite thin film is giving the specific interest to get the high selectivity membrane separation processes. The charged membranes facilitate to attain good separation even utilizing a realistically larger range of pore size hydrophilic zeolite membranes (Tsapatsis et al. 2002).

1.5.1 Zeolite membrane synthesis methods

In general, the methods used in the synthesis of zeolite membranes, require the synthesized zeolite layer to be supported on another material to acquire mechanical strength (Xu et al. 2009). The choice of support material is of great importance, since the properties of the support structure influence the characteristics of the nucleation growth that forms the zeolite layer (Chau et al. 2000). The types of supports that are used most frequently in the zeolite membrane industry are alumina and stainless-steel supports, mainly because the structure and other properties of their surfaces are compatible with the zeolite gel (Mabande et al. 2004). Several methods for synthesising zeolite membranes have developed in order to replace other traditional separation techniques that require major energy and capital cost. Generally, the

synthesising industry includes two well known methods for the preparation of zeolite membrane i.e., hydrothermal in-situ synthesis, and secondary growth method. The final synthesized forms of zeolite membranes should be a thin film with coherent structure of 5 - 20 μm thickness. To enhance the mechanical structure of these membranes, metallic or ceramic supports are used i.e., stainless steel, alumina or silicon (Nomura et al. 1998).

In-situ hydrothermal synthesis

In the in-situ hydrothermal synthesis, the solution is placed under the influence of temperature and generates autogenic pressure. For this technique, the precursor sols (consisting of sodium aluminate, sodium hydroxide, water and a template) are synthesized by reactions in an aqueous or organo-aqueous solution in the existence of an alkali or acid under the influence of heat and pressure. The in-situ hydrothermal method is the most common method for zeolite membrane preparation. There are considerable advantages of coating under the hydrothermal conditions over other methods (Kaya et al. 2002). Firstly, the particle size and the morphology can be controlled easily by changing synthetic conditions. Secondly, the required crystalline phase can be synthesized directly at lower temperature.

Secondary Growth Method

The secondary growth method (SGM) was first proposed by Tsapatsis and coworkers in 2002. This method has the advantage of lower crystallization temperature and time over the in-situ crystallization method. Moreover, SGM has a better control over membrane microstructure in terms of thickness and crystals organization (Pan et al. 2001). The experimental part of this method involves the deposition and growth of seeds on the surface of the membrane or film before it is introduced to the synthesized aqueous alkaline solution or gel.

This method allows a good distribution of the crystals over the surface of film or membrane. In general, most zeolite membranes are synthesized using one of these two methods and their experimental procedures are summarized in Figure 1.10.

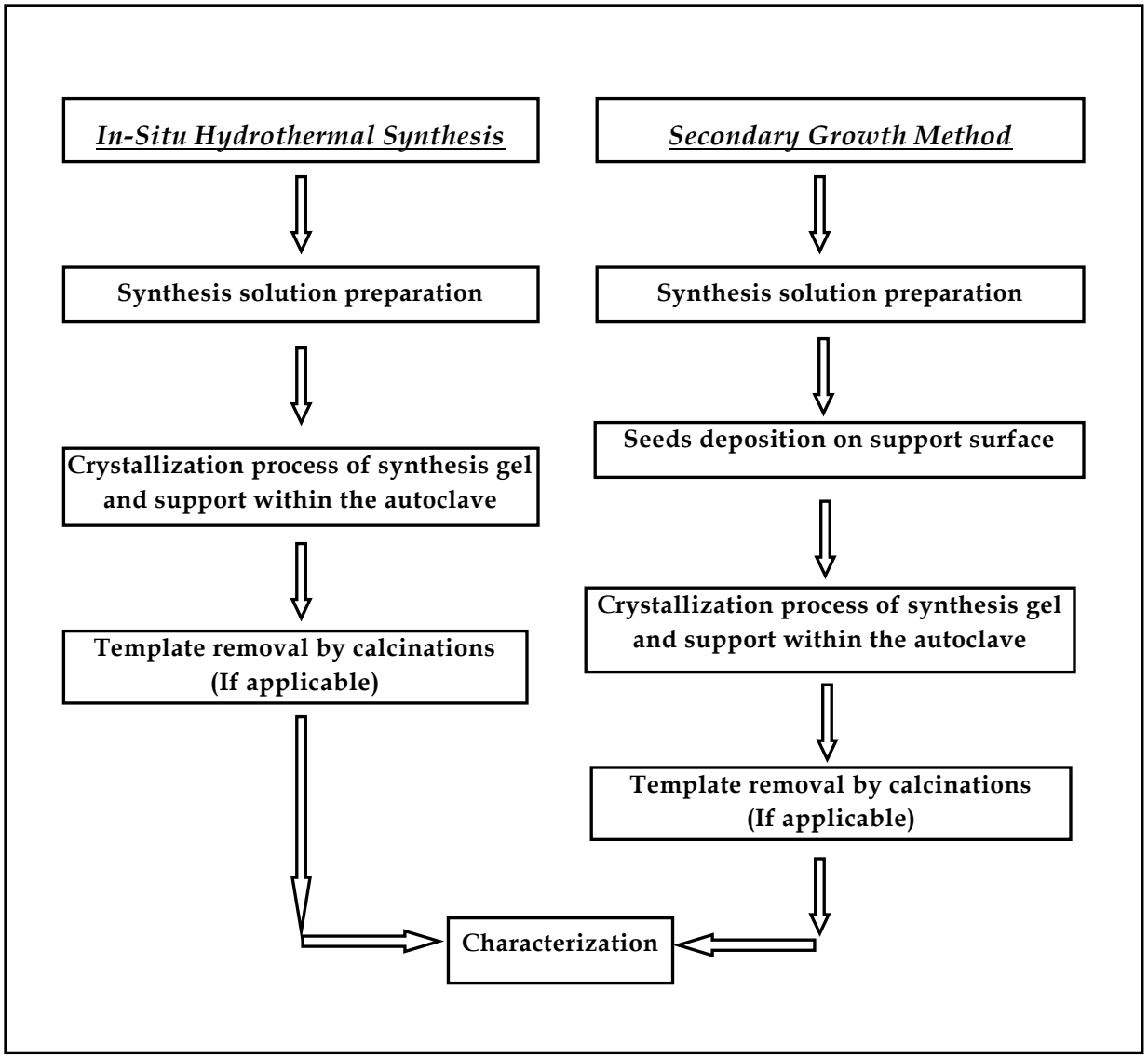

Figure 1.10: Illustration of the experimental procedure of in-situ and secondary growth methods.

1.6 State of the art

With a brief overview of the contemporary research, this section outlines the research outcome of various literatures so as to identify few promising areas of research that needs to be addressed in this thesis. The state of the art with possible scope of further research has been presented in three sub-sections namely, (a) fabrication of ceramic supports/membranes with tubular configuration, (b) fabrication of zeolite-ceramic composite membranes, (c) application of ceramic membranes for liquid phase separations (treatment of oily and dairy wastewater, removal of chromium and separation of bovine serum albumin from aqueous solutions).

1.6.1 Fabrication of ceramic supports/membranes with tubular configuration

Several literatures reported the fabrication of ceramic membranes using various types of starting materials such as α- alumina, γ-alumina, zirconia, titania and silica etc., (Judd and Jefferson 2003; Yoshino et al. 2005; DeFriend et al. 2003; Benito et al. 2005; Wang et al. 2006; Falamaki et al. 2004). The cost of these membranes was significantly high due to the higher costs of the raw materials. Moreover, most of the literature indicated that the sintering temperature required for preparation of membrane is more than 1100 °C. To overcome these problems, the research is currently directed towards the utilization of low cost raw materials, sintering temperature below 1000 °C and simple fabrication techniques. Numerous literatures reported the preparation of low cost membrane using raw clay, Moroccan clay, apatite powder, dolomite, kaolin, Tunisian clay, sepiolite clay and Algerian clay (Saffaj et al. 2005; Saffaj et al. 2006; Khemakhem et al. 2006; Weir et al. 2001; Khider et al. 2004; Bouzerara et al. 2006). In addition, preparation methods for ceramic membrane involve additional fabrication complexities that also contribute to the overall cost. The techniques (uniaxial/isostatic pressing, slip/centrifugal/gel casting and extrusion) employed for the fabrication of ceramic membranes

with different shapes (circular, tubular) were presented elaborately in literature. Amongst these fabrication techniques, extrusion is simple and very cost effective method for the production of tubular shaped membranes to treat the large volume of feed (Kaya and Blackburn 2004). This technique widely used in laboratory scale and industry scale fabrication methods to prepare ceramic membrane. Therefore, the preparation of tubular ceramic membranes with lower cost and excellent characteristics is the challenging tasks for the upcoming development of ceramic membranes for treatment of a large volume of feed. Tubular ceramic membranes are especially suitable in applications where the feed stream contains a relatively high proportion of large particles, and where the membranes are exposed to extreme pH and temperature conditions. In general, the size of the feed flow channels in tubular ceramic membranes is larger than other membrane modules. This type of open channel geometry reduces the risk of the blockage of the feed channels and also the requirement of costly pretreatment before microfiltration.

Okubo et al. (1991) synthesized tubular supports using α-Al_2O_3 as raw material by extrusion method and the supports were sintered at different temperatures (1427-1927 °C). The pore size of the support was in the rage of 0.2-6.0 µm. Qi et al. (2010) fabricated tubular support with α-Al_2O_3 and TiO_2 powders as raw materials. The ceramic support was prepared using extrusion method and sintered at 1400 °C. The membrane had average pore size and porosity of 6.8 µm and 41.4%, respectively. Patterson et al. (2006) fabricated tubular membrane support with α-Al_2O_3 as a raw material by centrifugal casting method and finally sintered at 1200 °C. The mean pore size of the tubular support was 0.16 µm. Terpstra et al. (1988) prepared α-alumina tubular ceramic substrate using extrusion method with outer diameter of 20 mm and length of 90 cm. The prepared tubular substrate possessed 0.9 µm at a sintering temperature of 1600 °C. Using α-alumina paste and extrusion method, Benito et al, (2005) prepared α-alumina ceramic tubes at a sintering temperature of 1600 °C. The membrane possessed an average pore size and porosity of

1.2 μm and 35%, respectively. Using α-alumina powder that possessed an average particle size of 3.5 μm, Yoshino et al. (2005) fabricated α-alumina tubular ceramic substrate using extrusion method at a sintering temperature of 1400 °C. The fabricated membrane possessed an average pore size and porosity of 0.7 μm and 40%, respectively. Bissett et al. (2008) manufactured and optimized the tubular α-alumina ceramic membrane supports derived from three different powder sizes (0.25, 0.31 and 0.61 μm) with different sintering temperature ranging between 1050 and 1400 °C. With the sintering temperature of 1150 °C, 37.2 % and 35.8 % porosity of the support were obtained for powder size of 0.25 and 0.31 μm, respectively. The support sintered at the lowest sintering temperatures had the highest porosity, water permeability and the largest pore sizes, while tensile strength was the lowest for all particle sizes used. Also the pore diameter of the supports produced by 0.31 and 0.61 μm powders were decreased, whereas powder size of 0.25 μm used remained constant with increasing sintering temperature.

The observation of the above literatures survey pointed out that the prepared tubular membranes are expensive due to higher sintering temperature (more than 1000 °C) and higher cost of the raw materials. These contributes towards higher raw materials cost and furnace power cost, respectively. In order to overcome such disadvantages, the researchers need to focus on exploring a new kind of low cost raw materials and simple fabrication techniques. Furthermore, lower sintering temperature (less than 1000 °C) would be beneficial for industrial applications. Recently, large number of research studies illustrated the manufacturing of ceramic membranes utilizing cheaper and naturally available raw materials such as clays (Saffaj et al. 2004; Dong et al. 2007; Masmoudi et al. 2007; Khemakhem et al. 2007; Saffaj et al. (2006); Kazemimoghadam et al. (2004); Fang et al. (2011); Majouli et al. (2012); Almandoz et al. (2004); Bouzerara et al. 2006). Saffaj et al. (2004) fabricated a tubular support using cordierite, amidon, methocel, polyethylene glycol and water as raw materials. The support was prepared using

extrusion method and sintered at 1275 °C. The membrane possessed the average pore size and porosity of 7 μm and 40%, respectively. Using extrusion method, Dong et al. (2007) manufactured a tubular support with low cost industrial grade cordierite powder and studied the effect of sintering temperature on the properties of tubular support. With increasing sintering temperature, the mechanical strength of the support increased and at the optimum sintering temperature of 1380 °C, the membrane possessed mean pore diameter of 8.66 μm and porosity of 36.20 %. Masmoudi et al. (2007) developed low cost tubular membrane support from natural apatite by extrusion method and sintered at various temperatures. The obtained result revealed that the pore diameter and mechanical strength increased with increasing sintering temperature and porosity of the support decreased with increasing temperature. The prepared ceramic support had a mean pore diameter of about 6 μm with an average porosity of 47 % at the sintering temperature of 1160 °C. The preparation of tubular support (10 mm diameter and 1.5 mm thickness) from Tunisian clay by extrusion process was reported by Khemakhem et al. (2007). The support was sintered at 1090 °C. The mean pore diameter and porosity of the support was found to be 6.3 μm, 48 %, respectively. In another study, Saffaj et al. (2006) fabricated a ceramic membrane support using Moroccan clay. The support was prepared by extrusion of the clay paste and sintered at different temperatures. The result showed that the pore diameter and mechanical strength increased with an increase in the sintering temperature and porosity of the support decreased with increasing sintering temperature. Finally the best condition to prepare the support is established for a firing temperature of 1225 °C. At this condition the average pore diameter was 10.25 μm and the mechanical resistance was 10 MPa. Kazemimoghadam et al. (2004) prepared the porous mullite ceramic support by extrusion method and the support was sintered at 1250 °C for 5 h. Fang et al. (2011) prepared the tubular supported ceramic microfiltration membranes via a slip-casting method using refined fly ash as

the raw material. Macroporous fly-ash-based substrate tubes of 10 mm external diameter, 5.5 mm internal diameter, and 100 mm length were fabricated by an extrusion method. The prepared tubular support was possessed 0.77 μm of pore size at a sintering temperature of 1150 °C. Majouli et al. (2012) elaborated the new tubular ceramic membrane from local Moroccan Perlite for microfiltration process, and applied for treatment of industrial wastewaters. Paste was extruded to form tubular supports with the following characteristics: length 15 cm, internal diameter 0.6 cm, external diameter 0.8 cm and a microfiltration layer, performed by slip casting method, with a mean pore size of 0.27 mm and sintering temperature of 1000 °C.

Very few researchers have used mixture of precursors instead of using single raw materials to obtain proper combination of better membrane characteristic such as good mechanical and chemical resistance with lower average pore size. Almandoz et al. (2004) used low cost ceramic materials such as ball clay, kaolin, alumina, quartz and calcium carbonate for the fabrication of membrane by paste method. The support was sintered at various temperatures ranging between 1100 and 1400 °C. The results indicated that an increase in sintering temperature led to a higher density, mechanical resistance and the smaller pore volume of the membrane. The authors found that optimum sintering temperature was in the range of 1200-1300 °C and the mean pore size of the membrane was between 0.1 and 1.0 μm. Bouzerara et al. (2006) prepared a tubular ceramic membrane support from kaolin and kaolin-dolama mixtures by extrusion technique. The effect of sintering temperature on the membrane properties (average pore size, mechanical strength and porosity) was investigated and the results revealed that the mechanical strength, porosity, average pore size and pore size distribution are strongly influenced by sintering temperature and processing route. A uniform pore size distribution within a total porosity ratio of 43% and 28 μm as an average pore size, were obtained for membrane sintered at 1250 °C for 1 h.

Conventional fabrication techniques such as extrusion and casting methods provide excellent low-cost manufacturing routes for tubular shaped ceramic support/membrane. Extrusion technique has been successfully used for the tubular ceramic membrane fabrication. In addition, recent studies on membrane manufacturing demonstrated the minimal macro-defects and homogeneous compact structure. Table 1.1 presents a summary of the research finding of various authors for the fabrication of tubular ceramic membrane supports.

Possible scope for further research

A critical review of above literatures and other relevant research findings (see Table 1.1) convey the following conclusions for the fabrication of ceramic membrane with tubular configuration. It can be observed that ceramic membrane research has been primarily addressing the fabrication of α-alumina membranes that are expensive due to higher cost of the inorganic precursors and sintering temperature. Using alumina precursors, the average pore size of the various fabricated membranes is in the range of 0.1 - 1.2 µm. Moreover, the sintering temperature used for fabricating alumina membrane is in the range of 1000 - 1600 °C. Further, the literature data indicates that membrane fabrication research was also carried out using low cost clay based raw materials such as cordierite, apatite powder, tunician clay, natural clay, mullite, fly ash, moroccan, dolomite and kaolin. Even though, these raw materials are inexpensive, the sintering temperature and pore size of the fabricated membranes are 0.7 - 28.0 µm and 1000 - 1350 °C, respectively. Therefore, ongoing research should target the (*i*) fabrication of low cost ceramic membranes using low cost precursors, (*ii*) lower sintering temperature and (*iii*) simple and cost effective fabrication technique (such as extrusion method). Similarly, MF membrane possessing submicron range average pore size (0.1 - 0.5 µm) using low cost precursors and sintering temperature lower than 1000 °C also need to be addressed. The larger and smaller pore size

possessing low cost MF membranes could potentially serve as inexpensive supports for MF and UF applications.

Table 1.1: Summary of literature survey on tubular ceramic support/membrane preparation

Materials	Method	Sintering temperature (°C)	Pore diameter (μm)	Authors
α-Al_2O_3	Extrusion	1427	0.2	Okubo et al. (1991)
α-Al_2O_3	Extrusion	1200	0.45	Gordon et al. (2008)
α-Al_2O_3	centrifugal casting	1200	0.16	Patterson et al. (2006)
α-Al_2O_3	Extrusion	1600	1.2	Benito et al. (2005)
α-Al_2O_3	Extrusion	1400	0.7	Yoshino et al. (2005)
α-Al_2O_3	Slip-casting	1050-1400	0.25-0.31	Bissett et al. (2008)
α-Al_2O_3	Extrusion	1600	0.9	Terpstra et al. (1988)
Cordierite	Extrusion	1275	7	Saffaj et al. (2004)
Cordierite powder	Extrusion	1380	8.66	Dong et al. (2007)
Apatite powder	Extrusion	1160	6	Masmoudi et al. (2007)
Tunician clay	Extrusion	1090	6.3	Khemakhem et al. (2007)
Natural clay	Extrusion	1100 - 1250	9.3 - 10.75	Saffaj et al. (2006)
Mullite	Extrusion	1250	-	Kazemimoghadam et al. (2004)
Fly ash	Slip-casting	1150	0.77	Fang et al. (2011)
Moroccan	Extrusion	1000	6.6	Majouli et al. (2012)
Ball clay, kaolin, alumina, quartz & calcium carbonate	Paste casting	1300	1	Almandoz et al. (2004)
Dolomite & kaolin	Extrusion	1250	28	Bouzerara et al. (2006)

1.6.2 Fabrication of zeolite-ceramic composite membranes

Zeolitic membranes can be classified as either symmetric membranes (self-supported) or asymmetric membranes (supported). The first type of membrane is constituted by a pure zeolitic phase and in the second type, a zeolitic thin layer is formed on a support (zeolitic layers on stable supports). To make the zeolite-ceramic composite membranes, a permanent support can be made of any of the numerous materials available. The resources generally used for the development of zeolite-ceramic composite membranes are α-alumina, γ-alumina, titania, zirconia and microporous glasses. In order to prepare these composite membranes, zeolite crystals need to grow on porous substrates for forming a continuous thin film, having the zeolitic pores. The growth of zeolites on porous supports, such as alumina, generally results in a random orientation of crystals, due to the roughness of the supports applied. Zeolite-ceramic composite membranes exhibit high thermal, chemical and mechanical stability, and can be used in continuous separation processes. The economic advantage of using a zeolite surface, which would allow carrying out such processes continuously have been recognized. In recent years many studies have demonstrated the potential of zeolites as coating materials for improving the separation performance of the membranes. Several research groups investigated the fabrication of zeolite composite membrane for the applications in pervaporation and gas phase separation due to their promising features such as uniform molecular sized pores, good adsorption properties, thermal stability, mechanical and chemical stability. Further, among all types of composites organic and inorganic membranes, zeolite composite membrane has the potential to attain both high flux and selectivity due to the presence of well-defined crystals microspores in the zeolite framework. Zeolite as a separating layer provides numerous benefits, for instance; pore size of the membrane can be regulated by using appropriate zeolite type. It can separate the component of gaseous or liquid mixtures based on molecular size due to its molecular sieve

function. Numerous experimental techniques were addressed to prepare the selective layer of polymer, ceramic and zeolite composite membranes. Unlike the polymeric membrane, zeolite composite membrane did not swell. Due to the swelling nature of polymeric membrane, it has higher permeability and low selectively (Praptowidodo 2005). A series of literature reported that various zeolite membranes, such as MCM-48 (Nishiyama et al. 2003; Kumar et al. 2008; Pedernera et al. 2009; Seshadri et al. 2011), MFI (Mordenite Framework Inverted) (Çulfaz et al. 2006; Zhang et al. 2012), FAU (Faujasite) (Jeong et al. 2003; Sato et al. 2007; Zhu et al. 2008; Covarrubias et al. 2008; Huang et al. 2012), LTA (Linde Type A) (Li et al. 2006; Huang et al. 2014), Silicate-1 (Jia et al. 1994; Wirawan et al. 2011), Analcime (Potdar et al. 2002, Kumar et al. 2006), ZSM-5 (zeolite socony mobil-5) (Yan et al. 1997, Oonkhanond and Mullins 2001), NaA (Ling et al. 2011; Jafari et al. 2013), CHA (Chabazite) (Maghsoudi and Soltanieh 2014; Hasegawa et al. 2010), were fabricated on porous and non-porous support.

Jia et al. (1993) prepared zeolite (silicate-1) membrane on a ceramic disk support using Teflon autoclave reactor at 180 °C for 3-72 h. To remove the organic surfactant, the fabricated membrane was calcined at 450 °C for 8 h. The prepared composite membrane was used for permeation study at room temperature and true selectivity of the membrane was found to be 2.81 for He over N_2 and 47.7 for N_2 over n-butane. Nishiyama et al. (2001) synthesized mesoporous silica MCM-48 composite membrane on alumina support with pore size of 0.1 μm by hydrothermal synthesis method at 90 °C for 96 h. The prepared MCM-48 membrane was investigated for the permeation of H_2, He, CH_4, O_2, N_2 and CO_2 gases at various applied pressures (100-270 kPa). The permeation of H_2 was independent of the feed pressure and no contribution of viscous flow to the total permeation.

In comparison with other composite membranes, mesoporous membranes are typically found several applications in many fields of charged mechanism separation processes due to the

presence of Si-O and Si-OH groups. FAU zeolite (NaX with Si/Al of 1.0-1.5) membranes have a three dimensional pore structure and 12-membered oxygen ring pores (0.74 nm) are suitable for separation of large molecules, in which LTA membrane (Jeong et al. 2002) cannot handled properly. Generally at low Si/Al ratio, FAU zeolite membrane is hydrophilic and it can be used for the dehydration of organic solvents by pervaporation or steam permeation (Zhu et al. 2009; Kita et al. 1997). Weh et al. (2002) fabricated FAU-type composite membrane on a porous α-Al_2O_3 support by hydrothermal method in two steps. First, a seed layer of Na-Y nanocrystals was deposited externally on the surface of ceramic support. Crystallization was kept under the reflux at 100 °C for 240 h. Secondly, the seeded support was again synthesized hydrothermally in Teflon autoclave at 90 °C for 12 h and it was treated with microwave oven at 100 °C for 2 h. The dense FAU layer was intergrown with Si/Al ratio of 1.3-1.8 and thickness in the range of 0.8-6.0 μm depending on synthesis condition. The observed result revealed that permeation of the single gas was in the order of $H_2 > CH_4 > N_2 > O_2 > CO_2 > nC_4H_{10} > SF_6$. Jeong et al. (2003) prepared FAU-type zeolite membrane on a porous α-Al_2O_3 support tube by treating hydrothermally at 90 °C for 24 h. The catalyst, 1.0 wt % Pt/Al_2O_3 was deposited on the membrane by an impregnation method in the temperature range of 150-250 °C. The fabricated membrane was utilized for the selective separation of benzene and hydrogen from cyclohexane. They indicated that the conversion of cyclohexane increased with increasing flow rate and the decrease in the feed rate of cyclohexane led to a higher cyclohexane conversion upto 72.1% at 200 °C. Zhu et al. (2008) fabricated FAU-type zeolite membrane by microwave assisted in situ crystallization on porous α-Al_2O_3 tubes. The synthesis solution was prepared by dissolving aluminum foil into sodium hydroxide solution, and then adding silica sol into the solution. The synthesis solution was transferred in a Teflon autoclave for 8 h at 60 °C and microwave heating was done at 90 °C for 20 min with 1400 W power. The authors reported the single gas

permeation of H_2, N_2, n-C_4H_{10} and i-C_4H_{10} through the fabricated membrane and H_2 showed a higher permeation. Guillou et al. (2009) synthesized FAU-type zeolite membrane on α-alumina tube using hydrothermal method at 85 °C for 24 h. The membrane was utilized for the separation of CO_2 /N_2. The obtained results demonstrated the CO_2 permeance of 3.5×10^{-7} mol $s^{-1}m^{-2}Pa^{-1}$ and selectivity of 12 for the separation of equimolar CO_2 /N_2 gas mixtures at 50 °C. Huang et al. (2012) prepared FAU zeolite membranes using 3-aminopropyltriethoxysilane (APTES) as covalent linker between the FAU layer and the alumina support by in-situ crystallization (about pH 7) at 75 °C for 24 h. The developed membrane was tested for the separation of gas from the mixture of gases. The separation factors for H_2/CO_2, H_2/N_2, H_2/CH_4 and H_2/C_2H_8 were found to be 6.5, 6.0, 4.0, and 11.1, respectively.

The zeolite MFI type (ZSM-5) has a suitable channel system, sinusoidal channels of circular cross-section 5.4 Å interconnected with straight channels of elliptical cross-section 5.6 Å × 5.7 Å. Low siliceous MFI type is hydrophilic in nature. Therefore, MFI designates the MFI-type that includes synthetic species with different chemical composition (Silicalite and ZSM-5). Matsukata et al. (2003) crystallized MFI-type zeolite on porous α-alumina support tubes by in situ hydrothermal synthesis. A gel was prepared tetrapropylammonium hydroxide (TPAOH) as a structural directing agent and carried out at 170 °C for 72 h. TPA cation contained in the membrane was removed by the calcination in air at 500 °C for 5 h. They suggested that the permeation properties of membranes synthesized by this method would be greatly affected by water adsorption. Even 500 ppb water stream influenced the single gas permeation properties of the membrane. These properties of the membranes were caused by strong hydrophilicity of highly aluminated MFI-type zeolite. Kazemimoghadam and Mohammadi (2007) synthesized the MFI membranes on mullite supports via hydrothermal crystallization using TPABr as a template at 180 °C for 24 h. The prepared MFI zeolite membranes have great potential for

applications in RO desalination of complex mixtures. RO of aqueous solutions using MFI zeolite membranes behaved very high rejection values for concentrated solutions containing different types of cations. Bernal et al. (2004) fabricated the MFI-type zeolite (ZSM5) membranes on alumina and stainless steel tubular supports using hydrothermal technique at 160 ^{o}C for 8 - 12 h and tested for the separation of CO_2/N_2 mixtures. They obtained larger permeate flux with a CO_2/N_2 separation factor of 13.7. Li et al. (2004) prepared the α-alumina supported MFI-type zeolite membranes by in situ crystallization for desalination by reverse osmosis. Hydrothermal treatment was conducted in an autoclave at 180 °C with an autogenous pressure for 4 h. After drying overnight at 50 °C, the membrane was activated by calcining at 450 °C in air for 5 h.

Liu et al. (2005) fabricated analcime zeolite membrane on α-alumina plate support (15 × 15 × 2 mm) by hydrothermal synthesis method at 180 °C for 72 h. The product obtained was dried at 180 °C for overnight and calcined at 500 °C for 6 h for the removal of template. The structural and thermal stability of the prepared membrane were confirmed by means of XRD, FTIR and DTA analysis. Cui et al. (2008) fabricated NaA zeolite composite membrane on α-alumina tube by hydrothermal synthesis method at 100 °C with various durations (i.e. 2, 4, 10 and 18 h). The support pore size was between 1 μm to 3 μm and porosity between 30 and 40%. The prepared composite membranes with pore sizes of 1.2 μm and 0.4 μm were used to treat oil-in-water emulsion containing 100 mg/ L oil and 99% oil rejection was reported. Sato et al. (2008) synthesized NaY zeolite membrane on a porous tubular shaped alumina support and used for the pervaporation of ethanol in industrial scale. The prepared zeolite membrane showed high performance for dehydration of the hydrous ethanol mixture at 75 °C. Jia et al. (1994) prepared ceramic-zeolite composite membrane on the inner surface of γ-alumina tube by in-situ hydrothermal synthesis at 180 °C for 12 h. SEM images showed that individual silicalite crystals were grown together continuous as silicalite-1 layer. The membrane displayed high permeance

for gases and shape-selectivity was found with n-C_4H_{10}/i-C_4H_{10} permeance ratio of 3:1. Maghsoudi and Soltanieh (2014) prepared the CHA-type zeolite membrane on the disk shaped α-alumina support by in-situ crystallization method for the separation of H_2S and CO_2 gases from methane. The separation results specified that both gases can be removed from methane with selectivity of 3.14 for H_2S/CH_4.

In summary, numerous synthetic techniques have been employed for the preparation of zeolite membrane such as in-situ (without seeding) hydrothermal synthesis (Noble and Falconer 1995), secondary (seeded) growth (Kim et al. 2013), vapor phase transport (Matsufuji et al. 2000) and post-treatments of zeolite membranes (Yan et al. 1997). FAU and MFI zeolite membranes have been prepared by hydrothermal synthesis method onto a porous support either in-situ or with a preliminary seeding step. Hydrothermal synthesis method is easy to implement in operation point of view as compared to other preparation techniques. Table 1.2 represents summary of various literatures for the fabrication of zeolite-ceramic composite membranes.

Possible scope for further research

Table 1.2 presents the summary of the literature survey for the preparation of zeolite-ceramic composite membranes. It can be noted that several literatures addressed the fabrication of zeolite-ceramic composite membranes using expensive α-alumina as a support material. Under this circumstance, future research for the fabrication of inexpensive zeolite-ceramic composite membranes should target (i) utilization of novel low cost ceramic support instead of alumina based support to reduce the cost of the composite membrane (ii) formation of various zeolite top layer such FAU and MFI (iii) simple and easy membrane preparation method such as hydrothermal treatment to minimize the cost. These approaches could identify potential pathways to the industrial competitiveness of the zeolite-ceramic composite membranes.

Table 1.2: State of the art on zeolite-ceramic composite membranes

Top/skin layer material	Support materials	Method of preparation	Authors
Silicate-1	Al_2O_3	In-situ hydrothermal	Jia et al. 1993
MCM-48	Al_2O_3	Hydrothermal treatment	Nishiyama et al. (2001)
FAU zeolite	Al_2O_3	Hydrothermal synthesis	Weh et al. (2002)
FAU zeolite	Al_2O_3	In-situ crystallization method	Huang et al. (2012)
NaA zeolite	α-Al_2O_3 tube	Hydrothermal synthesis	Cui et al. (2008)
ZSM-5	α-Al_2O_3	In-situ crystallization method	Yan et al. (1997)
MCM-48	α-Al_2O_3	Seeded growth technique	Kim et al. (2013)
FAU zeolite	α-Al_2O_3 tube	Hydrothermal synthesis	Guillou et al. (2009)
NaA zeolite	γ- Al_2O_3	Secondary growth method	Jafari et al. (2013)
Analcime zeolite	α-Al_2O_3	Hydrothermal synthesis	Liu et al. (2005)
LTA zeolite	α-Al_2O_3 tube	Hydrothermal synthesis	Huang et al. (2014)
MFI	α-Al_2O_3 tube	Dip-coating (seeding)	Çulfaz et al. (2006)
MFI	α-Al_2O_3	Hydrothermal crystallization	Zhang et al. (2012)
CHA zeolite	α-Al_2O_3	Crystallization method	Maghsoudi and Soltanieh (2014)
Silicate-1	α-Al_2O_3	Hydrothermal synthesis	Wirawan et al. (2011)
FAU zeolite	α-Al_2O_3 disk and tube	Seed growth and hydrothermal synthesis	Covarrubias et al. (2008)

1.6.3 Application of ceramic membranes for liquid phase separations

Till date, ceramic membranes have been found to be suitable in various separation applications such as desalination, industrial effluent treatment, food processing and drinking water production. Since, this work attempts to fabricate low cost ceramic membrane and zeolite-ceramic composite membranes with tubular configuration, we consider four major applications such as treatment of oily wastewater and industrial dairy wastewater, removal of chromium and separation of bovine serum albumin (BSA) from aqueous solutions. The reason for choosing the above application and its necessity, challenges involved in achieving the separation/removal, factors influencing its efficiency and optimum conditions to achieve greater efficiency are discussed in the following sub-sections.

1.6.3.1 Treatment of oily wastewater

The swiftly developments of various industries specifically, oil refineries, petrochemical, metallurgical, pharmaceutical, chemical and food industries, are bearing to produce a huge amount of both water-in-oil or oil-in-water emulsions. These contain bulk quantity of heavy hydrocarbons such as diesel oil, grease, crude oils, tars, and light hydrocarbons, such as gasoline, jet fuel, and kerosene. In addition, these comprise of cutting liquids, lubricants, total suspended solid (TSS), and other supplemental contaminates (Padaki et al. 2015; Salahi et al. 2015). The discharge of oil contaminated effluents to water bodies, generate environmental issues all over the globe. Concurrently, the population growth directs to the bigger demand for pure water, primarily in water scarcity regions (Salahi et al. 2013). Therefore, the removal of oil from the oily wastewater is necessary to protect our water resources in both an environmental and public health. Central pollution control board of India regulated the discharge limit of oil into the surface water and irrigation as 10 mg/L, public sewers and coastal water as 20 mg/L

from various process industries. Beside the treatment, the stable oily wastewater containing extremely physically and chemically emulsified oils are the major difficult ones in terms of efficient treatment (Abbasi et al. 2010). The conventional techniques utilized in water treatment plants to treat the wastewater can be classified as creational: chemical demulsification, gravity separation, adsorption, filtration, coagulation and coalescence (Srijaroonrat et al. 1999). These techniques have various demerits, including higher operation expenses, lower effectiveness, corrosion and recontamination issues (Rezvanpour et al. 2009). One of the best solutions to resolve these problems and reuse of water is using membrane technology. Currently, industries have paid increasing attention for the membrane technology (Sarfaraz et al. 2012). It is very attractive due to the advantages, such as compact design, lower energy requirement and higher separation efficiency as compared to other existing treatment processes (Cheryan and Rajagopalan 1998). In addition, the treatment cost can be further lowered by choosing microfiltration (MF) membranes since they do not require so high trans-membrane pressures and have higher flux than ultrafiltration membranes (Yi et al. 2013). In the membrane separation process, ceramic membranes have been proven to be well-suitable and more favorable for large scale applications compared to the polymeric membranes. Inorganic membranes have higher chemical, thermal and mechanical resistance and can be used in the wide range of pH, chlorinated and polar solvents (Nandi et al. 2010). Numerous authors have evaluated the potential aspects of ceramic membranes in oily wastewater treatment. However, the alumina based inorganic membranes are unfavorable to large scale industrial applications due to its high cost. Therefore, the research on ceramic membrane is directed to make low cost membranes by utilizing cheaper starting materials, such as kaolin, mullite, fly ash, apatite powder and dolomite (Karhu et al. 2013). In this context, manufacturing of reasonably inexpensive inorganic membranes for oil-in-water emulsion treatment is potentially useful for

future membrane development research. In addition, membranes come into four different configurations, including tubular, hollow fiber, plate and frame, and spiral. Tubular membranes are suitable for handling large size particles and high flow rates, and they can be cleaned easily (Cheryan 1998). Therefore, the low cost membrane with tubular configuration is well suitable particularly for oil-in-water emulsion treatment. Mohammadi et al. (2004) formulated a kaolin based tubular ceramic membrane with a pore diameter of 10 μm for the treatment of oily wastewater emulsions. The prepared membrane provided a good separation performance on various operating conditions. Zhong et al. (2003) examined the efficiency of ZrO_2 ceramic membrane (average pore diameter of 0.2 μm) in oily wastewater treatment. The prepared zirconia membrane displayed the oil removal of 99.4 - 99.9%. Yang et al. (1998) attained 99.8% of oil rejection utilizing the commercial tubular (ZrO_2/α-alumina) membrane with an average pore diameter of 0.2 μm. In another study, Cui et al. (2008) obtained 99% of oil rejection employing the zeolite membrane having the pore size of 1.2 μm in microfiltration of oily wastewater. Amongst many research perceptions, the development and employment of the ceramic membranes derived from inexpensive raw materials for oily wastewater treatment are getting interest in recent days. Abbasi et al. (2010) synthesized tubular inexpensive mullite microfiltration membrane from kaolin clay, which was obtained from Marand, Iran. The tubular shaped mullite membrane was suitably acquired through extrusion using 62 - 69% of kaolin and distilled water mixture. The potential of the fabricated membrane was investigated by the separation of oil-in-water emulsion and the influences of various significant conditions, namely pressure (50 - 400 kPa), cross flow velocity (0-2 m/s), and oil concentration (250-3000 ppm) were also examined. The investigation on oil-in-water emulsion treatment revealed that the prepared membrane has potential to get the highest rejection of 93.8%. Fang et al. (2013) elaborated new fly ash based low cost membrane for treatment of oily wastewater. Macroporous fly ash based

ceramic membrane was obtained by an extrusion process. The acquired membrane tested for microfiltration of oily wastewater by varying the operating parameters, such as transmembrane pressure (0.05 - 0.20 MPa), feed concentration (75 - 2000 ppm) and cross flow velocity (0.67 - 4 m/s). The highest rejection (98.2%) of oil was obtained with the feed concentration of 2000 ppm. Song et al. (2006) prepared the low cost tubular carbon membrane using coal via extrusion technique and used for oil-in-water emulsion treatment. This investigation was performed by altering various parameters, such as membrane pore size (0.6 - 1.4 μm), transmembrane pressure (60 - 140 kPa), feed oil concentration (120 - 400 ppm) and cross flow velocity (0.06 - 10 m/s). The maximum rejection of 98.6% was obtained with the feed concentration of 400 ppm.

Possible scope for further research

It is worth to mention that all the above investigations were performed using higher concentration of oil-in-water emulsion. The treatment of low concentration (≤100 ppm) of oily wastewater to bring down to the disposal limit (10 - 20 ppm) is difficult by most of the conventional separation techniques (Monash and Pugazhenthi 2011). For such complicating scenario, ceramic membrane technology could provide technological solutions. Therefore, this work attempts to address these issues by preparing novel low cost tubular ceramic membrane and application in oily wastewater treatment.

1.6.3.2 Treatment of dairy wastewater

Most of the wastewater from chemical industries, in general, and food industries, in particular, must be treated prior to discharge (Madaeni and Mansourpanah 2006). Food processing wastewater is very distinct from other industrial activities, and among the food industries, dairy is considered the most important as it requires very large quantities of freshwater and

generates large quantities of wastewater. This huge quantity of wastewater is produced due to the different unit operations, such as milk processing units, sanitization, cleaning and floor washing. Dairy industry generates 2.5 L (approximately) of wastewater for processing 1 L of milk and it contains a high lactose content, dissolved and suspended solids, fats and nutrients in the form of ammonia and phosphates (Al-Shammari et al. 2015). Even though the dairy industry generally does not deal with hazardous or toxic pollutants, different kinds of contaminants at high levels constitute the dairy wastewater, which can harm the environment. In particular, dairy wastewater contains a high concentration of nutrients along with a very high chemical and biological oxygen demand (COD and BOD) content and total suspended solids (TSS). An appropriate index to specify the quantity of organics in water is the COD, and the existence of such organic matter in dairy wastewater leads to numerous issues and dramatically contaminates the environment. Ideally, the COD value should be reduced to 200 mg/L to meet the environmental discharge standards (Madaeni and Mansourpanah 2006). Owing to these concerns, the dairy wastewater needs to be treated prior to its discharge into the environment.

A variety of techniques has been established to treat wastewater generated from dairy industries. In general, biological and physicochemical treatment methods are utilized for treating dairy wastewater. However, several studies have found that the COD removal using physicochemical methods is poor and the costs of chemical coagulants are high (Sharma 2014). Membrane technology has been applied for the reduction of organic materials. Membrane technology is the most promising and alternative emerging process particularly for wastewater treatment applications. Thus, membrane technology is gradually replacing to the conventional treatment methods, viz. adsorption, incineration, oxidation, stripping, biological treatment, etc. Among the various membrane based treatment options for reducing the COD of effluent from

dairy industry, microfiltration processes are more economical than the other (RO/NF/UF) processes in terms of achieving a high flux with a low energy input (Cowan et al. 1992). Tfiigdh and Johansson (1998) attempted to reduce the COD of dairy wastewater using zirconium-aluminum ceramic membrane and obtained 51% reduction in the feed COD (1650 mg/L). Bennani et al. (2015) prepared polyethersulfone ultrafiltration membrane for dairy wastewater treatment. They reported that the process efficiency and permeate quality are improved by operating under optimum conditions of transmembrane pressure (TMP) and volume reduction factor (VRF). Yip et al. (1996) used porous stainless steel micromembrane system for the investigation as a means of chemical recovery and effluent pretreatment for the dairy industry. They achieved 78 and 79% of COD reduction using microfiltration and nanofiltration membrane, respectively. Turan et al. (2002) synthesized thin film polyamide-polyethersulfone composite nanofiltration and reverse osmosis membranes and evaluated their potential for the treatment of the effluent of chemical-biological treatment plant. They obtained the COD removal 98% for nanofiltration and 99% for reverse osmosis membrane, respectively.

Possible scope for further research

Literature on ceramic membranes for dairy wastewater treatment application is very scarce. This is particularly important to further establish the potential of the same for large scale environment application. To best of our knowledge, the applicability of low cost ceramic membrane to treat dairy industry wastewater has not been studied till date. Therefore, this work attempts to study the applicability of novel low cost tubular configured ceramic membrane for the treatment of local dairy industry wastewater.

1.6.3.3 Removal of chromium from aqueous solution

The discharge of wastewater containing toxic heavy metals is increasing due to a rapid growth of various industries such as tanneries, metal plating, paper, mining operations, fertilizers and pesticides. Heavy metals, such as chromium, lead, cadmium, mercury, nickel, copper and zinc are unlike organic contaminants, non-biodegradable and lead to accumulation in the human body, which cause the health hazards due to their toxicity. Among the heavy metals, chromium is a widespread pollutant in surface water. For instance, in India alone about 2000-3000 tone of chromium escapes into the environment annually from tannery industries, with chromium concentrations ranging between 2000 and 5000 ppm in the aqueous effluent compared to the recommended permissible discharge limits of 2 ppm (Belay 2010). In addition, chromium is a widespread pollutant in surface water and presents principally either in trivalent or hexavalent oxidation states. Hexavalent chromium is highly toxic (10-100 times) than the trivalent chromium and also hard to eliminate from water. Moreover, it is carcinogenic to the human being and causes considerable hazards to the environment (Shpiner et al. 2009; Kim et al. 2015). Therefore, the World Health Organization (WHO) framed as 0.05 mg L^{-1} is the highest acceptable limit of chromium in drinking water (Mandal et al. 2015). A variety of techniques has been established to treat the chromium including, chemical precipitation (Gheju & Balcu 2011), liquid-liquid extraction (Sacmaci & Kartal 2011), chemical/electrochemical reduction (Dhaz et al. 2012), ion-exchange (Rengaraj et al. 2001), solvent extraction (Luo et al. 2013), adsorption (Selvi et al. 2001), coagulation/flocculation (Amuda et al. 2006), dialysis (Koseoglu et al. 2010) and reverse osmosis (Rad et al. 2009). Most of these methods have disadvantages, such as pretreatment, usage of additional costly chemicals, longer operation period, etc. Moreover, these techniques are expensive and the final metal recuperation needs further treatments. This

causes difficulties in the process and also considered to contaminate the processes itself (Canizares et al. 2002).

Membrane technology is the most prominent and alternative emerging process, particularly for the removal of heavy metals. Also, ceramic membrane is prepared with composite arrangement using an active top layer that will determine its separation efficiency. This active layer is formed using oxide inorganic materials through dip-coating, sol-gel technique and hydrothermal treatment. In general, the active layers are fabricated using inorganic oxides such as alumina, zeolites, zirconia, titania, etc. Among these, zeolites provide well-defined pore structures, better chemical and thermal stability and exhibit excellent applications in various separation processes. In addition, zeolites possess molecular dimension channels and distinct cavities, which are uniform in size, this resultant narrow pore size dispersion within the active top layer (Kumar et al. 2015). Therefore, the use of thin film of zeolite offers specific interest to get high selectivity in membrane separation processes. This charged membrane facilitates to attain excellent separation even employing a reasonably bigger pore sized zeolite membrane.

Recently, numerous investigations have been carried out to discover the potential of charged ultrafiltration and microfiltration membranes for the removal of chromium. Covarrubias et al. (2008) synthesized the FAU zeolite membrane using a secondary growth technique on alumina support and obtained the maximum rejection of 95% for Cr(III). Doke & Yadav (2014) produced the titania microfiltration membrane using nanocrystalline titania by sol-gel technique and obtained 99% removal of chromium from aqueous solution. Tang et al. (2012) prepared the magnetite membrane by sol-gel technique using porous stainless steel as support. The prepared membrane was effectively removed 92.5% of chromium presented in the aqueous medium. Shukla & Kumar (2007) prepared the analcime-O zeolite composite membrane via a hydrothermal method for the separation of chromic acid solution and attained about 50%

chromium rejection using the unmodified zeolite membrane. They reported that the charged membrane can separate the acid chromate ions even having a bigger pore size. Tijani et al. (2013) investigated the preparation of NaA zeolite membranes by hydrothermal treatment at various temperatures and applied for removal of hexavalent chromium. They strongly suggested that the zeolite membrane could be particularly useful for the separation of heavy metals. The above studies indicate that the chromium removal can be attained by utilizing charged membranes even having a bigger pore size.

Possible scope for further research

None of the literature reported the formation of zeolite top layer of FAU and MFI on low cost tubular ceramic substrate for the liquid phase separation application particularly for chromium removal. Hence, this work attempts to formation of FAU and MFI type zeolite membrane on novel low cost ceramic membrane derived from locally available clays and investigates the potential of the fabricated membranes in removal chromium from its aqueous solution.

1.6.3.4 Separation of bovine serum albumin (BSA) from aqueous solution

Bovine serum albumin (BSA) has abundant biochemical applications comprising immunoblots, Enzyme-Linked-Immunosorbent Assay (ELISAs) and immunohistochemistry. It is also used as a nutrient in microbial and cell culture. In addition, it is utilized in numerous biochemical reactions, because of its low cost and stability to increase a signal in assays. BSA is a single-chain globular protein has a prolate ellipsoidal shape with 66.7 kDa of molecular weight. The dimensions of the BSA is found to be 140×40×40 Å (Valiño et al. 2014). The downstream processing of BSA is a real bottleneck in biotechnological industries because of its size and shape. Nevertheless, the separation of BSA can be accomplished by changing the solution pH,

because it is a charged molecule (Monash et al. 2010). Chromatographic techniques, such as affinity chromatography and reverse-phase HPLC are widely used in industries in order to isolate ultra-pure protein (Valiño et al. 2014).

Membrane techniques such as microfiltration (MF) and ultrafiltration (UF) with polymeric and ceramic membranes have been used for protein recovery in industries. In recent years, ceramic MF membrane has received great attention by researchers for the separation of bio-molecules (Emilio et al. 2007). In addition, ceramic MF membranes can be considered as an alternative for chromatographic technique, because of their high efficiency, better chemical and thermal stability, excellent anti-fouling properties, good mechanical strength and readily scalable from the laboratory to industrial settings. These membranes are made up of inorganic oxides and have better tolerance to the wide range of pH. Owing to the very high cost of the commercially available ceramic membrane, a large scale industrial application is restricted. The production of ceramic membrane with low-cost materials might overcome this problem. Monash et al. (2010) fabricated the γ-Al_2O_3 ceramic composite membrane for BSA separation on low cost porous support. The prepared membrane was exhibited excellent rejection of BSA (95%). Emilio et al. (2007) fabricated the ceramic membrane containing mixture of aluminium/titanium/zirconium oxides with an active layer of zirconium oxide for BSA separation. The prepared membrane possessed 0.14 μm pore size and exhibited 71% of BSA rejection. In another study, Monash and pugazhenthi (2011) fabricated titanium-ceramic composite membrane with pore size of 0.83 μm and applied for separation of BSA from aqueous solution. Fakhfakh et al. (2010) prepared mesoporous silica layer by the sol–gel method using a SiO_2 sol on elaborated ceramic membranes from mineral oxides. The prepared silica membrane with pore size of 12.5 μm was tested for BSA separation.

Zeolites are crystalline aluminosilicate inorganic materials with unique intrinsic properties such as high surface area, excellent thermal/hydrothermal stability, high shape-selectivity and superior ion-exchange ability, which form the basis for their traditional applications in catalysis and separation of small molecules (Ozin 1989). Therefore, zeolites are expected to be novel chromatographic carriers for biomolecule separation. The FAU and MFI-type zeolites possess an appropriate channel structure with low siliceous in nature. Hence, these can be used as a potential applicant in removing diverse materials. It is well known that the separation of solutes by ultrafiltration (UF) and microfiltration (MF) are not only based on the pore size, but also depend on other factors such as surface charge of the membrane and electrostatic interactions between membrane and charged solutes. This means that the interaction between membrane and protein as well as protein and protein can significantly affect the performance of the UF/MF membranes (Monash et al. 2010). For the UF/MF of protein, the rejection is based on the chemical nature of the membrane, physico-chemical properties of solute and importantly electrostatic interactions between membrane and protein. It is noteworthy to mention that, the electrostatic repulsion and attraction between the protein and membrane is based on ionic strength and solution pH. Several attempts were made to study the ionic strength and pH influence on the separation of single and mixture of proteins through inorganic membranes (Persson et al. 2003; Shah et al. 2007; Ke et al. 2009). The BSA adsorption rate on the Al_2O_3 membrane with varying solution pH was studied by Bowen and Hughes 1990. The maximum adsorption rate was observed at the isoelectric point (pI) of BSA (pI of BSA is 4.9). The BSA transmission was found to be more with the zirconia membrane at pH 7 (Millesime et al. 1995). The higher rejection of BSA was obtained at lower pH in the study carried out by Monash and Pugazhenthi (2001).

Possible scope for further research

The literatures on application of ceramic membrane in bio-molecule separations are very limited. The selectivity of the ceramic membrane depends mainly on a zeolite layer deposited on the surface of the support. This separation layer makes the ceramic membrane more suitable for the separation of bio-molecules. With these understandings, the present study focuses on the separation of bio-molecule, BSA protein using tubular configured FAU and MFI-type zeolite microfiltration membranes with a cross-flow mode of operation. Therefore, it is our intent to fabricate FAU and MFI type zeolite membrane via an in-situ hydrothermal synthesis technique on low cost porous tubular ceramic substrate and application in separation of BSA. In addition to that, this study also attempts to optimize the BSA separation process by employment of effective multivariate statistical technique viz., Response surface methodology (RSM) and stochastical optimization approaches using genetic algorithm (GA).

1.7 Objectives of the thesis

Based on the above state of the art, the following major objectives are identified and addressed in the thesis.

- Fabrication of ceramic membrane in tubular configuration using locally available low cost raw materials by extrusion method.
- Treatment of oily and dairy wastewater using prepared novel low cost tubular ceramic membrane.
- Preparation and characterization of Faujasite (FAU) and Mordenite Framework Inverted (MFI) type zeolite-ceramic composite membranes on low cost tubular ceramic support by hydrothermal technique.

- Performance evaluation of prepared FAU and MFI type zeolite-ceramic composite membranes in removal chromium and separation of bovine serum albumin (BSA) from their aqueous solutions.

1.8 Organization of the thesis

The Doctoral thesis is organized in the seven chapters. The brief summary of the chapters are presented in the following sections.

Chapter 1 elaborates introduction, literature review and objectives of the thesis.

Chapter 2 summarizes the preparation of novel ceramic membrane with tubular configuration using locally available inexpensive raw materials. The raw materials and the fabricated membrane are characterized by standard techniques such as particle size distribution (PSD), scanning electron microscopy (SEM), energy dispersive X-ray spectroscopy (EDX), X-ray diffraction (XRD), thermogravimetric (TG) and field emission scanning electron microscopy (FESEM) analysis. The sintered membrane is subjected to investigate the its porosity, water permeability, an average pore size and mechanical strength and corrosion resistance in acidic and basic conditions. Finally, the estimation of the manufacturing cost of the acquired membrane is presented in detail.

Chapter 3 analyzes the potential of the fabricated novel tubular membrane by application to microfiltration of oily wastewater and dairy wastewater. The treatment of synthetic oily wastewater emulsion and local dairy industry wastewater experiments are carried out at various combinations of applied pressures, feed concentrations and cross flow rates. In this chapter, diverse pore blocking models (complete, standard, intermediate pore blocking and cake filtration model) to predict the permeate flux declination, as described by Hermia are employed to analyse the fouling mechanism associated with the microfiltration processes.

Finally, the performance of the membrane is compared with that of the other membranes reported in the literature for oily and dairy wastewater treatment.

Chapter 4 presents the fabrication of FAU and MFI type zeolite membrane on the novel low cost tubular ceramic membrane support by hydrothermal treatment method. The synthesized zeolite powders (FAU & MFI) as well as membranes are characterized by various standard techniques such as X-ray diffraction (XRD), Fourier transform infrared spectroscopy (FTIR), Thermogravimetric analysis (TGA) and Differential thermal analysis (DTA), field emission scanning electron microscopy (FESEM), porosity, pore size and water permeability measurements.

Chapter 5 describes the potential of FAU and MFI type zeolite membranes supported on low cost tubular ceramic support for chromium removal from an aqueous solution. The various influencing process parameters, such as applied pressure, initial feed concentration and cross flow rate are investigated. Additionally, the potential of the membranes are compared with other membranes reported in the literature for chromium removal application.

Chapter 6 explicates the application of FAU and MFI type zeolite membranes for the separation of bovine serum albumin (BSA) protein from its solution and optimization of critical parameters of the microfiltration system. Three operating parameters such as, BSA concentration, pH and applied pressure are optimized for the better separation efficiency of the membranes using response surface methodology (RSM) followed by bi-objective genetic algorithm (GA). The predicted conditions are experimentally validated for FAU membrane and MFI membrane.

Chapter 7 summarizes the inferences drawn from this work and provided some suggestions towards future research.

Chapter 2

Elaboration and characterization of novel tubular ceramic membrane from locally available low cost raw materials by extrusion method

---

Elaboration and characterization of novel tubular ceramic membrane from locally available low cost raw materials by extrusion method

The main aim of this chapter is to fabricate a novel tubular configured ceramic membrane having better porosity, lower average pore size, strong mechanical strength and excellent corrosion resistant. As mentioned earlier, the cost of the ceramic membrane mainly depends on the starting raw materials, sintering temperature and the method of fabrication. Therefore a new low cost starting materials (clay mixtures), which are locally available in India is used for the fabrication of membrane by the extrusion technique (simple and cost effective) and sintered at comparatively low temperature (<1000 °C) than that of commercial membrane (>1200 °C) is the main theme of this Chapter. In addition, the fabricated tubular membrane would be an alternative for high cost commercial α-alumina, zirconia and titania microfiltration membranes as well as used as a support for the manufacturing of composite membranes for industrial applications.

2.1 Experimental

2.1.1 Raw materials

The choice of raw materials and their relative composition is very important to achieve defect free membranes. The structural and morphological properties of a membrane are largely dependent upon the raw materials used and hence selection of raw materials and their composition is very important. In this work, several locally available low cost raw materials were selected to fabricate a tubular shaped ceramic membrane. Contemplation on reducing the price of the membrane and to assess our natural resources, the local clay materials: kaolin, quartz, ball clay, pyrophyllite, feldspar and calcium carbonate are utilized as raw materials. These clay materials utilized for elaboration of the membrane was of mineral grade and obtained in the vicinity (Kanpur, India). The composition of clay materials used for the

fabrication of membrane along with its significance is given in Table 2.1. The composition reported in this work was obtained with a trial and error approach using various ratios of raw materials. The reported raw material compositions in Table 2.1 enabled the fabrication of defect free membrane with good permeation, pore size distribution and porosity characteristics.

Table 2.1: Summary of identified raw material compositions for tubular membrane fabrication

Raw Materials	Composition (wt.%)	Significance
Kaolin ($Al_2SiO_5.(OH)_4$)	15	Low plasticity and high refractory property
Quartz (SiO_2)	28	Increases mechanical and thermal strength
Calcium Carbonate ($CaCO_3$)	18	Pore forming agent as well as sintering aid
Ball clay ($3\ SiO_2.Al_2.O_3$)	18	Provides plasticity and strength to the green support
Phyrophyllite ($Al_2.\ (SiO_5)_2.\ (OH)_2$	15	To reduce crazing
Feldspar ($Na,\ Ca\ AlSi_3\ O_8$)	6	Acts as a flux to form glassy phase at low temperature

2.1.2 Elaboration of tubular ceramic membrane

An extrusion process was adopted to form a tubular shaped membrane. The table top mechanized extruder (M/s. VB Ceramic Consultants, Chennai, India) made of stainless steel was used for obtaining tubular ceramic membrane. It essentially consists of a feed chamber, extruder screw shafts, cone and die assemblies. The procedure for the fabrication of membrane is diagrammatically presented in Figure.2.1. Tubular ceramic membrane was fabricated with length, inner and outer diameters of 100, 5.5, and 11.5 mm, respectively. Clay powders were

accurately weighed according to the composition and mixed with Millipore water (Elix-3 Milli-Q, USA) to make the paste for extrusion without the addition of any organic chemicals for plasticity. The obtained paste was fed into the extrusion cylinder. Then, evacuation piston forced the paste through a die in a tabletop extruder to form a tubular shape membrane. The tubular membrane was extruded in the horizontal direction with the forwarding velocity of ~0.7 cm/s at room temperature. When the tube reached the length of around 120 mm, the process extruder stopped and the tube was cut with sharp blades. Then, the obtained tubular membrane was subjected to natural drying at room temperature for 12 h. After which, the membrane was dried at 100 °C for 12 h and 200 °C for 12 h in a hot air oven. Subsequently, the membrane was taken to the sintering process with a heating rate of 2 °C/min and sintered at 950 °C for 6 h in a box furnace.

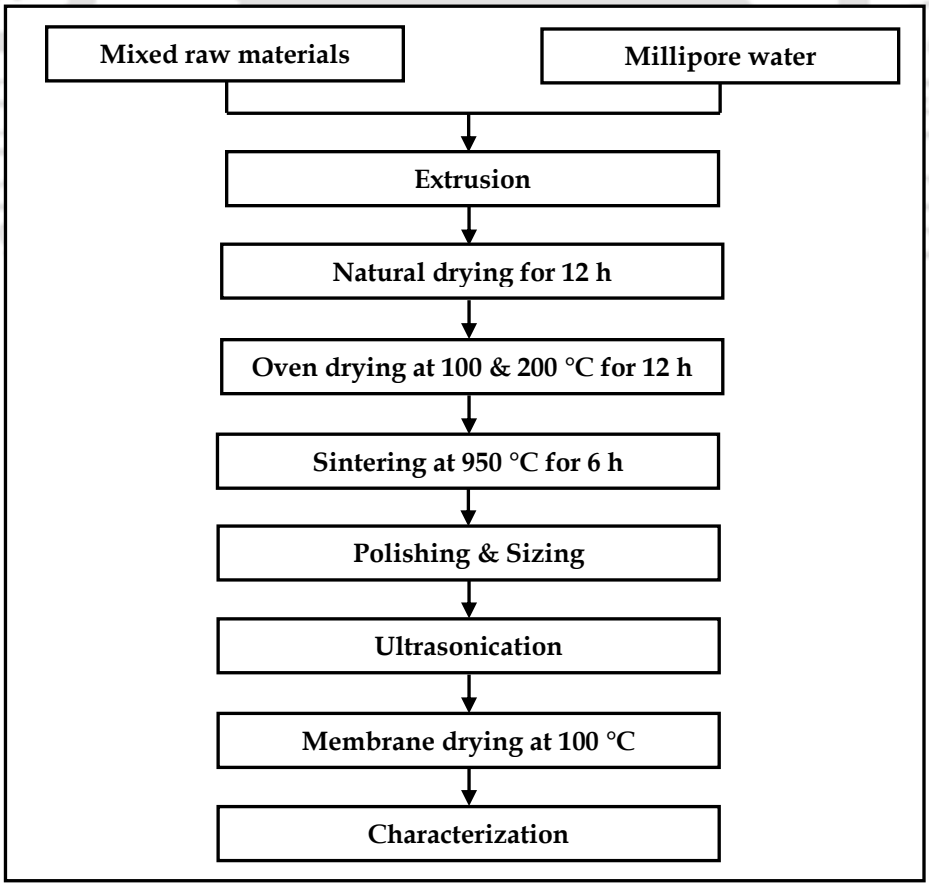

Figure 2.1: Schematic representation of tubular ceramic membrane fabrication

These restrained thermal treatment steps were followed to avoid the formation of micro cracks and bends in the membrane. The obtained rigid and porous sintered tubular membrane was finally polished and sized using silicon carbide abrasive paper (No. C - 220) to obtain a uniform smooth surface. Then the ceramic membrane was cleaned with Millipore water in an ultrasonic bath for 30 min to remove the loose particles created during polishing and sizing. Finally, the elaborated membrane was dried at 100 °C for further characterization. The table top mechanized extruder used for the fabrication of the tubular membrane and fabricated tubular membrane at different views are presented in Figure 2.2.

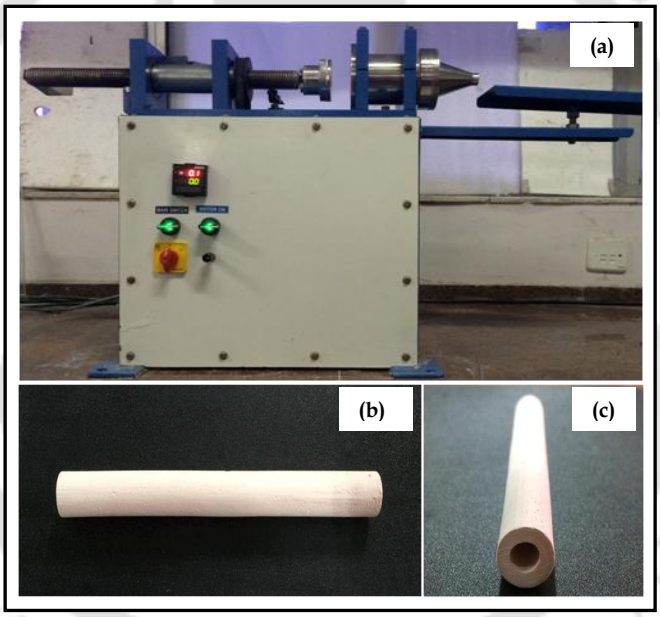

Figure 2.2: (a) Table top mechanized extruder and (b & c) fabricated membrane at different views.

2.1.3 Characterization techniques

The particle size distribution (PSD) of raw materials were analyzed in Malvern Mastersizer 2000 (APA5005® model, hydro MU) instrument in wet dispersion mode by circulating the heterogeneous feed at constant flow rate (pump speed = 2700 rpm) with an ultrasound to avoid the agglomeration of clay powders during analysis. Scanning electron microscopy (SEM)

investigations were conducted in a varying pressure digital scanning electron microscopy (LEO1430VP®) combined with an energy dispersive X-ray spectroscope. The X-ray diffraction (XRD) profiles recorded with Cu Kα (λ=1.5406 Å) radiation working at 40 kV and 40 mA in Bruker AXS machine in 2θ value ranging between 5 and 75° with a scan rate of 0.05°/s. Thermogravimetric (TG) and derivative thermogravimetric (DTG) analysis were performed using Mettler Toledo (TGA/SDTA 851®) thermogravimetric instrument (NETZSCH TG 209F1 Libra) to characterize the thermal decomposition activities of the individual and mixed clay powders in air atmosphere with a heating rate of 10 °C/min from 25 to 970 °C in a 150μL platinum container. Field emission scanning electron microscope (FESEM, JEOL JSM-5600LV) was used to analyze the presence of possible defects on the surfaces. A small size of the membrane sample was fixed on top of the stub and layered with gold using an auto fine coating instrument (JEOL JFC-1300) preceding to morphology assessment. The porosity of the membrane was measured by utilizing water as a soaking agent. The mechanical strength was measured using a standard three-point bending test by Computerized Universal Tester (DUTT-101, India). Four tubular ceramic membranes (length of 100 mm) were tested with the bending strength instrument. The instrument support span adjusted to 80 mm, before putting the sample on the support beam. Then the load was applied at a constant load rate of 10 Ns^{-1} until failure in the breaking force value was observed. The mechanical strength of the membrane was calculated from arithmetic mean of all values obtained. The corrosion resistance of the membrane was evaluated by means of loss of mass after treating in aggressive environments. The acid and alkali solutions were prepared with extreme conditions (HCl solution with pH 1 and NaOH solution with pH 14) and soaked the membrane into the solutions for one week. The corrosion resistance of the recovered membrane was evaluated by weight decrement of the membrane.

2.2 Results and discussion

2.2.1 Characterization of raw materials

2.2.1.1 PSD analysis

Sintering temperature and pore size of the ceramic membrane can be regulated by the particle size of raw materials used for membrane fabrication. The formation of pore on the ceramic membrane is a function of the initial particle size of the clay powders (Fukushima et al. 2009). The finer particles require reasonably lower temperature for sintering; however, it leads to the resistance of a larger transport due to extremely small effectual pore size. Conversely, courser materials require relatively high sintering temperature, and it leads to the resistance of a small transport due to macropores, but the mechanical strength is reduced (Wang et al. 2007). The particle size distributions of the individual clay powders are presented in Figure 2.3. All the analysis is done two times for the laser obscuration limit greater than 10% and the average value of the results is presented in the Table 2.2. The volume or mass moment mean, D[4,3] and surface area moment mean, D[3,2] are calculated using the following formula:

$$D[4,3] = \frac{\sum d^4}{\sum d^3} \tag{2.1}$$

$$D[3,2] = \frac{\sum d^3}{\sum d^2} \tag{2.2}$$

where, d is the particle diameter (μm).

The advantage of this method of calculation (eq. 1 and 2) is that formulae do not contain the number of particles and therefore the calculations of the means and distributions do not require knowledge of the number of particles involved. D[4,3] is usually reported in a prominent manner. The volume weighed mean formula is utilized to evaluate the diameter of the clay particles and their sizes vary between 5 and 10 μm. This range of particle size of clays is

favorable to manufacture the ceramic membranes. Similar particle size distributions of clays were applied for the fabrication of macroporous membrane (Almandoz et al. 2004). The surface area of the raw material in the increasing order is as follows: feldspar < pyrophyllite < ballclay < quartz < calcium carbonate < kaolin. This is also considered while choosing the composition of the raw materials for membrane preparation. This provides a knowledge regarding the composition of clays to be utilized for the fabrication of the membrane.

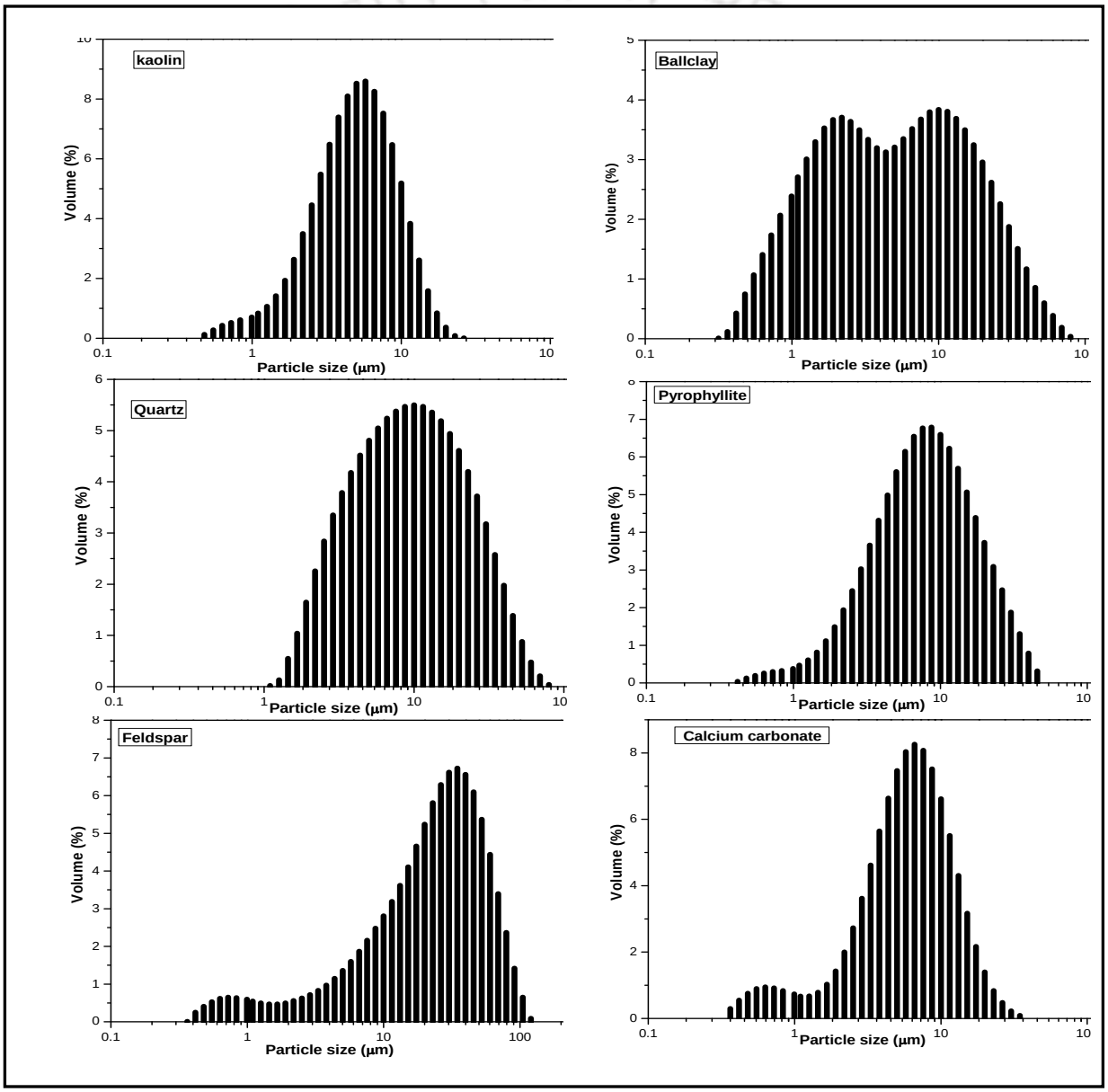

Figure 2.3: Particle size distribution of the raw materials used for preparation of membrane

Table 2.2: Particle size distribution of various clay powders used in the preparation of membrane

Clay Powder	Particle size			Span	Specific surface area (m^2/g)	D[3,2] (μm)	D[4,3] (μm)
	D(V,0.1) (μm)	D(V,0.5) (μm)	D(V,0.9) (μm)				
Kaolin	1.852	04.656	9.814	1.710	1.750	3.419	05.354
Feldspar	3.855	22.925	56.284	2.287	0.315	6.898	27.082
Quartz	2.680	08.650	27.107	2.824	0.994	6.034	12.242
$CaCO_3$	2.083	06.460	14.299	1.891	1.610	3.735	07.557
Ballclay	0.954	05.039	24.749	4.722	0.923	2.499	09.659
Pyrophyllite	2.805	08.428	22.786	2.371	0.379	5.581	10.926
Mixture	1.840	07.326	24.450	3.125	0.516	4.094	10.639

D[3,2] = surface area moment mean or the Sauter Mean Diameter (SMD)
D[4,3] = volume or mass moment mean or the De Broucker mean
D[v,0.5] = volume median diameter sometimes shown as D_{50} or $D_{0.5}$

Span is also another valuable consideration in calculating the applicability of the clay mixture that can be evaluated using the following expression:

$$\text{Span} = \frac{D_{90} - D_{10}}{D_{50}} \tag{2.3}$$

A larger span value could be owing to one or more of the following: (a) very high D_{90} and very small D_{10} (b) moderate D_{90} and D_{10}, but very small D_{50}. A higher span value with a very high D_{90} is unfavorable for the fabrication of ceramic membranes due to a higher percentage of coarser particles (Wang et al. 2007). Span values attained from the study are calculated to be in the similar range (1.8 to 3) for all clays, which specifies an equivalent width of the size distributions. This offers a well mixing and homogeneous distribution between the particles that could result in a good microfiltration membrane.

2.2.1.2 SEM and EDX analysis

Scanning electron microscope images of the clay powders along with the EDX are presented in Figure 2.4. The EDX analysis (qualitative analysis) of kaolin, ball clay and pyrophyllite indicates that the clay powders contain oxides of aluminium and silicon. However, no other peaks are obtained even using spot EDS at higher magnification, suggesting that it is free from other impurities or has only a trace amount of impurities (<5 wt.%) that cannot be detected by SEM. Quartz shows only the oxides of silicon that indicates its purity. The elemental peak of Ca obtained for feldspar signifies that the feldspar is of plagioclase type, which is triclinic in nature. The commercially purchased calcium carbonate shows only the peaks of Ca and O, which confirms its purity. The Si/Al ratio obtained with the EDX analysis of different clays is apparently closer to the theoretical value of those clays (Castellano et al. 2010).

2.2.1.3 XRD analysis

Similarly, all the clay powders were analyzed with XRD and the obtained patterns are well matching with the standard Joint Committee on Powder Diffraction Standards (JCPDS) files. The XRD patterns of the clay powders are presented in Figure 2.5. The XRD peaks of the kaolin match well with the reflections of standard JCPDS card number 14-164 and the other additional reflections match with the JCPDS card number 10-446. This indicates that kaolin also contains dickite, which is the same composition as kaolinite with different crystal structure (Castellano et al. 2010). The main crystalline phases observed in the ball clay corresponds to kaolin (2θ =12.25 and 24.85°) and quartz. The 2θ reflections (2θ =20.85 and 26.65°) of quartz match well with the JCPDS card number 46-1045, which corresponds to the pure quartz phase (González et al. 2007). Similarly, the 2θ reflections of pyrophyllite and feldspar are in good agreement with the standard JCPDS card number 12-203 and 09-456, respectively (Sugiyama et al. 1993). The cleaner pattern obtained for quartz, calcium carbonate and feldspar indicated the occurrence of their pure phases.

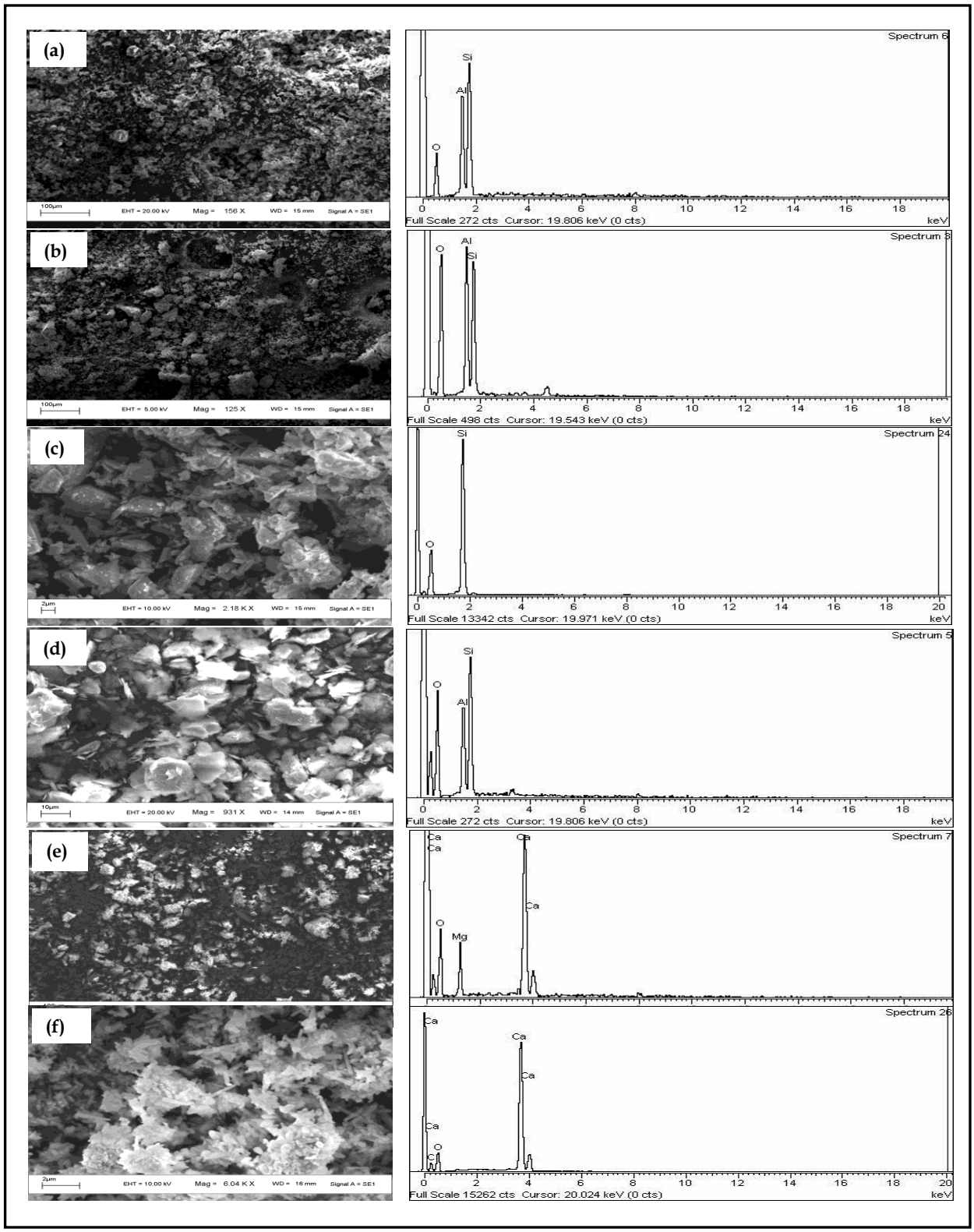

Figure 2.4: (a-f) SEM and EDX analysis of the raw materials used in membrane fabrication

(a) Kaolin, (b) Ball clay, (c) Quartz, (d) Pyrophyllite, (e) Feldspar and (f) $CaCO_3$

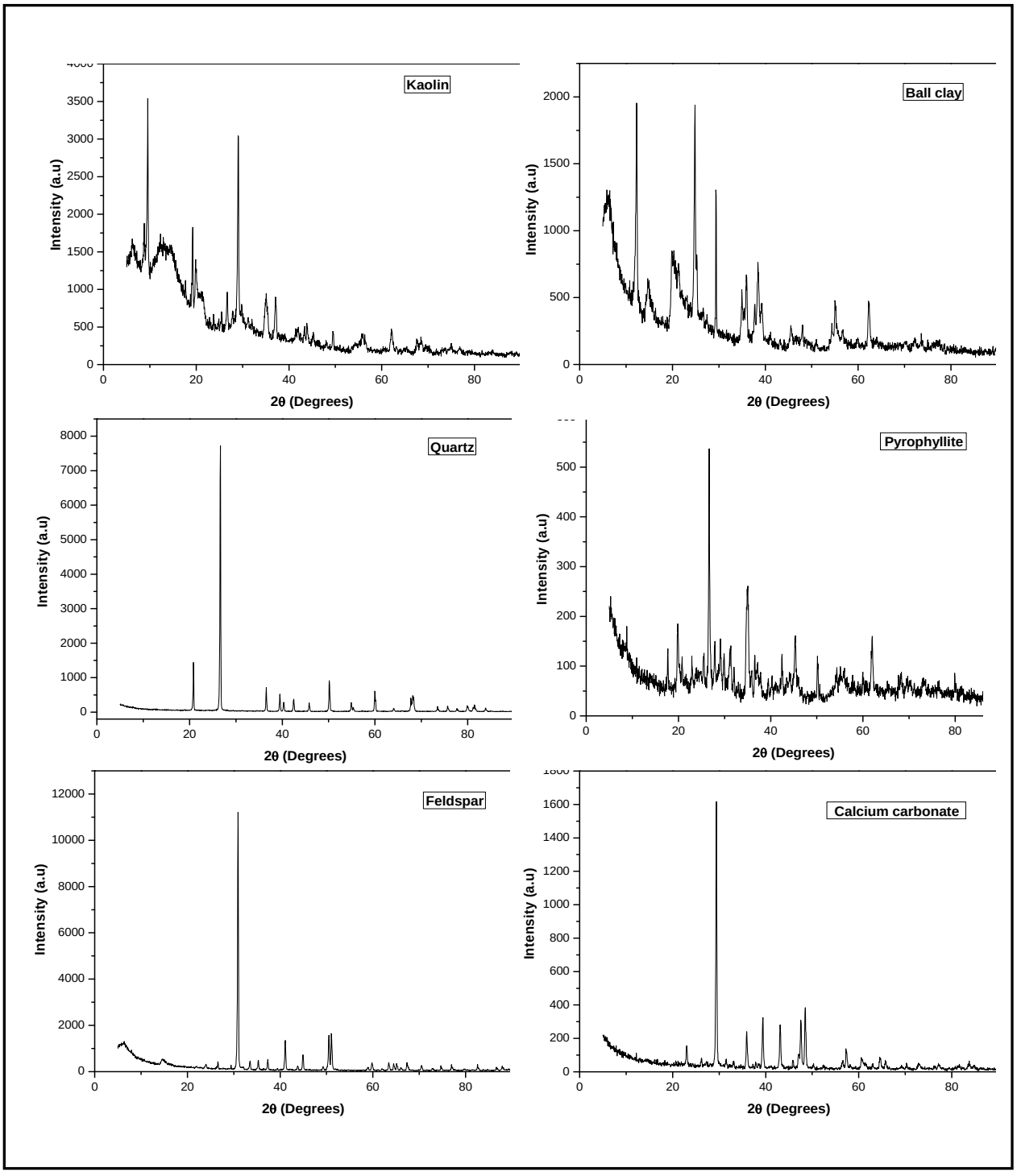

Figure 2.5: XRD patterns of the raw materials used for the preparation of membrane.

2.2.1.4 TGA and DTG analysis

Sintering temperature is an essential factor to control the mechanical strength, pore size and porosity of the ceramic membrane. TGA of clay powders was done to discover the minimum sintering temperature required for the fabrication of stable membrane and the obtained results are plotted in Figure 2.6. The weight decrement at temperature < 150 °C is mainly owing to the elimination of physisorbed water and at higher temperature (500 to 800 °C), the decrement is due to the dehyroxylation of the surface hydroxyl group or exclusion of structural water. Thermal decomposition (550 to 750 °C) of $CaCO_3$ results in major weight loss and forms CaO and CO_2. The porosity of the membrane primarily corresponds to the pathway occurred through the evolved CO_2 gas. Due to the increased release of OH groups attached to Al and Si and subsequent conversion of kaolin to metakaolin, ball clay shows a relatively higher weight loss (14.11%) than that of kaolin (5.04%) and pyrophyllite (9.70%).

The thermal investigations of mixed raw materials are performed to determine the sintering temperature to achieve a good solid membrane. TGA and DTG curves of mixed raw materials are presented in Figure 2.7. It is identified that above 850 °C, a negligible weight loss is observed in the TGA curve. It recommends that the membrane needs to be sintered at above 850 °C to obtain a good mechanical and thermal strength. DTG analysis shows an endothermic phenomenon from ambient to below 100 °C is associated to the physisorbed water and another endothermic phenomenon towards 480 °C is due to the dehydroxylation. A specific endothermic transformation at 650 °C - 750 °C is due to the loss of structural hydroxyl groups of the kaolinite.

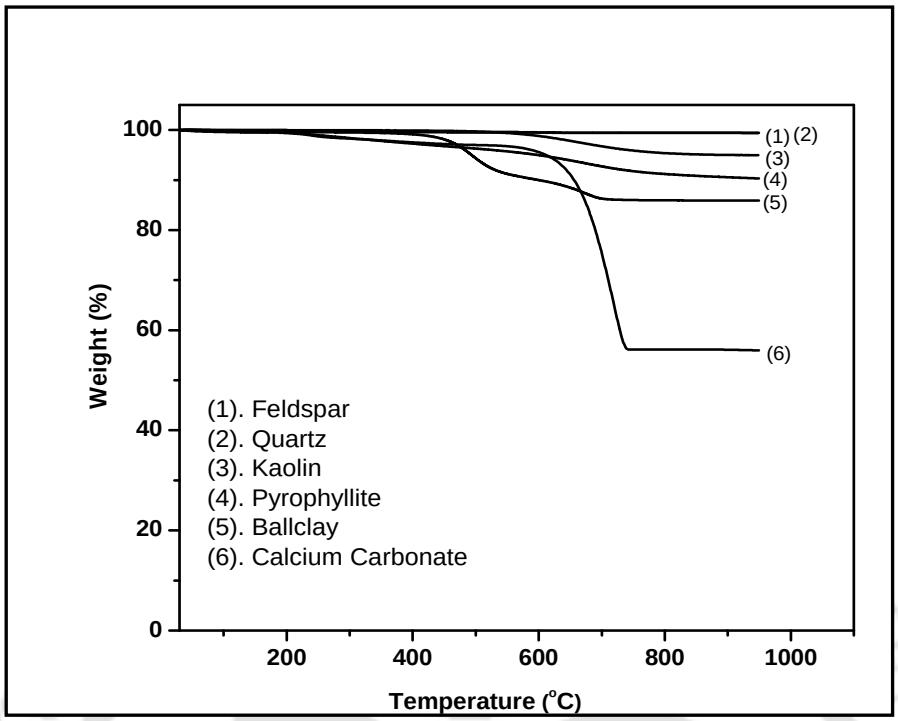

Figure 2.6: TGA profiles of the raw materials used for the preparation of membrane.

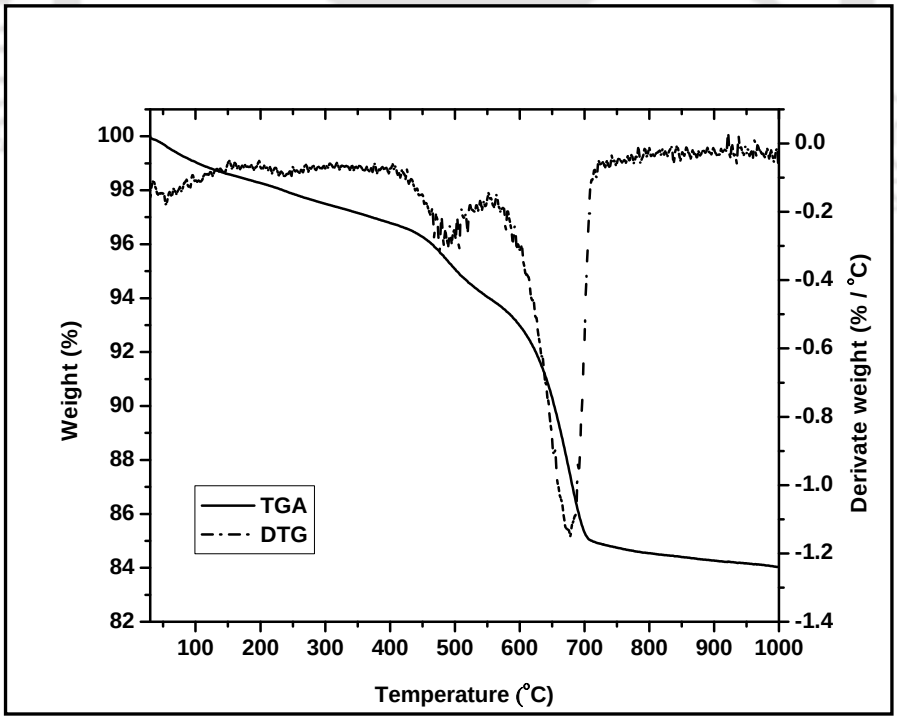

Figure 2.7: TGA and DTG curves of mixed raw materials

2.2.2 Characterization of tubular ceramic membrane

2.2.2.1 XRD analysis

The phase transformation activities of the membrane before and after sintering were analyzed through XRD patterns as depicted in Figure 2.8. The sintering process generates various phase transformations and reactions, which initiates the creation of new phases. This gives the absence as well as transfer of the position of the XRD peaks. The perfect crystalline phase is observed for the sintered membrane and the mainly identified phases for the membrane (after sintering) are mullite ($3Al_2O_3.2SiO_2$), quartz (SiO_2), Wollastonite ($CaSiO_3$) and anorthite ($CaO.Al_2O_3.2SiO_2$). Kaolin to mullite through metakaolinite phase transformation is identified in the temperature range of 800 °C to 1000 °C (Monash and Pugazhenthi (2001). This takes place due to the degradation of kaolin structure.

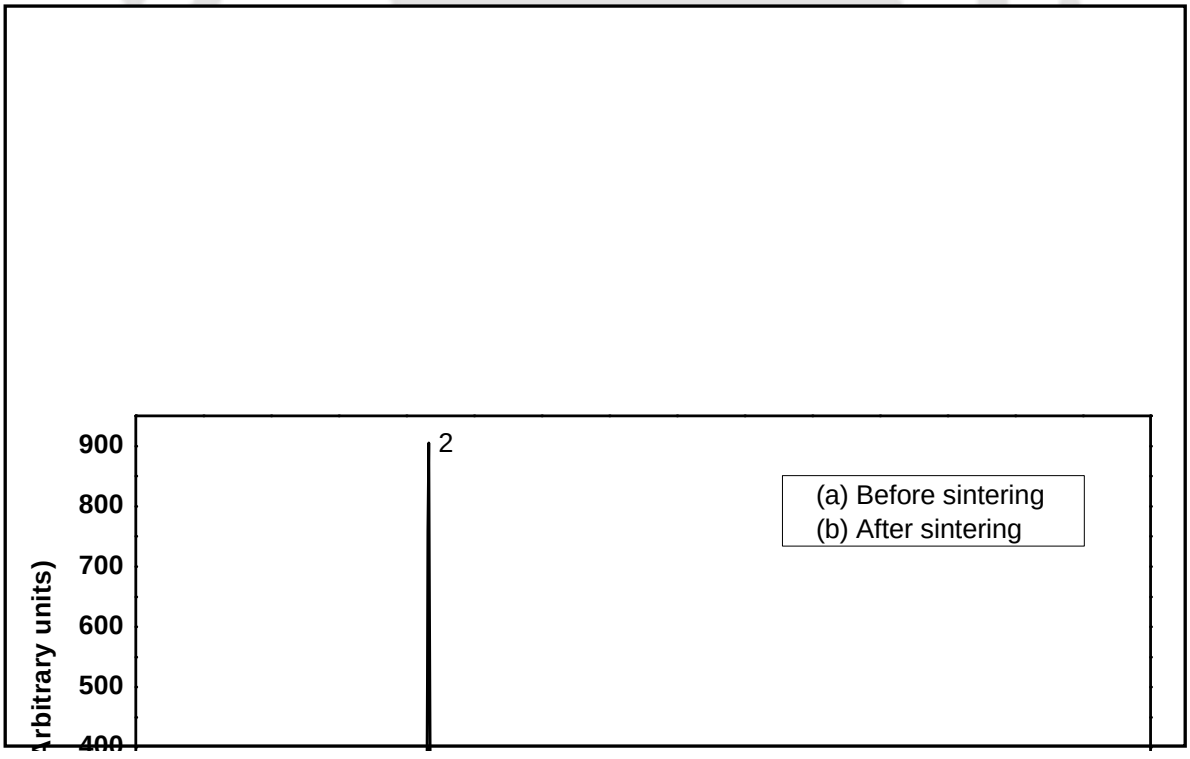

Figure 2.8: XRD patterns of the membrane (a) before sintering and (b) after sintering

(1- Kaolin, 2- Quartz, 3-Anorthite, 4- Calcium oxide, 5- Mullite, 6-Wollastonite)

2.2.2.2 Morphological analysis

The following possessions are most important for the development of a good quality membrane: excellent surface, including nonappearance of any big pores/defects/cracks, porosity, mechanical strength and corrosion resistance.

By following the optimized preparation procedure, the perfect tubular shaped ceramic membrane was successfully prepared. The tube obtained under this condition was straight with a constant thickness and diameter (see Figure 2.9). Photograph of the sintered membrane shown in Figure 2.9(a) confirms that the sintering process was successful. Figure 2.9(b) displays the universal serial bus (USB) microscope cross-sectional image of the membrane with their dimensions. It gives satisfactory cross-sectional circularity.

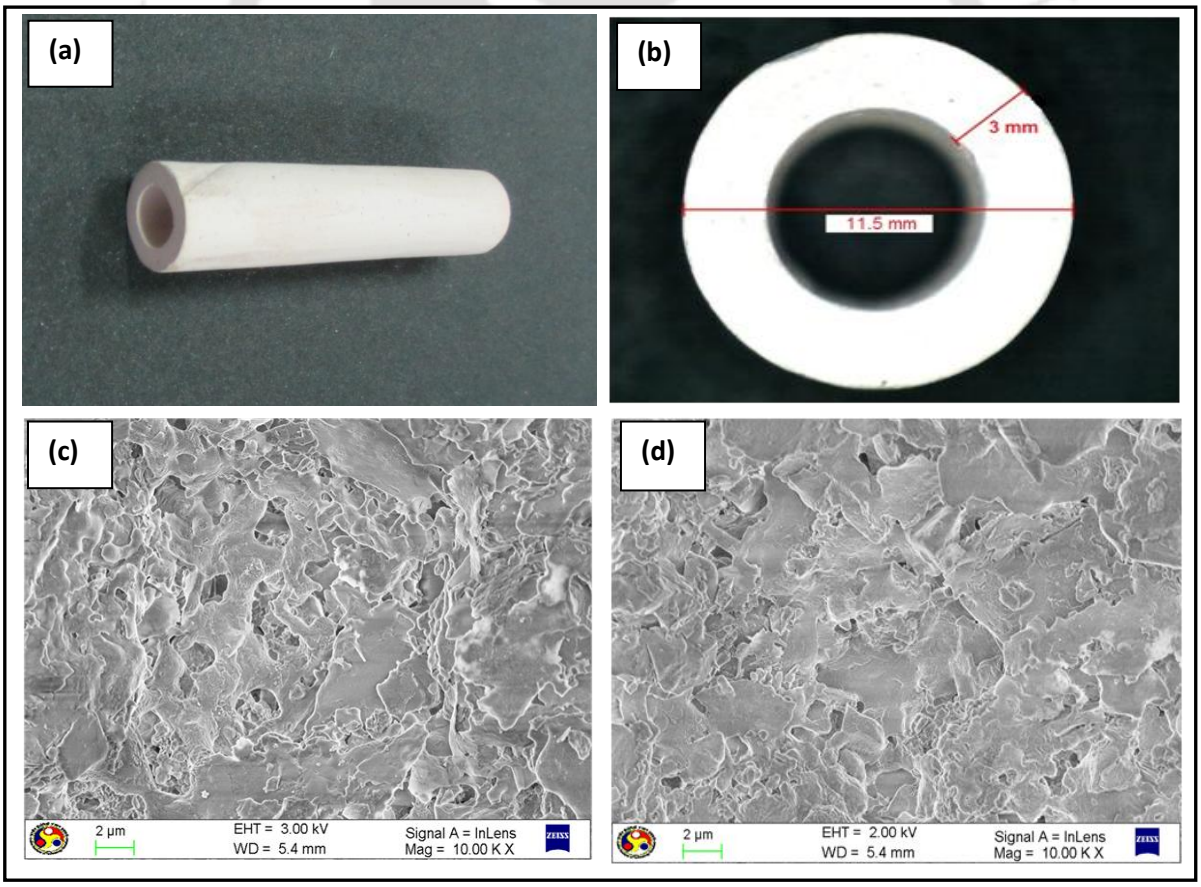

Figure 2.9: Photograph of the sintered membrane (a) Microscope image of cross sectional view of the membrane, (b) FESEM images of inner (c) and outer surfaces of the membrane (d).

In addition, FESEM images were used to analyze both inner and outer surface morphology of the fabricated membrane (see Figure 2.9(c, d)). These images provide information on consistency of prepared membrane surfaces. One can see a homogeneous surface with no cracks on the membrane surfaces. Also, the membrane is highly smooth and a flawless inner and outer surfaces. The overall surface morphological analysis recommends that the nonappearance of cracks/defects/ big pores is a key condition leading to a good quality membrane.

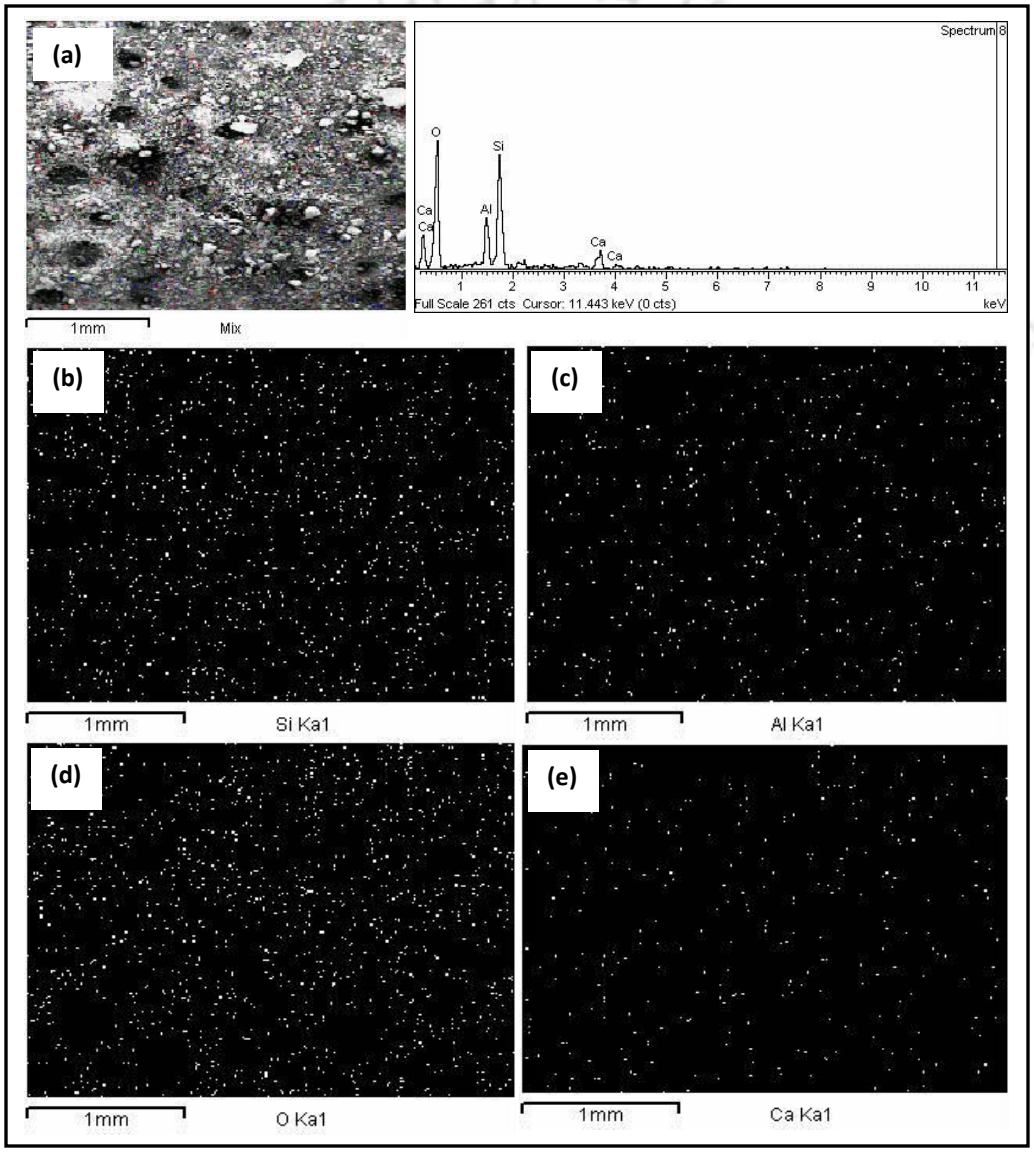

Figure 2.10: SEM mapping analysis of the sintered membrane. (a) Zone at which EDX and mapping analysis done, (b), (c), (d) and (e) represents the mapping results of Si, Al, O and Ca, respectively.

Mapping analysis of the SEM as shown in Figure 2.10 validates the homogeneous distribution of silica-aluminates throughout the membrane. The elements identified by the EDX are Al and Si, which are in the form of oxides (Al_2O_3 and SiO_2). Ca is in the form of CaO as well as wollastonite and anorthite.

2.2.2.3 Porosity, mechanical strength and corrosion resistance

The porosity of the membrane was measured using below expression (Kumar et al. 2015):

$$\text{Porosity } (\%) = \frac{W_{wet} - W_{dry}}{\rho_{water} \times V_{membrane}} \times 100 \qquad (2.4)$$

Where, W_{wet} is the wet weight of the membrane (placed in distilled water for overnight), W_{dry} is the dry weight of the membrane (dried at 120 °C for 3 h), $V_{membrane}$ is the total volume of the membrane and ρ_{water} is the density of the water. The average porosity of the tubular membrane is calculated to be 53%.

The standard three point bending test was performed to examine the mechanical strength of the membrane using the following expression (David et al. 2014):

$$\sigma = \frac{8FLd_{out}}{\pi(d_{out}^4 - d_{in}^4)} \qquad (2.5)$$

where, F is the applied force (N), L is the distance between the sample support points (mm), d_{in} and d_{out} are the inner and outer diameter of the tube (mm), respectively and σ is the mechanical strength of the membrane (MPa). The average mechanical stability of the membrane is calculated to be 12 MPa. This value is comparable and even better than the pyrophyllite membrane (5.5 MPa) prepared by Talidi et al. (2011).

The corrosion resistance test was performed with respect to weight decrement of the membrane after keeping in harsh environments (acid and alkali). The weight decrement of the membrane is calculated to be 9% in acidic condition and 0% in alkali condition. In acid and alkali conditions, the membrane displays an excellent result in resisting corrosion. The obtained results are more commensurable in comparison with the cordierite membrane fabricated by Dong et al (2007).

2.2.2.4 Experimental setup and measurement of water flux

In this work, the cross flow filtration system was employed for water flux measurement. Figure 2.11 illustrates a schematic along with the real depiction of overall experimental scheme. The system consisted of a series of feed tank, metering pump for circulation of the feed solution, membrane module with tubular configuration, pressure indicator and flow meter to measure the cross flow rate along with flow control valves (3 nos). The tubular ceramic membrane was incorporated into the module for tangential cross flow setup. The membrane module comprises of one hollow and two bolt parts that are made of stainless steel. The membrane was fixed between the two bolt parts using O-ring washers, and two end ducts are joined with two hosepipes. The pictorial representation of prepared tubular membrane before fixing and after fixing into the module is shown in the Figure 2.12. The feed was pumped to the module from the feed tank and retentate employed with the recirculation arrangement. The permeate flow through the membrane was determined using an electronic weighing balance at open atmospheric condition. The operating pressure was adjusted manually using the flow control valves each located at by-pass (V_1), inlet (V_2) and retentate (V_3) flow paths (Figure 2.11). Cross flow rate was adjusted with a flow control valve (V_3) at the retentate side flow path.

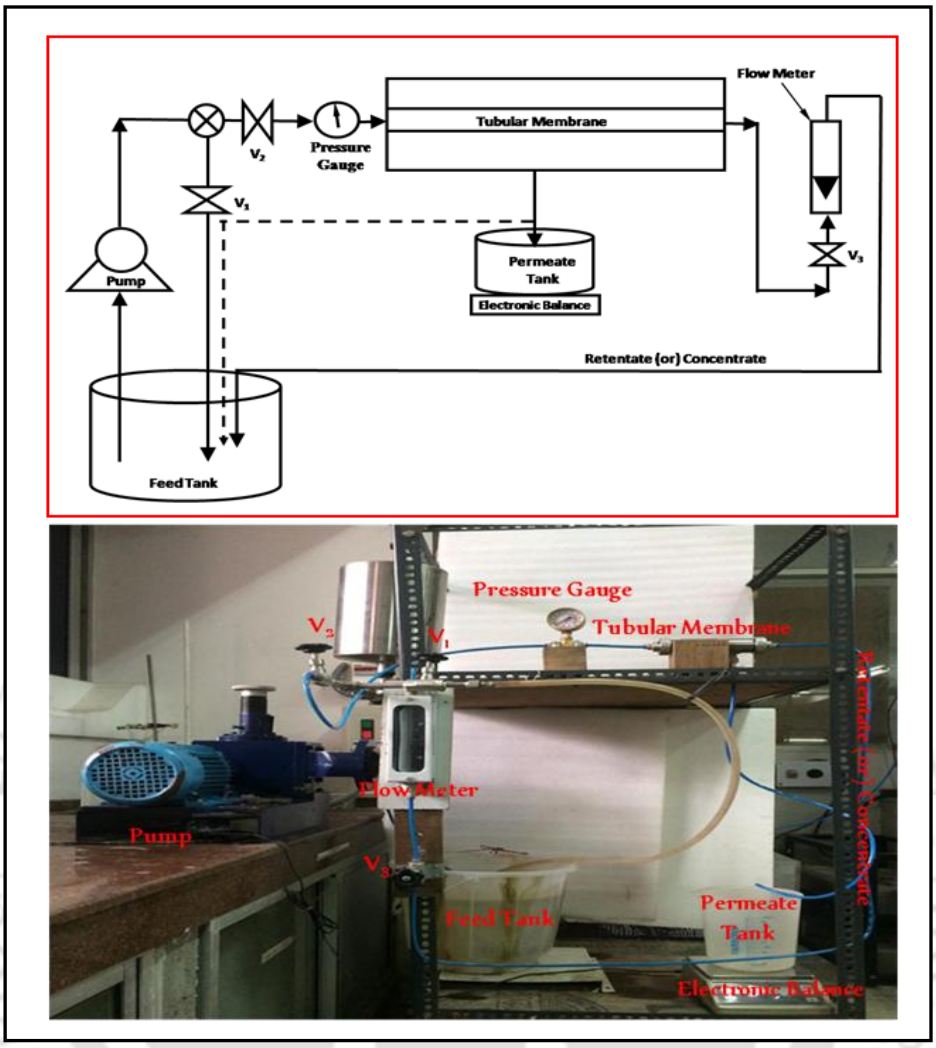

Figure 2.11: Schematic and optical representation of experimental system (V_1-by-pass valve, V_2- inlet valve, V_3- retentate valve)

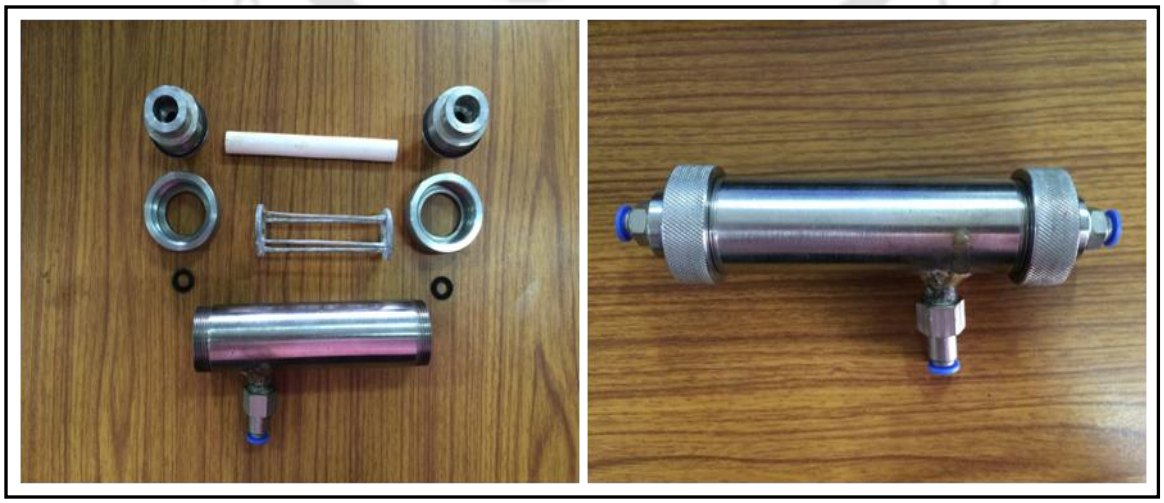

Figure 2.12: Tubular membrane before fixing and after fixing into module

In order to determine the water flux, the collection of permeate was measured at different applied pressures (69 - 345 kPa) as a function of time at a fixed cross flow rate using in-house made setup (see figure 2.11). The different pressures were regulated by a by-pass valve on the system starting from the lowest to the highest pressure.

The pure water flux (J_W) was measured by utilizing below expression:

$$J_W = \frac{Q}{At} \tag{2.6}$$

Where, Q is the permeated water in volume (m^3); A is the effective membrane area (m^2) and t is the measured time (s).

Figure 2.13(a) illustrates the water flux of the membrane as a function of time for different applied pressures. The steady flux is attained for the entire measured time. The variations of applied pressure on water flux are also presented in Figure 2.13(b). It can be noticed that the water flux increases linearly with an increase of applied pressures (69 - 345 kPa). This stipulates that the variation in pressure is the barely driving force for permeation. For transportation operation exclusively by convection, the flow rate is proportionate to the pressure, and is in accordance with Darcy's law.

The water permeability (L_h) of the membrane was determined by the water flux at different applied pressures. It was evaluated from the slope of the pure water flux (J_W) versus applied pressure across the membrane (ΔP) (see Figure 2.13(b)) using the equation.

$$J_W = L_h \Delta P \tag{2.7}$$

The water permeability (L_h) of the membrane is found to be 5.93×10^{-7} m^3/m^2s kPa. Hagen-Poiseuille equation was employed to estimate the average pore size of the membrane by assuming pores are cylindrical in shape (Almandoz et al. 2004; Bowen et al. 1997; Basumatary et al. 2015).

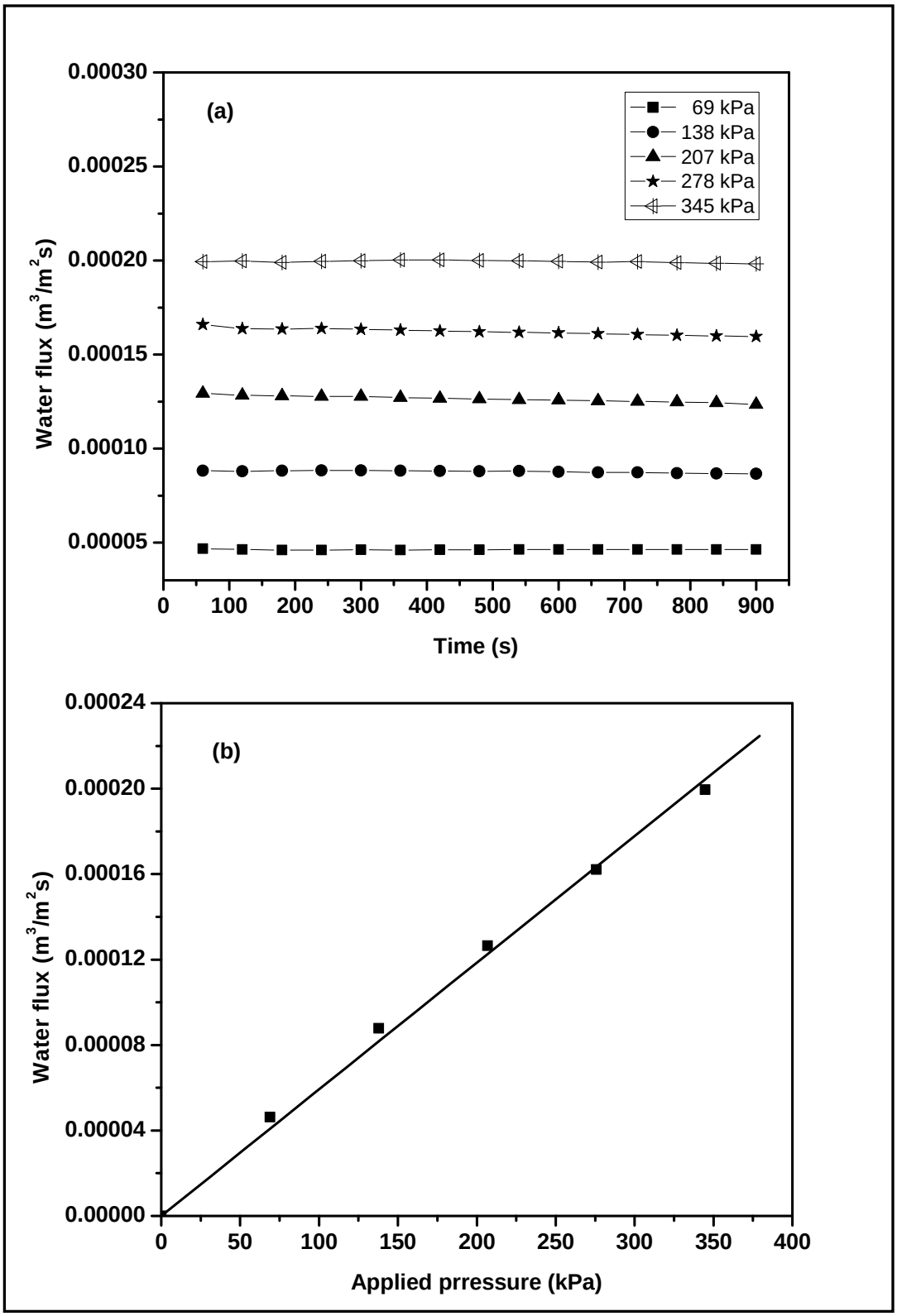

Figure 2.13: (a) Water flux as a function of time for five applied pressures and (b) water flux as a function of applied pressure

$$J_w = \frac{\varepsilon r^2 \Delta P}{8\mu\tau l} \quad (2.8)$$

where, ε is the porosity of the membrane (0.53), r is the pore radius of the membrane (m), ΔP is the applied pressures across the membrane (0 - 345 kPa), l is the pore length (0.003 m) which is generally taken as thickness of the membrane, τ is the tortuosity factor (generally used as 1), and μ is the viscosity of water (0.00089 Pa.s).

By combining equations 2.7 and 2.8, the corresponding pore radius of the membrane can be evaluated from

$$r = \left[\frac{L_h 8\mu\tau l}{\varepsilon}\right]^{1/2} \quad (2.9)$$

The average pore size of the membrane is calculated to be 0.309 µm (0.309×10^{-6} m). It is worth to mention that, this membrane can be directly utilized for making of ultrafiltration membranes with exclusion of intermediate layers.

Table 2.3 summarizes the overall properties (characterization results) of the prepared tubular ceramic membrane. It can be concluded that the prepared membrane could be applied for industrial utilization due to the excellent membrane characteristics such as quality surface, pore size, porosity, mechanical strength, corrosion resistance and water permeability.

2.2.3 Estimation of manufacturing cost of the membrane

A detailed analysis on manufacturing cost of the membrane is calculated and presented in the Table 2.4. The manufacturing cost is estimated in the preliminary economic evaluation at research level (Winter 1969). The manufacturing cost is the sum of all the direct costs and indirect costs of the actual manufacturing cost of the product. The direct manufacturing cost of the membrane includes the costs of raw materials, labor, electricity, maintenance and

laboratory. The raw material cost is estimated by consumption of raw materials to prepare the membrane. Labor cost is calculated by the use of a correlation of labor in a man-hour per day. The maintenance cost is estimated as 1% of the capital cost and laboratory cost is estimated as 20% of the labor cost (Winter 1969). The indirect manufacturing cost (capital cost), counting with the depreciation cost is calculated by straight line method. The manufacturing cost of the prepared tubular ceramic membrane is estimated to be 0.5 $/membrane (or 69 $/$m^2$). In comparison, α-alumina ceramic symmetric membranes cost approximately \$500/m^2 and symmetric stainless steel membrane costs approximately \$3000/m^2 (Vasanth et al. 2012). Therefore, it can be concluded from the cost estimation that the prepared membrane is very inexpensive as compared to alumina membranes, based on the sintering temperature and raw materials utilized in this study (Mavrov et al. 1998).

Table 2.3: Properties of the tubular ceramic membrane

Properties	**Membrane**
Dimensions:	
Outer diameter (mm)	11.5
Channel diameter (mm)	5.5
Thickness (mm)	3
Length (mm)	100
Unit surface (m^2)	1.72×10^{-3}
Average pore size (μm)	0.309
Porosity (%)	53
Water permeability (m^3/m^2s kPa)	5.93×10^{-7}
Mechanical strength (MPa)	12
Chemical stability:	
Acid - weight loss (%)	9
Base - weight loss (%)	0

Table 2.4: Estimation of manufacturing cost of the membrane

Items	Calculation basis for making hundred membranes				US$
Direct manufacturing costs:					
Raw materials	Raw Materials	Unit price (US$/kg)	Materials utilized (g)	Cost (US$)	
	Kaolin	0.18	142.8	0.03	
	Quartz	0.30	262.8	0.08	
	$CaCO_3$	5.40	169.4	0.92	
	Ball clay	0.09	173.7	0.02	
	Phyrophyllite	0.15	145.6	0.02	
	Feldspar	0.12	055.3	0.01	
				Total cost for raw materials:	1.08
Labor (including supervisory)	Labor cost = cost × total hours = 2.81 × 8				22.48
Electricity	*Furnace:* 12.25 h × 4 kW = 49 kW; 54.83 kW × US$ 0.09 = 4.93 *Hot air oven:* 30 h × 3 kW = 90 kW 90 × US$ 0.09 = 8.10 *Ultrasonicator:* 0.5 h × 2 kW = 1 kW 1 × US$ 0.09 = 0.09 *Extruder:* 1 kW/HP × 0.5 HP × 1.40 h 0.7 kW × US$ 0.09 = 0.06				
				Total electricity cost:	13.18
Maintenance	Maintenance cost = (Capital cost × 1%)/day *Extruder* = *1500* *Hot air oven* = *600* *Furnace* = *2250* *Ultrasonicator* = *375* Capital cost = 4725				
				Total maintenance cost:	0.13
Laboratory	Laboratory cost = 20% of labor cost				
				Laboratory cost:	4.50
Indirect manufacturing costs:					
Depreciation	Calculated by straight line method, $d = \frac{V-Vs}{n}$; where, d - annual depreciation cost, V - original cost, Vs - Salvage cost, n - service life.				0.50
Total manufacturing costs	Direct manufacturing costs + Indirect manufacturing costs				41.87
	Estimated manufacturing cost for one membrane				0.4187
	Estimated manufacturing cost for one membrane (Round off value):				***US$ 0.5***

2.3. Summary

A novel low cost tubular ceramic membrane has been effectively fabricated using inexpensive clay mixtures by the extrusion technique. The raw materials and membrane were characterized by PSD, SEM, EDX, XRD, TG and FESEM analysis. Initial analysis on the clays for the particle size distribution suggests that the particle diameter varies between 5 and 10 μm, which is suitable for macroporous ceramic membranes. The XRD and SEM analysis of the clays confirms that the clays are matching with the corresponding JCPDS files and mostly containing silica and alumina as well as trace amounts of other exchange ions, for example Ca. Thermal and XRD analysis infer various reactions and phase transformations undergone during sintering. The prepared membrane offers the better porosity of 53%, water permeability of 5.93×10^{-7} m^3/m^2s kPa, lower average pore size of 0.309 μm and strong mechanical strength of 12 MPa with excellent corrosion resistance in acidic and basic conditions. Finally, the manufacturing cost of the membrane estimated as 0.5 $/membrane (or 69 $/$m^2$). In addition, despite the use of simple fabrication method, lower sintering temperature and inexpensive raw materials, the excellent properties of the membrane substantiates that it could be effectively used as an alternative for high cost commercial α-alumina, zirconia and titania microfiltration membranes as well as the development of composite membranes for industrial applications.

Chapter 3

Treatment of oily and dairy wastewater using novel low cost tubular ceramic membrane and analysis of fouling mechanism using pore blocking models

---

Treatment of oily and dairy wastewater using novel low cost tubular ceramic membrane and analysis of fouling mechanism using pore blocking models

This chapter presents the potential application of elaborated novel low cost tubular membrane for the treatment of synthetic oily and local dairy industry wastewater. The main aim of the work reported in this chapter is to prove a potential suitability of the membrane in oil and dairy wastewater treatment by attaining acceptable limit of the permeate stream, which can be directly discharged into water bodies. The various process conditions, mainly the effect of applied pressure, feed concentration and cross flow rate were investigated on the treatment process. In this study, diverse pore blocking models (complete, standard, intermediate pore blocking and cake filtration model) to predict the permeate flux declination, as described by Hermia were employed to analyse the fouling mechanism associated with the microfiltration process of oily as well as dairy wastewater treatment. Finally, the performance of the membrane was compared with that of the other membranes reported in the literature for oily and dairy wastewater treatment.

3.1 Treatment of oily wastewater

3.1.1 Experimental

All the filtration tests were carried at an ambient temperature (~25 °C) by using the elaborated novel low cost tubular membrane in laboratory scale microfiltration system presented in chapter 2 (section 2.2.2.4). Crude oil procured from Guwahati Refinery, Indian Oil Corporation Limited (IOCL), India, was used without any treatment to prepare oily wastewater emulsions. The crude oil was obtained from Assam crude oil reservoirs. Assam crude is typically characterized to possess a high degree of aromatic and wax content (Kandwal et al. 2000).

3.1.1.1 Microfiltration of synthetic oily wastewater

The synthetic oily wastewater emulsions were made using crude oil with Millipore water as follows: a requisite quantity of crude oil was added into 10 L of Millipore water to make the various concentrations (50, 75, 100, 150 and 200 ppm) of feed stocks. The suspension was subjected to ultrasonication (Elma T460, India) for about 8 - 12 h to get stable oil-water emulsions. The emulsification process was carried out without the addition of any emulsifier agents. The oil droplet size in the feed was calculated by laser diffraction spectroscopy (Malvern Mastersizer, United Kingdom). The size dispersion of oil droplet is presented in the Figure 3.1 and the mean droplet size varies from 0.71 to 0.74 µm for 50, 75 and 100 ppm of oil concentrations and 1.18 to 1.21 µm for 150 and 200 ppm oil concentrations. The tangential microfiltration study on synthetic oily wastewater was performed for a period of 1 h at various operating conditions such as applied pressures of 69 - 345 kPa, feed concentrations of 50 - 200 ppm and cross flow rates of 5.55×10^{-7} - 1.66×10^{-6} m^3/s.

3.1.1.2 Analytical method

The observed oil rejection was determined by below expression:

$$R\,(\%) = \frac{C_f - C_p}{C_f} \times 100 \qquad (3.1)$$

Where C_f is the oil concentration in the feed stream, C_p is the oil concentration in the permeate stream and R is the observed rejection (%).

After performing the primary calibration studies, the accurate concentration of oily wastewater was determined by measuring the absorbance of the oily wastewater emulsions using ultraviolet-visible spectrophotometry (Thermo Scientific, UV-2300) at a wavelength of 236 nm.

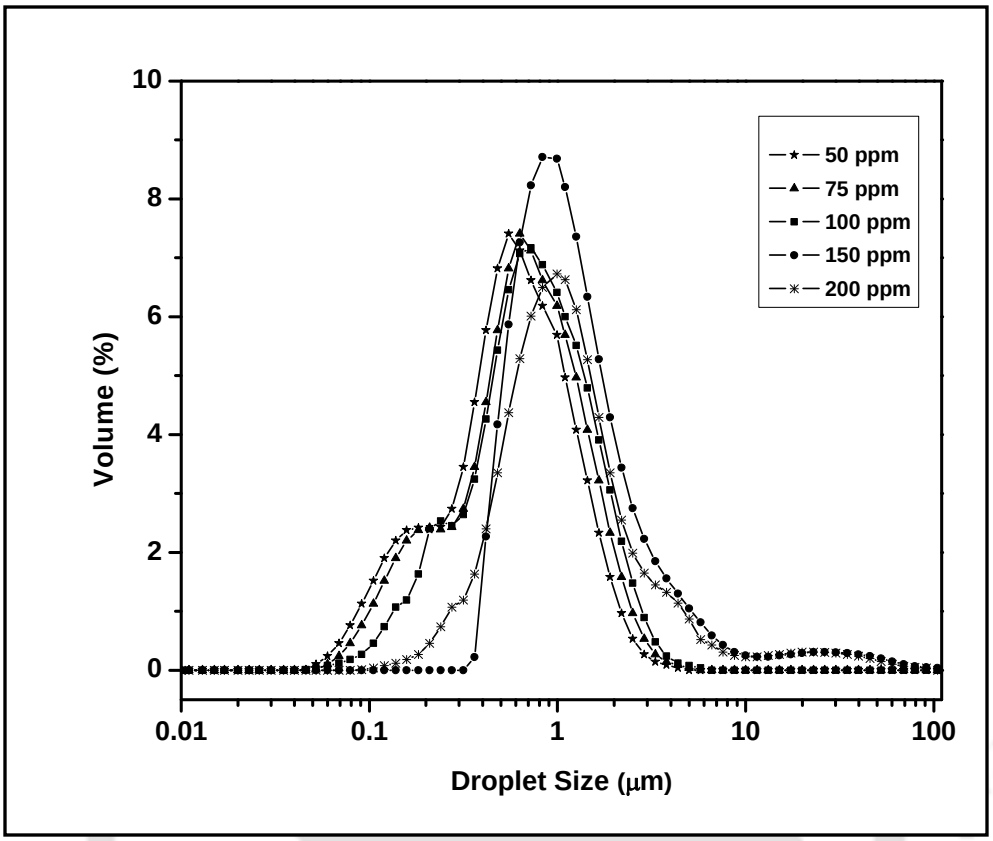

Figure 3.1: Droplet size distribution of oil-water emulsions

3.1.1.3 Membrane regeneration

The membrane was thoroughly rinsed and regenerated after every experimental run. For cleaning the membrane, the following steps were adopted sequentially: First, the membrane was washed by passing the cleansing agent (commercially acquired surf-excel powder solution of 1 g/L) to the filtration system for 1 h to eliminate the deposited oil on the surface of the membrane during the filtration. After which, the whole system was cleaned by passing Millipore water for 1 h. After conducting the cleaning process, the water flux of the membrane was evaluated to assure about negligible flux decline due to partial plugging. The full recuperation of the membrane was inspected by calculating the membrane hydraulic

permeability equal to the actual hydraulic permeability or within the limits of ±2% of actual permeability.

3.1.1.4 Analysis of fouling mechanism

Investigating the fouling mechanism facilitates the prediction of the flux behavior, thereby evaluation of the economic value of the process. Therefore, to analyse the fouling mechanism associated with the microfiltration process, Hermia's fouling models (Hermia 1982); namely, (a) complete, (b) standard, (c) intermediate pore blocking and (d) cake filtration models were applied. The description of these models is as follows and a pictorial representation of each of these models is shown in Figure 3.2. (a) Complete pore blocking takes place when the size of the solute particle is bigger than the pores of the membrane. It only causes the pore blocking on the surface of the membrane and does not block inside pores of the membrane. (b) Standard pore blocking occurs due to the non-uniform pore paths. When the solute particles are smaller than the membrane pores, inside pores of the membrane are blocked. Therefore, the membrane pore volume decrease proportionately to the filtered volume of permeate. (c) Intermediate pore blocking results when the solute particle size and membrane pore size are equivalent. This model considers no significantly blockage of the membrane pores due to the solute particles. The pore blocking may be due to some solute particles settling over others. As a result, the unblocked membrane surface area reduces with time. (d) Cake filtration model is applicable where particles bigger than the average pore size accumulate on the surface of the membrane thus forming a cake. Therefore, the cake volume builds with time and offers an extra porous barrier to the permeating liquid. The porous barrier may also mainly impact the membrane separation characteristics.

The assorted pore blocking models can be delineated with the following linearized equations of the membrane permeate flux (J) and time (t) as follows:

(a). Complete pore blocking : $\ln\ J^{-1} = \ln J_0^{-1} + k_b\, t$ (3.2)

(b). Standard pore blocking : $J^{-0.5} = J_0^{-0.5} + k_s\, t$ (3.3)

(c). Intermediate pore blocking : $J^{-1} = J_0^{-1} + k_i\, t$ (3.4)

(d). Cake filtration : $J^{-2} = J_0^{-2} + k_c\, t$ (3.5)

Hence, a plot of ln (J^{-1}) vs. t, $J^{-0.5}$ vs. t, J^{-1} vs. t and J^{-2} vs. t is a linear line with the slope of k_b, k_s, k_i and k_c, and a y-intercept of ln(J_o^{-1}), $J_o^{-0.5}$, J_o^{-1} and J_o^{-2} for the best fitting complete, standard, intermediate pore blocking and cake filtration model, respectively. Calculating the correlation coefficient (R^2) values acquired from linear regression plots, the suitable fitness and competency of various fouling models can be described in eqns. (3.2 - 3.5). Ultimately, the model that signifies experimental data with best fit R^2 value (nearby 1) is considered to refer the suitable fouling mechanism during microfiltration.

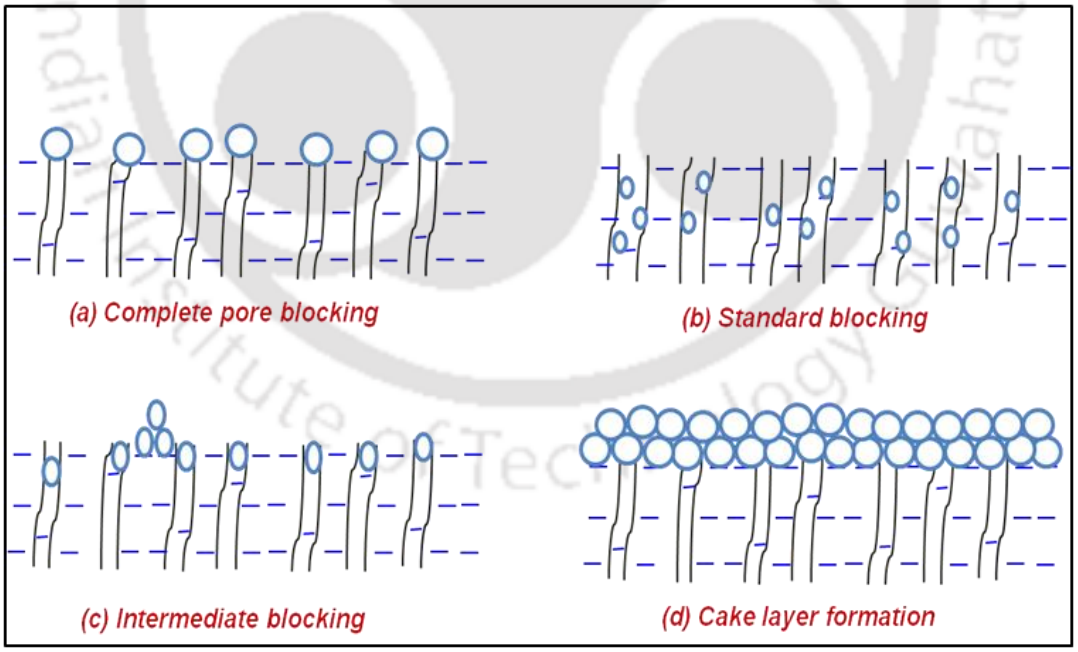

Figure 3.2: Fouling mechanism due to: (a) complete pore blocking, (b) intermediate blocking, (c) standard blocking, and (d) cake layer formation models

3.1.2 Results and discussion

3.1.2.1 Performance in synthetic oily wastewater treatment

The elaborated novel tubular ceramic membrane was applied for the treatment of synthetic oily wastewater emulsions. Applied pressure, feed oil concentration and cross flow rates are the important variables that affect the treatment process in terms of permeate flux and rejection. Hence, the effect of these parameters was investigated as a function of time.

3.1.2.1.1 Effect of applied pressure

Figure 3.3(a) shows the permeate flux profiles with time for various applied pressures (69, 138, 207, 278 and 345 kPa) at a cross flow rate of 1.11×10^{-6} m^3/s with feed concentration of 100 ppm. It can be seen from the figure that the permeate flux declines sharply at the initial period and becomes gradual thereafter in the microfiltration run. The reasons for the flux reductions are owing to concentration polarization on the surface of membrane and blocking of pore in the porous ceramic structure. In addition, it is noticed that the permeate flux increases with increasing applied pressures due to the higher driving forces acted on the membrane. However, the permeate flux profile on increasing applied pressure does not follow the linear trend (see Figure 3.3(a) (insert)). This is due to concentration polarization and adsorptive of oil on the surface that creates further resistances to transport liquid through the membrane (Chakrabarty et al. 2008). The rate of flux decline is higher at higher applied pressure due to the immediate formation of oil layer on the surface of the membrane, which makes membrane fouling faster while increasing the applied pressure. Figure 3.3(b) presents the rejection of oil with time for various applied pressures. It is noticed that the oil rejection declines with an increase in applied pressure. This occurs due to the fact that oil droplets can deform more at higher shear and the changed shape may enable their permeation at higher pressure. Moreover, the percentage of oil rejection slightly increases with duration of microfiltration. This is possibly due to the reduction

of membrane pore sizes, which happens by the adsorption of oil droplets on the surface of the membrane. The fabricated membrane exhibits excellent rejection performance according to the results depicted in Figure 3.3(b). The membrane shows the highest rejection of 99.98% at a lower applied pressure of 69 kPa with permeate flux of 3.16×10^{-5} m^3/m^2s.

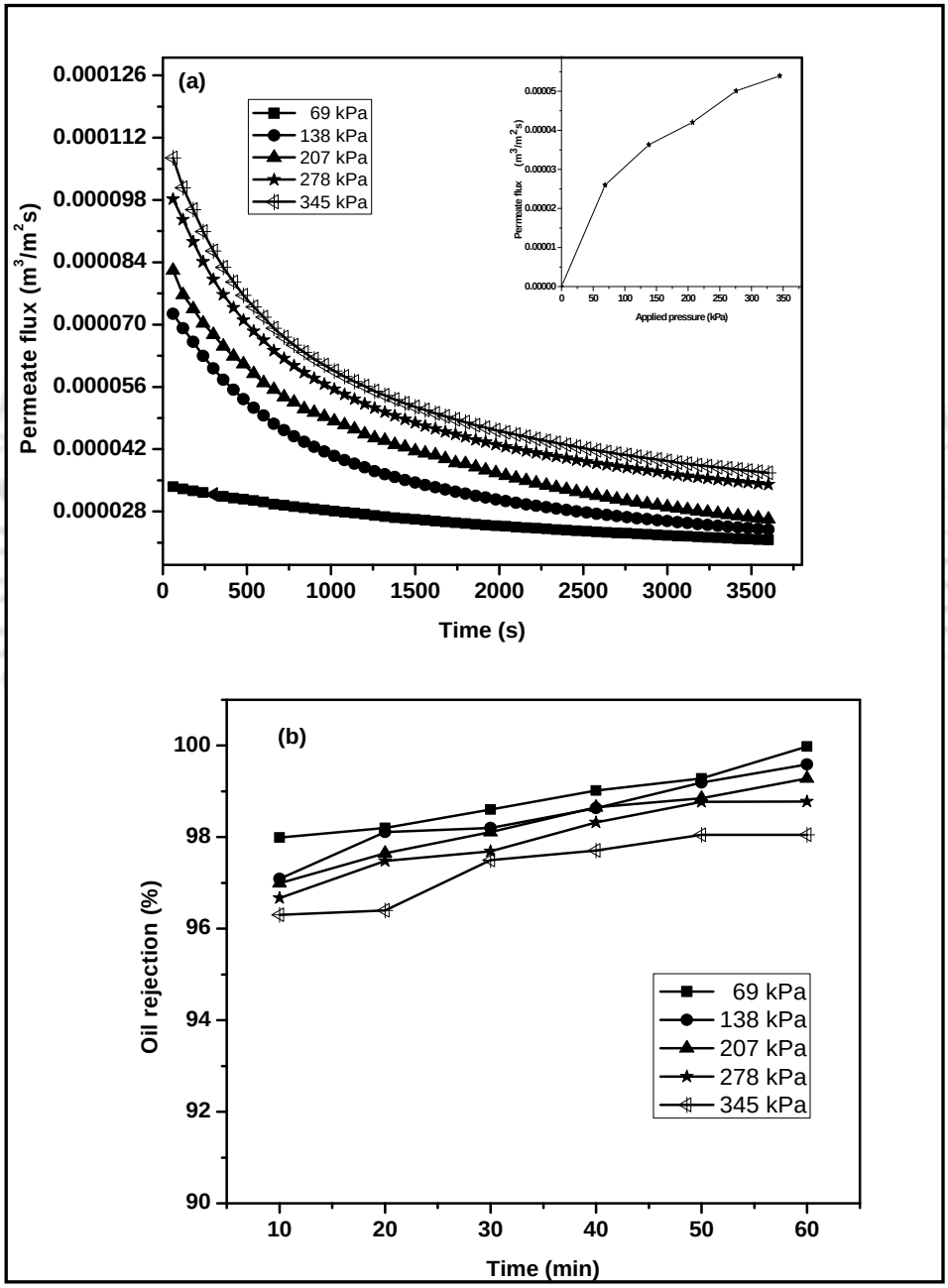

Figure 3.3: Influence of applied pressure on (a) permeate flux and (b) oil rejection

3.1.2.1.2 Effect of feed concentration

Figure 3.4(a) illustrates the permeate flux plots with time for various feed concentrations (50, 75, 100, 150 and 200 ppm) at applied pressure of 207 kPa with the cross flow rate of 1.11×10^{-6} m^3/s. Figure 3.4(a) clearly demonstrates that an increase in the oil concentration results larger flux decline. The coalesced oil sticks over the membrane, which creates fouling resulting a declined premeate flux at higher feed concentration (see Figure 3.4(a) (insert)). Similar kind of trends is also reported in the literature (Monash and Pugazhenthi 2011). From Figure 3.4(b), it is apparent that the rejection enhances with an increase in feed concentration due to the enhancement of oil droplet size and density of droplet at higher concentrations. At higher concentrations, the coalescence of the oil droplets forms a larger droplet that offers a greater rejection. The highest percentage of oil rejection (99.64%) is obtained for the feed concentration of 200 ppm with permeate flux of 1.74×10^{-5} m^3/m^2s.

3.1.2.1.3 Effect of cross flow rate

Figure 3.5(a) represents permeate flux plots with respect to time for different cross flow rates (5.55×10^{-7}, 1.11×10^{-6} and 1.66×10^{-6} m^3/s) at applied pressure of 207 kPa with feed concentration of 100 ppm. It is noticed that the permeate flux of the membrane enhances with increasing the cross flow rate (see Figure 3.5(a) (insert)). It can be explained that an increment of the cross flow rate reduces the concentration polarization. Additionally, increasing the cross flow rate offers enhancement in the shear stress on the membrane surface, which diminishes the thickness of the adhered oil layer on the surface of the membrane. Figure 3.5(a) signifies that an increase in the cross flow rate decreases the rate of flux decline. This is due to the fact that the increasing cross flow rate restricts the cake layer occurrence on the surface of the membrane. Figure 3.5(b) points out that the percentage of oil rejection reduces slightly with increasing cross flow rate. This is due to the reduction of oil layer thickness on the surface of the membrane at a

higher cross flow rate, as we discussed previously. At a lower cross flow rate, the formation of the cake layer is more, which acts as an additional barrier on the surface of the membrane resulting improved oil rejection. The higher cross flow rates depreciates the formation of cake layer, consequently the oil rejection decreases. For that reason, the percentage of oil rejection declines with rising cross flow rates. The highest percentage of oil rejection (99.86%) is obtained for lower cross flow rate of 5.55×10^{-7} m^3/s with permeate flux of 2.24×10^{-5} $m=/m^2s$.

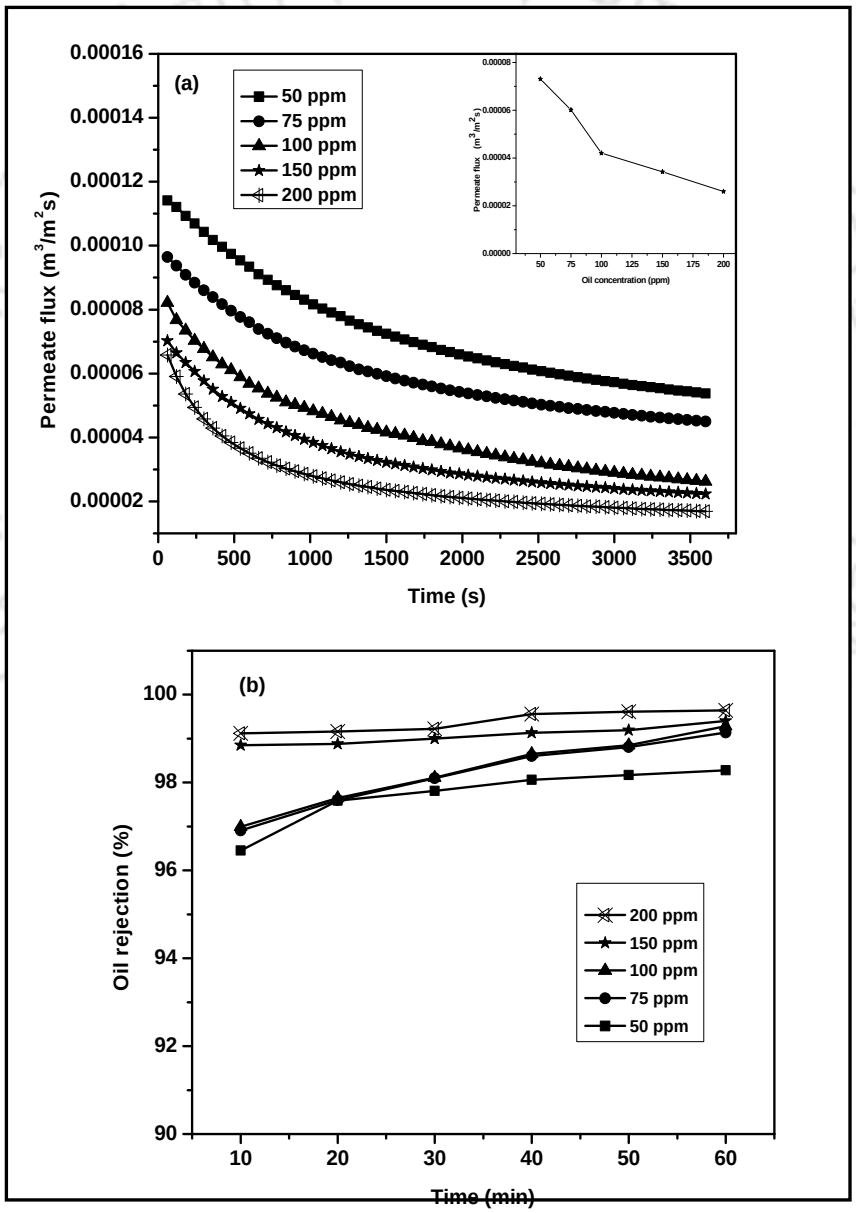

Figure 3.4: Effect of feed concentration on (a) permeate flux and (b) oil rejection

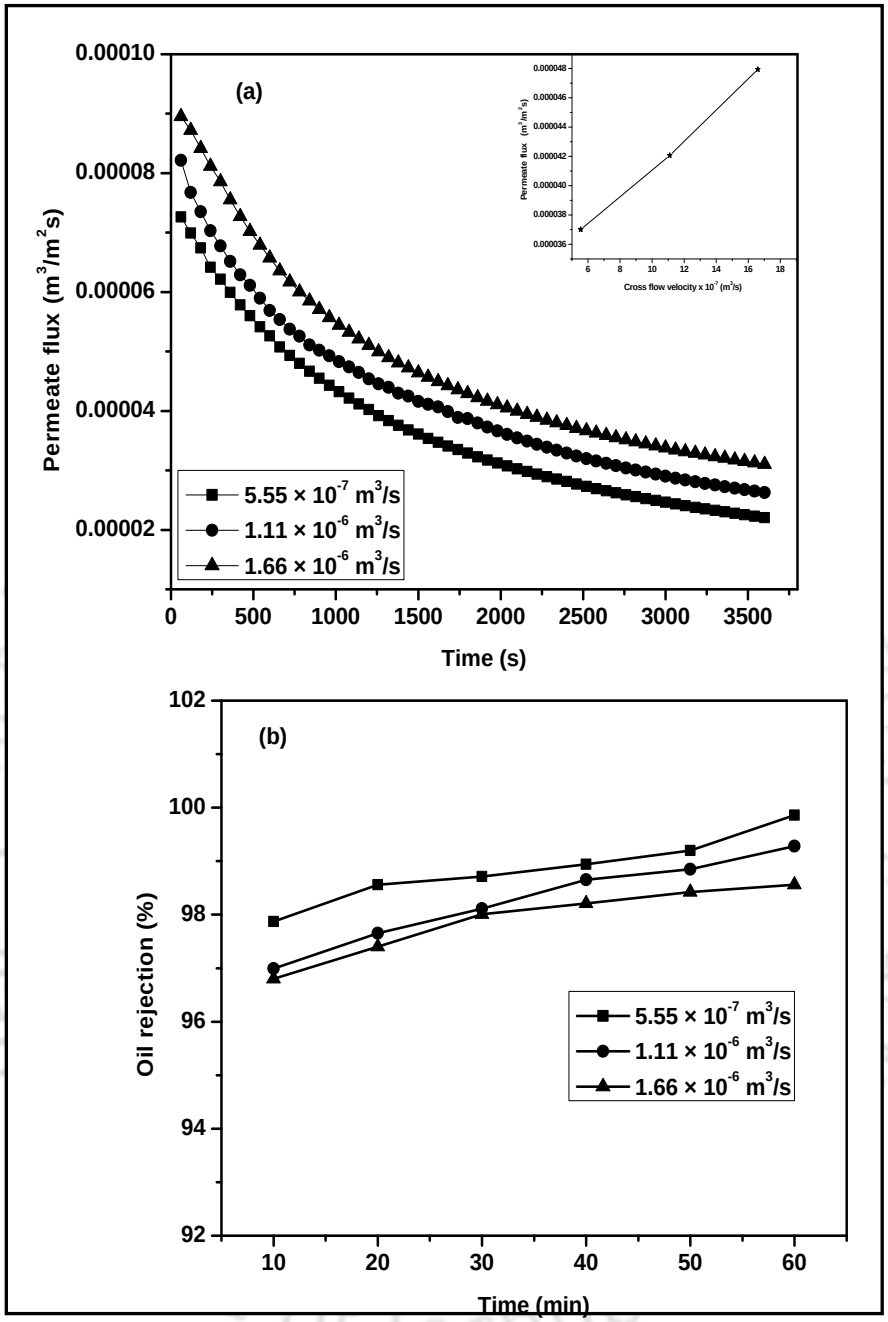

Figure 3.5: Effect of cross flow rate on (a) permeate flux and (b) oil rejection

3.1.2.2 Fouling analysis

For microfiltration processes, it is essential to indentify the pertinent flux decline mechanism. The permeate flux decline mechanisms are investigated using various pore blocking models during microfiltration of synthetic oily wastewater. These models provide the platform to study

the flux decline, which is influenced by pore blocking or cake filtration according to fitness of obtained data from microfiltration experiments. Figures (3.6 - 3.8) elucidate the fitness of pore blocking models for various applied pressures, feed concentrations and each cross flow rates. From these plots, it can be described that cake filtration model offers the best fit with the obtained experimental data. The various model parameters of four filtration models for microfiltration of oily wastewater are summarized in the Tables 3.1 -3.3. Based on the R^2 (correlation coefficient) values of various models, the best fit of the model can be identified. According to the R^2 value, the cake filtration model is regarded as best model to portray the flux decline mechanism for microfiltration of oily wastewater. The identical results reported by Salahi et al. (2010) also indicated that the flux decline throughout the microfiltration of oily wastewater with the polymer membrane was well described by the cake filtration model.

The values of model parameters (k) evaluated from different filtration models are also presented in the Tables 3.1 -3.3. As stated by the physical meaning and description of Hermia's model parameters, the value of 'k' designates the severity of fouling. It can be noticed that the initial permeate fluxes are calculated from intercept of various filtration models are lower than the initial permeate flux obtained from experimental results and thereby, all models have a tendency to underrate the initial flux. In addition, a huge variation is detected except for the cake filtration model, and it offers a fine conformity to the obtained experimental results as compared to other models. The entire study confirms that the cake filtration model best fits with the obtained experimental result. These examinations throughout the microfiltration are an auspicious act towards the life of the membrane, as cake filtration facilitates exterior fouling and may not provide considerably towards the irreversible fouling of the membrane.

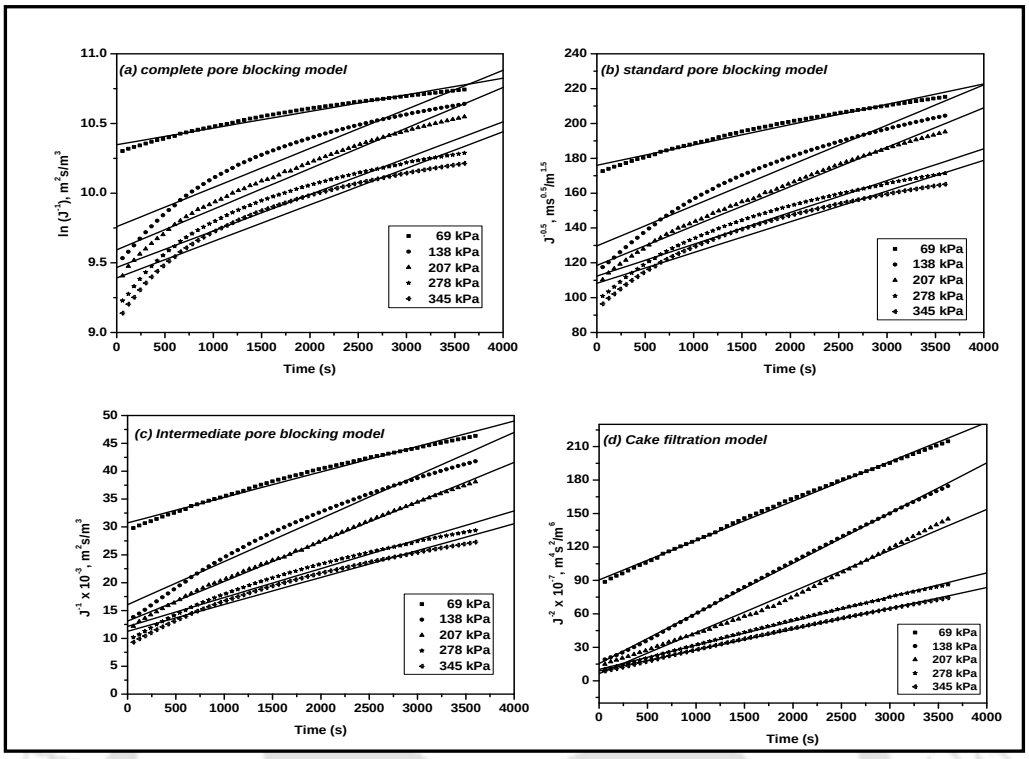

Figure 3.6: Linearized plots of permeate flux versus time for various pore blocking models (applied pressures: 69-345 kPa; feed concentration: 100 ppm; cross flow rate: 1.11 × 10^{-6} m^3/s).

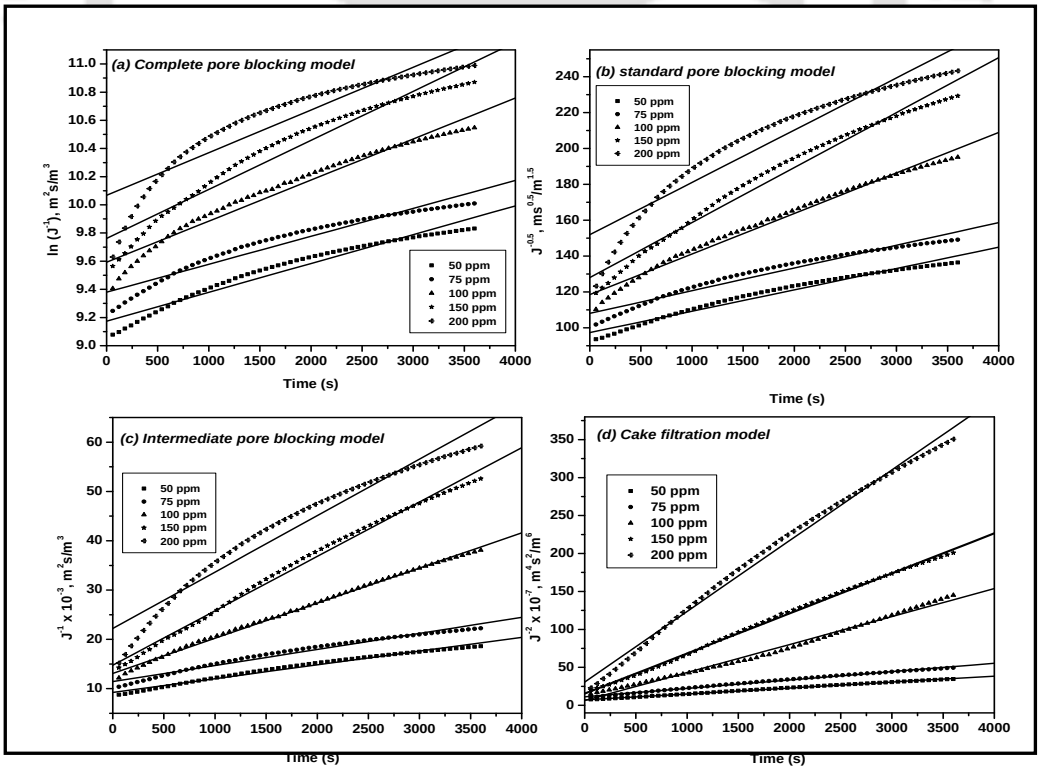

Figure 3.7: Linearized plots of permeate flux versus time for various pore blocking models (feed concentration: 50 - 200 ppm; applied pressure: 207 kPa; cross flow rate: 1.11 × 10^{-6} m^3/s).

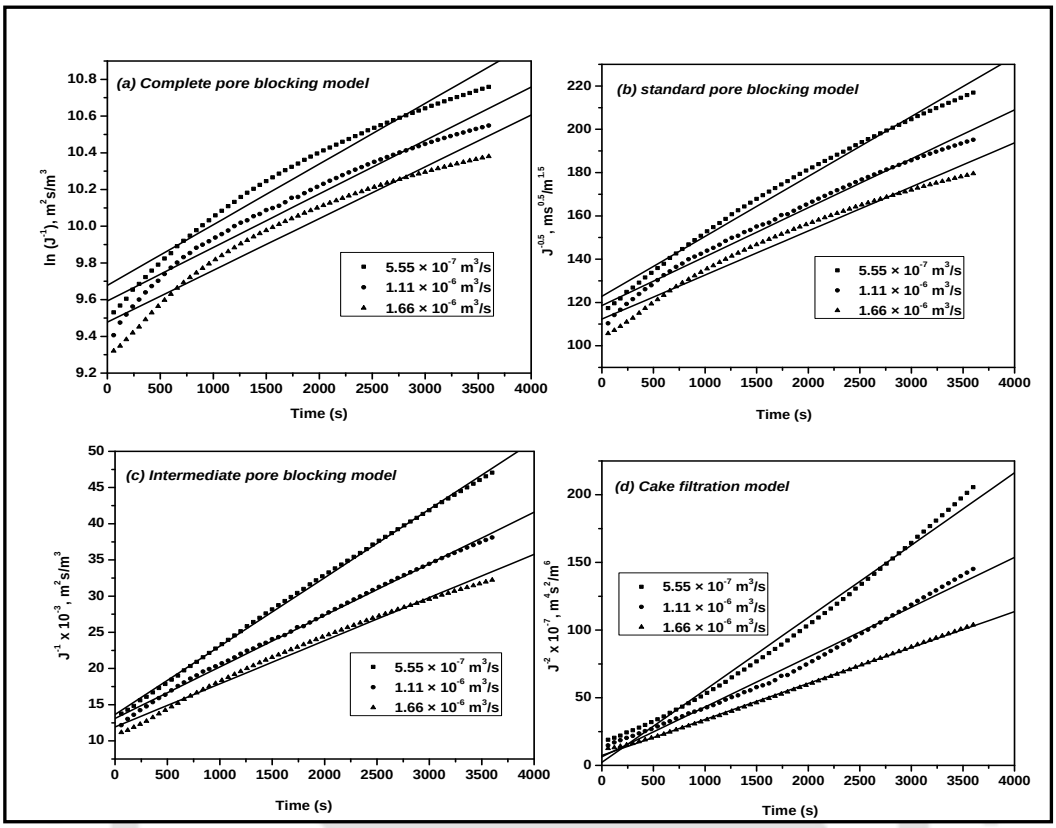

Figure 3.8: Linearized plots of permeate flux versus time for various pore blocking models (cross flow rates: 1.66 × 10^{-6} - 5.55 × 10^{-7} m^3/s; feed concentration: 100 ppm; applied pressure: 207 kPa).

Table 3.1: Summary of parameters associated with various pore blocking models for different applied pressures

Pressure	Complete pore blocking			Standard pore blocking			Intermediate pore blocking			Cake filtration		
(kPa)	R^2	k_b (s^{-1})	$\ln(J_0^{-1})$	R^2	k_s ($s^{0.5}\ m^{-0.5}$)	$J_0^{-1} \times 10^{-2}$	R^2	k_i (m^{-1})	$J_0^{-1} \times 10^{-4}$	R^2	k_c ($s\ m^{-2}$)	$J_0^{-2} \times 10^{-8}$
69	0.974	0.00011	10.34	0.982	0.01166	1.76	0.989	4.57046	3.07	0.997	353321.17	9.04
138	0.919	0.00028	9.75	0.954	0.02311	1.29	0.978	7.72818	1.60	0.999	450082.33	1.54
207	0.963	0.00029	9.59	0.986	0.02260	1.18	0.991	7.12208	1.30	0.997	368495.05	0.63
278	0.916	0.00026	9.46	0.950	0.01827	1.12	0.975	5.18478	1.21	0.998	216360.29	1.02
345	0.912	0.00026	9.39	0.948	0.01766	1.08	0.973	4.82586	1.12	0.998	186885.77	0.88

Table 3.2: Summary of parameters associated with various pore blocking models for different feed concentrations

Concentration	Complete pore blocking			Standard pore blocking			Intermediate pore blocking			Cake filtration		
(ppm)	R^2	k_b (s^{-1})	$\ln(J_0^{-1})$	R^2	k_s ($s^{0.5}\ m^{-0.5}$)	$J_0^{-1} \times 10^{-2}$	R^2	k_i (m^{-1})	$J_0^{-1} \times 10^{-4}$	R^2	k_c ($s\ m^{-2}$)	$J_0^{-2} \times 10^{-8}$
50	0.954	0.00020	9.17	0.972	0.01190	0.97	0.985	2.79117	0.92	0.998	78355.34	0.70
75	0.936	0.00019	9.37	0.958	0.01266	1.08	0.975	3.26004	1.14	0.995	110280.8	1.12
100	0.963	0.00029	9.59	0.986	0.02260	1.18	0.991	7.12208	1.30	0.997	368495.0	0.63
150	0.948	0.00034	9.76	0.978	0.030653	1.28	0.993	11.0281	1.47	0.994	528004.1	1.54
200	0.855	0.00030	10.06	0.910	0.029142	1.51	0.951	11.4484	2.22	0.993	931604.1	3.05

Table 3.3: Summary of parameters associated with various pore blocking models for different cross flow rates

Cross flow rate	Complete pore blocking			Standard pore blocking			Intermediate pore blocking			Cake filtration		
(m^3/s)	R^2	k_b (s^{-1})	$\ln(J_0^{-1})$	R^2	k_s ($s^{0.5}\ m^{-0.5}$)	$J_0^{-1}\times 10^{-2}$	R^2	k_i (m^{-1})	$J_0^{-1}\times 10^{-4}$	R^2	k_c ($s\ m^{-2}$)	$J_0^{-2}\times 10^{-8}$
1.66×10^{-8}	0.965	0.00033	9.67	0.988	0.02768	1.22	0.997	9.45363	1.36	0.999	534896.0	0.22
1.11×10^{-8}	0.963	0.00029	9.59	0.986	0.02260	1.11	0.991	7.12208	1.30	0.997	368495.0	0.63
5.55×10^{-7}	0.946	0.00028	9.47	0.973	0.02035	1.12	0.990	5.95845	1.19	0.999	265609.4	0.73

Table 3.4: Potential evaluation of other membranes with prepared membrane

Membrane material	Pressure (kPa)	Oil concentration (mg/L)	Cross flow rate (m^3/s)	Permeate flux (m^3/m^2s)	Rejection (%)	Authors
α- alumina	69	250	1.94×10^{-3}	8.33×10^{-6}	99.9	Mueller et al. (1997)
α- alumina	125	141(TOC)	1.82×10^{-2}	8.05×10^{-5}	97.8(TOC)	Abadi et al. (2011)
Zeolite/α- alumina	100	100	8.05×10^{-5}	1.66×10^{-5}	98.8	Cheryan and Rajagopalan (1998)
Zirconia/α- alumina	100	5500	2.43×10^{-2}	7.75×10^{-6}	94.3	Yang et al. (1998)
Mullite	300	1000	8.10×10^{-3}	1.11×10^{-5}	94(TOC)	Abbasi et al. (2010)
Carbon	100	120	8.11×10^{-4}	1.78×10^{-5}	97.8	Song et al. (2006)
Mixed clays	69	100	1.11×10^{-6}	3.16×10^{-5}	99.98	Present work

3.1.2.3 Potential evaluation of the elaborated membrane with other membranes

The performance of the present membrane in treatment of oily wastewater emulsion is analyzed with other membranes reported in the literature. It is evident from the Table 3.4 that the highest rejection of 99.98% achieved in this exertion at lower applied pressure and cross flow rate is considerably equivalent and more preferable than those described in the literature. In the work investigated by Mueller et al. (1997), α- alumina membrane exhibited 99.9% of oil rejection with permeate flux of 8.33×10^{-6} m^3/m^2s for oil concentration of 250 mg/L. It is noteworthy to mention that the prepared membrane provides a tough competitive to replace α-alumina membrane. In particularly, the synthesized membrane demonstrates one order higher permeate flux with keeping the same rejection value (99.98%) even at lower feed concentration (100 mg/L). From Table 3.4, it can be seen that most of the attempted studies on treatment oily wastewater is carried out with higher concentration and at elevated cross flow rates. As discussed in the chapter 1 (section 1.5.3.1), the treatment of oily wastewater containing lower concentration is difficult and higher cross flow rate directs to superior energy requirements to pump the feed stock. Thus, the selection of higher cross flow rates is not favorable in economical point of view. This study is attempted with a lower concentration of oil-in-water emulsion and low cross flow rate and the attained highest rejection is compared to those reported in literature. In few words, the prepared tubular ceramic membrane demonstrates to be best in comparison with other membranes in terms of rejection and economical point of view.

3.2 Treatment of dairy wastewater

3.2.1 Experimental

Raw dairy wastewater was obtained from a local dairy plant (Purabi Dairy, West Assam Milk Producer's Co-operative Union Ltd.,) in Guwahati, Assam, and was stored at 4 °C until further use. The complete characteristics of the wastewater are enlisted in Table 3.5. For its characterization, colour, pH, total fat content, total solids, total suspended solids (TSS), total dissolved solids, total carbohydrate content, biological oxygen demand (BOD), chemical oxygen demand (COD), total Kjeldahl nitrogen (TKN) and total phosphate content were determined as per the standard methods (Kumar et al. 2015; American Public Health Association (APHA) 1998). The COD measurement was carried out by closed reflux titrimetric method described in APHA (American Public Health Association). In this method, 2.5 mL of sample was added to COD digestion solution. Then, the COD vial was placed in preheated (150 °C) COD digester (HACH, USA) blocks and refluxed for 2 h. Following digestion, the vial was allowed to cool to room temperature. Finally, the sample was titrated against standard ferrous ammonium sulfate (FAS) solution. The change in color from blue-green to reddish brown was taken as the end point.

All experiments to treat the raw dairy wastewater were carried at an ambient temperature (~25 °C) by using the same laboratory scale microfiltration system, as illustrated in Figure 2.11 (chapter 2), under tangential flow mode at different applied pressure and cross flow rate in the rage 207 - 414 kPa and 5.55×10^{-7} - 2.22×10^{-6} m^3/s, respectively. Due to the chemical complexity of the effluent, COD was used as an indicator to assess the performance of the membrane (Sanyal et al. 2015). The percentage of COD removal from the wastewater was calculated using the expression (eq.3.6):

$$R[\text{Removal},(\%)]=1-\frac{C_p\,[\text{COD in permeate}]}{C_f\,[\text{COD in feed}]}\times 100 \qquad (3.6)$$

After every experimental run, the membrane was cleaned and regenerated as procedure mentioned earlier (section 2.1.1.3). Furthermore, the membrane fouling which inevitably occurs due to the adsorption of proteins in the pores as well as on surface of the membrane during the separation process was studied by using empirical model described by Hermia (1982).

Table 3.5: Composition of the raw dairy wastewater

Parameter	Value
Color	Dark grey
Smell	Pungent
pH	5.64
Total suspended content	976 mg/L
Total suspended solids	254 mg/L
Total dissolved solids	722 mg/L
Total fat content	294 mg/L
Total carbohydrate	366 mg/L
BOD	758 mg/L
COD	1462 mg/L
Total phosphate content	0.45 mg/L
Conductivity	853 mS/cm
TKN	24.5 mg/L

3.2.2 Results and discussion

3.2.2.1 Potential application of low cost membrane in dairy wastewater treatment

The fabricated novel tubular ceramic membrane was applied for the treatment of dairy wastewater. Applied pressure and cross flow rates are the key parameters, which influence the

treatment process in terms of permeate flux and COD removal. Consequently, the influences of these parameters are studied as a function of time.

3.2.2.1.1 Effect of applied pressure on treatment process

Figure 3.9(a) shows permeate flux profiles with time for various applied pressures (207, 278, 345 and 414 kPa) at a cross flow rate of 1.11×10^{-6} m^3/s. It can be seen from the figure that the permeate flux declines dramatically within a short time period and becomes gradual thereafter during the microfiltration. The decrease in flux is attributed to concentration polarization on the membrane surface and blocking of pores in the porous ceramic structure. In addition, it is noticed that the permeate flux increases with an increase in the applied pressures due to a high driving force acting on the membrane. However, the permeate flux profile does not follow a linear trend with the applied pressure (see Figure 3.9(a) (insert)). This is due to concentration polarization and adsorption of solutes on the surface that creates further resistance to transport liquid through the membrane. The decrease in rate of flux is high for a high applied pressure owing to the formation of boundary layer on the membrane surface, which enhances the membrane fouling rate with an increase in the applied pressure. Figure 3.9(b) shows the removal of COD with time at different applied pressure, which reveals that the COD removal reduces with an increase in the applied pressure. At high operating pressure, COD content increases in permeate stream because of an enhanced convective flux through the membrane (due to greater driving force) (Chakrabarty et al. 2008; Bennani et al. 2015). The presence of large quantity of retained organic matter on the membrane surface further facilitates the permeation of organic matter through the membrane at a higher pressure. This results in an increase in the COD on the permeate side (Zheng et al. 2013). Moreover, the percentage of COD removal increases with microfiltration time, which is possibly due to the development of cake layer, owing to the accumulation of particles on the membrane surface with time. The formed

cake layer acts as secondary mechanism of the membrane process, which leads to an increase in the COD removal efficiency (Coskun et al. 2013). The fabricated membrane exhibits good COD removal according to the results depicted in Figure 3.9(b). The membrane shows a maximum COD removal of 91% at an applied pressure of 207 kPa with a permeate flux of 2.59×10^{-6} m^3/m^2s.

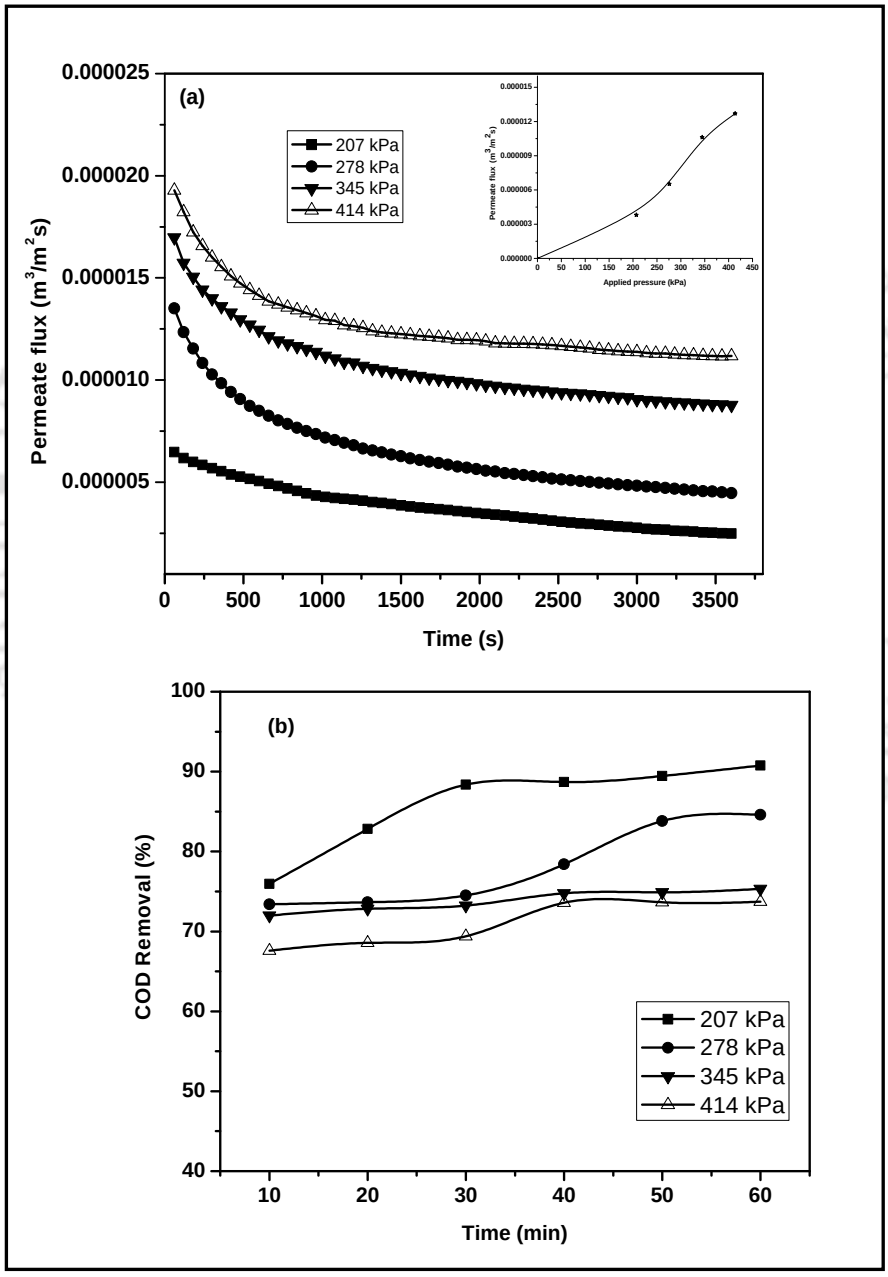

Figure 3.9: Effect of applied pressure on (a) permeate flux and (b) COD removal

3.2.2.1.2 Effect of cross flow rate on treatment process

Figure 3.10(a) represents permeate flux with respect to time for different cross flow rates (5.55×10^{-7}, 1.11×10^{-6}, 1.66×10^{-6} and 2.22×10^{-6} m^3/s) at an applied pressure of 278 kPa. It is observed that the membrane permeate flux enhances with an increase in the cross flow rate (see Figure 3.10(a) (insert)). This can be explained on the basis of reduction in concentration polarization with an increase in the cross flow rate. Additionally, increasing the cross flow rate induces shear stress on the surface of the membrane, thereby diminishing the thickness of the fouling layer on the membrane surface (Farizoglu and Keskinler 2006). Figure 3.10(a) reveals that an increase in the cross flow rate decreases the flux rate, which is due to the fact that an increase in the cross flow rate restricts the cake layer formation on the membrane surface. Figure 3.10(b) shows that the percentage of COD removal reduces slightly with increasing cross flow rate. This is due to the reduction of cake layer thickness on the membrane surface at a high cross flow rate, as quoted previously. At a low cross flow rate, the formation of the cake layer is more, which acts as an additional barrier on the surface of the membrane resulting in an improved COD removal efficiency. A high cross flow rate negatively impacts the formation of cake layer, consequently the removal decreases. For this reason, the percentage of COD removal decreases with a raise in the cross flow rate. Thus, a maximum COD removal of 89% is obtained for a low cross flow rate of 5.55×10^{-7} with a permeate flux of 3.26×10^{-6} m^3/m^2s.

3.2.2.2 Fouling analysis

The permeate flux decline mechanism was investigated using various pore blocking models (during microfiltration of the dairy wastewater). These models provide a platform to study the flux decline, which is influenced by pore blocking or cake filtration according to the fitness of the data obtained from microfiltration experiments.

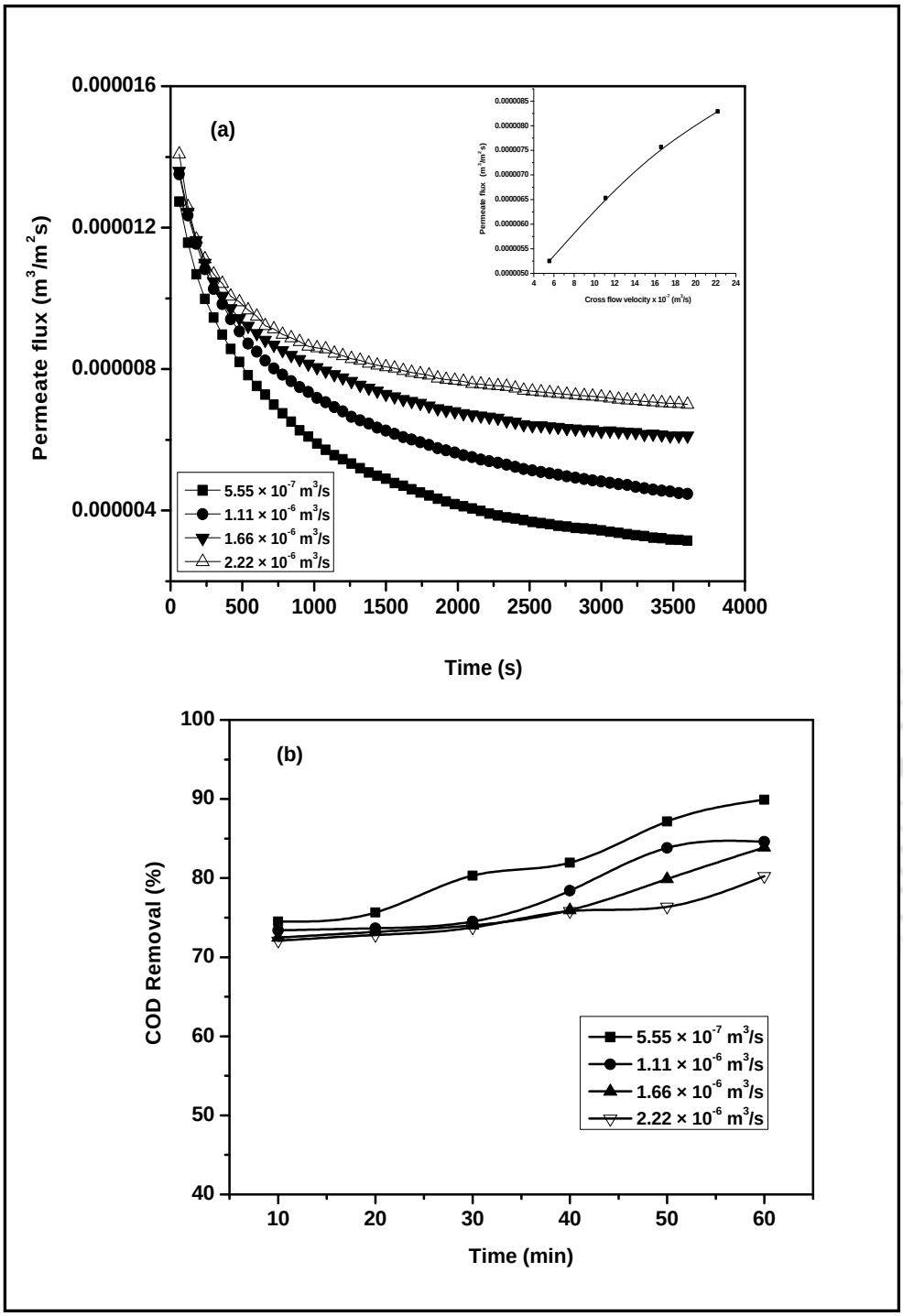

Figure 3.10: Effect of cross flow rate on (a) permeate flux and (b) COD removal

Figures 3.11 and 3.12 describe the fitness of the different pore blocking models to the experimental data for different applied pressures (207, 278, 345 and 414 kPa) and cross flow

rates (5.55×10^{-7}, 1.11×10^{-6}, 1.66×10^{-6} and 2.22×10^{-6} m^3/s), respectively. From these plots, it can be well said that the cake filtration model offers the best fit with the obtained permeate flux data. The estimated model parameters of the four filtration models applied for microfiltration of dairy wastewater are summarized in Tables 3.6 and 3.7. Based on the R^2 (determination coefficient) values obtained for the various models, the cake filtration model is regarded the best model to describe accurately the flux decline mechanism for microfiltration of dairy wastewater. A similar observation on the application of the cake filtration/gel layer model for explaining the flux decline of dairy wastewater using two different polymer membranes has been reported by Brião and Tavares (2012).

The values of the model parameter (k) estimated from the different filtration models are presented in Tables 3.6 and 3.7, which indicate the severity of membrane fouling in this microfiltration study. It can be noticed that the value of the initial permeate flux calculated from the various filtration models is lower than the experimentally determined initial permeate flux, which indicate that, all these models have a tendency to under rate the initial flux. In addition, a variation is detected except for the cake filtration model, and it offers a fine conformity to the obtained experimental results as compared to other models. All these results confirm that the cake filtration model best fits the obtained experimental data. Furthermore, for a prolonged life of membrane, cake filtration is important to facilitate exterior fouling, thereby preventing the irreversible fouling of the membrane. Hence, according to the results obtained in this study, it can be well said that the cake filtration for dairy wastewater treatment contributes to the longer life span of the membrane.

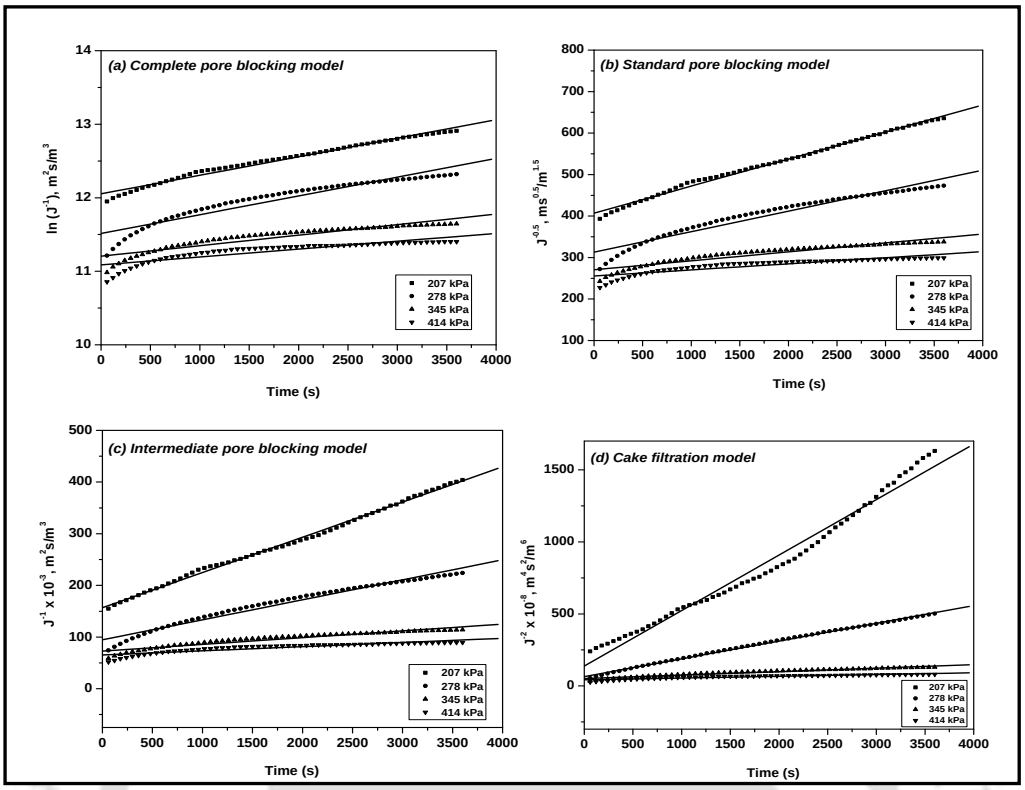

Figure 3.11: Linearized plots of permeate flux versus time for various pore blocking models (applied pressures = 207 - 414 kPa; cross flow rate = 1.11 × 10^{-6} m^3/s)

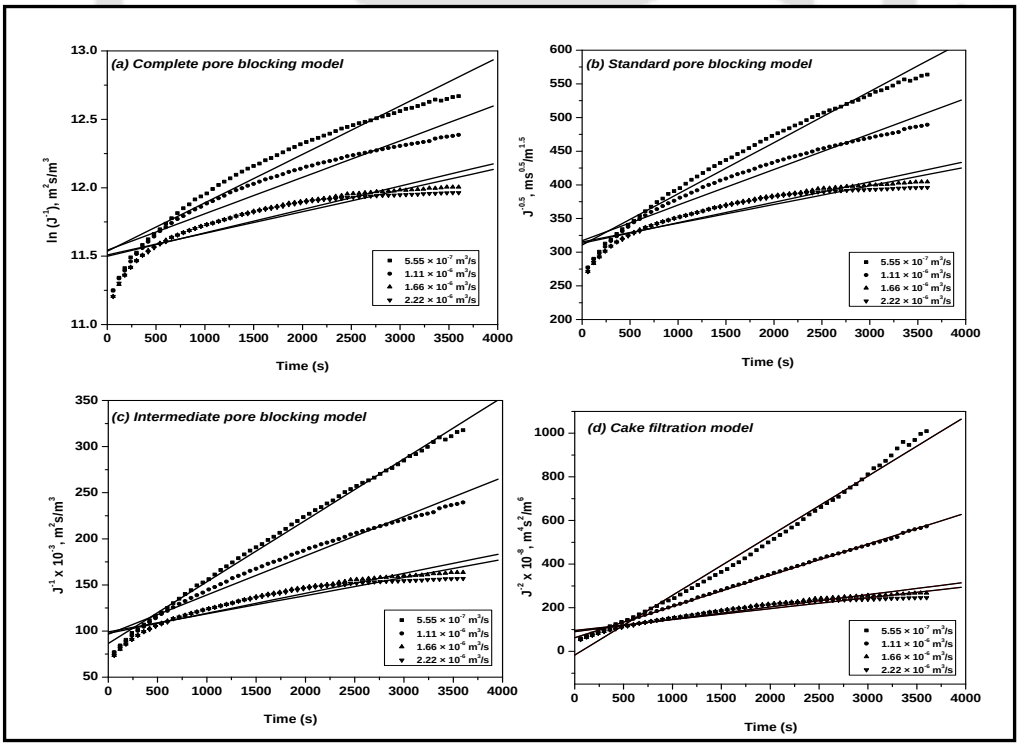

Figure 3.12: Linearized plots of permeate flux versus time for various pore blocking models (cross flow rates = 5.55 × 10^{-7} - 2.22 × 10^{-6} m^3/s; applied pressure = 278 kPa)

Table 3.6: Summary of parameters associated with various pore blocking models for different applied pressures

Pressure	Complete pore blocking			Standard pore blocking			Intermediate pore blocking			Cake filtration		
(kPa)	R^2	k_b (s^{-1})	$\ln(J_0^{-1})$	R^2	k_s ($s^{0.5}\ m^{-0.5}$)	$J_0^{-1} \times 10^{-2}$	R^2	k_i (m^{-1})	$J_0^{-1} \times 10^{-4}$	R^2	k_c ($s\ m^{-2}$)	$J_0^{-2} \times 10^{-8}$
207	0.982	0.00025	12.05	0.994	0.06516	4.06	0.980	68.1848	15.6	0.997	38517667.3	138.0
278	0.905	0.00025	11.51	0.943	0.04936	3.13	0.970	38.6935	9.46	0.998	12326097.3	64.96
345	0.864	0.00014	11.20	0.892	0.02156	2.70	0.916	13.0560	7.27	0.955	2425153.72	51.05
414	0.821	0.00010	11.08	0.868	0.01468	2.55	0.904	8.06509	6.52	0.936	1229463.28	42.41

Table 3.7: Summary of parameters associated with various pore blocking models for different cross flow rates

Cross flow rate	Complete pore blocking			Standard pore blocking			Intermediate pore blocking			Cake filtration		
(m^3/s)	R^2	k_b (s^{-1})	$\ln(J_0^{-1})$	R^2	k_s ($s^{0.5}\ m^{-0.5}$)	$J_0^{-1} \times 10^{-2}$	R^2	k_i (m^{-1})	$J_0^{-1} \times 10^{-4}$	R^2	k_c ($s\ m^{-2}$)	$J_0^{-2} \times 10^{-8}$
1.66×10^{-8}	0.912	0.00034	11.60	0.954	0.07461	3.24	0.981	66.4808	9.69	0.998	27966636.1	14.89
1.11×10^{-8}	0.905	0.00025	11.51	0.943	0.04936	3.13	0.970	38.6935	9.46	0.998	12326097.3	64.96
5.55×10^{-7}	0.839	0.00017	11.49	0.874	0.03031	3.13	0.904	21.6826	9.75	0.949	5655551.21	90.40
2.22×10^{-6}	0.803	0.00013	11.47	0.839	0.02248	3.09	0.870	15.3180	9.54	0.921	3606063.79	89.43

3.2.2.3 Potential evaluation of the elaborated membrane with other membranes

The performance of the membrane utilized in this study was compared with that of the other membranes reported in the literature for dairy wastewater treatment. In this study, the membrane exhibited a maximum COD removal of 91% at an applied pressure of 207 kPa with a cross flow rate of 1.11×10^{-6} m^3/s. The COD content (135 mg/L) in the permeate stream is well within the permissible limit for direct discharge into the environment. From Table 3.7, it can be seen that the COD removal of dairy wastewater using the novel low cost tubular membrane is comparable or even better than those reported in the literature. Thus, the prepared tubular ceramic membrane proved to be the best in comparison with other membranes for COD removal from industrial wastewater.

Table 3.7: Potential evaluation of other membranes with the prepared membrane

Membrane material	Method	COD in feed (mg/L)	COD in permeate (mg/L)	Pressure (kPa)	COD removal (%)	Authors
Polyamide/ polyethersulfone	NF	470	9	1000	98	Turan et al. (2000)
Polyamide/ polyethersulfone	RO	10500	80	1000	99	Turan et al. (2000)
Polyethersulfone	UF	346	16	250	95	Bennani et al. (2015)
Stainless steel	MF	3000	630	-	79	Yip et al. (1996)
Stainless steel	UF	3000	660	379	78	Yip et al. (1996)
Polysulfone	UF & NF	3200	70	-	97	Gong et al. (2012)
Zirconium/ aluminum	UF	1650	800	190	51	Tfiigdh and Johansson (1998)
Low cost clays	MF	1462	135	207	91	Present work

3.3 Summary

The novel low cost tubular ceramic microfiltration membrane was successfully applied for treating oily and local dairy industry wastewater. The tangential mode of microfiltration operation was investigated at different applied pressure, feed concentration and cross flow rate on treatment processes. Microfiltration of oily wastewater studies demonstrated that the permeate flux increases and the oil rejection decreases when the applied pressure and cross flow rate increase. The highest oil rejection of 99.98% is attained with permeate flux of 3.16×10^{-5} m^3/m^2s at applied pressure of 69 kPa. An increment in applied pressure and cross flow rate on microfiltration process of dairy wastewater resulted in a decrease in percentage of COD removal. It is important to mention that the elaborated novel membrane achieved a maximum reduction in COD up to 91% (135 mg/L) in the permeate stream at an applied pressure of 207 kPa. The obtained rejection value for oily wastewater as well as dairy wastewater meets the permissible limit for wastewater discharge into the environment. The investigation on fouling mechanisms with various pore blocking models proved that the cake filtration model describes accurately the experimental data for both the wastewater treatment process. Finally, the comparison of the membrane performance with reported for other membranes in the literature demonstrated its very good suitability for oily and dairy wastewater treatment. Moreover, the permeated water from the membrane can be utilized for makeup water of cooling towers and other applications.

Chapter 4

Fabrication and characterization of tubular configured FAU and MFI type zeolite composite membranes on low cost tubular ceramic support

---

Fabrication and characterization of tubular configured FAU and MFI type zeolite composite membranes on low cost tubular ceramic support

This chapter presents the fabrication and characterization of FAU (Faujasite) and MFI (Mordenite Framework Inverted) type zeolite composite membranes. Zeolite composite membranes were prepared on the novel low cost tubular ceramic support by hydrothermal treatment method. The synthesized zeolite powders (FAU & MFI) as well as membranes were characterized by various standard techniques such as X-ray diffraction (XRD), particle size distribution (PSD), Fourier transform infrared spectroscopy (FTIR), thermogravimetric analysis (TGA), zeta potential measurements, field emission scanning electron microscopy (FESEM), porosity, pore size and water permeability measurements. The porosity, pore size and water permeability values were reduced and weight of the membranes was increased due to the incorporation of the zeolite layers on the ceramic support by hydrothermal treatment.

4.1 Experimental

4.1.1 Materials

Sodium hydroxide was purchased from Merck (I) Ltd, Mumbai. Fumed silica was acquired from Central Drug House (P) Ltd., Mumbai. Tetrapropylammonium hydroxide (TPAOH) was obtained from Loba Chemie laboratory reagents & fine chemicals, Mumbai. Water was used in this work was taken from the Millipore water system (ELIX-3).

4.1.2 Preparation of FAU and MFI zeolite composite membranes

The prepared novel low cost tubular ceramic microfiltration membrane, which is presented in chapter 2, was used as a support material to fabricate FAU and MFI zeolite composite

membranes due its excellent characteristics. FAU type zeolite membrane was fabricated hydrothermal treatment technique according to the synthesis procedure reported by Huang et al. (2012). To formulate the FAU zeolite layer on the surface of the porous ceramic support, the reaction mixture for hydrothermal reaction was made by combining aluminate and silicate solutions.

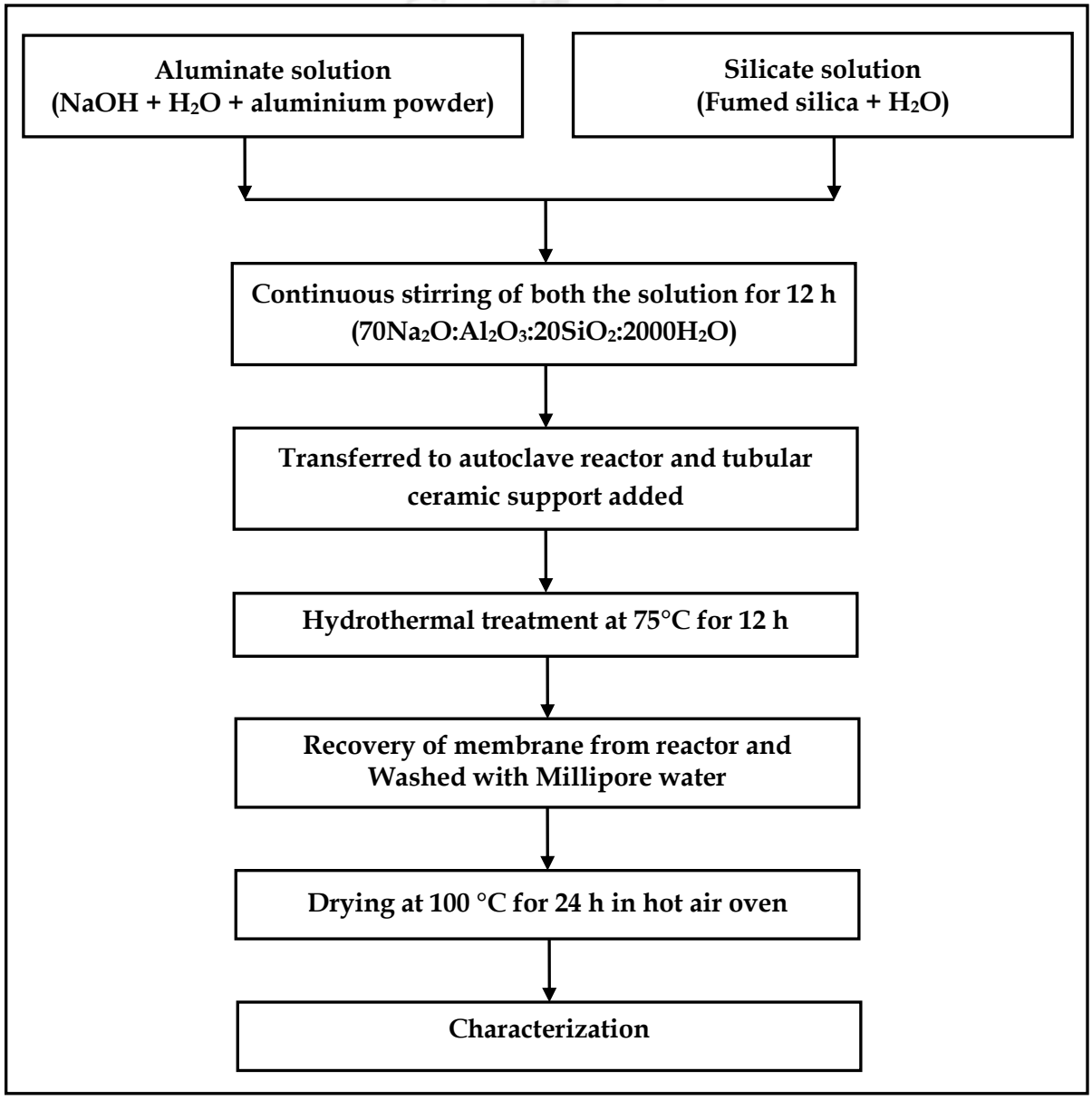

Figure 4.1: Preparation of FAU type zeolite composite membrane

In order to obtain the aluminate solution, 31.12 g of NaOH was dissolved in 60 mL of Millipore water and the calculated quantity of aluminum powder was added. Separately, the silicate solution was obtained by dissolving 13.34 g of fumed silica in 140 mL of Millipore water with effective stirring condition. After which, the obtained aluminate solution was poured into the silicate solution and stirred for 12 h in order to make a clear homogenous solution. The molar composition of the prepared clear homogeneous solution was $70Na_2O:Al_2O_3:20SiO_2:2000H_2O$. The synthesized reaction mixture was poured into Teflon lined stainless steel autoclave reactor, which contained vertically placed tubular ceramic support. Subsequently, the reactor was subjected to hydrothermal treatment for 12 h at 75 °C. After treatment, the membrane and FAU powder were recovered from the reactor and rinsed with Millipore water for many times, and consequently dried at 100 °C for 24 h in a hot air oven. Figure 4.1 illustrates the schematic diagram for the preparation of FAU type zeolite composite membrane.

MFI type zeolite composite membrane was prepared by a hydrothermal technique reported by Wegner et al. (1999) as follows: To prepare the hydrothermal solution, 2.8 g of sodium hydroxide was dissolved in 200 ml of 1 M tetrapropylammonium hydroxide solution in a glass beaker. Then 40 g of fumed silica was added to the solution at 90 °C under strong stirring conditions. After which, the solution was stirred for overnight and then 6.4 ml of Millipore water was added to obtain the desired composition of the gel mixture of $100SiO_2:5(TPA)_2O:5.3Na_2O:1420H_2O$. Then, the prepared hydrothermal solution was poured into a Teflon coated stainless steel autoclave reactor having a capacity of 300 mL. The prepared tubular ceramic support was vertically positioned in the reactor. The tightly closed reactor was subjected to in-situ hydrothermal treatment for 4 h at 185 °C in a hot air oven. After treatment, the membrane was extensively washed using Millipore water and dried at 40 °C for 72 h. To eliminate the structure directing agent/template (TPA) from the zeolite channels, the

membrane was calcined at 400 °C for 5 h in an air atmosphere at heating rate of 0.5 °C /min. The procedure adopted for the fabrication of MFI type zeolite composite membrane is presented in Figure 4.2.

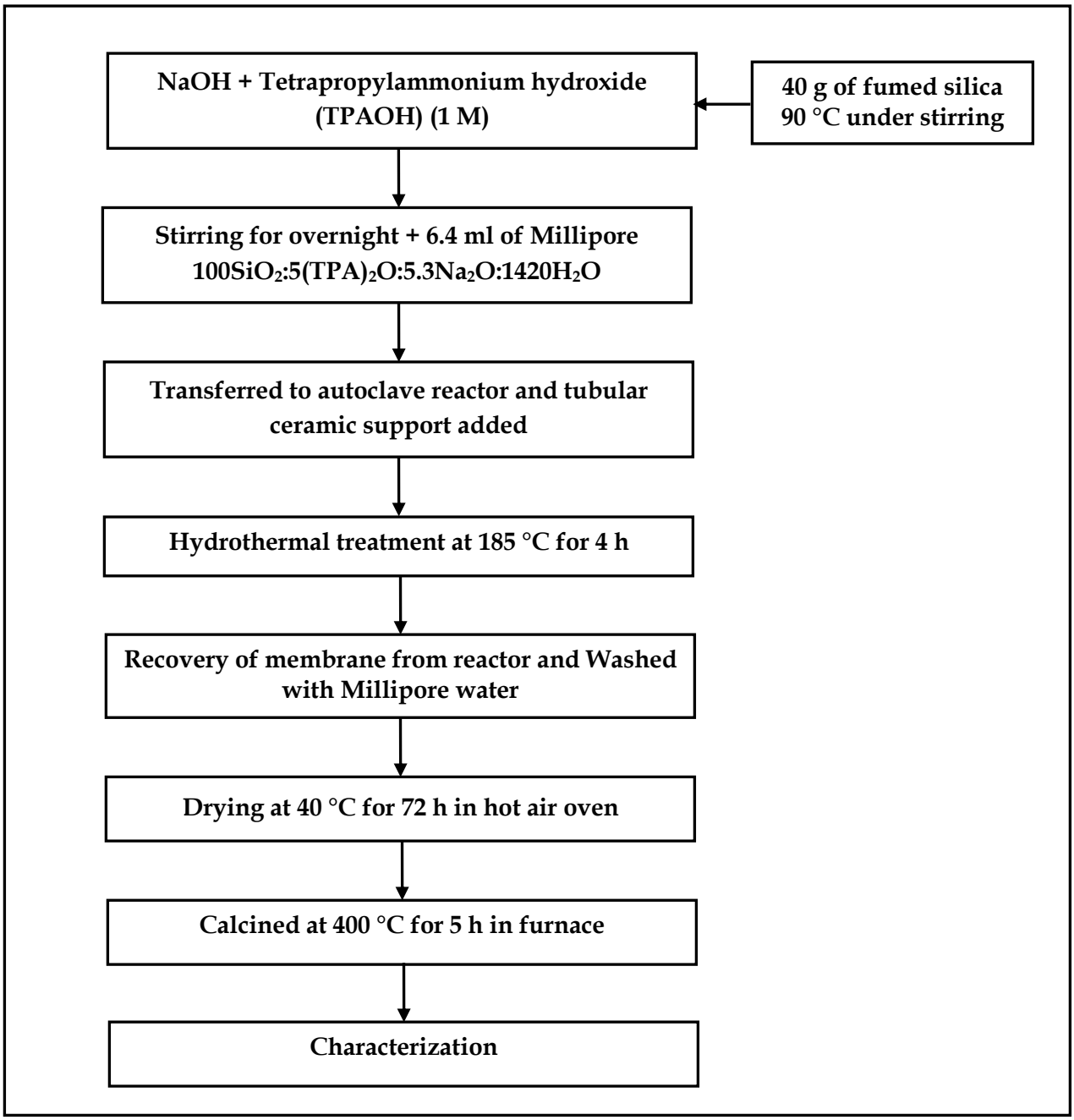

Figure 4.2: Preparation of MFI type zeolite composite membrane

4.1.3 Characterization

The XRD analysis was carried out at room temperature on a Bruker A8 advance instruments under air atmosphere operating at 40 kV and 40 mA using CuKα (λ = 1.5406 Å) radiation. The patterns were recorded in the 2θ range of 1-50° at a scanning speed of 0.05 $°s^{-1}$. The thermal behavior was studied by thermogravimetric analysis (TGA) using Mettler Toledo TGA/SDTA 851® instrument in an air atmosphere from 25 to 950 °C in 150 µL platinum crucibles with a heating rate of 10 °C/min. The FTIR spectrum was measured in the range of 4000 to 450 cm^{-1} with KBr powder in a Shimadzu IR Affinity-1 model spectrometer. The particle size and particle size distribution (PSD) was measured in wet dispersion mode using a Beckman Coulter model Delsa Nano instrument. Zeta potential measurement was carried out using Beckman Coulter model Delsa Nano instruments. The morphological investigations were carried out with a field emission scanning electron microscope (FESEM, JEOL JSM-5600LV). A small size of the sample was fixed on top of the stub and layered with gold using an auto fine coating instrument (JEOL JFC-1300) preceding to morphology assessment. In addition to the above characterization, the pure water flux of the fabricated membranes was measured at various applied pressures. The porosity of the membranes was evaluated by Archimedes' using water as a soaking agent. The average pore size of the membrane was estimated using Hagen-Poiseuille equation by assuming pores are cylindrical in shape. The procedure to calculate porosity, average pore size and water permeability of membranes has been described in the chapter 2 of the thesis.

4.2 Results and discussion

4.2.1 Characterization of FAU and MFI zeolite powder

4.2.1.1 XRD analysis

Figure 4.3 illustrates the powder XRD pattern of FAU zeolite with high crystallinity and the obtained profile is in good agreement with patterns of FAU zeolites described elsewhere (Treacy and Higgins 2007). It is evident that the FAU zeolite is present in reaction products after hydrothermal treatment of silicate solutions. The observed peak at 2θ value of 12.40 demonstrates the formation of a high degree of crystallinity and all peaks are consistence with FAU zeolite powder (Huang et al. 2012; Treacy and Higgins 2007).

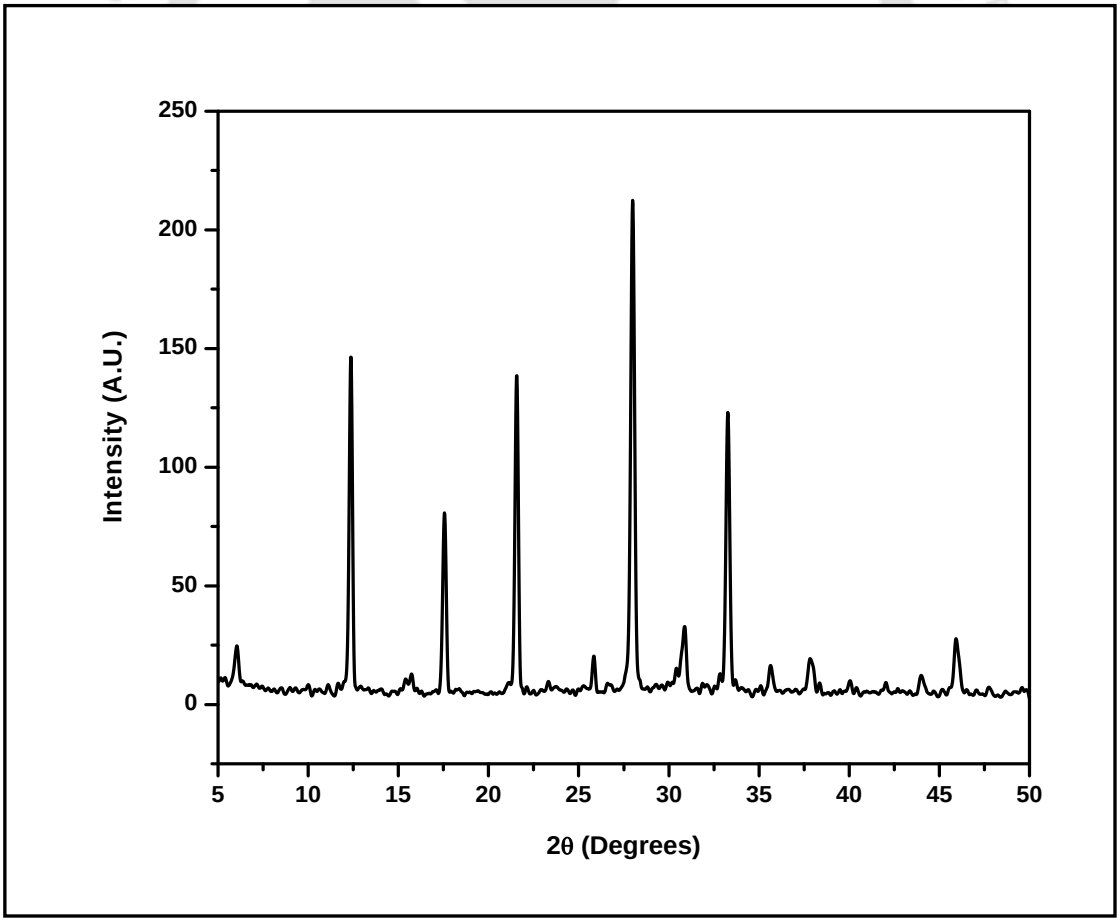

Figure 4.3: XRD pattern of FAU zeolite

MFI-type zeolites (as-synthesized and calcined) were characterized to verify its purity and structure through XRD profile as illustrated in Figure 4.4. The powder XRD pattern of MFI zeolite shows the high crystallinity and the obtained profile is good agreement with patterns of MFI zeolites described elsewhere (Wegner et al. 1999). The distinctive peaks are obtained in 2θ range around 7.5 and 23.5 with some other bearing peaks in both samples signifying the occurrence of pure phase of the zeolite.

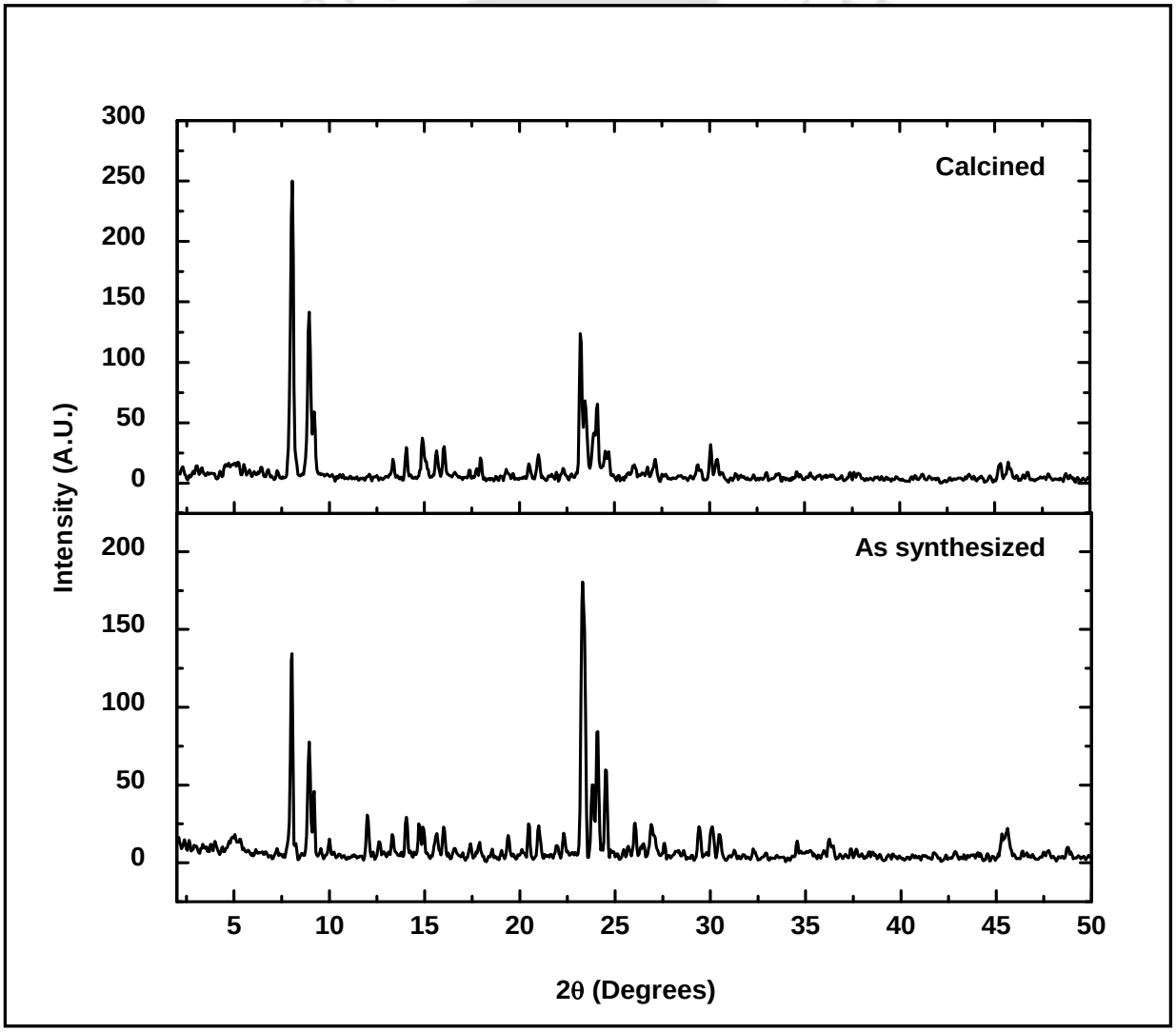

Figure 4.4: XRD pattern of MFI zeolite

4.2.1.2 FTIR analysis

The FTIR spectrum of the FAU zeolite is illustrated in Figure 4.5. The spectrum exhibits a strong and broad band at the region of 3200-3600 cm^{-1} due to the presence of the silanol OH group (Si-OH). The dominant absorbance peak appeared at 979 cm^{-1} is attributed to Si-O-Al groups. The bands observed between 456 and 740 cm^{-1} correspond to Al-O, Si-O, Si-Al, and Si-O-Si. The absorption band appeared at 668 cm^{-1} is due to Si-O-Na groups (Sadeghi et al. 2014).

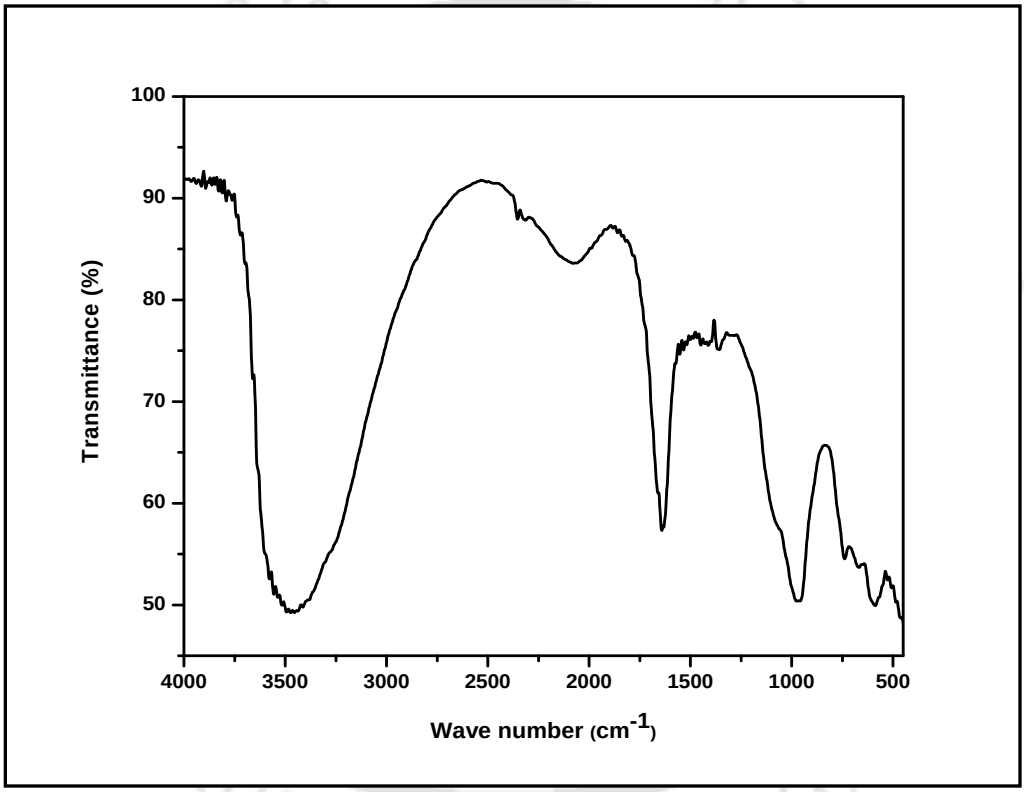

Figure 4.5: FTIR spectrum of FAU zeolite

In Figure 4.6, FTIR spectrum of MFI zeolite confirms that the creation of zeolite phase in both samples presenting well defined bands around 450 cm^{-1}(T-O bending), 540 cm^{-1} (double ring vibration), 790 cm^{-1} (external symmetric stretch) and 1080 cm^{-1} (internal asymmetric stretch) (Szostak 1998). The external asymmetric stretching vibration near 1225 cm^{-1} occurred in the

pattern of MFI structures is allocated to four chains of 5-member rings formed around a two-fold screw axis. The band appeared at 1622 cm^{-1} belongs to the bending vibration of adsorbed water. For the as-synthesized sample, the sharp intense bands occurred near 2,900 and 2,850 cm^{-1} correspond to the presence of C-H stretching of the structure directing agent (TPA). Moreover, the spectrum verifies the decrease of silanol group after calcination of zeolite at 400°C. The bands representing 3200-3700 cm^{-1} (OH groups), also including water, as well as the band allied with silanol nests (950 cm^{-1}) evidently show a reduced intensity after calcination due to the removal of the structure directing agent (TPA) (Kuhn et al. 2007).

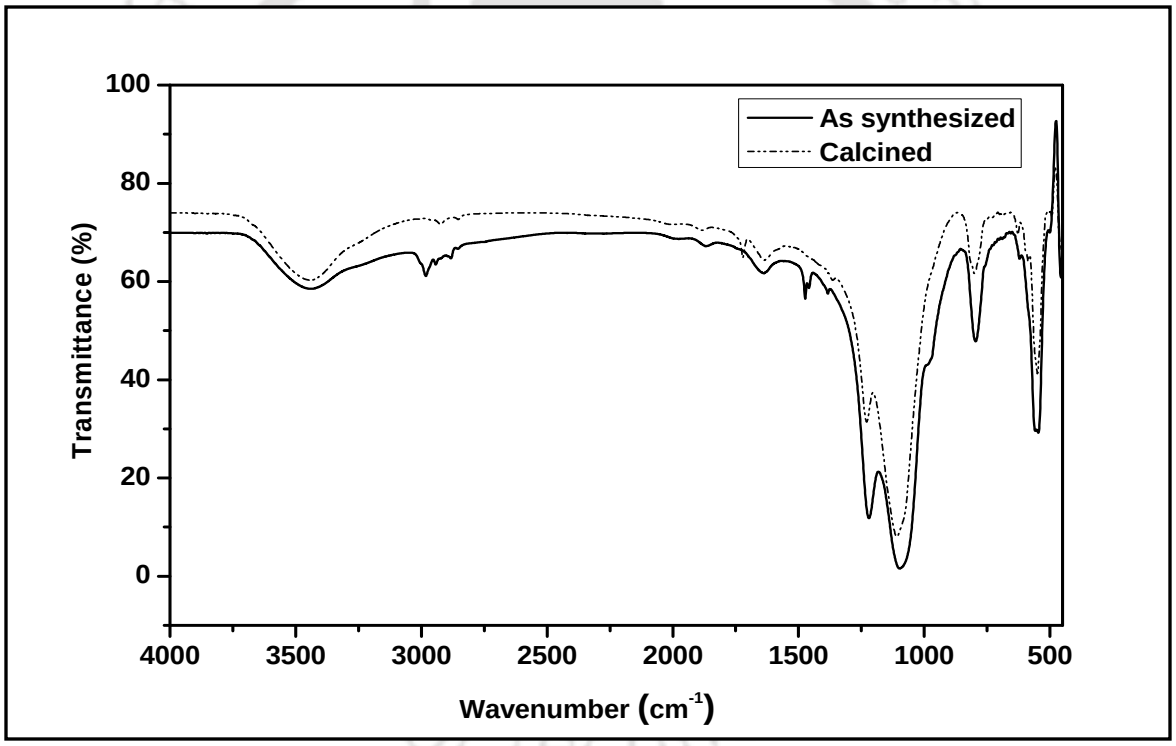

Figure 4.6: FTIR spectra of MFI zeolite

4.2.1.3 TGA and DTG analysis

The thermogravimetric (TGA) analysis curve of the FAU zeolite is displayed in Figure 4.7. It can be seen from TGA data that the majority of weight loss occurs at the temperature ranging

between 80 and 330 °C and total weight loss is found to be 18%. The weight loss below 110 °C is attributed to the loss of water molecules present in the framework of the zeolite. The first stage of weight loss occurred above 130 °C is most likely due to intrazeolite water desorption (Figueiredo et al. 2006). The second stage of weight loss at 150-330 °C is due to the liberation of crystal water from the sample and no further significant weight loss is noticed after 330 °C.

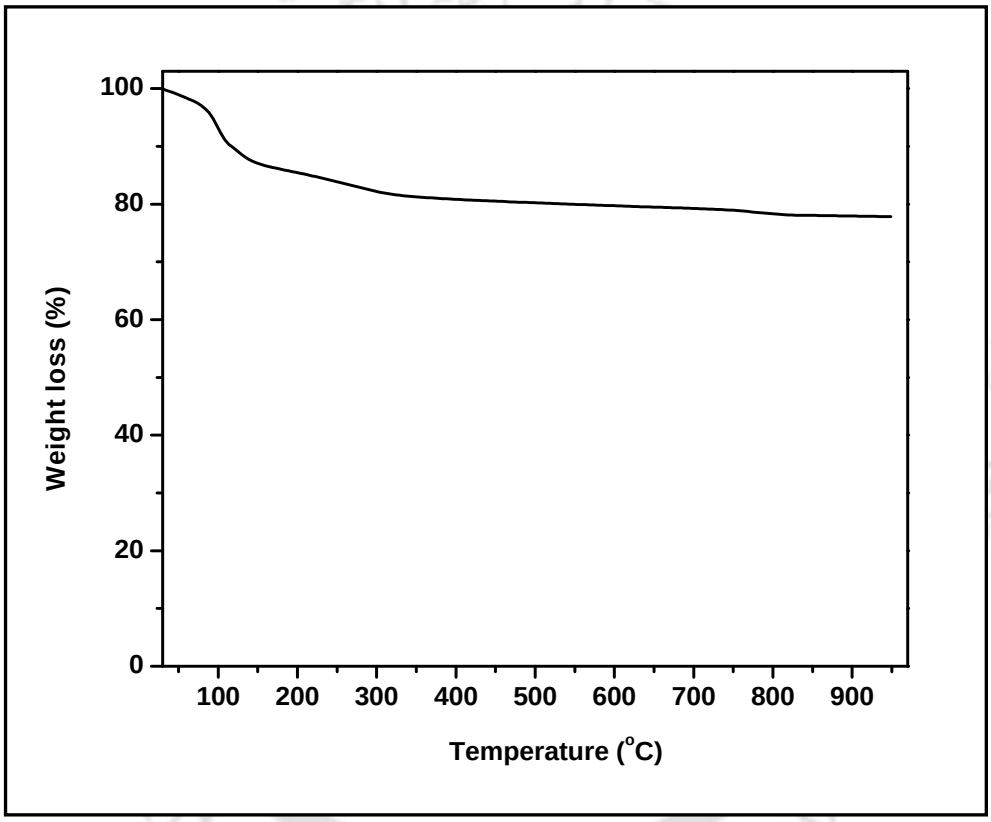

Figure 4.7: TG analysis of FAU

The TGA and derivative thermogravimetric (DTG) curves of as-synthesized MFI zeolite material are presented in Figure 4.8. The weight loss below 150 °C corresponds to the removal of the physically adsorbed water present in the sample and the loss at 500 °C is due to condensation of silanol groups. The sample exhibits a derivative peak in the range of 350-500

°C, which belongs to the release of structure directing agent (template) present inside the zeolite channels. The total weight loss of the zeolite is found to be 23.22%, which is mainly due to the structure directing agent loosely occluded inside the zeolite channels, resultant in a mass loss (Li et al. 2014).

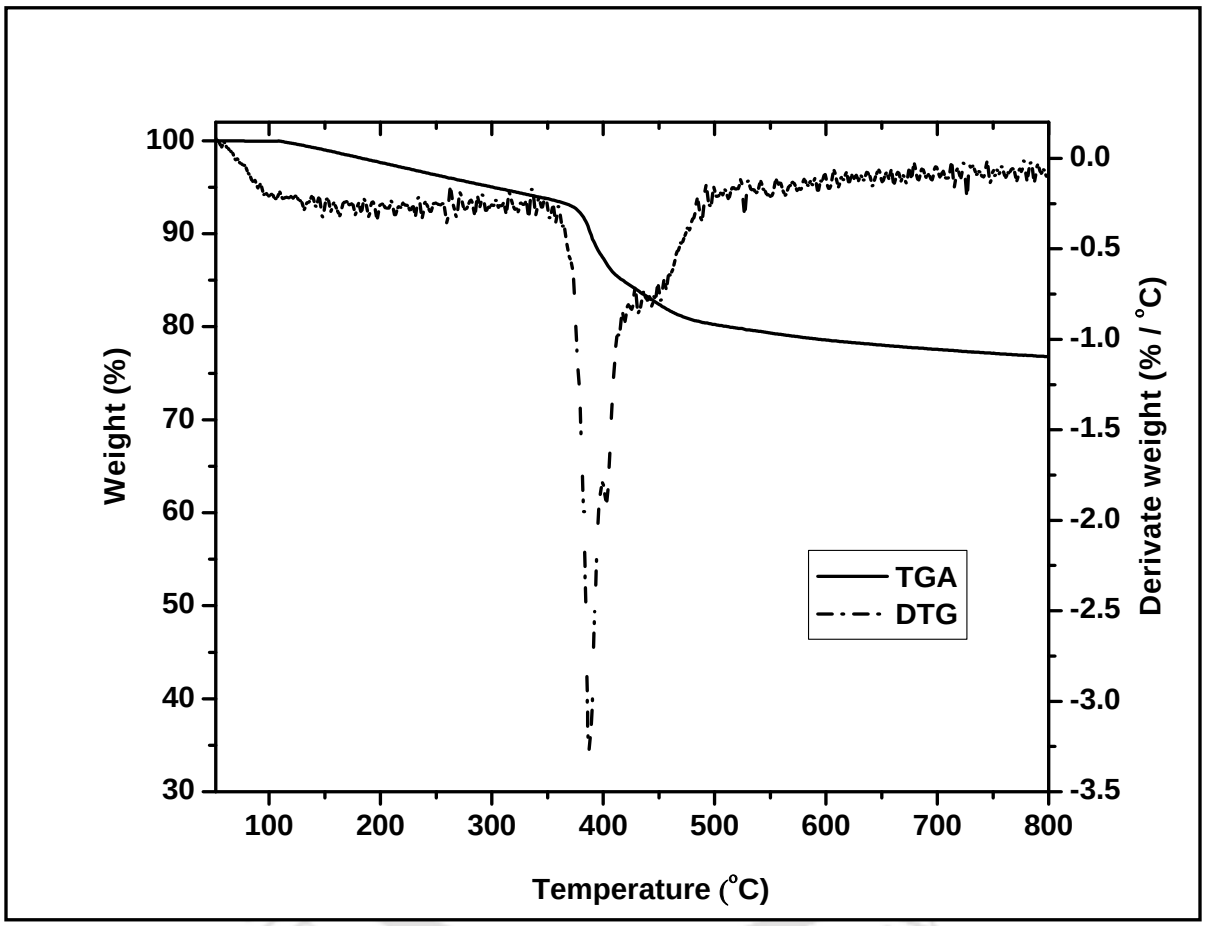

Figure 4.8: TGA and DTG curves of MFI zeolite

4.2.1.4 Zeta potential measurements

Figure 4.9 displays the variation of zeta potential of FAU and MFI zeolite powder at various pH. The surface charge of the membrane will be positive or negative, depending upon the pH of the contact solution. In order to find out the surface charge of the zeolite composite

membranes, the zeta potential of FAU and MFI zeolite powder particles in solution is measured by electrostatic light scattering method. The surface potential of zeolite powders is altered by the addition of NaOH to make higher pH and HCl solution is added to make lower pH. The surface charge of zeolites becomes positive due to larger amount of H^+ ions at lower pH and at higher pH, negative hydroxyl (OH^-) ions become more. Therefore, the zeta potential value is 4 mV for FAU zeolite and 11.5 mV for MFI zeolite at pH 2 while it is approximately -45 mV for FAU zeolite and -62.42 mV for MFI zeolite at pH 12, respectively. Hence, electrostatic interactions play a major role in the surface activity of FAU zeolite. The iso-electric point (IEP) of FAU and MFI zeolite powder is obtained to be 3.8 and 4.0, respectively. When pH is < IEP, the zeolite membrane is positively charged and if pH > IEP, it is negatively charged.

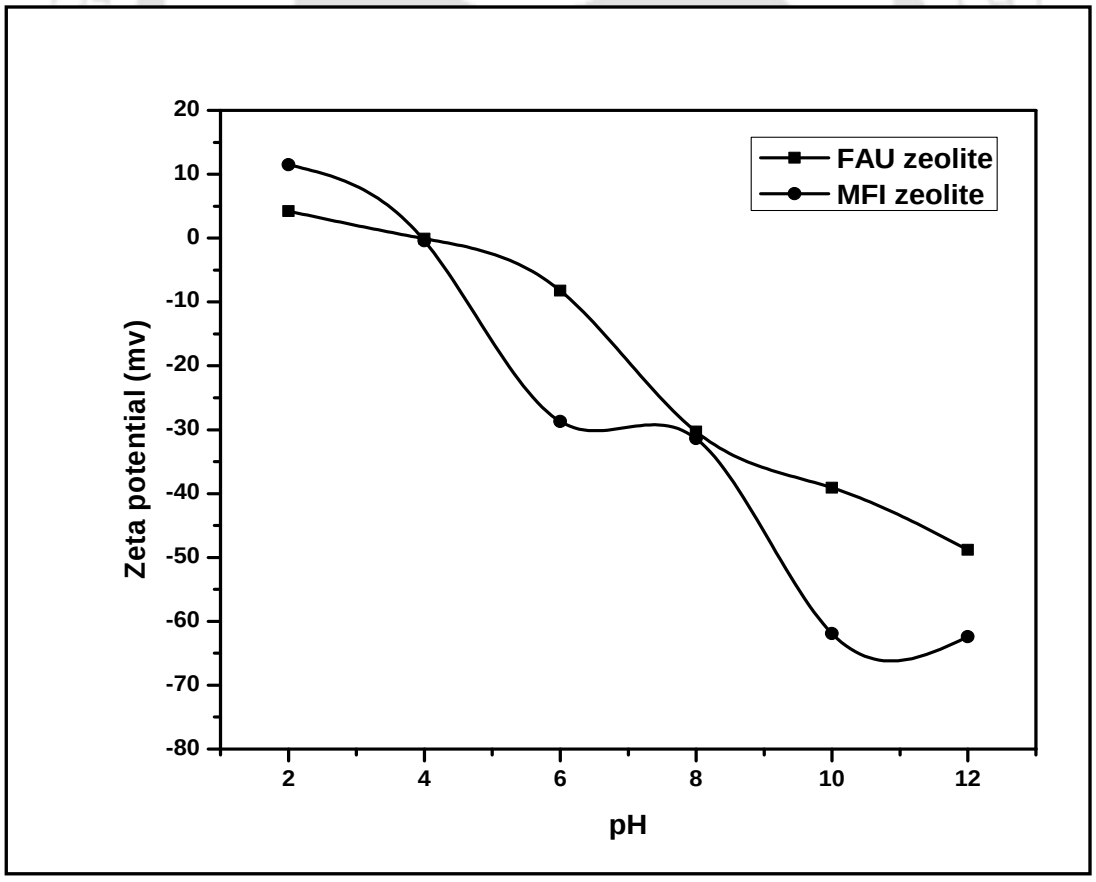

Figure 4.9: Zeta potential measurement of FAU zeolite

4.2.1.5 Particle size distribution

Particle size and shape of the particle is important parameter that controls the porosity and pore size of membrane. Smaller particles (less than the membrane pore size) can easily penetrate in the membrane pores and reduce the pore size. On the other hand, larger particles are stick on the membrane surface and also reduce the pore size. Figure 4.10 shows the particle size distribution of the as synthesized FAU zeolite particles. The average particle size of the FAU zeolite is calculated to be 157 nm.

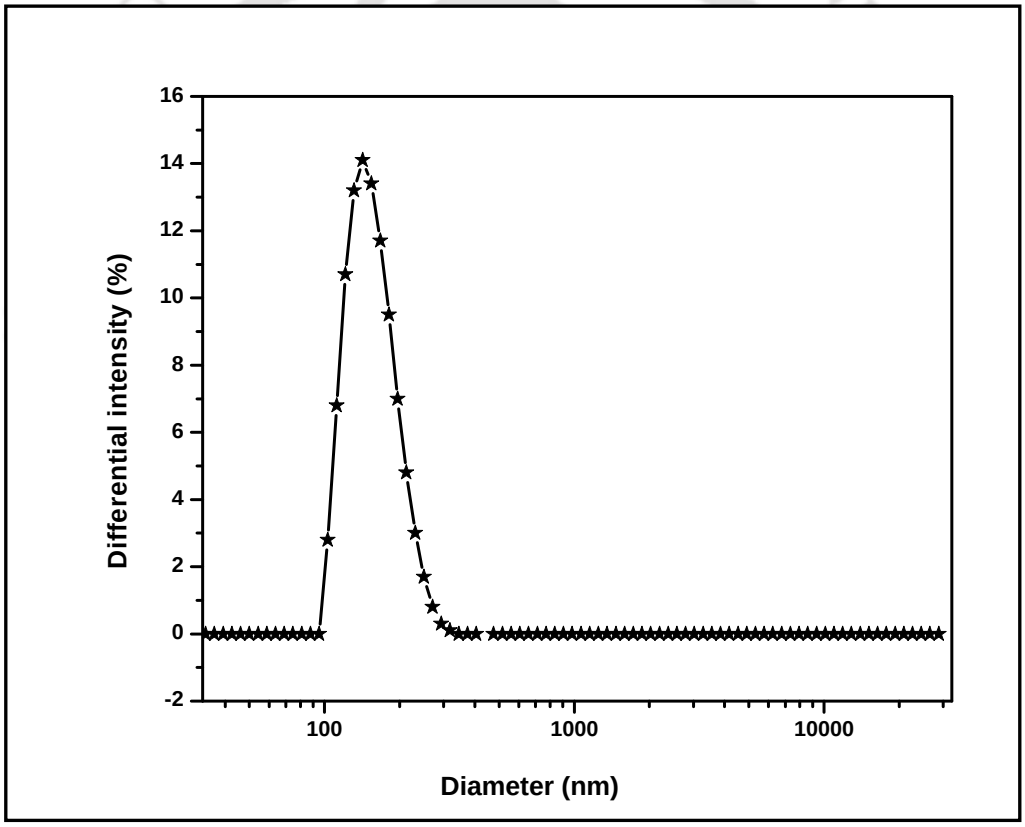

Figure 4.10: PSD of FAU zeolite

Figure 4.11 illustrates the particle size distribution of the MFI zeolite particles before and after calcination. It is to be noted that the average particle size is 972.4 nm and 1,005 nm for

before and after calcination, respectively. This indicates that the average particle size is slightly increased after calcination.

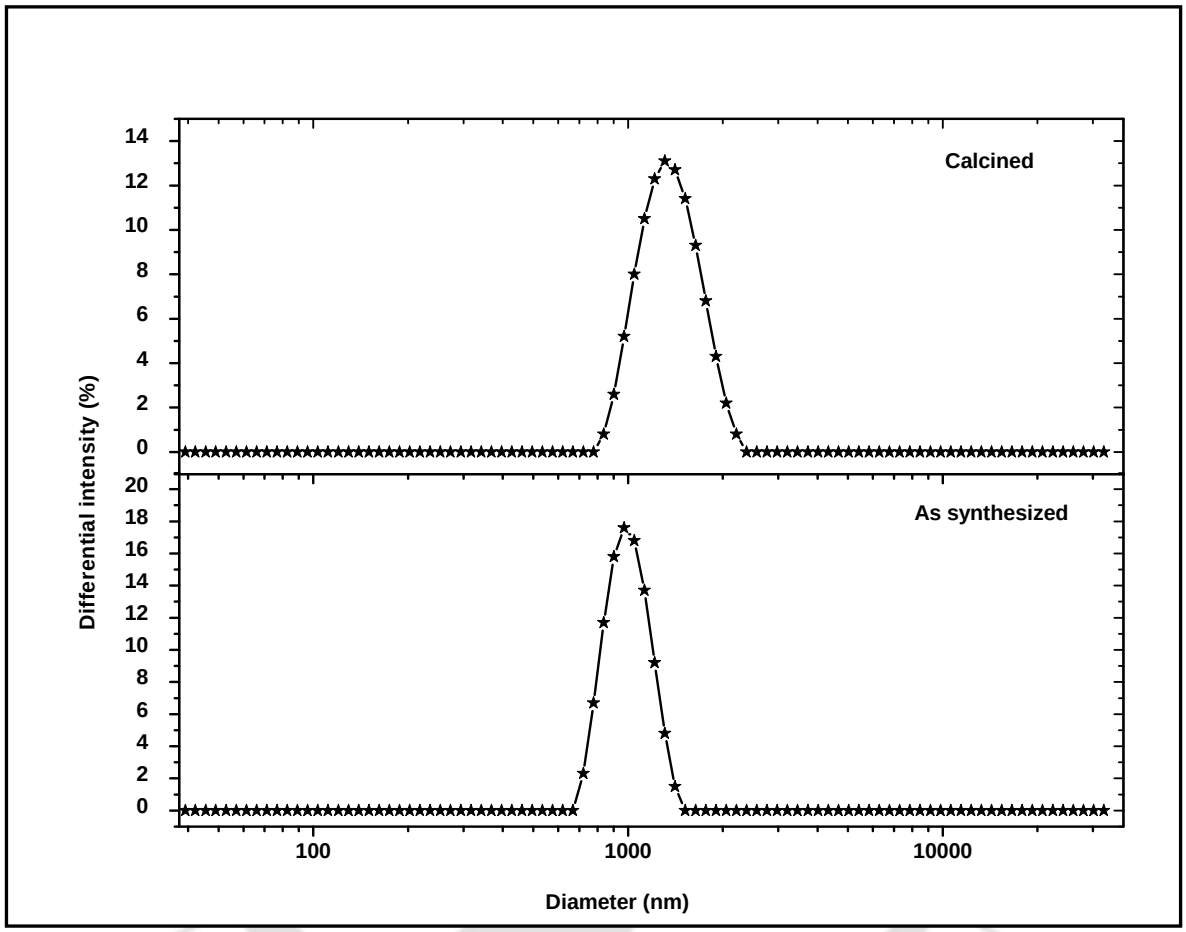

Figure 4.11: PSD of MFI zeolite

4.2.2 Characterization of FAU and MFI zeolite composite membranes

Figure 4.12 shows the FESEM images of inner (a) and outer (b) surfaces of ceramic support, inner (c) and outer (d) surfaces of FAU zeolite composite membrane and inner (e) and outer (f) surfaces MFI zeolite composite membrane. It can be clearly seen that the synthesized zeolites are homogeneously dispersed in the cubic structure of FAU and interconnected pattern of MFI

zeolite crystals on the membrane surfaces. These images illustrate the inner and outer top surfaces of the membranes after hydrothermal coating of zeolites at the same magnifications.

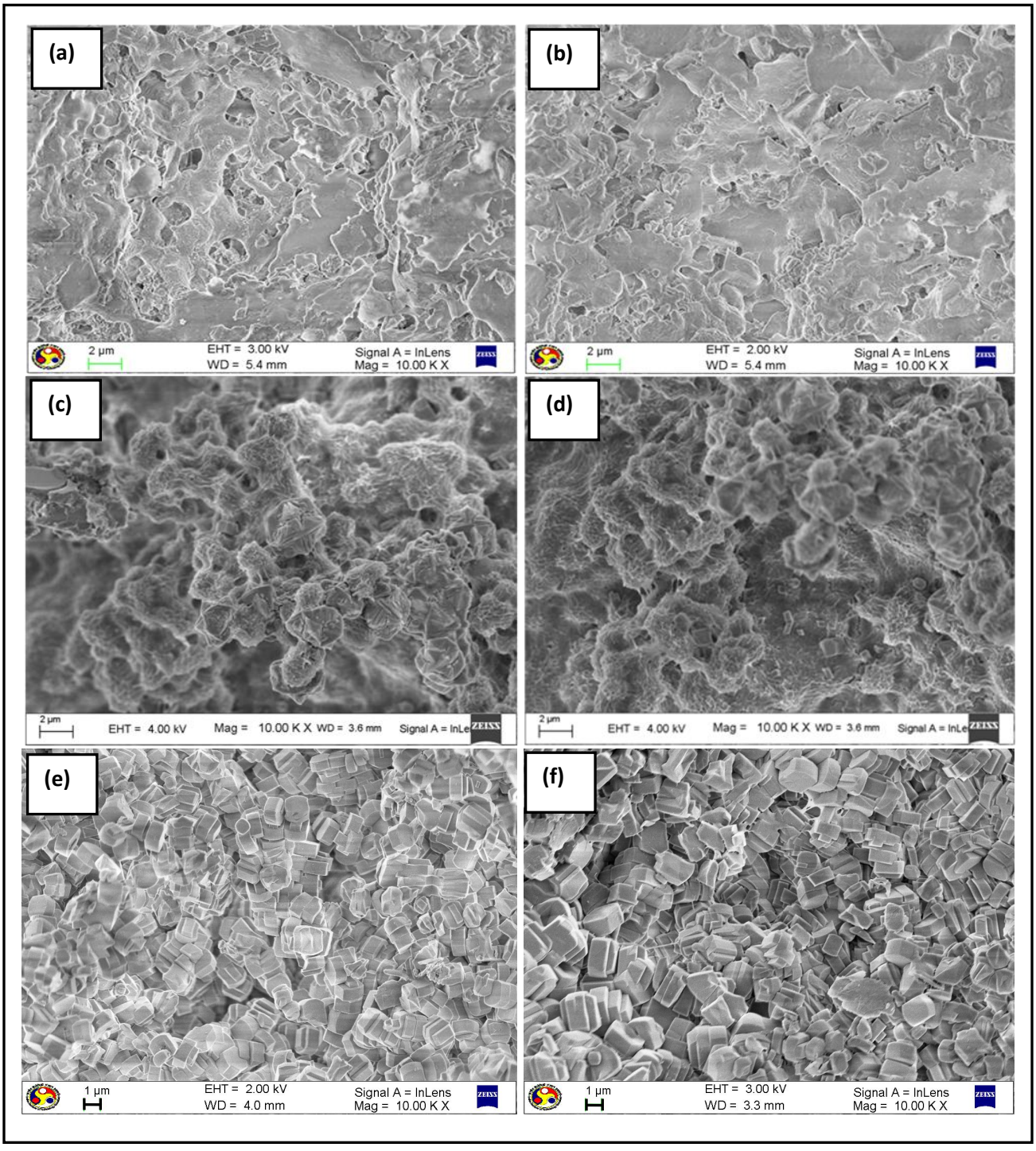

Figure 4.12: FESEM images of (a) inner and (b) outer surfaces of ceramic support, (c) inner and (d) outer surfaces of FAU and inner (e) and outer (f) surfaces MFI zeolite composite membranes.

It can be clearly seen that the synthesized FAU and MFI zeolites are homogeneously dispersed on the both sides of membrane surfaces. In the zeolite deposition process, the layers of FAU and MFI zeolite crystals completely covered the ceramic support with no observable macro-cracks. Figure 4.13 shows FAU (a) and MFI (b) zeolite crystals, as well as cross sectional views of FAU (c) and MFI (d) zeolite composite membranes. These figures (4.13 a-b) evidently proves that the pores of the ceramic support blocked by the zeolite particles. The overall morphological study concludes that the sufficient amount of zeolite crystals is loaded on the ceramic support surface, resulting in the formation of a compact composite membrane.

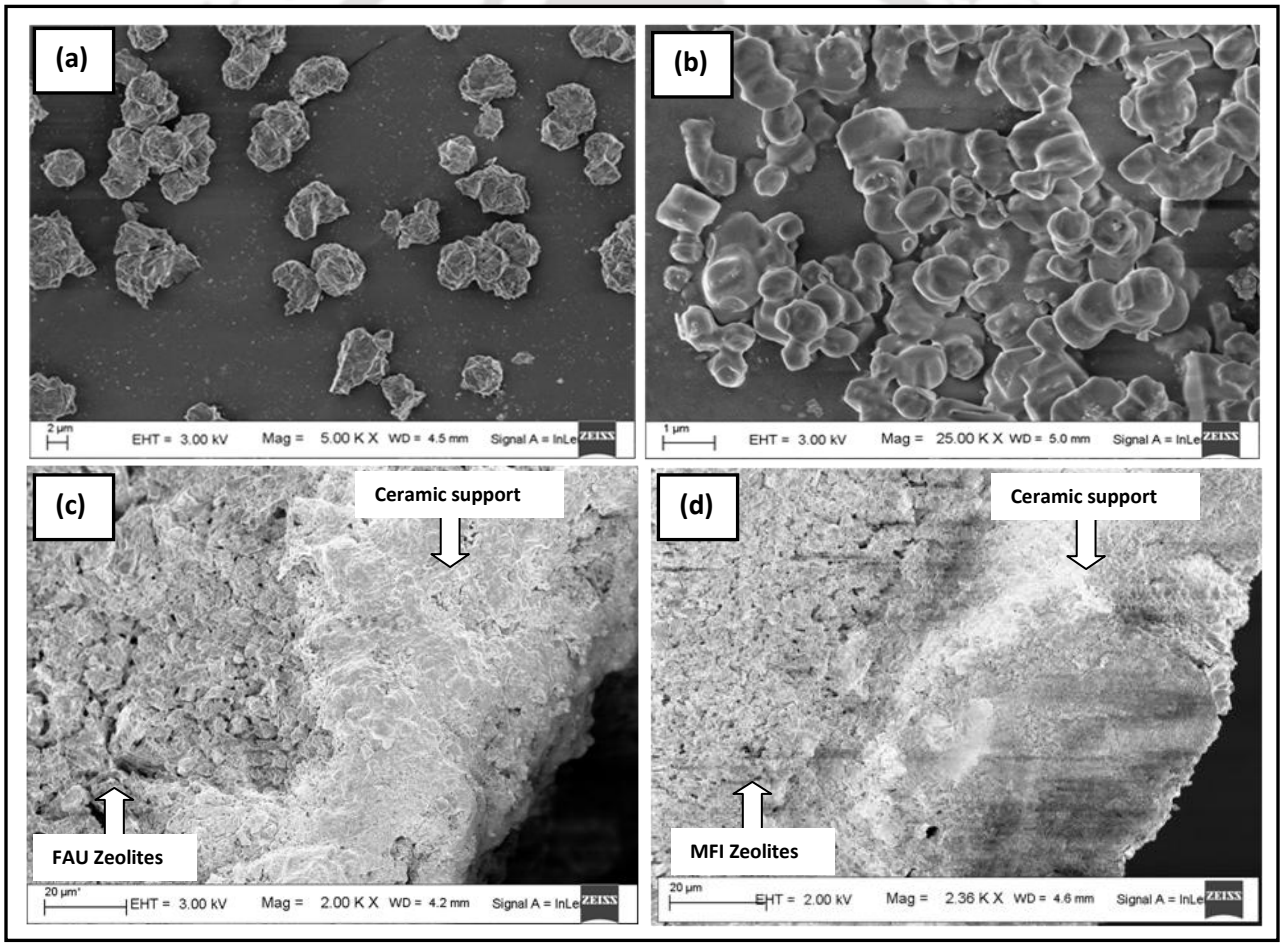

Figure 4.13: FESEM images of FAU (a) and MFI (b) zeolite crystals, as well as cross sectional views of FAU (c) and MFI (d) zeolite composite membranes.

The average porosity is evaluated to be 53%, 43% and 51%, for ceramic support, FAU and MFI zeolite membrane, respectively. The reduction in the porosity of the composite membranes clearly points out the deposition of zeolite materials on the ceramic support. The water flux obtained for the ceramic support, FAU and MFI zeolite composite membranes as a function of time for various applied pressures is presented in Figure 4.14(a-c). The steady flux is attained for the entire measured time for support as well as composite membranes. Figure 4.14(d) depicts the pure water flux of ceramic support along with zeolite membranes as a function of applied pressure. It can be noticed that the water flux increases linearly with an increase in the applied pressures (69 - 345 kPa). This stipulates that the variation in the pressure is the barely driving force for permeation. For transportation operation exclusively by convection, the flow rate is proportionate to the pressure, and is in accordance with Darcy's law. It is also evident from figure that the water flux of the zeolite composite membranes is reduced, which is accredited by the reduction in pore radius on hydrothermal treatment. The water permeability of the membrane was calculated from the slope of water flux versus applied pressure across the membrane (from Figure 4.14(d)) and pore size estimated using Hagen Poiseuille equation was explained in chapter 2. The water permeability of the ceramic support, FAU and MFI composite zeolite membrane is calculated as 5.93×10^{-7} $m^3/m^2s.kPa$, 1.62×10^{-7} $m^3/m^2s.kPa$ and 4.43×10^{-7} $m^3/m^2s.kPa$, respectively. Workneh and Shukla (2008) reported water permeability value for sodalite octahydrate zeolite-clay composite membrane as 7.50×10^{-8} $m^3/m^2s.kPa$. In another study, the values of water permeability determined were 7.94×10^{-8}, 5.54×10^{-8} and 3.89×10^{-8} m/s kPa for unmodified, nitrated and aminated zeolite composite membranes, respectively by Shukla and Kumar (2007). It is identified that the water permeability of the prepared FAU and MFI zeolite membranes are higher than that of others membranes reported in the literature (Workneh and Shukla 2008; Shukla and Kumar 2007). The pore size of the FAU

and MFI zeolilte membrane is evaluated to be 0.179 and 0.272 µm, respectively, which is lower than that of ceramic support (0.309 µm). For FAU coating, the weight of the membrane was increased from 8.7993 g (support) to 9.9273 g (FAU membrane) and for the MFI coating, the weight of the membrane was increased from 8.8347 g (support) to 9.5191 g (MFI membrane), respectively.

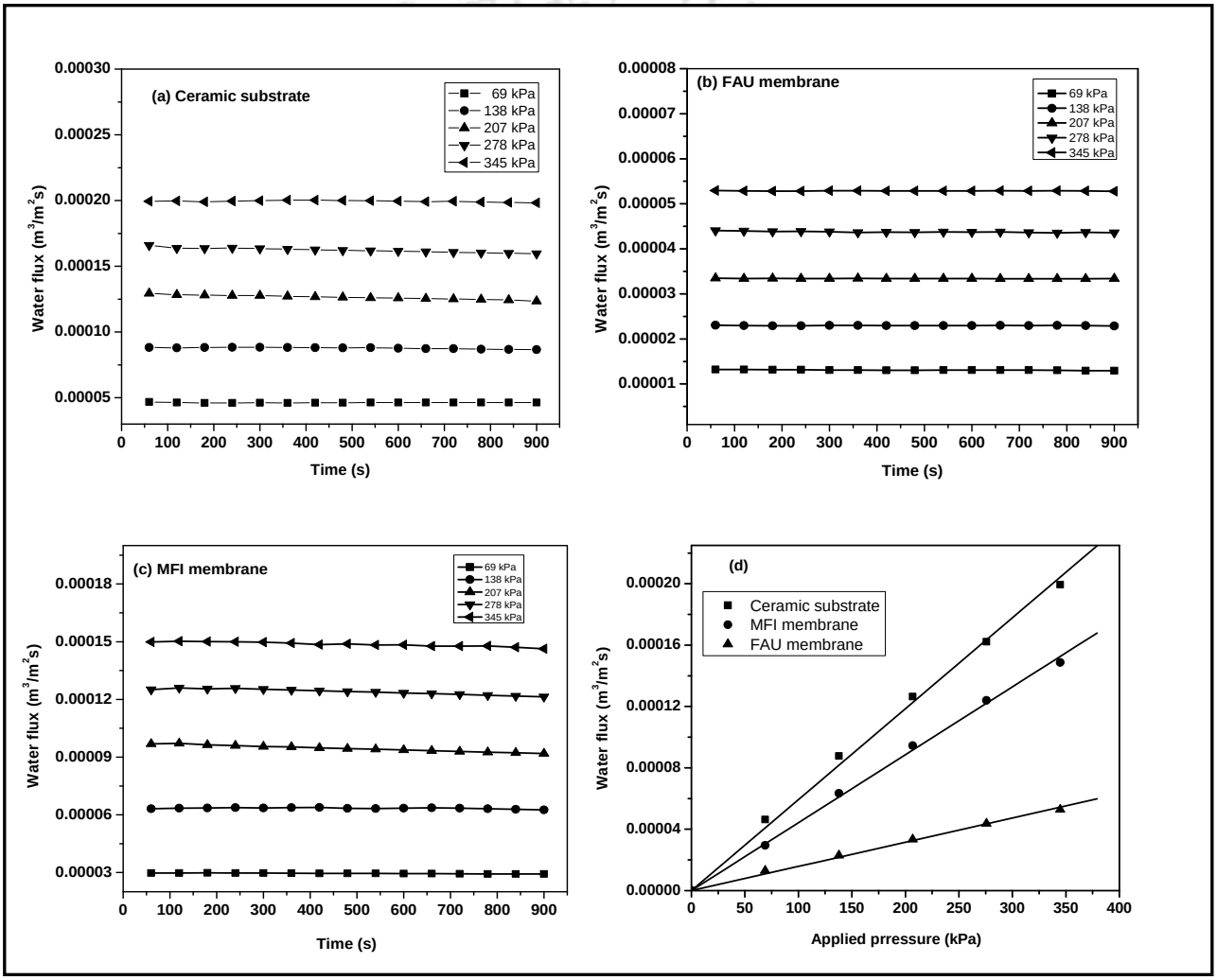

Figure 4.14: Water flux as a function of time for (a) ceramic substrate, (b) FAU membrane, (c) MFI membrane and (d) pure water flux as a function of applied pressure for substrate and zeolite membranes

The porosity, pore size and water permeability of the MFI zeolite membrane is higher as compared to FAU zeolite membrane. This is due the quantity of FAU zeolite deposition (1.128 g) on ceramic support is more than that of MFI (0.6844 g). As stated above, the porosity, water permeability and pore size of the zeolite membrane are decreased and mass of the membrane is increased after coating, which is obviously due to the incorporation of respective zeolite layer on the ceramic support by hydrothermal treatment. The overall characterization results obtained for the ceramic support, FAU and MFI zeolite composite membrane is presented in the Table 4.1.

Table 4.1: Characterization results of ceramic support, FAU and MFI zeolite composite membrane

Properties	**Ceramic support**	**FAU zeolite membrane**	**MFI zeolite membrane**
Porosity (%)	53	43	51
Average pore size (μm)	0.309	0.179	0.272
Water permeability ($m^3/m^2s.kPa$)	5.93×10^{-7}	1.62×10^{-7}	4.43×10^{-7}
Weight (g)	8.7993	9.9273	9.5191

4.3 Summary

FAU and MFI type zeolite composite membranes were effectively fabricated on porous low cost tubular ceramic support by hydrothermal treatment method. In XRD patterns, the observed peak at 2θ value of 12.40 demonstrated the formation of a high degree of crystallinity and all peaks are consistence with FAU zeolite. The distinctive peaks obtained at 2θ value of 7.5 and 23.5 signified the occurrence of pure phase of the MFI zeolite. The ceramic support was layered with homogeneous dispersion of FAU and MFI zeolite crystals and the zeolites facilitated to

form a uniform FAU and MFI zeolite membranes. The porosity of ceramic support (53%) was reduced by the deposition of FAU (43%) and MFI (51%) zeolite layers. The pore size of the FAU and MFI zeolilte membrane was evaluated to be 0.179 and 0.272 μm, respectively, which is lower than that of support (0.309 μm). The water permeability of the ceramic support, FAU and MFI zeolite membrane was calculated as 5.93×10^{-7} $m^3/m^2s.kPa$, 1.62×10^{-7} $m^3/m^2s.kPa$ and 4.43×10^{-7} $m^3/m^2s.kPa$, respectively. As stated above, these decreased values obtained are obviously due to the incorporation of the zeolite layers on the ceramic support by hydrothermal treatment.

Chapter 5

Removal of chromium from aqueous solution using FAU and MFI type zeolite membranes supported on low cost tubular ceramic substrate

---

Removal of chromium from aqueous solution using FAU and MFI type zeolite membranes supported on low cost tubular ceramic substrate

This chapter describes the potential of FAU and MFI type zeolite membranes supported on low cost tubular ceramic support for the removal of chromium from an aqueous solution with homemade cross flow filtration setup. The various influencing process parameters, such as applied pressure, initial feed concentration and cross flow rate on permeate and rejection were investigated. Additionally, the potential of the membranes were compared with other membranes reported in the literature for chromium removal application.

5.1 Experimental

All the chromium removal tests were carried at an ambient temperature (~25 °C) by using the fabricated FAU and MFI zeolite membranes on low cost tubular support in laboratory scale cross flow microfiltration system presented in chapter 2 (section 2.2.2.4) and 3 (section 4.12), respectively. The analytical grade chromium (VI) oxide obtained from Merck (India) Ltd., Mumbai was utilized for filtration tests. The required concentration aqueous solution of chromium was prepared with Millipore water and its concentration was calculated using conductivity meter (Eutech Instruments, Model: CON 2700). In order to avoid the contribution of surface adsorption of chromate ions, the first ~50 ml of permeate solution was thrown away and subsequent permeated solution through membrane was considered to calculate the percentage removal of chromium at each conditions. At the end of each experiment, the membrane was properly washed with Millipore water followed by flushing with Millipore water for 1 h at higher pressure to regain the original pure water flux. The permeate flux and

the rejection of chromium solution were investigated as a function of operating parameters such as applied pressure, concentration of the feed solution and cross flow rate of the filtration process. In order to study the inference of applied pressure, the experiments were performed for a period of 1 h at five different pressures (69-345 kPa) for a fixed concentration of chromium solution (1000 ppm) with natural pH of the solution (~2.35). The effect of concentration on the permeate flux and rejection was conducted by changing five different concentrations (250-3000 ppm) at an applied pressure of 69 kPa. The influence of cross flow rate in the range of 5.55×10^{-7} - 1.66×10^{-6} m^3/s was also examined at a fixed feed concentration (1000 ppm) and an applied pressure of 69 kPa.

The percentage removal of chromium was determined by below expression:

$$R(\%) = \frac{C_f - C_p}{C_f} \times 100 \qquad (5.1)$$

where, C_f is the concentration of chromium in the feed stream, C_p is the concentration of chromium in the permeate stream and R is the observed rejection (%).

5.2 Results and discussion

5.2.1 Potential of FAU and MFI zeolite in chromium removal

The fabricated FAU and MFI zeolite ceramic membranes were applied for the removal of chromium present in the aqueous medium. Applied pressure, initial feed concentration and cross flow rates are the important variables that influence the filtration process in terms of permeate flux and rejection. Hence, the effect of these parameters was investigated as a function of time.

5.2.1.1 Influence of applied pressure on zeolite composite membranes

Figure 5.1 shows permeate flux profiles of FAU and MFI zeolite membranes with time for various applied pressures (69, 138, 207, 278 and 345 kPa) at a fixed cross flow rate of 1.11×10^{-6} m^3/s with feed concentration of 1000 ppm. It is observed from these figures that the flux of zeolite composite membranes is augmented with an increase in the applied pressure owing to enhancement of driving force. It can also be noticed from Figure 5.1(a) that the variation of permeate flux with time is almost negligible in 1 h operation and similar patterns are also observed with MFI zeolite composite membranes (Figure 5.1(b)). The permeate flux varies almost linearly with increasing applied pressure for both the zeolite composite membranes. This may be due to the fact that there is no significant contribution of additional transport resistance from concentration polarization and adsorption. On the other hand, the chromium flux is marginally lesser than to water flux of the membrane. This typical trend is obtained owing to the generation of osmotic pressure by the retained ions, which leads to decrease the effectual pressure on the membrane surface. Rashdi et al. (2015) also observed the improvement of permeate flux with enhancing applied pressure for the separation of heavy metal ions by cross flow nanofiltration with commercial NF270 membrane. Figure 5(c) illustrates the permeate flux of FAU and MFI zeolite membranes as a function of applied pressure. Compare to FAU membrane, the MFI membrane displays marginally higher flux value; this may be due to a bigger pore size of MFI membrane (0.272 μm) when compared to FAU membrane (0.179 μm). The deposition of zeolites on the ceramic support acquires promising steady permeate flux with the removal of chromium. This may be due to better compatibility of liquid phase separation of both zeolite membranes.

Figure 5.2(a-b) shows percentage removal of chromium with time for FAU and MFI zeolite membranes at different applied pressures with fixed cross flow rate of 1.11×10^{-6} m^3/s. For both

the zeolite membranes, the percentage removal of chromium gradually augments for all the studied pressure with the filtration time. This is possibly due to the development of concentration polarization until reach the steady state with time on the surface of the membrane. The percentage of chromium removal increases with an increment in the applied pressure. This is possible due to the formation of concentration polarization effect doesn't occur at the initial period of operation and at low applied pressure.

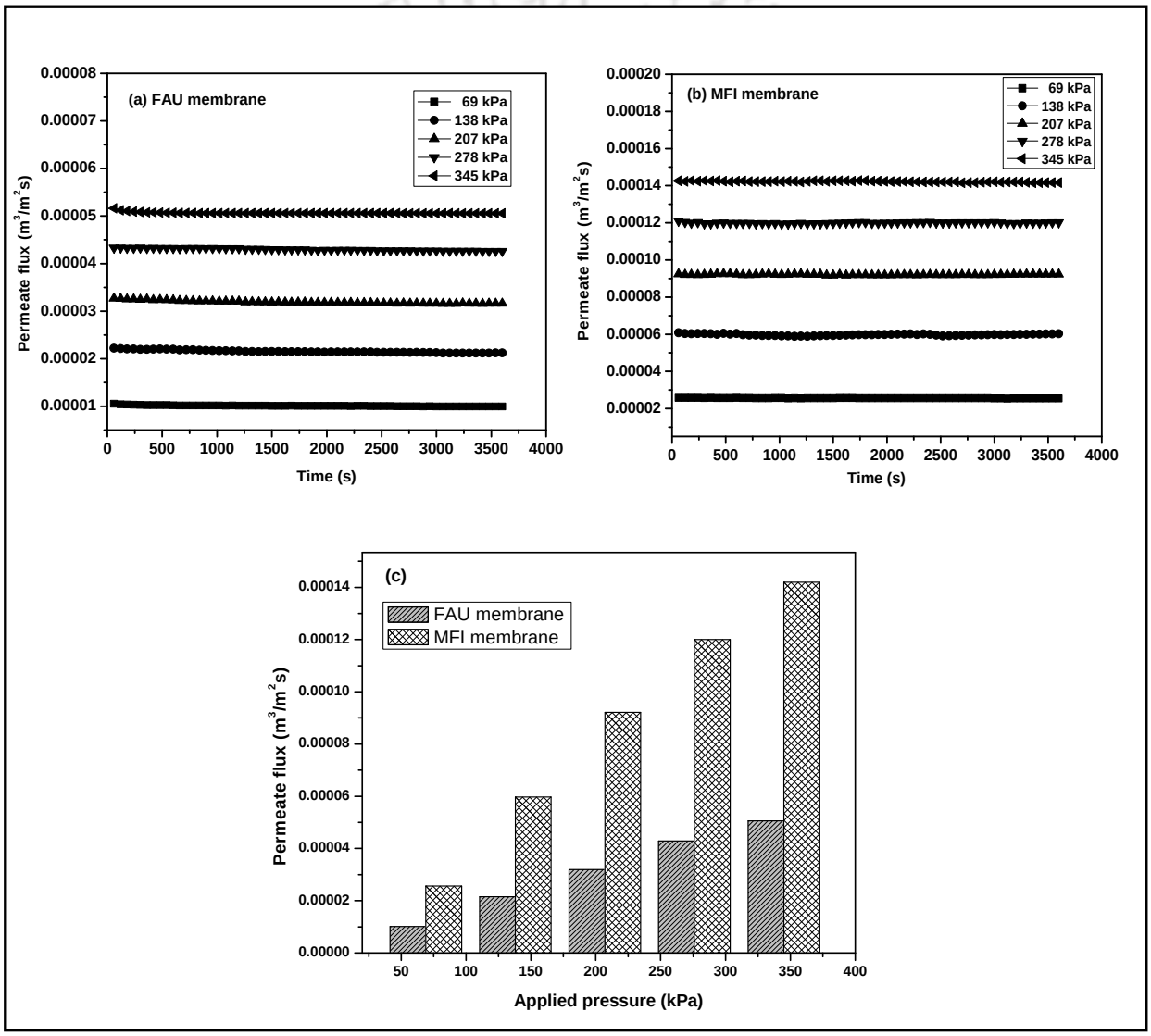

Figure 5.1: Influence of applied pressure on permeate flux with time for (a) FAU zeolite membrane, (b) MFI zeolite membrane and (c) permeate flux as a function of applied pressure for zeolite membranes (feed concentration = 1000 ppm, natural pH~ 2.35)

Conversely, it develops with increasing time owing to retention of ions within the membrane pores. When the applied pressure increases, the convective transport turns more significant than the diffusive transport. As a result, the percentage removal of chromium enhances with increasing pressure due to the dilution effect, as the higher transport of solvent flux would result in a dilution of permeate. Therefore, the higher applied pressure facilitates to attain higher removal of chromium (Gherasim and Mikulasek 2014).

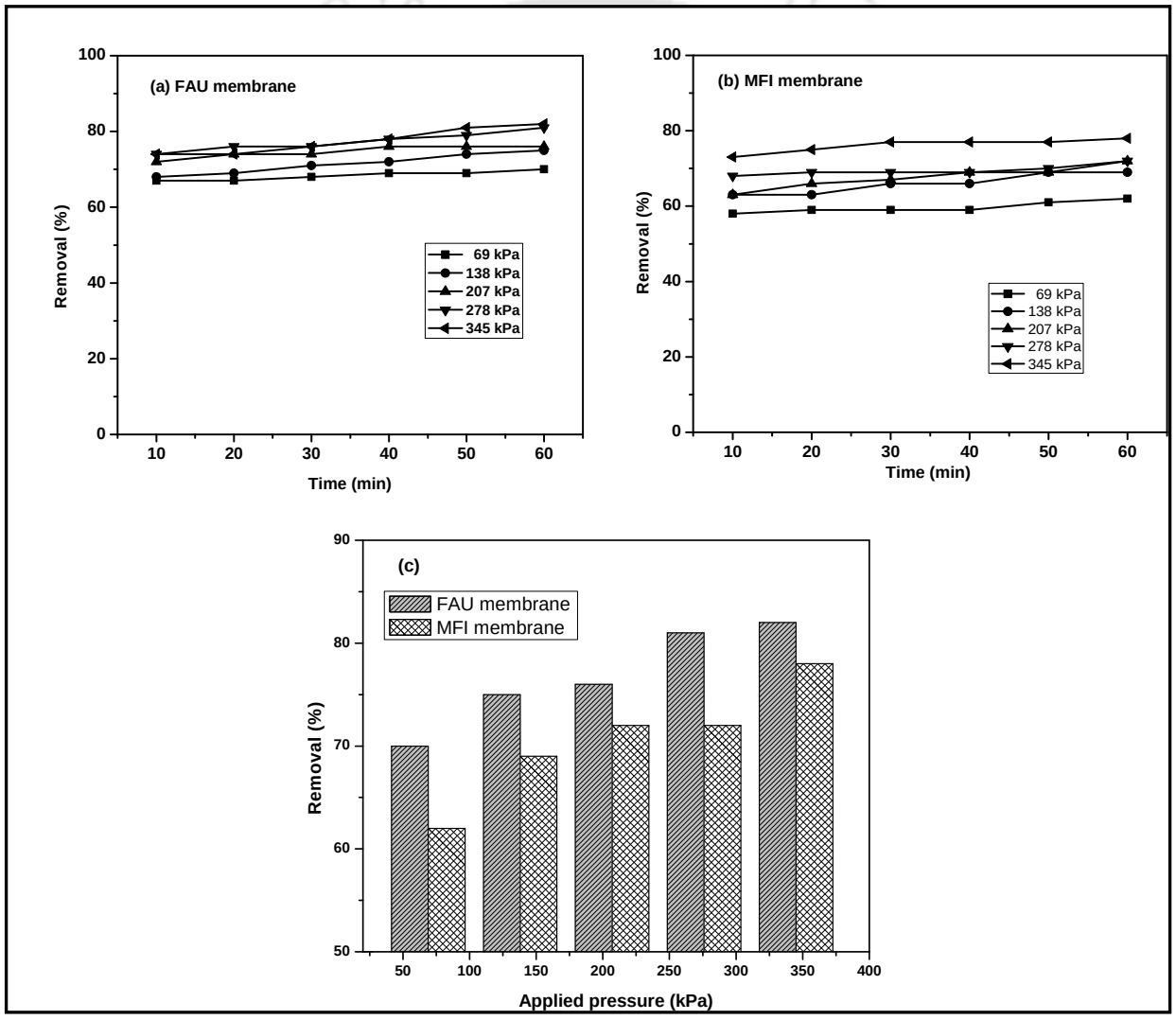

Figure 5.2: Influence of applied pressure on removal (%) with time for (a) FAU zeolite membrane, (b) MFI zeolite membrane and (c) removal as a function of applied pressure (feed concentration = 1000 ppm, natural pH~ 2.35)

In order to get comprehensive information on the influence of applied pressure on the removal of chromium, the removal against applied pressure is plotted. Figure 5.2(c) illustrates the removal of chromium as a function of applied pressure for both the zeolite composite membranes. It represents increasing the percentage removal of chromium with an increase in the applied pressure (Mehiguene et al. 1999). The maximum removal of chromium is achieved as 82% for FAU membrane and 78% for MFI membrane under the applied pressure of 345 kPa.

The membrane surface charge is a major factor for the influential removal efficacy of the membrane while dealing with ionic solution and also it varies with the pH of the solution. The isoelectric point (IEP) of FAU and MFI zeolite membrane is estimated as 3.8 and 4, respectively, which are determined using zeta potential measurements (Chapter 4). It means, at pH of the solution less than IEP, membranes are positively charged and when pH of the solution is greater than IEP, membranes are negatively charged. FAU and MFI zeolite membrane have zeta potential value of +2.95 mV and +10.76, respectively, at natural pH (2.35) of chromium solution (1000 ppm). In aqueous solution, chromium is usually present in the form of $HCrO_4^-$, $Cr_2O_7^{2-}$ and $Cr_2O_4^{2-}$ based on the pH (Benhamou et al. 2013). In this study, the removal experiments were conducted at the natural pH of the chromium solution (~2.35). The chromium predominantly presents in the form of acid chromate ions ($HCrO_4^-$) along with H_3O^+ in this experimental condition (Benhamou et al. 2013; Basumatary et al. 2015). Since the membrane is positively charged at this pH condition, therefore, the repulsion between positively charged membrane and positive species (H_3O^+) will take place. As the cation and anion cannot act autonomously, thereby, $HCrO_4^-$ is also rejected to maintain electroneutrality of the system, as shown in Figure 5.3 (Benhamou et al. 2013; Kumar et al. 2015a; Basumatary et al. 2015). In addition to charge density, the removal of chromium also depends on the amount of zeolite

materials deposited on the ceramic support. The quantity of FAU zeolite deposition (1.128 g) on ceramic substrate is more than that of MFI (0.6844 g). Hence, the removal efficiency of FAU membrane is slightly higher compared to MFI membrane.

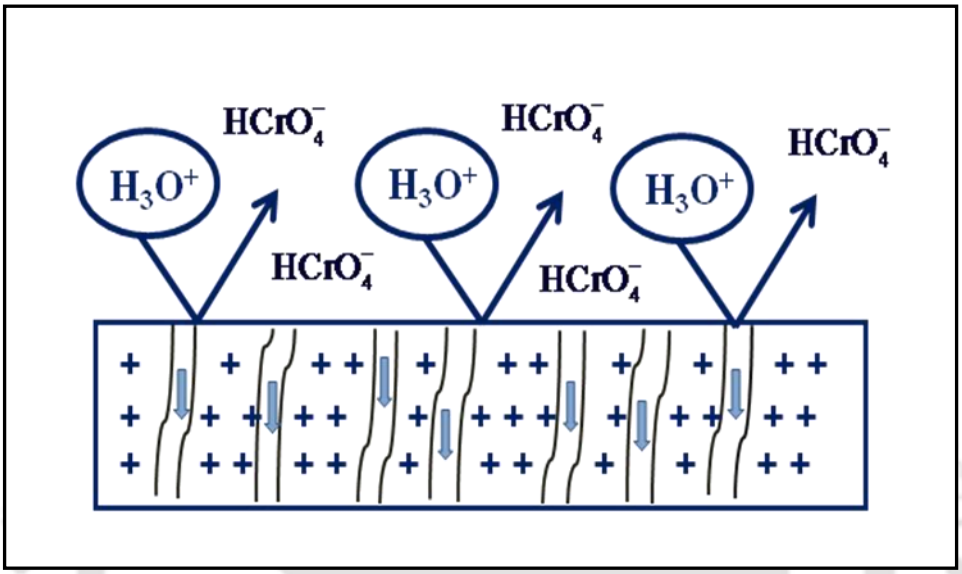

Figure 5.3: Schematic representation of chromium separation by zeolite membranes

5.2.1.2 Influence of initial feed concentration on zeolite composite membranes

Figure 5.4(a, b) demonstrates the variation of permeate flux of FAU and MFI membranes with time for various feed concentrations (250, 500, 1000, 2000 and 3000 ppm) at applied pressure of 69 kPa and the cross flow rate of 1.11×10^{-6} m^3/s. It is evident from the figure that there is a marginal decline in permeate flux for the both zeolite membranes when the chromium concentration gradually increases. This is probably due to the occurrence of incomplete plugging of the membrane pores. This leads to the creation of another barrier layer, which may have reduced the flux at higher concentration of chromium. The permeate flux of chromium slightly declines with the extension of operation time. This decrement in permeate flux is probably due to the chromium ions fouling (Habibi et al. 2015). As shown in the Figure 5.4(c),

the MFI membrane provides higher permeate flux in comparison with FAU membrane. This is due to higher pore size of MFI membrane over FAU membrane as discussed in the earlier section. It is apparent that the percentage removal of chromium augments with an increment in the initial feed concentration of chromium as displayed in Figure 5.5.

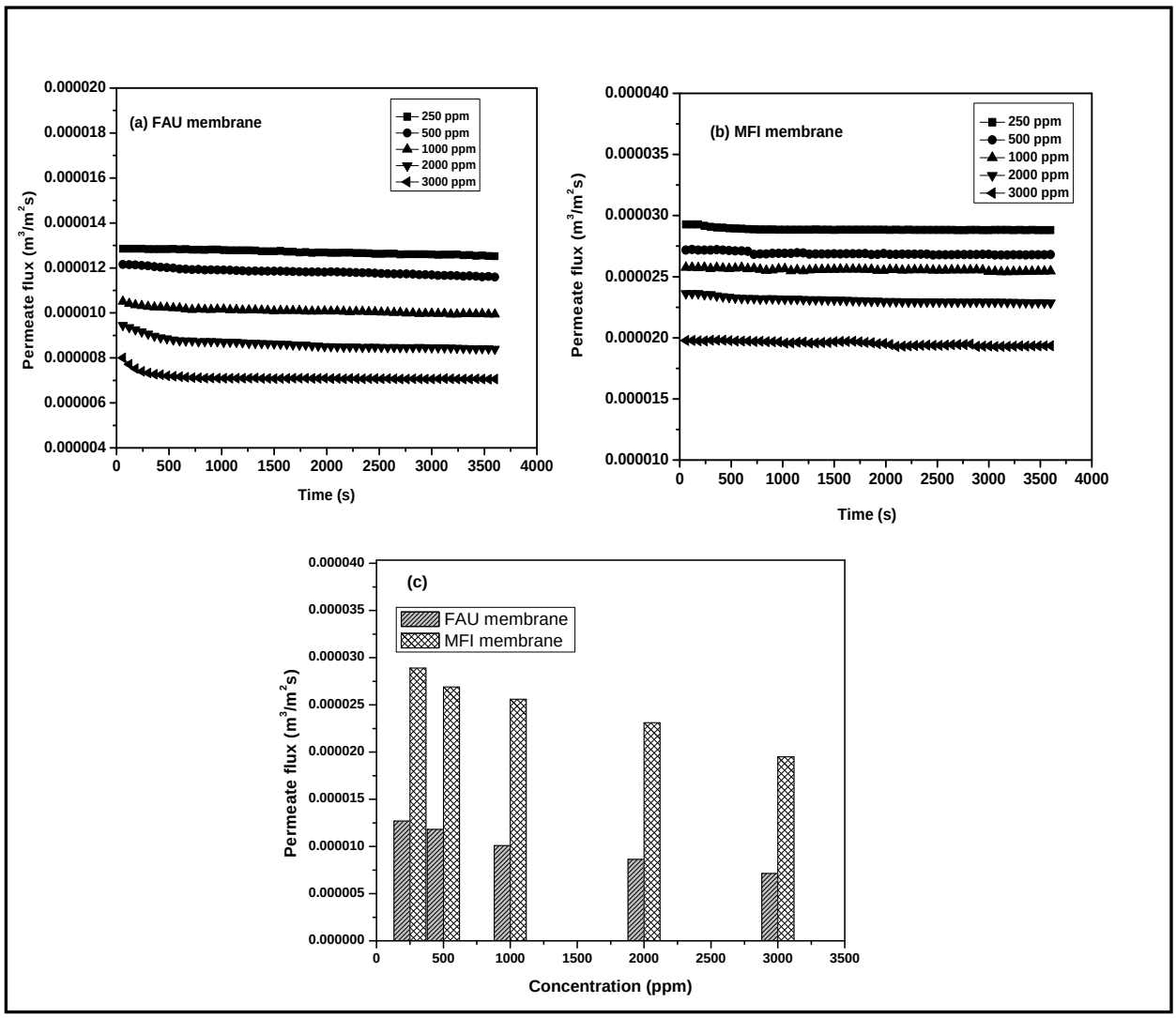

Figure 5.4: Influence of initial feed concentration on permeate flux with time for (a) FAU zeolite membrane, (b) MFI zeolite membrane and (c) permeate flux as a function of feed concentration for zeolite membranes (Applied pressure = 69 kPa, cross flow rate: 1.11×10^{-6} m^3/s).

This is primarily attributed to various factors such as, concentration polarization, osmotic pressure and membrane fouling across the membrane surface. In the studied concentration ranges, the highest percentage of removal 81% and 76% is obtained using FAU and MFI zeolite composite membrane, respectively for the feed concentration of 3000 ppm.

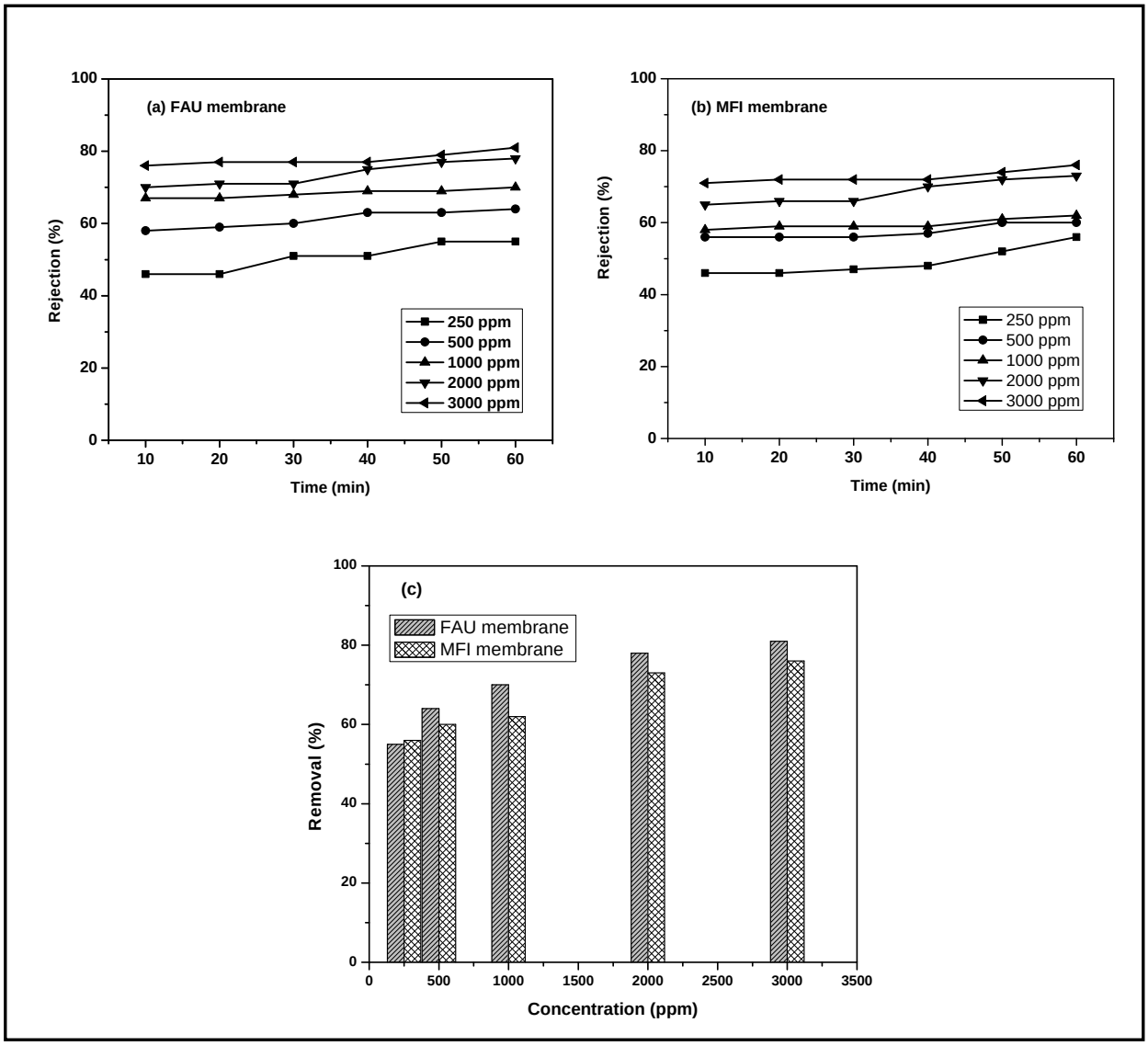

Figure 5.5: Influence of of initial feed concentration on removal (%) with time for (a) FAU zeolite membrane, (b) MFI zeolite membrane and (c) removal as a function of feed concentration (Applied pressure = 69 kPa, cross flow rate: 1.11×10^{-6} m^3/s).

5.2.1.3 Influence of cross flow rate on zeolite composite membranes

Figure 5.6 represents permeate flux plots of FAU and MFI membranes with respect to time for different cross flow rates (5.55×10^{-7}, 1.11×10^{-6} and 1.66×10^{-6} m^3/s) at the applied pressure of 69 kPa and the initial feed concentration of 1000 ppm. The permeate flux augments with increasing cross flow rate due to decrement in concentration polarization at higher cross flow rate. Increment in cross flow rate induces the shear stress across the membrane surface, thereby minimizes the chance of chromium adsorption on the membrane surface. Cross flow rate plays substantiate role in diminishing the concentration polarization by its wiping behavior on the membrane surface. Therefore, the probability of causing resistance as well as fouling is lesser for both the zeolite membranes as shown in Figure 5.6(a, b). Moreover, the convective force is improved while decrement in concentration polarization, thereby enhances the solvent flux owing to its uncoupling nature of the solvent and solute flux during operation. Figure 5.6(c) depicts the permeate flux of chromium against three cross flow rate of 5.55×10^{-7}, 1.11×10^{-6} and 1.66×10^{-6} m^3/s for FAU and MFI zeolite composite membranes. This figure indicates that with increasing cross flow rate, the permeate flux of both the zeolite composite membrane (FAU and MFI) increases almost linearly. It is noticeable that the percentage removal of chromium slightly declines with an increment in cross flow rate as depicted in Figure 5.7. This is probably attributed to thinner boundary layer on the membrane surface at a high cross flow rate. The balance between convective transport from bulk to membrane surface and solute's diffusive transport from membrane surface to bulk at steady state may result in higher concentration of solute at the membrane. Therefore, the chromate ions can easily reach permeate side and decrease the removal (Danis and Keskinler 2009). For this reason, the percentage of chromium removal decreases with a rise in the cross flow rate. Similar trends are observed in both zeolite composite membranes (FAU and MFI) (Figure 5.7(a, b)). In the investigated cross flow rates, the

highest chromium removal of 77 % and 70% is obtained for FAU and MFI membranes, respectively, at lower cross flow rate of 5.55 × 10^{-7} m^3/s with a fixed applied pressure (69 kPa). Figure 5.7(c) demonstrates the rejection with three flow rates for the both zeolite composite membranes. A slight decrease in rejection is observed with increasing cross flow rate for both the zeolite composite membranes. The FAU zeolite composite membrane displays a higher rejection at lower cross flow rate. The reason may be due to more quantity of FAU zeolites deposited on the ceramic support.

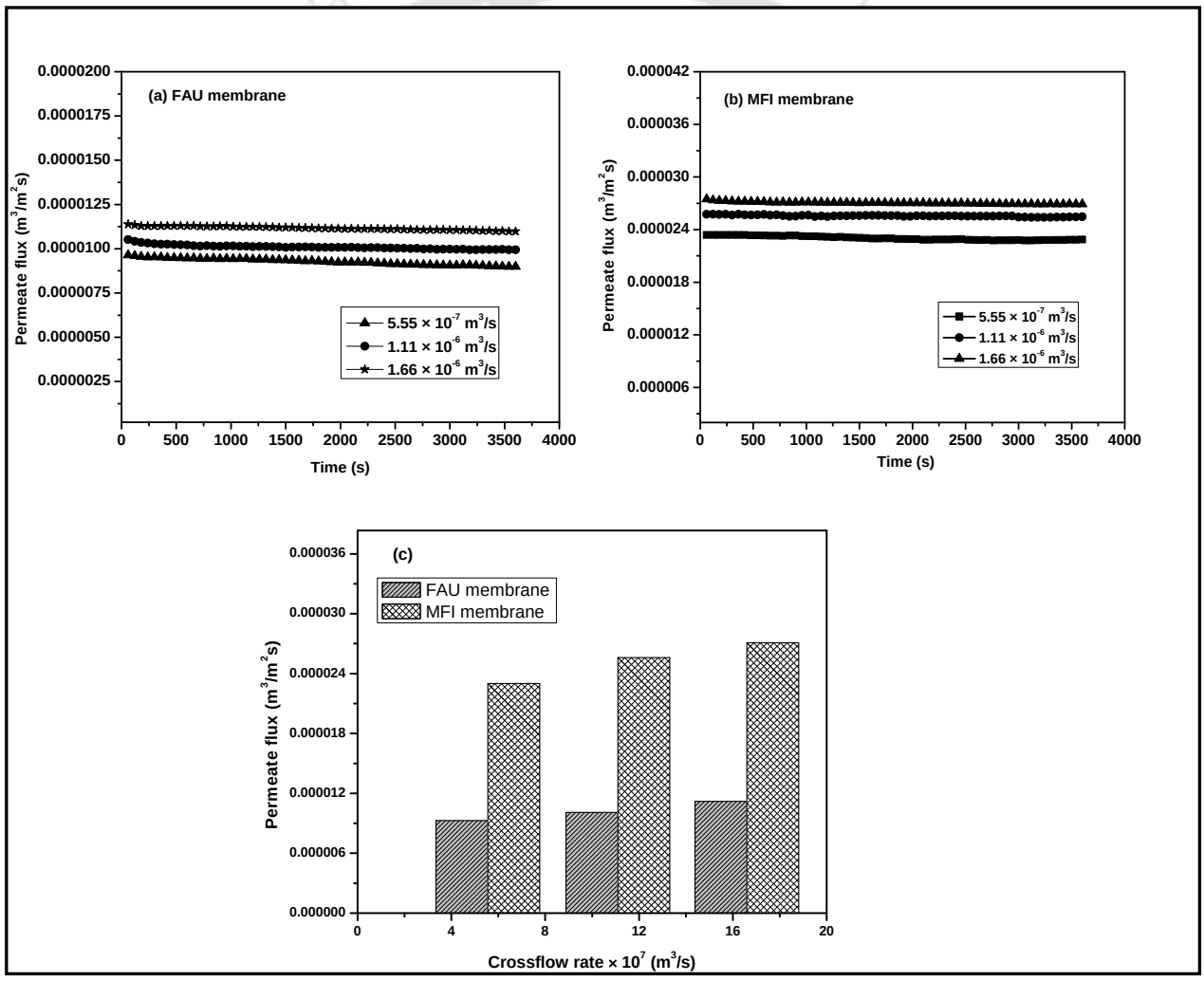

Figure 5.6: Influence of cross flow rate on permeate flux with time for (a) FAU zeolite membrane, (b) MFI zeolite membrane and (c) permeate flux as a function of cross flow rate for zeolite membranes (Applied pressure = 69 kPa, Concentration = 1000 ppm).

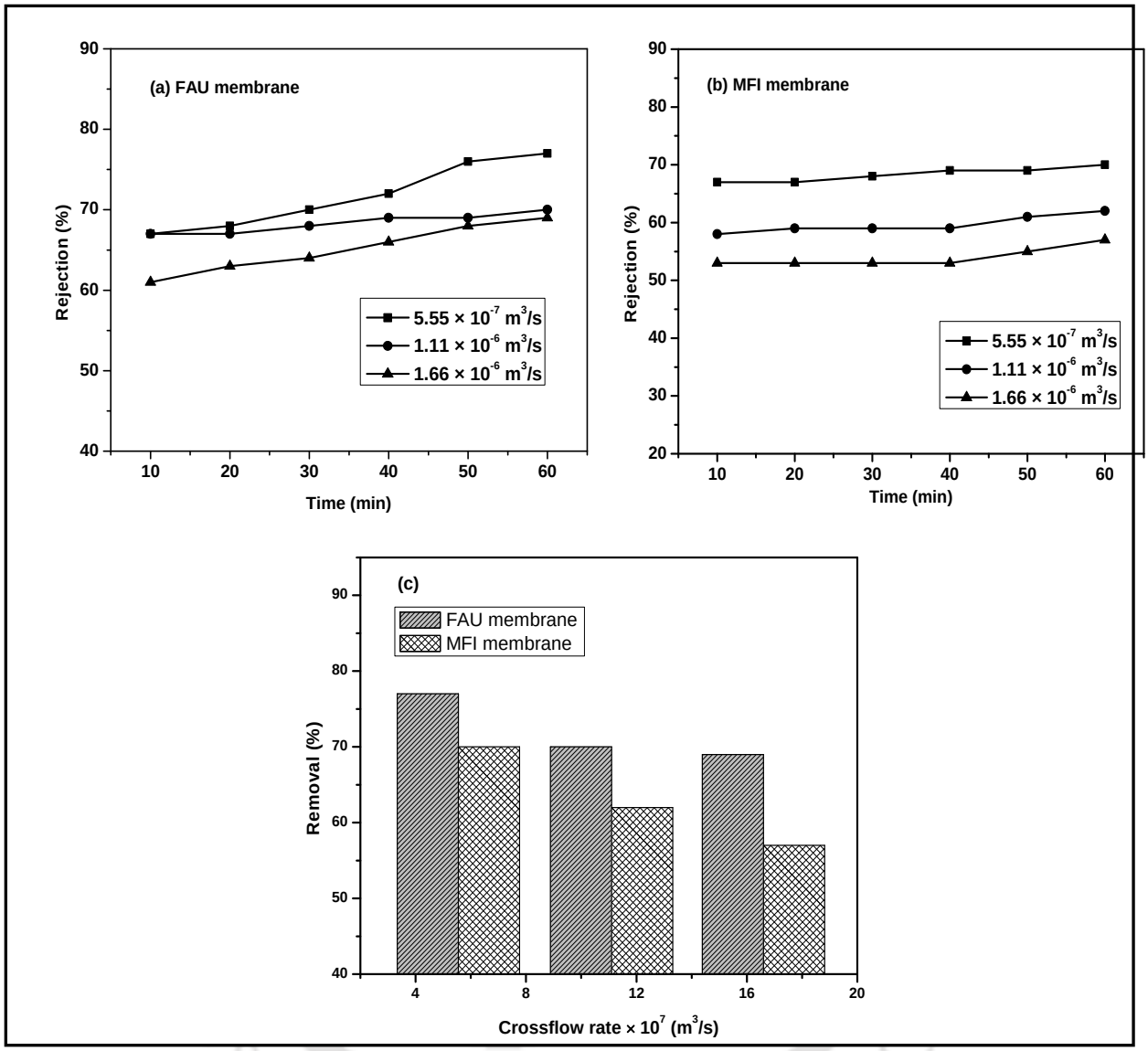

Figure 5.7: Influence of cross flow rate on removal (%) with time for (a) FAU zeolite membrane, (b) MFI zeolite membrane and (c) removal as a function of feed concentration (Applied pressure = 69 kPa Concentration = 1000 ppm).

5.2.1.4 Potential assessment of the prepared membrane with other membranes

The performance of the FAU and MFI zeolite membranes in chromium removal is analyzed with other membranes reported in the literature. It is evident from the Table 5.1 that the highest

removal of 82% with permeate flux of 5.05 × 10^{-5} m^3/m^2s for FAU membrane and 78% with permeate flux of 1.42 × 10^{-4} m^3/m^2s for MFI membrane achieved in this exertion is considerably equivalent and more preferable than those described in the literature. Neelakandan et al. (2003) obtained 68% of chromium rejection with lower permeate flux of 5.96 × 10^{-10} m^3/m^2s using NO_x modified PMMA-EGDM composite membrane. Shukla and Kumar (2007) acquired 66% of chromium rejection with permeate flux of 2.73 × 10^{-6} m^3/m^2s by zeolite-clay composite membrane. In the work investigated by Pugazhenthi et al. (2005), carbon membrane exhibited 96% of chromium rejection with permeate flux of 1.464 × 10^{-8} m^3/m^2s for feed concentration of 1000 ppm.

Table 5.1: Potential assessment of FAU and MFI zeolite composite membranes with other membranes on chromium(VI) removal

Membrane Material	Pore size	Feed concentration (ppm)	Solute permeability (m^3/m^2s)	Rejection (%)	Authors
PMMA-EGDM	8.5 kDa	1000	5.96 ×10^{-10}	68	Neelakandan et al. (2003)
Zeolite-clay membrane	30 nm	1000	2.73×10^{-6}	66	Shukla and Kumar (2007)
Clay -carbon	2 nm	1000	1.46×10^{-8}	96	Pugazhenthi et al. (2005)
Styrene acrylonitrile	55 nm	1000	2.38×10^{-6}	90	Sachdeva and Kumar (2008)
FAU zeolite membrane	0.179 µm	1000	5.05×10^{-5}	82	This study
MFI zeolite membrane	0.272 µm	1000	1.42×10^{-4}	78	This study

In another study, the styrene acrylonitrile composite membrane prepared by Sachdeva and Kumar (2008) demonstrated around 90% removal with permeate flux of 2.38×10^{-6} (m^3/m^2s). Even though, some of the membranes showed higher percentage removal of chromium in comparison with the present work, the flux (5.05×10^{-5} m^3/m^2s for FAU and 1.42×10^{-4} m^3/m^2s for MFI) of present study is 1 - 6 order higher when compared with other membranes reported in the literature (see Table. 5.1) and also the membrane displays a reasonable removal percentage (82% and 78%). From the assessment survey, it can be stated that the fabricated FAU and MFI zeolite membranes are better than that of other membranes reported in the literature. Among the investigated composite membranes (FAU and MFI) in this study, FAU zeolite membrane is better in terms of removal efficiency. Besides, it requires lesser hydrothermal synthesize temperature (75°C) and no calcination step involved in the fabrication, which leads to minimize the manufacturing cost of the composite membrane.

In order to check the stability of membrane in the presence of chromium solution, the weight of dry membrane checked before and after conducting the separation studies and there was no weight loss of membrane. This implies that the membrane is very stable in the chromium solution. In addition to this, water flux was determined through these membranes after each separation experiments and the water flux was found to be same as the initial water flux of the membrane. These analyses clearly demonstrate that the prepared membranes are highly stable in chromium separation process.

5.3 Summary

Low cost supported FAU and MFI type zeolite composite membranes were successfully applied for the removal of chromium from aqueous solution. Various influencing parameters such as applied pressure (69-345 kPa), initial feed concentration (250 - 3000 ppm) and cross flow rate

(5.55×10^{-7} - 1.66×10^{-6} m^3/s) on permeate flux and removal of chromium were investigated. It was apparent that the prepared zeolite composite membranes do not have the tendency of fouling and cake layer deposition on the surface of the membrane layer in the removal of chromium. It was observed that the percentage of chromium removal increased with increasing applied pressure and feed concentration. On the other hand, the percentage of removal reduced slightly with enhancing the cross flow rate for both the zeolite membranes. A maximum chromium removal of 82% with permeate flux of 5.05×10^{-5} m^3/m^2s and 78% with permeate flux of 1.42×10^{-4} m^3/m^2s was obtained with FAU and MFI membrane, respectively at an applied pressure of 345 kPa and the initial feed concentration of 1000 ppm with natural pH of the solution. For both the membranes, no decline trends in the permeate flux was observed during the period of filtration study, indicating that these membranes can be utilized for longer duration without frequent regeneration of the membrane. The separation results pointed out that these zeolite composite membranes (FAU and MFI) can be effectively utilized for the removal of Cr (VI) from aqueous solution based on the interaction between the charged membrane and chromium ions. The performance comparison analysis was clearly indicated that the prepared membranes have better potential in removal of chromium with offering 1 to 6 order higher fluxes. Overall, it can be concluded that the FAU zeolite composite membrane is better candidate for chromium removal application when compared to MFI zeolite membrane due to higher removal efficiency, lower synthesize temperature involved in fabrication, and no requirement of calcination step as surfactant is not used as a templating agent in the development of FAU zeolite membrane.

भारतीय प्रौद्योगिकी संस्थान गुवाहाटी
Indian Institute of Technology Guwahati

Chapter 6

Separation of BSA using zeolite membranes and optimization of microfiltration process through hybrid RSM-GA approach

---

Separation of BSA using zeolite membranes and optimization of microfiltration process through hybrid RSM-GA approach

This chapter explicates the application of FAU and MFI type zeolite membranes for the separation of bovine serum albumin (BSA) protein from its solution and optimization of critical parameters of the microfiltration system. The separation efficiency of both the membranes in terms of permeate flux and rejection was studied with BSA as a model protein. Three operating parameters such as, BSA concentration, pH and applied pressure were optimized for the better separation efficiency of the membranes using response surface methodology (RSM) followed by bi-objective genetic algorithm (GA). The non-linear models predicted by RSM were further optimized by GA. The appropriate optimum conditions were obtained and the predicted conditions were experimentally validated. Further, the separation efficiency of membranes was compared with other membranes used for the BSA separation stated in literature.

6.1 Experimental

6.1.1 Materials

Sodium hydroxide, hydrochloric acid, sodium dodecyl sulfate and calcium carbonate were purchased from Merck (India) Ltd, Mumbai. Bovine albumin fraction V (powder) was obtained from Loba Chemie laboratory reagents & fine chemicals, Mumbai.

6.1.2 Microfiltration of BSA using FAU and MFI zeolite membranes

Microfiltration of BSA experiments was carried out at room temperature with in-house made cross flow filtration system as described in chapter 2. Two zeolite membranes namely, FAU and MFI supported on low cost tubular ceramic supports were applied for the separation of BSA.

The preparation and characterization of FAU and MFI zeolite membranes are extensively presented in chapter 4 of the thesis. Various concentrations of BSA solution (100-500 ppm) were prepared with Millipore water. In order to prevent the foam formation, shaking was circumvented, because, the foam can extremely interfere during the analysis of protein. Hence, the solutions were taken for analysis only after the natural dissipation of foam occurred. BSA solutions were prepared freshly and utilized within 6 h in order to avoid the aggregation of protein. To investigate the effect of pH on the rejection and permeate flux, experiments were performed at various pH values fluctuating between 2 and 4. The pH of the solutions was adjusted with NaOH and HCl. Also, the effects of applied pressure ranging between 68.94 kPa and 275.79kPa were investigated. All the cross-flow experiments were performed using 6 L of feed solution. For each experimental run, the initial 10-20 mL of protein solution passed through the membrane was discarded in order to attain a steady flux. The separation of BSA was performed for a period of 1 h at each operating conditions. The volume of the permeate was noted for 1 h in each experimental run to evaluate the permeate flux. Aliquots were taken to measure the concentration of BSA by UV-visible spectrophotometer (Thermo Scientific, UV-2300) at a wavelength of 280 nm. The percentage rejection was calculated using the equation given below.

$$R[\text{rejection},(\%)]=1-\frac{C_p\,[\text{concentration in permeate}]}{C_f\,[\text{concentration in feed}]}\times 100 \qquad (6.1)$$

In order to regenerate the membrane, immediately after every experimental run, the membrane was thoroughly washed with Millipore water followed by a solution containing mixture of sodium dodecyl sulfate (SDS) (2 g/L) and NaOH (20 g/L) for 30 min. After that the membrane was again washed with Millipore water to reach neutrality. Water permeability experiment was performed to check the complete regeneration of the membrane.

6.1.3 Response surface methodological approach

Response surface methodology (RSM) is a statistical and systematic approach employed to estimate main effects, interaction effects and quadratic effects of the variables on the response. In the RSM, two values can be assigned to each factor *i.e.*, -1 for low values (x_{min}) and +1 for high values (x_{max}). Transformed variables -1 and +1 are called coded variables (Z) and they have no unit of measure. The centre values of all variables were coded as zero. The transformation used for coded values are as follows:

$$Z = \frac{x - [(x_{min} + x_{max})/2]}{[(x_{max} - x_{min})/2]} \tag{6.2}$$

Uncoded or actual values (x) can be estimated from the coded values by:

$$x = Z\frac{(x_{max} - x_{min})}{2} + \frac{(x_{max} + x_{min})}{2} \tag{6.3}$$

In this study, Face Centred Central Composite Design (FCCCD) was used to analyse the permeate flux and percentage rejection of BSA. Variables such as concentration of BSA in ppm, pH of the solution and applied pressure in kPa were used to find the effects on the permeate flux and rejection. Table 6.1 shows the variable ranges and experimental design according to FCCCD. The FCCC design consists of 20 experimental runs, which includes 8 runs in the two-level full factorial portion, 6 runs in an axial portion and 6 runs in center portion. For the pure error estimation, the center portion is repeated for 6 times. The following second-order non-linear polynomial equation was used to fit the experimental data.

$$Y = \beta_o + \sum_{i=1}^{n}\beta_i X_i + \sum_{i=1}^{n}\beta_{ii} X_i^2 + \sum_{i=1}^{n-1}\sum_{j=i+1}^{n}\beta_{ij} X_i X_j + \varepsilon \tag{6.4}$$

where Y is the response (permeate flux and rejection), n is the number of variables, β_0 is the model intercept term and β_i is the linear effect term, β_{ii} is the square effect term, β_{ij} is the

interaction effect term, X_i and X_j is the level of the independent variables and ε is the random error. For most of the cases, the second order model represented by Eq. (6.4) was adequate. The fitted models (Eq. (6.4)) were used to find the optimum set of operating conditions for permeate flux and rejection. In order to optimize the responses, a useful approach is Derringer's desirability function methodology (Ozin et al. 1989). This approach is frequently used to optimize multiple responses. In this approach, Y_i, the responses were converted into an individual desirability function d_i. The desirability function d_i varies over the range of 0 to 1; 0 being a completely undesirable and 1 being a completely desirable or ideal response value. The overall desirability function could be written by combining all the individual desirability as given below.

$$D = \left(\prod_{i=1}^{n} d_i \right)^{\frac{1}{n}} \tag{6.5}$$

where, D is the overall desirability, d_i is the individual desirability and n is the number of response. Criteria used for individual desirability of each response are given below.

$$d = \begin{cases} 0, & y < L \\ \left(\dfrac{y - L}{U - L} \right)^r, & L \le y \le U \\ 1, & y > U \end{cases} \tag{6.6}$$

where, r is a weight factor, L is the lower response and U is the higher response. The statistical analyses of the experimental data were performed using Design Expert 8.0.7.1, Stat-Ease, Inc., Minneapolis, USA. All the experiments were carried out in duplicate and average values were used for further studies.

Table 6.1: Variables and its levels for RSM-FCCCD experimental design

Particulars	Variables	Levels				
		-α level	-1 level	0 level	+1 level	+α level
X_1	Concentration of BSA (ppm)	100	100	300	500	500
X_2	pH	2	2	3	4	4
X_3	Applied pressure (kPa)	68.94	68.94	172.365	275.79	275.79

6.1.4 Genetic algorithm based optimization

Genetic algorithm (GA) is a powerful global non-linear optimization tool, which can be used to find the optimum conditions of the RSM predicted model. GA can also be used in multi-objective optimization problems. In general, most of the optimization problems have many objectives to be minimized or maximized or conflicting with each other. Commonly, such problems are solved by two widely used GA approaches, such as a single composite function of all objectives through the weighted sum method and finding the Pareto optimal sets of solution. In practice, the selection of the utility functions and accurate weight functions are much difficult in the case of weighted sum approach. Hence, the Pareto optimal sets of solution approach were adopted in this present investigation, in order to find the optimal solution set. In this study, there are two objective functions, *viz,* permeate flux and percentage rejection that has to be maximized through GA. The general multi-response GA problem steps are given below.

$$x = \{x_1, x_2, \cdots x_n\} \tag{6.6}$$

where x is the input decision variable vector with n-dimension.

$$\vec{x}^* = \left[x_1^*, x_2^*, \cdots x_n^*\right]^T \tag{6.7}$$

where $\vec{x}^*$ is the vector, that can be obtained through the Eq. (6.6), which will stratify the equality

and inequality constrains. Then the Eq. (6.7) can be used to optimize the objective function of vector, which is given below.

$$\vec{f}\left(\vec{x}\right)=\left[\, f_1(\vec{x}),\, f_2(\vec{x})\cdots f_n(\vec{x})\right] \tag{6.8}$$

In this study, three input vectors such as concentration of BSA (ppm), solution pH and the applied pressure (kPa) were used. The initial populations of input vectors called chromosomes, are randomly formed. Then, according to objective functions, the input vectors fitness was evaluated. Finally, the most important genetic algorithm operations like mutation followed by cross-over were implemented to the appropriate chromosomes to generate another set of chromosomes. This procedure continued until optimal Pareto representative subset solutions were found. In this present investigation, the models predicted by RSM were used as the objective function for multi-response GA for the maximization of permeate flux and rejection according to the method described by Konak et al. (2006). The parameters and the conditions of multi-response GA are described below.

1. Double vector population type with the population size of 20 was used.
2. To generate the initial population, the constraint dependent uniform distribution function was implemented.
3. Tournament selection function was used to choose the appropriate individual vector.
4. The reproduction crossover fraction of 0.8 was used with constrain dependent mutation function and scattered crossover function to create children for the next generation.
5. The forward direction migration option was adopted for the migration of individuals between populations. According to the forward direction migration, the individual migrates to the subsequent subpopulations.
6. Population Pareto front fraction of 0.35 was used to preserve the maximum population fit and to retain a diverse population.

The fitness function used in this study is mentioned below.

$$\max y_i = f(x);\ i = 1, 2.\cdots n \tag{6.9}$$

where y_i represents the responses of RSM predictive models, such as permeate flux and rejection; $f(x)$ represents the non-linear quadratic model equations obtained by RSM modelling and x represents the independent vector. Equation (6.9) was subjected to the following criteria of lower and upper bound of input vectors.

$$\begin{aligned} &100 \le x_1 \le 500; && x_1 - Concentration\ of\ BSA\ in\ ppm \\ &2 \le x_2 \le 4; && x_2 - Solution\ pH \\ &68.94 \le x_3 \le 275.74; && x_3 - Applied\ pressure\ in\ kPa \end{aligned} \tag{6.10}$$

GA multi-objective tool box of MATLAB 7.10.0 (R2010a) (The Mathworks, Inc., Natick, MA, USA) was used for the maximization of permeate flux and rejection.

6.1.5 Validation of optimum conditions predicted by hybrid RSM-GA

Experiments were carried out at the optimized conditions predicted by hybrid RSM-GA in duplicate in order to validate the feasibility, suitability and accuracy of the optimized conditions. The average values of the permeate flux and rejection were compared with the predicted values of RSM-GA.

6.2. Results and discussion

6.2.1 Microfiltration of bovine serum albumin

The prepared FAU and MFI zeolite membranes (Chapter 4) were utilized for the separation of BSA. The concentration of BSA, initial pH of the solution and applied pressures are the

important variables that affect the separation process in terms of permeate flux and rejection. Hence, the effect of these parameters was investigated.

6.2.2 Response surface methodological approach

To achieve a maximum permeate flux and percentage rejection of BSA for FAU and MFI membranes, three important process parameters such as concentration of BSA, initial pH of the solution and applied pressure were considered in the cross-flow microfiltration. Initially, pH of the solution was varied from 3 to 8. It was observed from the preliminary experimental runs that the rejection is considerably very low (10-20%) beyond the isoelectric point (pI) of BSA for both the zeolite membranes. The pI of BSA is 4.9. At pH<pI, the charge of BSA is positive, whereas the solution pH>pI, the charge of BSA is negative. The change in solution pH will affect the electrical charge of BSA, its molecular shape and size and membrane electrical charge (Monash et al. 2010). In addition, the pH of the solution will also affect the permeation flux and rejection. Based upon the preliminary experimental results, it was decided to maintain the solution pH below than that of pI of BSA. Hence, the pH of the solution altered between 2 and 4. According to the FCCCD, experiments were performed with different combinations of three independent parameters (see Table 6.2) in the tubular cross-flow microfiltration experimental setup for both zeolite membraens. Permeate was collected for 1 h and the flux as well as BSA concentration in the permeate solution was measured. The data were fitted with a second-order polynomial equation represented to FAU membrane by Eqs. (6.11) and (6.12) and MFI membrane by Eqs. (6.13) and (6.14) for the permeate flux and percentage rejection of BSA, respectively in terms of actual values of independent variables.

Table 6.2: Coded and actual levels of the independent variables according to the RSM-FCCCD experimental design and experimental results of FAU and MFI membranes separation efficiency

	Run no	BSA Concentration (ppm)	pH	Applied pressure (kPa)	Permeate flux (m^3/m^2s) (Y_1) [FAU Membrane]			Rejection (%)(Y_2) [FAU Membrane]			Permeate flux (m^3/m^2s) (Y_1) [MFI Membrane]			Rejection (%)(Y_2) [MFI Membrane]		
					Y_{exp}	Y_{pre}	Error	Y_{exp}	Y_{pre}	Error	Y_{exp}	Y_{pre}	Error	Y_{exp}	Y_{pre}	Error
Full factorial portion	1	100 (-1)	2 (-1)	68.94 (-1)	1.38E-05	1.37E-05	1.42E-07	94.06	94.71068	-0.65068	2.47×10^{-5}	2.48×10^{-5}	-1.1×10^{-7}	87.56	87.67	-0.1067
	2	500 (+1)	2 (-1)	68.94 (-1)	1.21E-05	1.23E-05	-1.2E-07	82.27	82.43168	-0.16168	1.52×10^{-5}	1.51×10^{-5}	1.14×10^{-7}	61.68	61.69	-0.0077
	3	100 (-1)	4 (+1)	68.94 (-1)	1.75E-05	1.76E-05	-1.8E-07	35.2	35.28668	-0.08668	2.69×10^{-5}	2.69×10^{-5}	4.09×10^{-9}	38.92	38.69	0.2273
	4	500 (+1)	4 (+1)	68.94 (-1)	6.85E-06	6.8E-06	5.02E-08	41.2	41.70768	-0.50768	1.67×10^{-5}	1.68×10^{-5}	-7.6×10^{-8}	42.84	43.02	-0.1787
	5	100 (-1)	2 (-1)	275.79 (+1)	2.63E-05	2.64E-05	-1.7E-08	87.65	87.57168	0.078318	4.60×10^{-5}	4.59×10^{-5}	6.41×10^{-8}	81.68	81.54	0.1433
	6	500 (+1)	2 (-1)	275.79 (+1)	1.79E-05	1.77E-05	2.18E-07	90.8	91.14268	-0.34268	4.18×10^{-5}	4.18×10^{-5}	-1.6×10^{-8}	69.98	70.24	-0.2627
	7	100 (-1)	4 (+1)	275.79 (+1)	4.75E-05	4.74E-05	1.55E-07	55.74	56.00768	-0.26768	5.54×10^{-5}	5.55×10^{-5}	-1.3×10^{-7}	48.11	48.14	-0.0277
	8	500 (+1)	4 (+1)	275.79 (+1)	2.91E-05	2.93E-05	-1.1E-07	78.5	78.27868	0.221318	5.11×10^{-5}	5.10×10^{-5}	9.41×10^{-8}	67.22	67.15	0.0713
Axial portion	9	100 (-1)	3 (0)	172.365 (0)	2.09E-05	2.1E-05	-9.5E-08	65.4	64.47327	0.926727	3.43×10^{-5}	3.41×10^{-5}	1.64×10^{-7}	63.95	64.19	-0.2362
	10	500 (+1)	3 (0)	172.365 (0)	1.12E-05	1.12E-05	-3.7E-08	70.26	69.46927	0.790727	2.69×10^{-5}	2.70×10^{-5}	-1.2×10^{-7}	61.08	60.7	0.3778
	11	300 (0)	2 (-1)	172.365 (0)	8.14E-06	8.36E-06	-2.2E-07	72.3	71.22327	1.076727	2.20×10^{-5}	2.21×10^{-5}	-5.6×10^{-8}	61.55	61.32	0.2338
	12	300 (0)	4 (+1)	172.365 (0)	1.62E-05	1.61E-05	8.91E-08	35.72	35.07927	0.640727	2.78×10^{-5}	2.77×10^{-5}	1.04×10^{-7}	35.19	35.28	-0.0922
	13	300 (0)	3 (0)	68.94 (-1)	6.99E-06	6.88E-06	1.15E-07	61.3	59.89327	1.406727	1.28×10^{-5}	1.27×10^{-5}	6.36×10^{-8}	52.38	52.31	0.0658
	14	300 (0)	3 (0)	275.79 (+1)	2.42E-05	2.44E-05	-2.5E-07	74.92	74.60927	0.310727	4.04×10^{-5}	4.04×10^{-5}	-1.6×10^{-8}	61.39	61.31	0.0758
Center portion	15	300 (0)	3 (0)	172.365 (0)	1.13E-05	1.13E-05	2.71E-08	57.12	58.24082	-1.12082	2.36×10^{-5}	2.36×10^{-5}	-4.9×10^{-8}	52.07	52.65	-0.5755
	16	300 (0)	3 (0)	172.365 (0)	1.15E-05	1.13E-05	2.27E-07	57.89	58.24082	-0.35082	2.38×10^{-5}	2.36×10^{-5}	1.51×10^{-7}	52.59	52.65	-0.0555
	17	300 (0)	3 (0)	172.365 (0)	1.11E-05	1.13E-05	-1.7E-07	58.09	58.24082	-0.15082	2.35×10^{-5}	2.36×10^{-5}	-1.5×10^{-7}	53.04	52.65	0.3945
	18	300 (0)	3 (0)	172.365 (0)	1.14E-05	1.13E-05	1.27E-07	57.98	58.24082	-0.26082	2.37×10^{-5}	2.36×10^{-5}	5.09×10^{-8}	52.81	52.65	0.1645
	19	300 (0)	3 (0)	172.365 (0)	1.12E-05	1.13E-05	-7.3E-08	56.72	58.24082	-1.52082	2.35×10^{-5}	2.36×10^{-5}	-1.5×10^{-7}	51.96	52.65	-0.6855
	20	300 (0)	3 (0)	172.365 (0)	1.14E-05	1.13E-05	1.27E-07	58.21	58.24082	-0.03082	2.37×10^{-5}	2.36×10^{-5}	5.09×10^{-8}	53.12	52.65	0.4745

$$Y_1 = 2.983\times10^{-5} - 4.569\times10^{-8}X_1 - 5.326\times10^{-6}X_2 - 1.528\times10^{-7}X_3 - 1.178\times10^{-8}X_1X_2 - 8.776\times10^{-11}X_1X_3 + 4.1207\times10^{-8}X_2X_3 + 1.1955\times10^{-10}X_1^2 + 9.4017\times10^{-7}X_2^2 + 4.0735\times10^{-10}X_3^2 \quad (6.11)$$

$$Y_2 = 161.0771 - 22.161\times10^{-2}X_1 - 61.5489\times10^{-1}X_2 - 47.874\times10^{-2}X_3 + 23.375\times10^{-3}X_1X_2 + 19.156\times10^{-5}X_1X_3 + 67.343\times10^{-3}X_2X_3 + 21.826\times10^{-5}X_1^2 - 50.8955\times10^{-1}X_2^2 + 84.236\times10^{-5}X_3^2 \quad (6.12)$$

$$Y_1 = 4.46502\times10^{-5} - 1.31875\times10^{-7}X_1 - 7.51846\times10^{-6}X_2 - 3.5214\times10^{-8}X_3 - 5\times10^{-10}X_1X_2 + 6.76819\times10^{-11}X_1X_3 + 1.81291\times10^{-8}X_2X_3 + 1.73182\times10^{-10}X_1^2 + 1.22727\times10^{-6}X_2^2 + 2.73661\times10^{-10}X_3^2 \quad (6.13)$$

$$Y_2 = 144.05618 - 29.992527\times10^{-2}X_1 - 47.9240003\times10^{-1}X_2 - 25.702464\times10^{-2}X_3 + 37.88125\times10^{-3}X_1X_2 + 17.748\times10^{-5}X_1X_3 + 37.64805\times10^{-3}X_2X_3 + 24.497\times10^{-5}X_1^2 - 43.4636364\times10^{-1}X_2^2 + 38.971\times10^{-5}X_3^2 \quad (6.14)$$

where, Y_1 and Y_2 are permeate flux in m^3/m^2s and percentage rejection of BSA, respectively.

6.2.3 Model adequacy checking

It is more essential to verify that the developed model gives an adequate approximation to experimental values. Optimization of the developed model will give misleading or poor results, unless otherwise the developed model shows the reasonable fit (Myers et al. 2009). Various statistical parameters were determined to check the adequacy of the model. Besides, various diagnostic and influence plots were constructed to validate the model adequacy. They were discussed in the following section.

6.2.3.1 Statistical parameters for model adequacy

The statistical significance of each individual, interaction and quadratic terms in the model equations (Eq. 6.11-6.14) were evaluated by the *F*-test for analysis of variance (ANOVA). Tables 6.3 and 6.4, shows the quadratic models of FAU and MFI membranes permeate flux and

rejection of BSA for three independent variables. All the model terms are significant ($p<0.05$ at 95% confidence level), apart from the interaction terms between BSA concentration and solution pH for the response permeate flux. As shown in Tables 6.3 and 6.4, the model F-value for each response (FAU membrane: $Y_1 = 4727.29$ and $Y_2 = 608.34$; MFI membrane: $Y_1 = 15300.27$ and $Y_2 = 2095.651$) is high with a low probability value ($p<0.0001$) that reveals a high significance of the developed regression model. The F-value of lack of fit for FAU membrane is found to be 2.83 and 4.43, (MFI membrane is found to be 1.624 and 0.397), respectively for the response Y_1 and Y_2 with the probability p-value greater than 0.05. This indicates that each response is not significant relative to pure error, suggesting that the predicted models correlate well with the experimental data (Box et al. 1978). A high determination coefficient (R^2) of each response (FAU membrane: $Y_1 = 0.9998$ and $Y_2 = 0.9982$; MFI membrane: $Y_1 = 0.99992$ and $Y_2 = 0.99947$) indicates a better correlation between experimental and predicted values. Besides, the adjusted R^2 (FAU membrane: $Y_1 = 0.9996$ and $Y_2 = 0.9965$; MFI membrane: $Y_1 = 0.99986$ and $Y_2 = 0.9989$) and predicted R^2 (FAU membrane: $Y_1 = 0.9976$ and $Y_2 = 0.9913$; MFI membrane: $Y_1 = 0.99935$ and $Y_2 = 0.99776$) are good agreement with the determination coefficient, indicating that the aptness of the models (Haaland, 1989). Adequate precision measures the signal to noise ratio, in general the value greater than 4 is desirable. Adequate precision values for FAU membrane are found to be 281.494 and 84.875 whereas for MFI membrane, these are found to be 436.20 and 181.05 for the response Y_1 and Y_2, respectively. These high values signify that both the models could be used to navigate the design space. In addition, a relatively low value of coefficient of variation (FAU membrane: $Y_1 = 1.25\%$ and $Y_2 = 1.54\%$; MFI membrane: $Y_1 = 0.48\%$ and $Y_2 = 0.71\%$) suggests that experiments conducted are precise and reliable (Box et al. 1978; Weisberg, 2005). Absolute average deviations (AAD) between the predicted and observed data are calculated to check the accuracy of the models. AAD was calculated by the following equation:

$$AAD = \left\{ \frac{\left[\sum_{i=1}^{n} \left(\left| y_{i,\exp} - y_{i,cal} \right| / y_{i,\exp} \right) \right]}{n} \right\} \times 100 \qquad (6.15)$$

where, $y_{i,\exp}$ and $y_{i,cal}$ are the experimental and calculated responses, respectively, and n is the number of experimental runs. A relatively small value of AAD (FAU membrane: Y_1 = 0.0165% and Y_2 = 0.0355%; MFI membrane: Y_1 = 0.0073% and Y_2 = 0.0042%) displays that the model equation defines the true behaviour of the system and it could be used for interpolation in the experimental domain. Predicted error sum square (PRESS) measures how a model fits each point in the design. Generally, a small value of PRESS is desirable. PRESS values of each response for FAU membrane are found to be 4.323×10^{-12} and 47.08; for MFI membrane, these are found to be 1.7034×10^{-12} and 7.0596. It implies that the predicted models are well fitted and can be used to predict the response of a new experiment. Bias is an estimator used to find out the normal distribution of errors between the experimental and predicted value. Bias can be calculated as follows:

$$Bias = \exp\left[\frac{1}{n} \sum_{i=1}^{n} \ln \frac{y_{i,\exp}}{y_{i,cal}} \right] \qquad (6.16)$$

In this study, bias value of 1 for each response points out that errors are normally distributed, demonstrating a good model fit.

Table 6.3: Analysis of variance of the developed second-order polynomial models for FAU membrane separation efficiency as per the RSM-FCCD experimental design

Source	Coefficient estimate	Sum square	Degree of freedom	Mean square	*F*-value	*p*-value
Permeate flux (m^3/m^2s) (Y_1)						
Model	2.983×10^{-5}	1.77×10^{-09}	9	1.96×10^{-10}	4727.29	< 0.0001*
X_1	-4.569×10^{-8}	2.38×10^{-10}	1	2.38×10^{-10}	5741.19	< 0.0001*
X_2	-5.326×10^{-6}	1.51×10^{-10}	1	1.51×10^{-10}	3634.98	< 0.0001*
X_3	-1.528×10^{-7}	7.71×10^{-10}	1	7.71×10^{-10}	18569.7	< 0.0001*
X_1X_2	-1.178×10^{-8}	4.44×10^{-11}	1	4.44×10^{-11}	1068.42	< 0.0001*
X_1X_3	-8.776×10^{-11}	2.64×10^{-11}	1	2.64×10^{-11}	634.774	< 0.0001*
X_2X_3	4.1207×10^{-8}	1.45×10^{-10}	1	1.45×10^{-10}	3498.96	< 0.0001*
X_1^2	1.1955×10^{-10}	6.29×10^{-11}	1	6.29×10^{-11}	1514.27	< 0.0001*
X_2^2	9.4017×10^{-7}	2.43×10^{-12}	1	2.43×10^{-12}	58.5345	< 0.0001*
X_3^2	4.0735×10^{-10}	5.22×10^{-11}	1	5.22×10^{-11}	1257.3	< 0.0001*
Residual		4.15×10^{-13}	10	4.15×10^{-14}		
Lack of fit		3.07×10^{-13}	5	6.14×10^{-14}	2.83331	0.1388**
Pure error		1.08×10^{-13}	5	2.17×10^{-14}		
Cor total		1.77×10^{-09}	19			
Rejection (%)(Y_2)						
Model	161.0771	5405.116	9	600.5684	608.3382	< 0.0001*
X_1	-0.22161	62.40004	1	62.40004	63.20734	< 0.0001*
X_2	-6.15489	3265.972	1	3265.972	3308.225	< 0.0001*
X_3	-0.47874	541.4016	1	541.4016	548.406	< 0.0001*
X_1X_2	0.023375	174.845	1	174.845	177.107	< 0.0001*
X_1X_3	0.000192	125.6113	1	125.6113	127.2363	< 0.0001*
X_2X_3	0.067343	388.0898	1	388.0898	393.1107	< 0.0001*
X_1^2	0.000218	209.6073	1	209.6073	212.3191	< 0.0001*
X_2^2	-5.08955	71.23455	1	71.23455	72.15614	< 0.0001*
X_3^2	0.000842	223.2678	1	223.2678	226.1563	< 0.0001*
Residual		9.872278	10	0.987228		
Lack of fit		8.054795	5	1.610959	4.43184	0.0640**
Pure error		1.817483	5	0.363497		
Cor total		5414.988	19			

*significant; **not significant

Table 6.4: Analysis of variance of the developed second-order polynomial models for MFI membrane separation efficiency as per the RSM-FCCD experimental design

Source	Coefficient estimate	Sum square	Degree of freedom	Mean square	*F*-value	*p*-value
Permeate flux (m^3/m^2s) (Y_1)						
Model	4.46502×10^{-5}	3×10^{-9}	9	2.94×10^{-10}	15300.27	< 0.0001*
X_1	-1.31875×10^{-7}	1×10^{-10}	1	1.27×10^{-10}	6585.243	< 0.0001*
X_2	-7.51846×10^{-6}	8×10^{-11}	1	7.95×10^{-11}	4132.093	< 0.0001*
X_3	-3.5214×10^{-8}	2×10^{-9}	1	1.92×10^{-9}	99527.71	< 0.0001*
X_1X_2	-5×10^{-10}	8×10^{-14}	1	8×10^{-14}	4.156826	0.0688
X_1X_3	6.76819×10^{-11}	2×10^{-11}	1	1.57×10^{-11}	814.7378	< 0.0001*
X_2X_3	1.81291×10^{-8}	3×10^{-11}	1	2.81×10^{-11}	1461.384	< 0.0001*
X_1^2	1.73182×10^{-10}	1×10^{-10}	1	1.32×10^{-10}	6856.92	< 0.0001*
X_2^2	1.22727×10^{-6}	4×10^{-12}	1	4.14×10^{-12}	215.222	< 0.0001*
X_3^2	2.73661×10^{-10}	2×10^{-11}	1	2.36×10^{-11}	1224.421	< 0.0001*
Residual		2×10^{-13}	10	1.92×10^{-14}		
Lack of fit		1×10^{-13}	5	2.38×10^{-14}	1.62438	0.3037**
Pure error		7×10^{-14}	5	1.47×10^{-14}		
Cor total		3×10^{-9}	19			
Rejection (%)(Y_2)						
Model	144.0562	3157.829	9	350.8699	2095.651	< 0.0001*
X_1	-0.29993	30.34564	1	30.34564	181.2463	< 0.0001*
X_2	-4.7924	1694.423	1	1694.423	10120.33	< 0.0001*
X_3	-0.25702	202.5	1	202.5	1209.478	< 0.0001*
X_1X_2	0.037881	459.1965	1	459.1965	2742.657	< 0.0001*
X_1X_3	0.000177	107.8246	1	107.8246	644.0073	< 0.0001
X_2X_3	0.037648	121.2903	1	121.2903	724.4343	< 0.0001*
X_1^2	0.000245	264.0365	1	264.0365	1577.019	< 0.0001*
X_2^2	-4.34636	51.94991	1	51.94991	310.2828	< 0.0001*
X_3^2	0.00039	47.78821	1	47.78821	285.4261	< 0.0001*
Residual		1.674276	10	0.167428		
Lack of fit		0.475593	5	0.095119	0.396763	0.8334**
Pure error		1.198683	5	0.239737		
Cor total		3159.503	19			

*significant; **not significant

6.2.3.2 Diagnostic and influence plots for model adequacy

Figure 6.1 and 6.2 show diagnostic plots for FAU and MFI membranes, used for model adequacy checking. Diagnostic plots were constructed based on the residues obtained. Residual or random error is the difference between the experimental and predicted value of response. Figures 6.1 and 6.2 (a-i & a-ii) show the normal probability plot of the studentized residual for the permeate flux and percentage rejection of microfiltration of BSA. From these plots, it is clearly seen that the residuals of the response are normally distributed, as they lie on very close to a straight line, which shows no deviation of variation. Figures 6.1 and 6.2 (b-i & b-ii) shows the plot of the residuals versus the ascending predicted response values. It tests the assumption of constant variance. From these plots, there is no evidence of obvious patterns established in both the responses; moreover, the plots are random scatter, indicating there is no need for a transformation. The plot of the actual response versus predicted response values is illustrated in Figures 6.1 and 6.2 (c-i & c-ii) for each response. It is clearly evident that the actual responses are relatively close to the predicted responses, and the points of all actual and predicted responses fall very close to the 45˚ line. These results indicate that the model developed are successful in confining the correlation between the process variables on the permeate flux and rejection of BSA. Figures 6.1 and 6.2 (d-i & d-ii) displays the plot of residuals versus run number. These plots are used to find the lurking variables that possibly affect the dependent variable in the course of experimentation. The data points in the plot must be scattered. From these figures, it is apparent that all data points are scattered randomly and lies within the limit (± 3). Thus, the experimental data were found satisfactory.

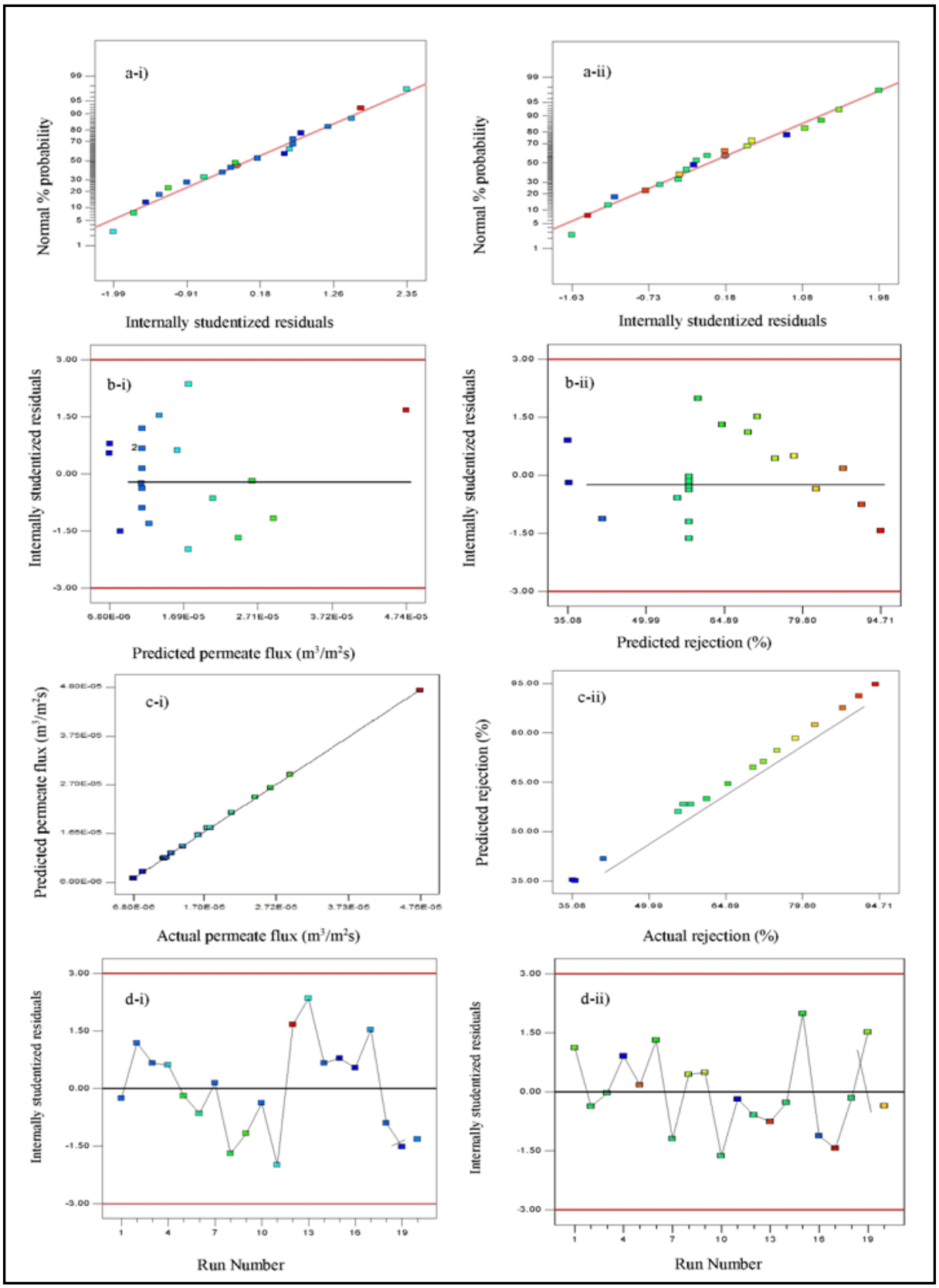

Figure 6.1: Diagnostic plots for the adequacy of predictive models obtained for FAU membrane

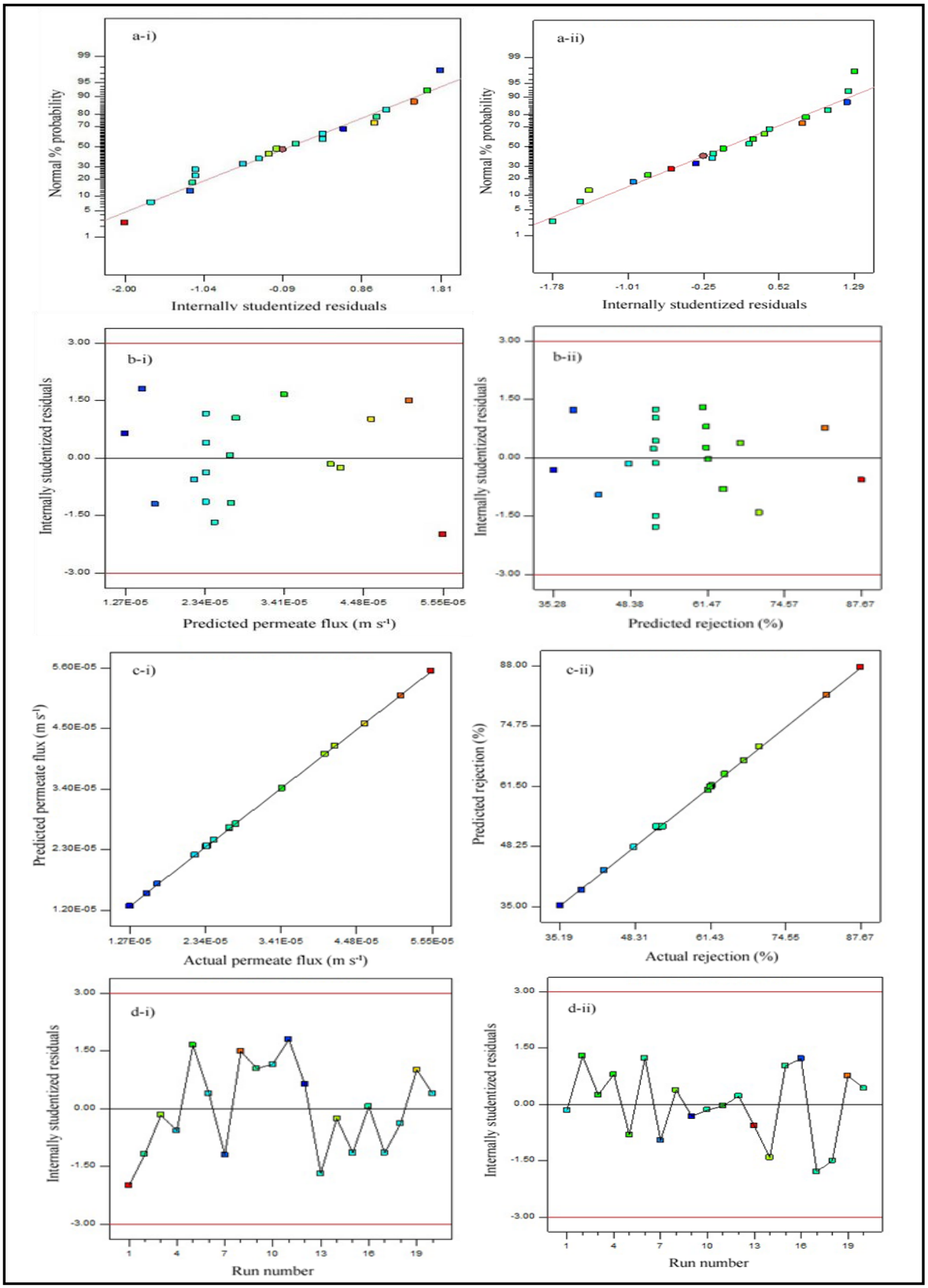

Figure 6.2: Diagnostic plots for the adequacy of predictive models obtained for MFI membrane

Figures 6.3 and 6.4 show influence plots for FAU and MFI membranes, used for model adequacy checking. Figures 6.3 and 6.4 (a) shows the plot of leverage versus run number. Leverage is the potential for a design point to influence the fit of the model coefficients, based on its position in the design space. Leverage equal to 1 indicates that there is a problem with the data point, and this unexpected error strongly influences the model. In this investigation, there is no evidence of unexpected errors and no outliers in the developed models, since the leverage value is less than 1 for both the responses (Figure 6.3-4(a-i) & (a-ii)).

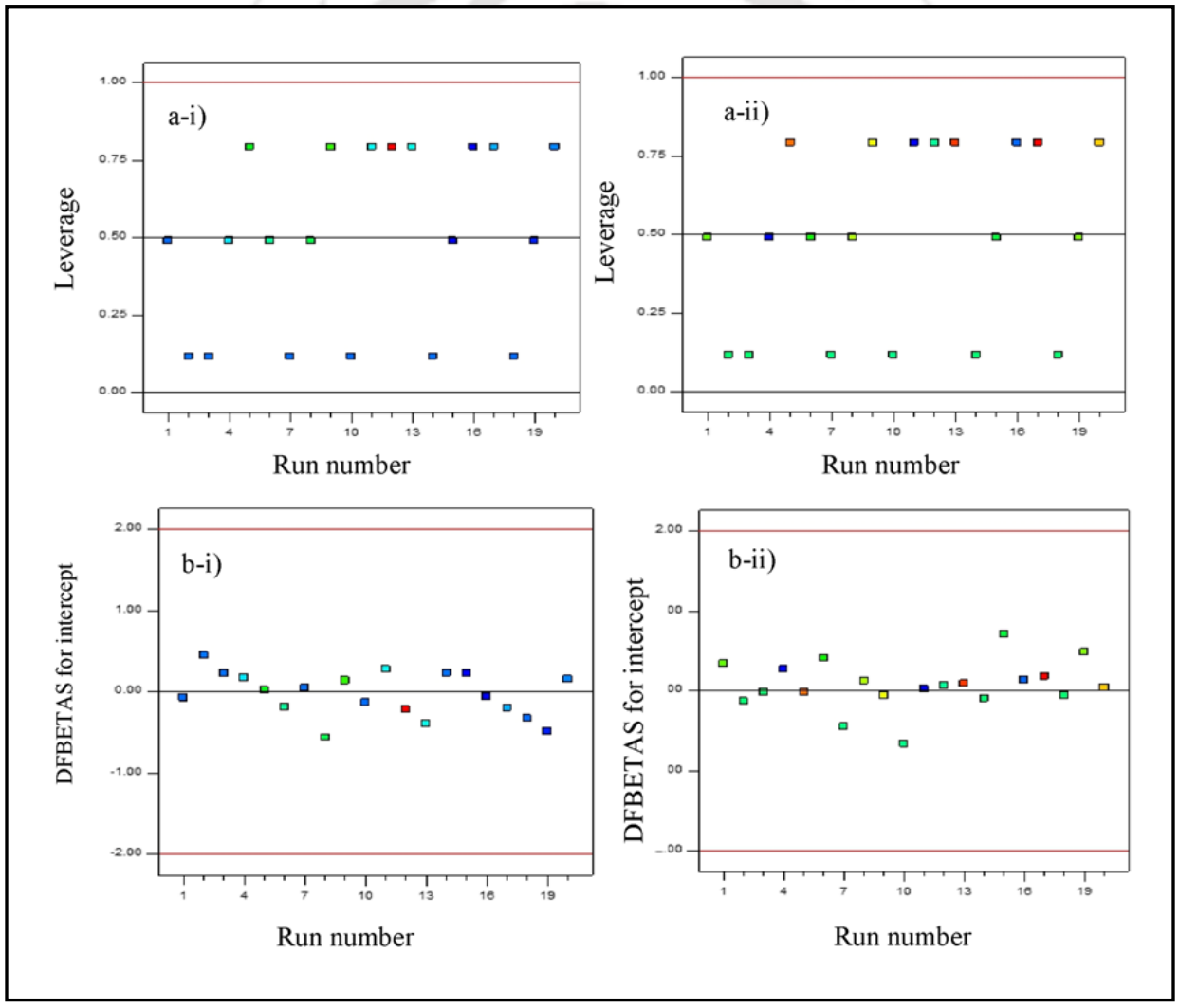

Figure 6.3: Influence plots of MFI membrane for the adequacy of predictive models

The variation in beta values (DFBETAS) plots (Figures 6.3 and 6.4 (b)) measures the influence of each experimental run on each regression coefficient. A large DFBETAS value indicates that the particular observation has a lot of influence on the particular regression coefficient. In this study, DFBETAS plot (Figures 6.3 and 6.4 (b-i) & (b-ii)) demonstrates no influence of any observation on any regression coefficients of the developed models for the permeate flux and rejection of BSA.

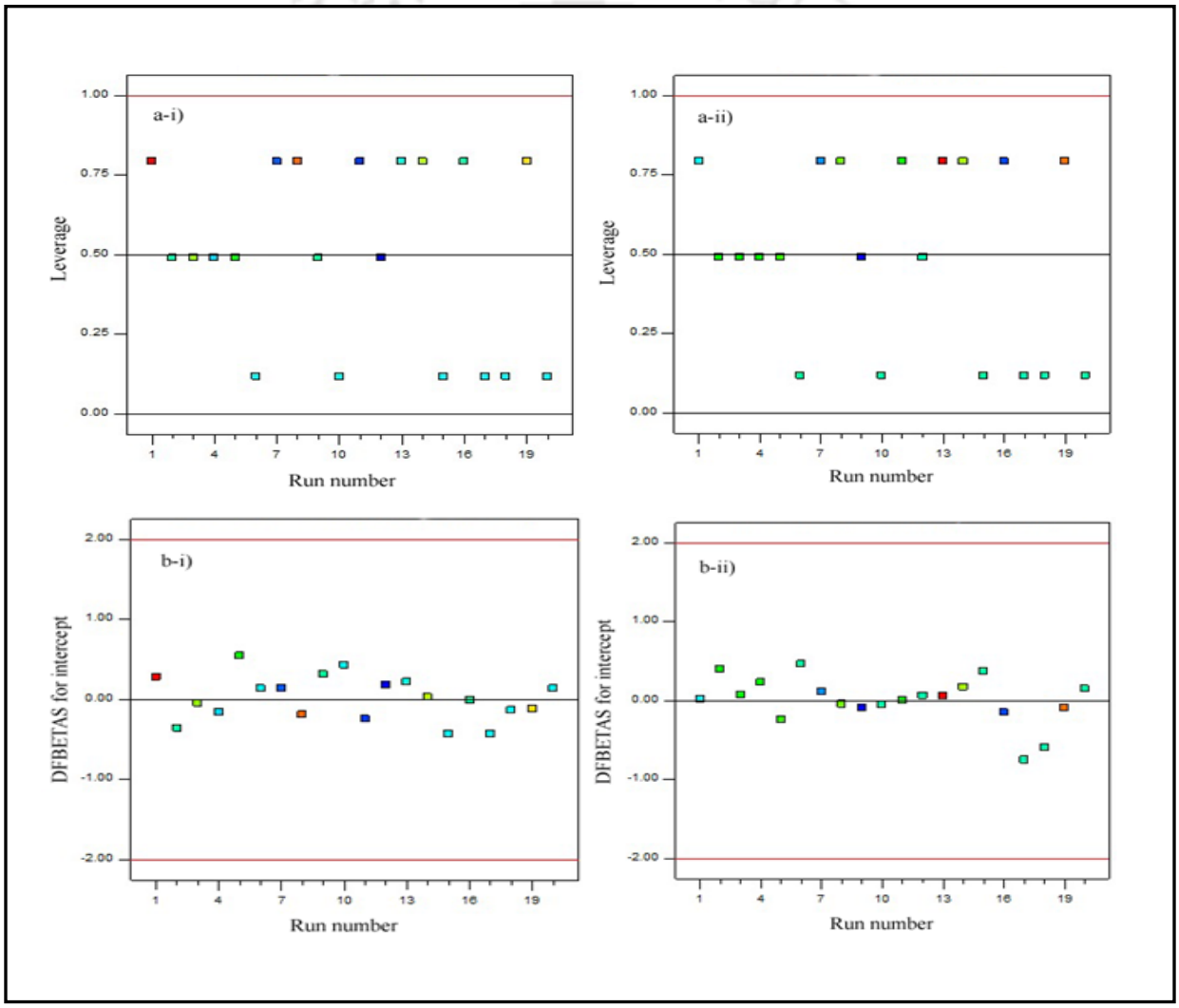

Figure 6.4: Influence plots of MFI membrane for the adequacy of predictive models

6.2.1 Effects of process variables on separation efficiency

The effect of three parameters (concentration of BSA, solution pH and applied pressure) were investigated at three levels (-1, 0 and +1) as per face centred central composite design in order to know the potential of FAU and MFI zeolite membranes. The interaction effects of these variables on the responses for both membranes are shown in Figures 6.5 and 6.6. These contour plots of response surface are plotted on the basis of a model equation to determine the interaction among the variables. These graphs are constructed by plotting against any two independent variables respectively for x and y axis with the response as a parameter, while another variable is maintained at its center (0) level.

6.2.1.1 Effect of concentration of BSA

The substantial decrease in permeate flux and rejection is observed with an increase in the concentration of BSA for the both zeolite membranes. The concentration of BSA molecules on the surface of the membrane increases with an increase in the feed concentration, which causes additional fouling resistances. Therefore, the declination in permeate flux is observed owing to concentration polarization and partial plugging of the membrane at higher concentration. The rejection values obtained at these concentrations also demonstrate that the observed rejection decreases with increasing feed concentration. This is a typical characteristic of charged membranes, for which Donnan exclusion plays a vital role (Persson et al. 2003; Monash and Pugazhenthi, 2011; Cabatingan et al. 2001). With increasing BSA concentration, the effect of Donnan exclusion declines and also the surface concentration increases, this leads to the harsh concentration polarization. Consequently, the solute permeation by diffusion increases and hence the permeate concentration also raises. The effect of each linear, interaction and square terms on the response was determined by the coefficient of estimate of each terms, which are

given in the Tables 6.3 (for FAU membrane) and 6.4 (for MFI membrane). The negative sign indicated that the particular variable exhibited negative effect on the response. Similarly, the positive sign indicated that the particular term exhibited positive effect on the response. From Tables 6.3 and 6.4, it is clearly seen that the coefficients of the linear term of BSA concentration exhibits negative effect on both responses. However, the quadratic term coefficients of feed concentration displays significant ($p<0.05$ at 95% confidence level) positive effect on both responses. The interaction terms except the interaction between the feed concentration and solution pH, demonstrate positive effects on permeate flux and rejection. The interaction effects of BSA concentration on responses are shown in Figure 6.5 for FAU membrane and Figure 6.6 for MFI membrane.

6.2.1.2 Effect of pH

The solution pH is the most significant physico-chemical parameter that influences the separation efficiency of microfiltration of BSA (Velasco et al. 2015). BSA separation efficiency is very low at its pI for both the zeolite membranes. At pI, BSA molecules possess the neutral charge. Moreover, the solubility of BSA in aqueous solution is less at pI. Below the pI, the BSA exhibitsa positive charge, while above the pI, the charge of BSA is negative. Generally, the membrane surface charge is strongly dependent upon the solution pH. The point of zero charge (PZC) of FAU and MFI- type zeolite was found to be 3.8 and 4.0, respectively by zeta potential measurements (refer chapter 4). The solution pH less than PZC, the membranes exhibits a positive charge, whereas, pH greater than PZC, the membranes are negatively charged. In this present study, the effect of pH ranging between 2 and 4 was examined to evaluate the separation efficiency of the membrane. Hence, the charge is almost positive for both the BSA molecule and the fabricated zeolite membranes. A significant interaction effects are observed

between the process variables as depicted in Figures 6.5 and 6.6. The coefficients of the linear term of pH show negative effect for both the responses (see Tables 6.3 and 6.4). However, the interaction terms, excluding the interaction between BSA concentration and pH, display significant effects with probability, $p<0.05$. In addition, the coefficient of the quadratic effect is positive for the permeate flux and negative for the percentage rejection (Tables 6.3 and 6.4). It is noteworthy to mention that, a higher rejection of 87.45% with permeate flux of 2.65×10^{-5} m^3/m^2s is observed for FAU membrane at lower pH value of 2. On the other hand, the maximum rejection is obtained as 81.68% with permeate flux of 4.6×10^{-5} m^3/m^2s for MFI membrane at a same pH. At the lower pH, both the membranes and BSA are positively charged, which induces the electrostatic repulsive force between BSA molecules and membranes, causing a higher rejection. The percentage rejection is found to be low (FAU membrane: 35.2-78.5% and MFI membrane: 42.84-48.11%) at pH 4 (Table 6.2). Nevertheless, the permeate flux decreases at lower pH, and increases at pH 4. The permeate flux is strongly influenced the three process parameters. From the Figures 6.5 and 6.6, it can be shown that the strong interaction between the variables studied on the permeate flux. Persson et al. (2003) also observed a higher flux and transmission of BSA at lower pH (pH-3). Similarly, Monash et al. (2010) obtained a maximum rejection of BSA (89%) at pH 3.

6.2.1.3 Effect of applied pressure

The permeate flux and rejection trend of BSA with FAU and MFI zeolite membranes at various applied pressures are shown in Figures 6.5 and 6.6, repectively. The permeate flux increases with increasing applied pressure. However, the decrease in flux is observed with increasing concentration of BSA, which is mainly due to fouling. The effects of linear, interactive and square terms are given in the Tables 6.3 and 6.4.

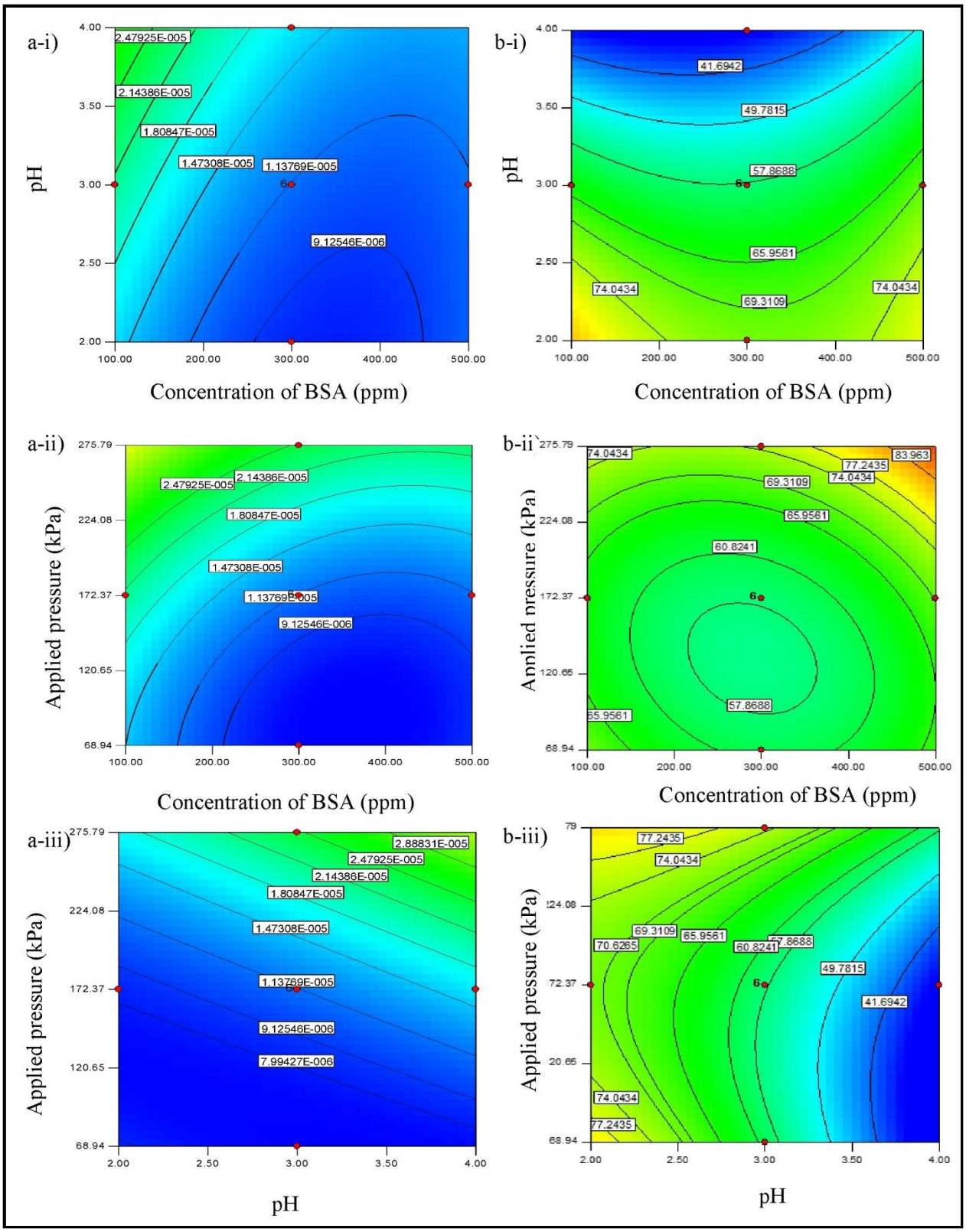

Figure 6.5: Contour plots representing relative effects on the responses for FAU membrane

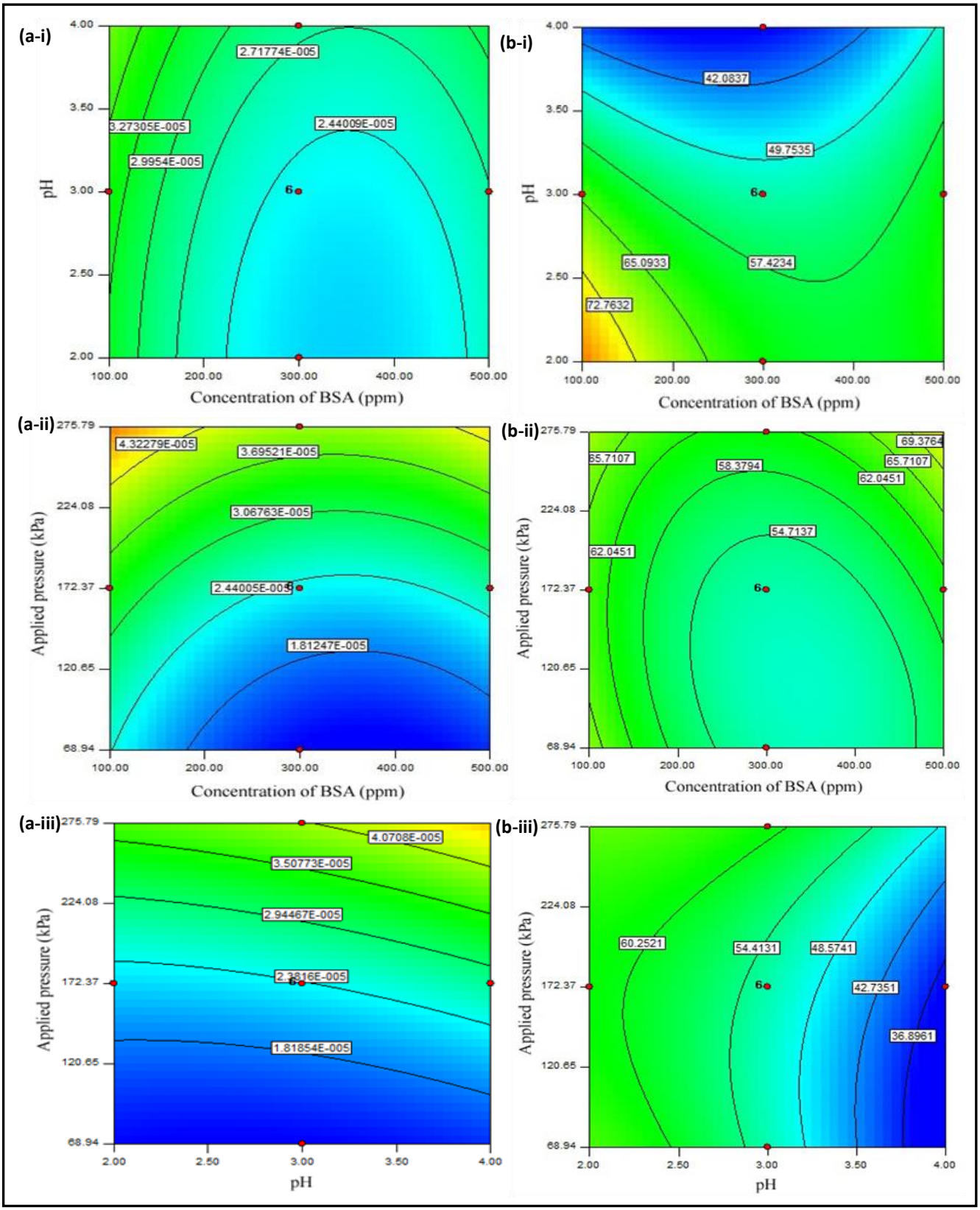

Figure 6.6: Contour plots representing relative effects on the responses for MFI membrane

It is evident from the Tables 6.3 and 6.4, that all the effects of linear, interactive and square terms are statistically significant with the probability, $p < 0.05$ at 95% confidence level. The higher permeate flux (FAU membrane: 4.75×10^{-5} m^3/m^2s and MFI membrane: 5.54×10^{-5} m^3/m^2s) is obtained at 275.79 kPa. Owing to the larger driving force at higher pressure results in increased permeate flux (Kumar et al. 20150). Nonetheless, the flux of BSA solution is considerably lesser than that of pure water flux. This indicates that the presence of BSA molecules causes an additional resistance to flow. The non-linear trend of rejection was observed with varying applied pressure (see Table 6.2). Although, the applied pressure shows a significant effect on the percentage rejection, the concentration of BSA and solution pH are predominate factors than that of applied pressure.

6.2.2 Prediction of optimum conditions through hybrid RSM-GA

The Derringer's desired function methodology (see section 6.1.3) was adopted for predicting optimum conditions for separation efficiency with maximum desirability. In this numerical optimization technique, the possible goal for the process input variables were set as in range, whereas, the goal of the responses were set as maximize with the weight factor of 1 according to the equation 6.6. According to this approach, optimal values for both the zeolite membranes were found to be as follows: BSA concentration of 100 ppm, solution pH value of 2 and applied pressure of 275.79 kPa. The maximum permeate flux and rejection were predicted for FAU membrane as 2.65×10^{-5} m^3/m^2s and 87.45%, respectively at the optimum conditions with the reasonable desirability function value of 0.66. For MFI membrane, the highest permeate flux and rejection were predicted as 4.594×10^{-5} m^3/m^2s and 81.54%, respectively at the optimum conditions with the reasonable desirability function value of 0.830. Further, the multi-response GA was adopted as mentioned in the section 6.1.2, to obtain appropriate parameters for the

separation efficiency. The RSM numerical optimization gives a local solution to the non-linear model, whereas, GA offers global solution (Yuen et al. 2000). Hence, GA was implemented in this study to obtain a global optimum solution of RSM predictive models. The predicted RSM models for the permeate flux and rejection were used as the fitness functions in GA. The multi-objective GA yields a set of non-inferior Pareto optimal solutions. The plot of Pareto front was drawn between two objective functions such as permeate flux and rejection and is illustrated in Figure 6.7. From the Pareto front analysis, the appropriate conditions were estimated to be BSA concentration of 100 ppm, pH value of 2 and applied pressure of 275.79 kPa, at which the permeate flux of 2.64×10^{-5} m^3/m^2s and rejection of 87.57% were observed for FAU membrane. Conversely, the permeate flux of 4.69×10^{-5} m^3/m^2s and 82.17 % of rejection were achieved for MFI membrane at the same estimated optimum conditions. The permeate flux and rejection values for both the zeolite membranes obtained by GA were found to be relatively higher than that of those obtained by RSM. These results revealed that the conditions found by RSM were not assured to be optimal. Hence, GA is a powerful tool for the optimization of non-linear problems (Yuen et al. 2000; Mondal et al. 2011; Soleimani et al. 2013).

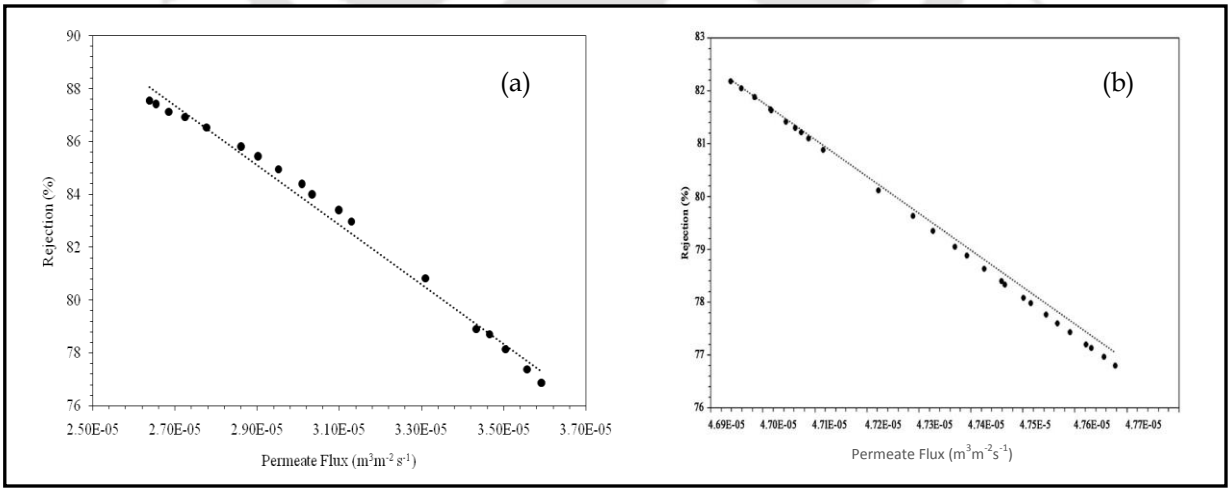

Figure 6.7: Pareto front plot of optimal solution set obtained from multi-response genetic algorithm technique (a) FAU membrane (b) MFI membrane

6.2.3 Validation of the predicted model

In order to validate the models based on RSM-GA for separation efficiency, microfiltration experiments were carried out under optimized conditions. Permeate was collected and analysed for flux and concentration of BSA. The experiments were repeated for at least two times in order to validate the accuracy of the predicted model. The average permeate flux and rejection for FAU membrane were found to be 2.66×10^{-5} m^3/m^2s and 88.02%, respectively. For MFI membrane, these values were obtained as 4.63×10^{-5} m^3/m^2s and 81.98%. These experimental results were good agreement with the results predicted by hybrid RSM-GA. In addition, the percentage deviation between the experimental and predicted permeate flux and rejection was found to be 0.75 and 0.51%, respectively for FAU membrane, while for MFI membrane, these found to be 1.278 and 0.256%, respectively.

Compare to FAU membrane, the MFI membrane displays marginally higher permeate flux value; this may be due to a bigger pore size of MFI membrane (0.272 μm) when compared to FAU membrane (0.179 μm) as discussed in chapter 4. However, the rejection percentage of BSA for FAU membrane is higher compared to MFI membrane due to a higher quantity of FAU deposition (1.128 g) on the ceramic support as seen in the chapter 4. The permeate flux and rejection of both the zeolite membranes were comparable with the other reports as shown in Table 6.5. From the Table 6.5, it is apparent that the fabricated FAU and MFI zeolite membranes exhibit better separation efficiency in terms of permeate flux and rejection than the other membranes reported in literature. These results also suggest that the statistical and stochastical approaches could be effectively used to optimize the operating parameters of the membrane separation operation.

Table 6.5: Comparison of separation efficiency of FAU and MFI zeolite membrane with other membranes

Membrane type	Pore size	Permeate flux (m^3/m^2s)	Rejection (%)	Authors
TiO_2-mixed clays	0.83 µm	-	40	Ke et al. 2009
γ-Al_2O_3 -clay composite membrane	5.4-13.6 nm	3×10^{-5}	95	Yi et al. 2011
Zirconia- aluminium/titanium membrane	0.14 µm	4×10^{-5}	71	Kosmulski, 2009
Silica ceramic membrane	12.5 µm	4.31×10^{-5}	78	Desai et al. 2006
FAU-type zeolite membrane	0.179 µm	2.66×10^{-5}	88	Present work
MFI-type zeolite membrane	0.272 µm	4.63×10^{-5}	82	Present work

6.3 Summary

The separation efficiency of the FAU and MFI-type zeolite membranes was checked with the model protein BSA in a cross-flow mode of operation. The effects of operating parameters such as BSA concentration (100-500 ppm), solution pH (2-4) and applied pressure (68.94 kPa-275.79 kPa) on the separation efficiency of the membranes were studied. It was experimentally demonstrated that the hybrid RSM-GA could be used to determine the parameters influencing the cross-flow microfiltration of BSA. It was observed that all the individual, interaction and quadratic terms of variables had significant influence on separation efficiency. The appropriate optimum conditions were obtained as BSA concentration of 100 ppm, solution pH of 2 and applied pressure of 275.79 kPa for both the membranes. These predicted conditions were

experimentally validated and a higher permeate flux and rejection of BSA were obtained as 2.66×10^{-5} m^3/m^2s & 88% for FAU membrane and 4.63×10^{-5} m^3/m^2s & 82% for MFI membrane, respectively. The separation efficiency of the membranes in terms of permeate flux and rejection was observed to be better than that of those reported in literature. The results suggested that membrane separation is cost effective and environmental compatible method for the separation of proteins. Hence, microfiltration is a promising alternate technique to the conventional separation methods of protein. Besides, this work would offer advantages in terms of the reduction in purification cost and improved recovery of BSA for the large scale operation.

Chapter 7

Conclusions and Scope for Future work

Conclusions and Scope for Future work

This chapter summarizes the inferences drawn from the various research work presented in this thesis. Also, some suggestions towards the scope for future research are outlined. The main aim of this research is to fabricate low cost ceramic and zeolite ceramic composite membranes by simple and cost effective fabrication technique and their application in liquid phase separation. The novel low cost tubular membrane and zeolite ceramic membranes prepared in this study exhibited characteristics best suited for liquid phase separation applications. The application potential of the prepared membranes was evaluated by conducting microfiltration experiments on oily wastewater, dairy wastewater, toxic heavy metal and protein separation. In this thesis, highly interesting results and discussion were presented, which are summarized in the following section.

7.1 Conclusions

- A novel low cost tubular ceramic membrane was successfully fabricated using inexpensive clay mixtures following the extrusion technique, which is simple, cost effective and involved a low sintering temperature (950 °C).
- The prepared membrane offered the best properties in terms porosity 53%, water permeability 5.93×10^{-7} m^3/m^2s kPa, low average pore size 0.309 µm and strong mechanical strength 12 MPa along with an excellent resistance to corrosion in acidic and basic conditions.
- The manufacturing cost of the membrane at the laboratory level is estimated to be 0.5$/membrane (or 69 $/$m^2$).
- The novel low cost tubular ceramic microfiltration membrane was successfully applied for treating oily wastewater as well as dairy wastewater. An applied pressure of 69 kPa

offered the highest rejection of the oily wastewater (99.98%) with a permeate flux of 3.16×10^{-5} m^3/m^2s. A maximum COD reduction of up to 91% in the permeate stream with a flux of 2.59×10^{-6} m^3/m^2s was achieved using the membrane for treating the dairy wastewater. The obtained rejection values for both these wastewaters were well within the permissible limits for wastewater discharge into the environment.

- The investigation on fouling mechanisms employing various pore blocking models proved that the cake filtration model accurately describes the experimental data for oily and dairy wastewater treatment processes.
- FAU and MFI type zeolite ceramic composite membranes were successfully fabricated using the porous low cost tubular ceramic as the support by hydrothermal treatment method, which is both simple and easy.
- The ceramic support was layered with a homogeneous dispersion of FAU/MFI zeolite crystals, which facilitates the preparation of FAU and MFI zeolite membranes, respectively.
- Upon deposition of FAU (43%) and MFI (51%) zeolite layers the porosity of ceramic support was reduced. The pore size of the FAU and MFI zeolilte membranes was evaluated to be 0.179 and 0.272 µm, respectively, which is lower than that of the support (0.309 µm). The water permeability of the ceramic support, FAU and MFI zeolite membrane was estimated to be 5.93×10^{-7} $m^3/m^2s.kPa$, 1.62×10^{-7} $m^3/m^2s.kPa$ and 4.43×10^{-7} $m^3/m^2s.kPa$, respectively. All these excellent properties of the composite membrane were attributed to the incorporation of FAU/MFI zeolite layer on the ceramic support by hydrothermal treatment.
- FAU and MFI type zeolite composite membranes were successfully applied for the removal of chromium from aqueous solution. Maximum chromium removal of 82%

with a permeate flux of 5.05×10^{-5} m^3/m^2s and 78% removal with a permeate flux of 1.42×10^{-4} m^3/m^2s were obtained with FAU and MFI membrane, respectively, at an applied pressure of 345 kPa,1000 ppm initial feed concentration and unadjusted solution pH.

- For both the membranes, no reduction in the permeate flux was observed during the experiments, indicating that these membranes can be utilized for a prolonged duration without any intermediate and frequent regeneration of the membrane.
- The separation results pointed out that these zeolite composite membranes (FAU and MFI) can be effectively utilized in the removal of chromium from aqueous solution based on the interaction between the charged membrane and chromium ions. A comparison of the performance of these membranes with that reported in the literature for chromium removal are superior with 1 to 6 order high fluxes.
- The separation efficiency using the FAU and MFI-type zeolite membranes was further checked for aqueous solution containing the model protein BSA in a cross-flow mode of operation. This study also demonstrated that the hybrid RSM-GA optimization method can be used to optimize the parameters influencing the cross-flow microfiltration of BSA for an enhanced performance of the membranes.
- Following the hybrid RSM-GA method, the optimum value of the process parameters were obtained as: 100 ppm BSA concentration, solution pH 2 and 275.79 kPa applied pressure for both these membranes. A high permeate flux and BSA rejection values were obtained for both the FAU and MFI membranes.

- Results obtained in this study demonstrated that membrane separation is cost effective and environmentally sound method for the separation of proteins. Thereby, proving that microfiltration is a promising alternate technique to the conventional protein separation methods. Besides, it offers advantages in terms of the reduction in purification cost and improved recovery of BSA for large scale.

In summary, the use of simple fabrication method, low sintering temperature and inexpensive raw materials along with the excellent properties of the novel tubular ceramic membrane substantiates its utility for microfiltration application at large scale compared with the high cost commercial α-alumina, zirconia and titania microfiltration membranes. Comparison of the performance of the novel ceramic and zeolite ceramic membranes with that reported for other membranes in the literature demonstrates an excellent application potential of these novel membranes for both wastewater treatment as well as protein purification. Compared with the MFI zeolite membranes, the FAU zeolite composite membrane is better for chromium removal and BSA separation applications, due to high removal efficiency, lower manufacturing temperature, and no requirement of calcination step for its synthesis.

7.2 Future scopes

- The elaborated low cost tubular ceramic membrane can be developed as a water purification unit for drinking purpose.
- The prepared membranes can be evaluated for the treatment of wastewater from other industrial sources, such as tanneries, metal plating, paper, mining operation, fertilizer and pesticide, etc.

- Multi channel tubular ceramic membrane can be developed using the same inexpensive precursors used in this research work in order to attain a high flux by increasing the surface area and its performance can be investigated for liquid phase separations.
- Reduction in the pore size of MFI and FAU membranes can be achieved further by multiple coating of the respective zeolites through hydrothermal route and can be tested their potential in separation of gas phase application.

References

Abadi, S. R. H., Sebzari, M. R., Hemati, M., Rekabdar, F. and Mohammadi, T., 2011. Ceramic membrane performance in microfiltration of oily wastewater, *Desalination*, **265**, 222-228.

Abbasi, M., Mirfendereski, M., Nikbakht, M., Golshenas, M. and Mohammadi, T., 2010. Performance study of mullite and mullite-alumina ceramic MF membranes for oily wastewaters treatment, *Desalination*, **259**, 169-178.

Almandoz, M. C., Marchese, J., Pradanos, P., Palacio, L. and Hernandez, A., 2004. Preparation and Characterization of Non-Supported Microfiltration Membranes from Aluminosilicates, *Journal of Membrane Science*, **241** 95-103.

Al-Shammari, S. B., Bou-Hamad, S., Al-Saffar, A., Salman, M. and Al-Sairafi, A., 2015. Treatment of dairy processing wastewater using integrated submerged membrane microfiltration system, *Journal of Environmental and Analytical Toxicology*, **5: 4**, 1-6.

Amuda, O. S., Amoo, I. A., Ipinmoroti, K. O. and Ajayi, O. O., 2006. Coagulation/flocculation process in the removal of trace metals present in industrial wastewater, *Journal of Applied Science and Environmental Management,* **10**, 159-162.

APHA, Standard Methods for the Examination of Water and Wastewater, 20th ed., American Public Health Association, Washington, DC, 1998.

Basumatary, A. K., Kumar, R. V., Ghoshal, A. K. and Pugazhenthi, G., 2015. Synthesis and characterization of MCM-41-ceramic composite membrane for the separation of chromic acid from aqueous solution, *Journal of Membrane Science*, **475**, 521-532.

Belay, A. A., 2010. Impacts of Chromium from Tannery Effluent and Evaluation of Alternative Treatment Options, *Journal of Environmental Protection,* **1**, 53-58.

Benhamou, A., Basly, J. P., Baudu, M., Derriche, Z. and Hamacha, R., 2013. Amino-functionalized MCM-41 and MCM-48 for the removal of chromate and arsenate, *Journal of Colloid Interface Sci*ence, **404**, 135-139.

Benito, J. M., Conesa, A., Rubio, F. and Rodriguez, F., 2005. Preparation and characterization of tubular ceramic membranes for treatment of oil emulsions, *Journal of the European Ceramic Society,* **25**, 1895-1903.

Bennani, C. F., Ousji, B. and Ennigrou, D. J., 2015. Reclamation of dairy wastewater using ultrafiltration process, Desalin, *Water Treatment*, **55**, 2, 287-303.

Bernal, M. P., Coronas, J., Menendez, M. and Santamaria, J., 2004. Separation of CO_2/N_2 Mixtures Using MFI-Type Zeolite Membranes, *AIChE Journal,* **50**, 1,127-135

Bissett, H., Zah, J. and Krieg, H. M., 2008. Manufacture and Optimization of Tubular Ceramic Membrane Supports, *Powder Technology*, **181,** 57-66.

Bouzerara, F., Harabi, A., Achour, S. and Larbot, A., 2006. Porous ceramic supports for membranes prepared from kaolin and doloma Mixtures, *Journal of the European Ceramic Society,* **26**, 1663-1671.

Bowen, W. R. and Hughes, D. T., 1990. Properties of microfilteration membranes. Adsorption of bovine serum aibumin at aluminium oxide membrane, *Journal of Membrane Science,* **51**, 189-200.

Bowen, W. R., Mohammad, A. W. and Hilal, N., 1997. Characterisation of nanofiltrtation membranes for predictive purposes-use of salts uncharged solutes and atomic force microscopy, *Journal of Membrane Science*, 91-105.

Box, G., Hunter, W. G. and Hunter, J., *Statistics for experiments: an introduction to design, data analysis and modeling*,Wiley, 1978.

Brião, V. B. and Tavares, C. R. G., 2012. Pore blocking mechanism for the recovery of milk solids from dairy wastewater by ultrafiltration, *Brazilian Journal of Chemical Engineering*, **29 (2)**, 393-407.

Burggraaf, A.J. and Cot, L., 1996. Fundamentals of inorganic membranes science and technology, *Elsevier*, Amsterdam, The Netherlands.

Cabatingan, L. K., Agapay, R. C., Rakels, J. L., Ottens, M. and van der Wielen, L. A., 2001. Potential of biosorption for the recovery of chromate in industrial wastewaters, *Industrial and Engineering Chemistry Research*, **40**, 2302-2309.

Canizares, P., Perez, A. and Camarillo, R., 2002. Recovery of heavy metal by means of ultrafiltration with water-soluble polymers: calculation of design parameters, *Desalination,* **144**, 279-285.

Castellano, M., Turturro, A., Riani, P., Montanari, T., Finocchio, E. and Ramis, G., 2010. Bulk and surface properties of commercial kaolins, *Applied Clay Science*, **48**, 446-454.

Chakrabarty, B., Ghoshal, A. K. and Purkait, M. K., 2008. Ultrafiltration of stable oil-in-water emulsion by polysulfone membrane, *Journal of Membrane Science,* **325**, 427-437.

Cheryan, M. and Rajagopalan, N., 1998. Membrane processing of oily streams. Waste water treatment and waste reduction, *Journal of Membrane Science*, **151,** 13-28.

Cheryan, M., 1998. Ultrafiltration and Mircofiltration Handbook, *Technomic Publishing Co. Inc. Lancaster*, Pennsylvania.

Cheryan, M., Ultrafiltration and microfiltration handbook, CRC press, Florida, 1998.

Coskun, T., Yildirim, A., Balcik, C., Demir, N. M. and Debik, E., 2013. Performances of Reverse Osmosis Membranes for Treatment of Olive Mill Wastewater, *Clean - Soil, Air, Water,* **41(5)**, 463-468.

Covarrubias, C., Garcia, R., Arriagada, R., Yanez, J., Ramanan, H., Lai, Z. and Isapatsis, M., 2008. Removal of Trivalent Chromium Contaminant from Aqueous Media using FAU-type Zeolite Membranes, *Journal of Membrane Science*, **312,** 163-173.

Cowan, J. A. C., MacTavish, F., Brouckaert, C. J. and Jacobs, E. P., 1992. Membrane treatment strategies for red meat abattoir effluents, *Water Science Technology*, **25**, 137-148.

Cui, J., Zhang, X., Liu, H., Liu, S. and Yeung, K. L., 2008. Preparation and Application of Zeolite/Ceramic Microfiltration Membranes for Treatment of Oil Contaminated Water, *Journal of Membrane Science*, **325,** 420-426.

Cui, Z.F. and Muralidhara, H.S., 2010. Membrane Technology, a Practical Guide to Membrane Technology and Applications in Food and Bioprocessing, Volume **(1),** *Butterworth-Heinemann/IChemE.*

Çulfaz, P. Z., Çulfaz, A. and Kalıpçılar, H., 2006. Preparation of MFI type Zeolite Membranes in a Flow System with Circulation of the Synthesis Solution, *Microporous and Mesoporous Materials*, **92,** 134-144.

Danis, U. and Keskinler, B., 2009. Chromate removal from wastewater using micellar enhanced cross flow filtration: Effect of transmembrane pressure and cross flow velocity, *Desalination*, **249**, 1356-1364.

David, O., Gendel, Y. and Wessling, M., 2014. Tubular macro-porous titanium membranes, *Journal of Membrane Science*, **461**, 139-145.

DeFriend, K.A., Wiesner, M.R. and Barron, A.R., 2003. Alumina and aluminate ultra-filtration membranes derived from alumina nanoparticles, *Journal of Membrane Science*, **224**, 11-28.

Desai, K., Akolkar, S., Badhe, Y., Tambe, S. and Lele, S., 2006. Optimization of fermentation media for exopolysaccharide production from Lactobacillus plantarum using artificial intelligence-based techniques, *Process Biochemistry*, **41**, 1842-1848.

Dhaz, C. E. B., Lugo, V. L. and Bilyeu, B., 2012. A review of chemical, electrochemical and biological methods for aqueous Cr(VI) reduction, *Journal of Hazardous Material,* **223-224**, 1-12.

Doke, S. M. and Yadav, G. D., 2014. Process efficacy and novelty of titania membrane prepared by polymeric sol-gel method in removal of chromium(VI) by surfactant enhanced microfiltration. *Chemical Engineering Journal,* **255**, 483-491.

Dong, Y., Feng, X., Dong, D., Wang, S., Yang, J., Gao, J., Liu, X. and Meng, G., 2007. Elaboration and Chemical Corrosion Resistance of Tubular Macro-Porous Cordierite Ceramic Membrane Supports, *Journal of Membrane Science*, **304,** 65-75.

Dyer, A. (1988). An introduction to zeolite molecular sieves, Wiley, Chichester.

Emilio, J., Guadix, A., Ibáñez, R. and Guadix, E. M., 2007. Influence of pH and salt concentration on the cross-flow microfiltration of BSA through a ceramic membrane, *Biochemical engineering journal*, **33**, 110-115.

Fakhfakh, S., Baklouti, S., Baklouti, S. and Bouaziz, J., 2010. Preparation, characterization and application in BSA solution of silica membranes, *Desalination*, **262**, 188-195.

Falamaki, C., Afarani, M. S. and Aghaie, A., 2004. Initial sintering stage pore growth mechanism applied to the manufacture of ceramic membrane supports, *Journal of the European Ceramic Society,* **24**, 2285-2292.

Fang, J., Qin, G., Wei, W. and Zhao, X., 2011. Preparation and characterization of tubular supported ceramic microfiltration membranes from fly ash, *Separation and Purification Technology*, **80,** 585-591.

Fang, J., Qin, G., Wei, W., Zhao, X. and Jiang, L., 2013. Elaboration of new ceramic membrane from spherical fly ash for microfiltration of rigid particle suspension and oil-in-water emulsion, *Desalination* ,**311**, 113-126.

Farizoglu, B. and Keskinler, B., 2006. Sludge characteristics and effect of crossflow membrane filtration on membrane fouling in a jet loop membrane bioreactor (JLMBR), *Journal of Membrane Science*, **279**, 578-587.

Figueiredo, H., Neves, I. C., Quintelas, C., Tavares, T., Taralunga, M., Mijoin, J. and Magnoux, P., 2006. Oxidation catalysts prepared from biosorbents supported on zeolites, *Applied Catalysis* B: *Environmental*, **66**, 274-280.

Fukushima, M., Zhou, Y. and Yoshizawa, Y.I., 2009. Fabrication and microstructural characterization of porous SiC membrane supports with Al_2O_3-Y_2O_3 additives, *Journal of Membrane Science*, **339,** 78-84.

Gheju, M. and Balcu, I., 2011. Removal of chromium from Cr(VI) polluted wastewaters by reduction with scrap iron and subsequent precipitation of resulted cations. *Journal of Hazardous Materials,* **196,** 131-138.

Gherasim, C. V. and Mikulasek, P., 2014. Influence of operating variables on the removal of heavy metal ions from aqueous solutions by nano filtration, *Desalination*, **343**, 67-74.

Gong, Y. W., Zhang, H. X. and Cheng, X. N., 2012. Treatment of dairy wastewater by two-stage membrane operation with ultrafiltration and nanofiltration, *Water Science and Technology,* **65**,915-919.

González, J., Carreras, A. and Ruiz, M. D. C., 2007. Phase transformations in clays and kaolins produced by thermal treatment in chlorine and air atmospheres, *Latin American Applied Research*, **37**, 133-139.

Gordon, C. C. Y. and Chi-Ming Sai, T., 2008. Effects of starch addition on characteristics of tubular porous ceramic membrane substrates, *Desalination,* **233**, 1-3, 129-136.

Guillou, F., Rouleau, L., Pirngruber, G. and Valtchev, V., 2009. Synthesis of FAU-type Zeolite Membrane: An Original in Situ Process Focusing on the Rheological Control of Gel-like Precursor Species, *Microporous and Mesoporous Materials*, **119,** 1-8.

H. Chau, J. L., Tellez, C., Yeung, K. L. and Ho, K., 2000. The role of surface chemistry in zeolite membrane formation, *Journal of Membrane Science*, **164**, 1, 257-275.

Haaland, P.D. Experimental design in biotechnology, CRC press, 1989.

Habibi, S., Nematollahzadeh, A. and Mousavi, S. A., 2015. Nano-scale modification of polysulfone membrane matrix and the surface for the separation of chromium ions from water, *Chemical Engineering Journal,* **267**, 306-316.

Hasegawa, Y., Abe, C., Nishioka, M., Sato, K., Nagase, T. and Hanaoka, T., 2010. Formation of High Flux CHA-type Zeolite Membranes and their Application to the Dehydration of Alcohol Solutions, *Journal of Membrane Science*, **364,** 318-324.

Hermia, J. 1982 Constant pressure blocking filtration laws-application to power-law non-newtonian fluids, *Transaction of the Institution of Chemical Engineers*, **60**, 183-187.

Hsieh, H.P., 1996. Inorganic membranes for separation and reaction, Elsevier, Amsterdam.

Huang, A., Wang, N. and Caro, J., 2012. Seeding-Free Synthesis of Dense Zeolite FAU Membranes on 3-Aminopropyltriethoxysilane-Functionalized Alumina Supports, *Journal of Membrane Science*, **389,** 272-279.

Huang, B., Liu, Q., Caro, J. and Huang, A., 2014. Iso-Butanol Dehydration by Pervaporation using Zeolite LTA Membranes Prepared on 3-Aminopropyltriethoxysilane-Modified Alumina Tubes, *Journal of Membrane Science*, **455,** 200-206.

Huang,A.,Wang,N. and Caro,J., 2012. Seeding-free synthesis of dense zeolite FAU membranes on 3-aminopropyltriethoxysilane-functionalized alumina supports, *Journal of Membrane Science*, **389**, 272-279.

Jafari, M., Bayat, A., Mohammadi, T. and Kazemimoghadam, M., 2013. Dehydration of Ethylene Glycol by Pervaporation using Gamma Alumina/NaA Zeolite Composite Membrane, *Chemical Engineering Research and Design*, **91,** 2412-2419.

Jeong, B. H., Hasegawa, Y., Sotowa, K. I., Kusakabe, K. and Morooka, S., 2002. Separation of Mixtures of Benzene and n-Alkanes using an FAU-type Zeolite Membrane, *Journal of Chemical Engineering Japan,* **35,** 167-172.

Jeong, B. H., Hasegawa, Y., Sotowa, K.-I., Kusakabe, K. and Morooka, S., 2003. Permeation of Binary Mixtures of Benzene and Saturated C_4-C_7 Hydrocarbons through an FAU-type Zeolite Membrane, *Journal of Membrane Science*, **213,** 115-124.

Jia, M. D., Chen, B., Noble, R. D. and Falconer, J. L., 1994. Ceramic-Zeolite Composite Membranes and their Application for Separation of Vapor/Gas Mixtures, *Journal of Membrane Science*, **90,** 1-10.

Jia, M. D., Peinemenn, K. V. and Behling, R. D., 1993. Ceramic Zeolite Composite Membranes: Preparation, Characterization and Gas Permeation, *Journal of Membrane Science*, **82,** 15-26.

Judd, S. and Jefferson, B., 2003. Membranes for industrial Wastewater Recovery and Re-use, *Elsevier*, Oxford OX5 IGB, UK.

Kandwal, V. C., Agrawal, K. M., Nautiyal, S. P. and Khan, H.U., 2000. Paraffin deposition and viscosity temperature behaviour of Assam crude oil, *Petroluem Science and Technology*, **18**, 755-769.

Karhu, M., Kuokkanen, T., Rämö, J., Mikola, M. and Tanskanen, J., 2013. Performance of a commercial industrial-scale UF-based process for treatment of oily wastewaters, *Journal of Environmental Management*, **128**, 413-420.

Kaya, C. and Blackburn, S., 2004. Extrusion of ceramic tubes with complex structures of non-uniform curvatures made from nano-powders, J *Journal of the European Ceramic Society*, **24**, 14, 3663-3670.

Kazemimoghadam, M. and Mohammadi, T., 2007. Synthesis of MFI zeolite membranes for water desalination, *Desalination*, **206**, 547–553.

Ke, X. B., Shao, R. F., Zhu, H. Y., Yuan, Y., Yang, D. J., Ratinac, K. R. and Gao, X. P., 2009. Ceramic membranes for separation of proteins and DNA through in situ growth of alumina nanofibres inside porous substrates, *Chemical Communications*, 1264-1266.

Khemakhem, S., Amar, R. B. and Larbot, A., 2007. Synthesis and Characterization of a New Inorganic Ultrafiltration Membrane Composed Entirely of Tunisian Natural Illite Clay, *Desalination*, **206,** 210-214.

Khemakhem, S., Larbot, A. and Amara, R. B., 2006. Study of performances of ceramic microfiltration membrane from tunisian clay applied to cuttlefish effluents treatment, *Desalination*, **200**, 307-309.

Khider, K., Akretche, D. E. and Larbot, A., 2004. Purification of water effluent from a milk factory by ultrafiltration using algerian clay support, *Desalination*, **167**, 147-151.

Kim, H. J., Jang, K.-S., Galebach, P., Gilbert, C., Tompsett, G., Conner, W. C., Jones, C. W. and Nair, S., 2013. Seeded Growth, Silylation, and Organic/Water Separation Properties of MCM-48 Membranes, *Journal of Membrane Science*, **427,** 293-302.

Kim, M. K., Sundaram, K. S., Iyengar, G. A. and Lee, K. P., 2015. A novel chitosan functional gel included with multiwall carbon nanotube and substituted polyaniline as adsorbent for efficient removal of chromium ion. *Chemical Engineering Journal*, **267,** 51-64.

Kita, H., Inoue, T., Asamura, H., Tanaka, K. and Okamoto, K., 1997. NaY Zeolite Membrane for the Pervaporation Separation of Methanol-Metylert-Butyl Ether Mixtures, *Chemical Communication*, 45-46.

Konak, A., Coit, D. W. and Smith, A. E., 2006. Multi-objective optimization using genetic algorithms: A tutorial, *Reliability Engineering and System Safety*, **91**, 992-1007.

Koseoglu, T. S., Kir, E., Ozkorucuklu, S. P. and Karamizrak, E., 2010. Preparation and characterization of P2Fan/PVDF composite cation-exchanger membranes for the removal of Cr(III) and Cu(II) by Donnan dialysis, *Reactive and Functional Polymers*, **11,** 900-907.

Kosmulski, M., 2009. pH-dependent surface charging and points of zero charge. IV. Update and new approach, *Journal of Colloid Interface Science*, **337**, 439-448.

Kuhn, J., Gross, J., Jansen, J.C., Kapteijn, F. and Jansens, P.J., 2007. Investigating mass transport in zeolite pores by tuning the framework polarity, *Studies in Surface Science and Catalysis*, 2007, **170**, 942-948.

Kumar, M., Agarwal, S., Pugazhenthi, G., Shukla, A. and Kumar, A., 2006. Preparation and Characterization of Iron Salt Embedded Electrodialysis Analcime-C Zeolite Clay Composite Membrane, *Journal of Membrane Science*, **275,** 110-118.

Kumar, P., Ida, J., Guliants, V. V., 2008. High Fflux Mesoporous MCM-48 Membranes: Effects of Support and Synthesis Conditions on Membrane Permeance and Quality, *Microporous and Mesoporous Materials*, **110,** 595-599.

Kumar, R. V., Basumatary, A. K Ghoshal, A. K. and Pugazhenthi, G. 2015 Performance assessment of an analcime-C zeolite-ceramic composite membrane by removal of Cr(VI) from aqueous solution, *RSC Advance*, **5,** 6246-6254.

Kumar, S., Gupta, N. and Pakshirajan, K., 2015. Simultaneous lipid production and dairy wastewater treatment using *Rhodococcus opacus* in a batch bioreactor for potential biodiesel application, *Journal of Environmental Chemical Engineering*, **3**, 1630-1636.

Li, L., Dong, J., Nenoff, T.M, and Lee, R., 2004. Reverse osmosis of ionic aqueous solutions on a MFI zeolite membrane, *Desalination*, **170**, 309-316.

Li, Y., Chen, H., Liu, J. and Yang, W., 2006. Microwave Synthesis of LTA Zeolite Membranes Without Seeding, *Journal of Membrane Science*, **277,** 230-239.

Li,C. G.,Xu,L., Wu,P.,Wu, H. and He,M., 2014.Efficient cycloaddition of epoxides and carbon dioxide over novel organic–inorganic hybrid zeolite catalysts,*Chemical Communications*,**50**, 15764-15767.

Ling, W. S., Thian, T. C. and Bhatia, S., 2011. Synthesis, Characterization and Pervaporation Properties of Microwave Synthesized Zeolite A Membrane, *Desalination*, **277,** 383-389.

Liu, B. S., Tang, D. C. and Au, C. T., 2005. Fabrication of Analcime Zeolite Fibers by Hydrothermal Synthesis, *Microporous and Mesoporous Materials*, **86,** 106-111.

Luo, J. H., Li, J., Qi, Y. B. and Cao, Y. Q., 2013. Study on the removal of chromium(III) by solvent extraction, *Desalination and Water Treatment,* **51**, 2130-2134.

Mabande, G. T. P., Pradhan, G., Schwieger, W., Hanebuth, M., Dittmeyer, R., Selvam, T., and Herrmann, R., 2004. A study of Silicalite-1 and Al-ZSM-5 membrane synthesis on stainless steel supports, *Microporous and Mesoporous Materials*, **75**, 3, 209-220.

Madaeni, S. S. and Mansourpanah, Y., 2006. Screening membranes for COD removal from dilute wastewater, *Desalination*, **197**, 23-32.

Maghsoudi, H. and Soltanieh, M, 2014. Simultaneous Separation of H_2S and CO_2 from CH_4 by a High Silica CHA-type Zeolite Membrane, *Journal of Membrane Science*, **470,** 159-165.

Majouli. A.,Tahiri, S., Younssi, A., Loukili, H. and Albizane, A., 2012. Elaboration of new tubular ceramic membrane from local Moroccan Perlite for microfiltration process, Application to treatment of industrial wastewaters, *Ceramics International*, **38,** 4295-4303.

Mandal, S., Mahapatra, S. S. and Patel, R. K., 2015. Neuro fuzzy approach for arsenic(III) and chromium(VI) removal from water. *Journal of Water Process Eng*ineering, **5,** 58-75.

Manohar, 2012. Development & Characterization of Ceramic Membranes, *International Journal of Modern Engineering Research (IJMER)*, **2**, 4, 1492-1506.

Masmoudi, S., Larbot, A., Feki, H. E. and Amar, R. B., 2007. Elaboration and Characterization of Apatite Based Mineral Supports for Microfiltration and Ultrafiltration Membranes, *Ceramic International*, **33,** 337-344.

Matsufuji, T., Nishiyama, N., Matsukata, M. and Ueyama, K., 2000. Separation of Butane and Xylene Isomers with MFI-type Zeolitic Membrane Synthesized by a Vapor-Phase Transport Method, *Journal of Membrane* Science, **178,** 25-34.

Matsukata, M., Nara, T. and Kikuchi, E., 2003. Effect of water adsorption on MFI-type zeolite membrane prepared by in situ hydrothermal crystallization, *Fuel Chemistry Division Preprints* **48**, 1, 487.

Mavrov, V., Chmiel, H., Kluth, J., Meier, J., Heinrich, F., Ames, P., Backes, K. and Usner, P., 1998. Comparative study of different MF and UF membranes for drinking water production, *Desalination,* **117**, 189-196.

Mehiguene, K., Garba, Y., Taha, S., Gondrexon, N. and Dorange, G., 1999. Influence of operating conditions on the retention of copper and cadmium in aqueous solutions by nanofiltration: experimental results and modeling, *Separation and Purification Technology*, **15**, 181-187.

Millesime, L., Dulieu, J. and Chaufer, B., 1995. Protein retention with modified and unmodified inorganic ultrafiltration membranes : model of ionic strength controlled retention, *Journal of membrane science*, **108**, 143-159.

Mohammadi, T., Pak, A., Karbassian, M. and Golshan, M., 2004. Effect of operating conditions on microfiltration of an oil-water emulsion by a kaolin membrane, *Desalination*, **168**,201-205.

Monash, P. and Pugazhenthi, G., 2011. Addition of TiO_2 on the properties of ceramic membrane supports and its influence on the separation of oil and BSA protein from its solution, *Desalination*, **279**, 104-114.

Monash, P. and Pugazhenthi, G., 2011. Development of ceramic supports derived from low-cost raw materials for membrane applications and its optimization based on sintering temperature, *International Journal of Applied Ceramic Technology*, **8,** 227-238.

Monash, P. Majhi, A. and Pugazhenthi, G., 2010. Separation of bovine serum albumin (BSA) using γ-Al_2O_3–clay composite ultrafiltration membrane, *Journal of chemical technology and biotechnology*, **85**, 545-554.

Mondal, D. N., Sarangi, K., Pettersson, F., Sen, P. K., Saxen, H. and Chakraborti, N., 2011. Cu—Zn separation by supported liquid membrane analyzed through Multi-objective Genetic Algorithms, *Hydrometallurgy*, **107**, 112-123.

Mueller, J., Cen, Y. W. and Davis, R. H., 1997. Crossflow microfiltration of oily water, *Journal of Membrane Science,* **129**, 221-235.

Mulder, M., 1991. Basic Principles of Membrane Technology, *Kluwer Academic Publishers*, Dordrecht.

Myers, R. H., Montgomery, D. C. and Anderson-Cook, C. M., Response surface methodology: process and product optimization using designed experiments, John Wiley & Sons, 2009.

Nandi, A., Moparthi, R., Uppaluri and Purkait, M., 2010. Treatment of oily wastewater using low cost ceramic membrane: Comparative assessment of pore blocking and artificial neural network models, *Chemical Engineering Research and Design*, **88**, 881-892.

Neelakandan, C., Pugazhenthi, G. and Kumar, A., 2003. Preparation of NO_x modified PMMA-EGDM composite membrane for the recovery of chromium (VI), *European polymer Journal,* **39**, 2383-2391.

Nishiyama, N., Park, D. H., Egashira, Y. and Ueyama, K., 2003. Pore Size Distributions of Silylated Mesoporous Silica MCM-48 Membranes, *Separation and Purification Technology*, **32**, 127-132.

Nishiyama, N., Park, D. H., Koide, A., Egashira, Y. and Ueyama, K., 2001. A Mesoporous Silica (MCM-48) Membrane: Preparation and Characterization, *Journal of Membrane Science*, **182,** 235-244.

Noble, R. D. and Falconer, J. L., 1995. Silicate-1 Zeolite Composite Membranes, *Catalysis Today*, **25**, 209-212.

Noble, R.D. and Stern, S.A., 1995. Membranes separations technology, principles and application, *Elsevier*, Amsterdam, The Netherlands.

Nomura, M., Yamaguchi, T. and Nakao, S. I., 1998. Ethanol/water transport through silicalite membranes, *Journal of Membrane Science*, **144**, 1, 161-171.

Nunes, S.P., Peinemann, K.V., 2001. Membrane Technology in the Chemical Industry, *Wiley-VCH Verlag GmbH*, Germany.

Okubo, T., Haruta, K., Kusakabe, K. and Morooka, S., 1991. Preparation of a Sol-Gel Derived Thin Membrane on a Porous Ceramic Hollow Fiber by the Filtration Technique, *Journal of Membrane Science*, **59,** 73-80.

Oonkhanond, B. and Mullins, M. E., 2001. The Preparation and Analysis of Zeolite ZSM-5 Membranes on Porous Alumina Supports, *Journal of Membrane Science*, **194,** 3-13.

Ozin, G. A., Kuperman, A. and Stein, A., 1989. Advanced zeolite, Materials science, *Angewandte Chemie International Edition in English,* **28**, 359-363.

Ozin, G. A., Kuperman, A. and Stein, A., 1989. Advanced Zeolite material science, *Advanced Materials*, **1**, 69-86.

Padaki, M., Murali, R.S., Abdullah, M., Misdan, N., Moslehyani, A. and Kassim, M., 2015. Membrane technology enhancement in oil-water separation. A review, *Desalination*, **357**, 197-207.

Pan, M., and Lin, Y. S., 2001. Template-free secondary growth synthesis of MFI type zeolite membranes, *Microporous and Mesoporous Materials*, **43**, 3, 319-327.

Patterson, V. A, Krieg, H. M, Kriek, R. J. and Bisset, H., 2006. Direct Synthesis of a Titania Membrane on a Centrifugally Casted Tubular Ceramic Support, *Journal of Membrane Science*, **285**,1-3.

Pedernera, M., Iglesia, O. de la, Mallada, R., Lin, Z., Rocha, J., Coronas, J. and Santamaria, J., 2009. Preparation of Stable MCM-48 Tubular Membranes, *Journal of Membrane Science*, **326,** 137-144.

Persson, A., Jönsson A.S. and Zacchi, G., 2003. Transmission of BSA during cross-flow microfiltration: Influence of pH and salt concentration, *Journal of Membrane Science*, **223**, 11-21.

Potdar, A., Shukla, A. and Kumar, A., 2002. Effect of Gas Phase Modification of Analcime Zeolite Composite Membrane on Separation of Surfactant by Ultrafiltration, *Journal of Membrane Science*, **210,** 2009-225.

Praptowidodo, V. S., 2005. Influence of Swelling on Water Transport through PVA-Based Membrane, *Journal of Molecular Structure*, **739**, 207-212.

Pugazhenthi, G., Sachan, S., Kishore, N. and Kumar, A., 2005. Separation of chromium(VI) using modified ultrafiltration charged carbon membrane and its mathematical modeling, *Journal of Membrane Science,* **254**, 229-239.

Qi, H., Fan, Y., Xing, W. and Winnubst, L., 2010. Effect of TiO_2 Doping on the Characteristics of Macroporous Al_2O_3/TiO_2 Membrane Supports, *Journal of European Ceramic Society*, **30,** 1317-1325.

Rad, S. A., M. Mirbagheri, S. A. and Mohammadi, T., 2009. Using reverse osmosis membrane for chromium removal from aqueous solution, *World Academic of Science Engineering Technology,* **57**, 348-352.

Rashdi, B. A. M., Johnson, D. J. and Hilal, N., 2015. Removal of heavy metal ions by nanofiltration, *Desalination*, **315**, 2-17.

Rengaraj, S., Yeon, K. H. and Moon, S. H., 2001. Removal of chromium from water and wastewater by ion exchange resins, *Journal of Hazardous Materials,* **87**, 273-287.

Rezvanpour, A., Roostaazad, R., Hesampour, M., Nyström, M. and Ghotbi, C., 2009. Effective factors in the treatment of kerosene-water emulsion by using UF membranes, *Journal of hazardous Material*, **161**, 1216-1224.

Sachdeva, S. and Kumar, A., 2008. Synthesis and modeling of composite poly (styrene-*co*-acrylonitrile) membrane for the separation of chromic acid, *Journal of Membrane Science,* **307**, 37-52.

Sacmaci, S. and Kartal, S., 2011. Separation and enrichment of Cr(III) and Cr(VI) in environmental samples by ion-pair solvent extraction using a β-diketone ligand, *International Journal of Environmental and Analytical Chemistry,* **5,** 448-461.

Sadeghi,B.,Lasemi, Z.,Tavasoli,F. A.,Hashemian,S. and Zahedi,H., 2014. Synthesis of FAU Zeolite Nanoparticles as Heterogeneous Catalyst for One-Pot Synthesis of 2-Substituted Aryl (Indolyl) Kojic Acid Derivatives under Solvent-Free Condition, *Synthesis and Reactivity in Inorganic Metal-Organic and Nano-Metal Chemistry* , **44**, 1497-1503.

Saffaj, N., Persin, M., Younssi, S. A., Albizan, A., Bouhria, M., Loukili, H., Dacha, H. and Larbot, A., 2005. Removal of salts and dyes by low $ZnAl_2O_4$–TiO_2 ultrafiltration membrane deposited on support made from raw clay, *Separation and Purification Technology*, **47**, 36-42.

Saffaj, N., Alami Younssi, S., Albizane, A., Messouadi, A., Bouhria, M., Persin, M., Cretin, M., Larbot A., 2004. Elaboration and Properties of TiO_2-$ZnAl_2O_4$ Ultrafiltration Membranes Deposited on Cordierite Support, *Separation and Purification Technology,* **36**, 107-114.

Saffaj, N., Persin, M., Younsi, S. A., Albizane, A., Cretin, M. and Larbot, A., 2006. Elaboration and characterization of micro-filtration and ultra-filtration membranes deposited on raw support prepared from natural moroccan clay: application to filtration of solution containing dyes and salts, *Applied Clay Science*, **31**, 110-119.

Salahi, A., Gheshlaghi, A., Mohammadi, T. and Madaeni, S. S., 2010. Experimental performance evaluation of polymeric membranes for treatment of an industrial oily wastewater, *Desalination*, **262**, 235-242.

Salahi, A., Noshadi, I., Badrnezhad, R., Kanjilal, B. and Mohammadi, T., 2013. Nano-porous membrane process for oily wastewater treatment: optimization using response surface methodology, *Journal of Environmental Chemical Engineering*, **1**, 218-225.

Salahi, T., Mohammadi, R., Behbahani, M., Hemmati, M., 2015. Asymmetric polyethersulfone ultrafiltration membranes for oily wastewater treatment: Synthesis, characterization, ANFIS modeling, and performance, Journal of Environmental Chemical Engineering, **3,** 170-178.

Sanyal, O., Liu, Z., Meharg, B. M., Liao, W. and Lee, I., 2015. Development of polyelectrolyte multilayer membranes to reduce the COD level of electrocoagulation treated high-strength wastewater, *Journal of Membrane Science,* **496**, 259-266.

Sarfaraz, M.V., Ahmadpour, E., Salahi, A., Rekabdar, F. and Mirza, B., 2012. Experimental investigation and modeling hybrid nano-porous membrane process for industrial oily wastewater treatment, *Chemical Engineering Research and Design*, **90**, 1642-1651.

Sato, K., Sugimoto, K., and Nakane, T., 2008. Synthesis of Industrial Scale NaY Zeolite Membranes and Ethanol Permeating Performance in Pervaporation and Vapor Permeation up to 130 °C and 570 kPa, *Journal of Membrane Science*, **310,** 161-173.

Sato, K., Sugimoto, K., Sekine, Y., Takada, M., Matsukata, M. and Nakane, T., 2007. Application of FAU-type Zeolite Membranes to Vapor/Gas Separation Under High Pressure and High Temperature upto 5 MPa and 180 °C, *Microporous and Mesoporous Materials*, **101,** 312-318.

Selvi, K., Pattabhi, S. and Kadirvelu, K., 2001. Removal of Cr(VI) from aqueous solution by adsorption onto activated carbon, *Bioresource and Technology,* **80**, 87-89.

Seshadri, S. K. and Lin, Y. S., 2011. Synthesis and Water Vapor Separation Properties of Pure Silica and Aluminosilicate MCM-48 Membranes, *Separation and Purification Technology*, **76,** 261-267.

Shah, T. N. Foley, H. C and Zydney, A. L. Development and characterization of nanoporous carbon membranes for protein ultrafiltration, *Journal of membrane science*, 2007, **295**, 40-49.

Sharma, D., 2014. Treatment of dairy waste water by electro coagulation using aluminum electrodes and settling, filtration studies, *International Journal of Chemical Technology and Research*, **6**, 591-599.

Shpiner, R., Vathi, S. and Stuckey, D. C., 2009. Treatment of oil well ''produced water'' by waste stabilization ponds: Removal of heavy metals. *Water Research*, **43,** 4258-4268.

Shukla, A. and Kumar, A., 2007. Separation of Cr(VI) by zeolite-clay composite membranes modified by reaction with NOx. *Separation and Purification Technology*, **52**, 423-429.

Soleimani, R., Shoushtari, N. A., Mirza, B. and Salahi, A., 2013. Experimental investigation, modeling and optimization of membrane separation using artificial neural network and multi-objective optimization using genetic algorithm, *Chemical Engineering Research and Design*, **91**, 883-903.

Song, C. W., Wang, T. H., Pan, Y. Q. and Qiu, J.S., 2006. Preparation of coal-based microfiltration carbon membrane and application in oily wastewater treatment, *Separation and Purification Technology*, **51**, 80-84.

Song, T., Wang, Y., Pan, and Qiu, J., 2006. Preparation of coal-based microfiltration carbon membrane and application in oily wastewater treatment, *Separation and Purification Technology*, **51**, 80-84.

Srijaroonrat, P., Julien, E. and Aurelle, Y., 1999. Unstable secondary oil/water emulsion treatment using ultrafiltration: fouling control by backflushing, *Journal of Membrane Science*, **159**, 11-20.

Sugiyama, K., Ryu, H. and Waseda, Y., 1993. Local ordering structure of meta-kaolinite and meta-dickite by the X-ray radial distribution function analysis, *Journal of Material Science*, **28**, 2783-2788.

Szostak, R., *Molecular Sieve*, Blackie-Academic and Professional, 1998.

Talidi, A., Saffaj, N., Kacemi, K. E. Younssi, S. A. Albizane, A. and Chakir, A., 2011. Processing and characterization of tubular ceramic support for microfiltration membrane prepared from pyrophyllite clay, *Scientific Study & Research Chemistry & Chemical Engineering, Biotechnology, Food Industry,* **12**, 263-268.

Tang, W., Peng, Z., Li, L., Yue, T., Wang, J., Li, Z., Li, R., Chen, J., Colvin, V. L. and Yu, W.W., 2012. Porous stainless steel supported magnetite crystalline membranes for hexavalent chromium removal from aqueous solutions. *Journal of Membrane Science,* **392-393**, 150-156.

Terpstra, R. A., Bonekamp, B. C. and Veringa, H. J., 1988. Preparation, Characterization and some properties of tubular alpha alumina ceramic membranes for microfiltration and as a support for ultrafiltration and as support for ultrafiltration and gas separation membranes, *Desalination*, **70,** 395-404.

Tfiigdh, G. and Johansson, D., 1998. Purification of alkaline cleaning solutions from the dairy industry using membrane separation technology, *Desalination*, **119**, 21-29.

Tijani, N., Ahlafi, H., Smaihi, M. and Mansouri, A. E., 2013. Preparation and Characterization of NaA Zeolite Membranes and its Application for Removal of Heavy Metals. *Mediterraneen Journal of Chem*istry, **2**, 484-492.

Treacy,M. M. J. and Higgins,J. B., 2007. Collection of simulated XRD Powder Diffraction Pattern for Zeolites, fifth revised ed., Elsevier, Amsterdam.

Tsapatsis, M. 2002. Molecular sieves in the nanotechnology era, *AIChE Journal*, **78**, 654-659.

Turan, M., Koyuncu, I., Topacik, D. and Ateş, A., 2000. Comparative evaluation of nanofiltration and reverse osmosis treatment of an effluent from dairy industry, *Journal of Environmental Science and Health*, **A35**, 5, 741-754.

Valiño, V., San Román, M. F., Ibañez R. and Ortiz, I., 2014. Improved separation of bovine serum albumin and lactoferrin mixtures using charged ultrafiltration membranes, *Separation and Purification Technology*, **125**, 163-169.

Vasanth, D., Pugazhenthi, G. and Uppaluri, R., 2013. Performance of Low Cost Ceramic Microfiltration Membranes for the Treatment of Oil-in-water Emulsions, *Separation Science and Technology*, **48**, 849–858,

Velasco, C., Calvo, J., Palacio, L., Carmona, J., Prádanos, P. and Hernández, A., 2015, Flux kinetics, limit and critical fluxes for low pressure dead-end microfiltration. The case of BSA filtration through a positively charged membrane, *Chemical Engineering Science*, **129**, 58-68.

Wang, S. and Kammermeyer, K., 1975. Membranes in Separations; Techniques in Chemistry, Volume (**7**), *Verlag Chemie*, GmbH, Germany.

Wang, Y. H., Tian, T. F., Liu, X. Q. and Meng, G. Y., 2006. Titania membrane preparation with chemical stability for very hash environments applications, *Journal of Membrane Science*, **280**, 261-269.

Wang, Y. H., Zhang, Y., Liu, X. Q. and Meng, G. Y., 2007. Sol-coated preparation and characterization of macroporous α-Al_2O_3 membrane support, *Journal of Sol-Gel Science and Technology*, **41**, 267-275.

Wegner, K., Dong, J. and Lin, Y.S., 1999. Polycrystalline MFI zeolite membranes: xylene pervaporation and its implication on membrane microstructure,*Journal of Membrane* Science, **158**, 17-27.

Weh, K., Noack, M., Hoffmann, K., Schroder, K. P. and Caro, J., 2002. Change of Gas Permeation by Photoinduced Switching of Zeolite-Azobenzene Membranes of type MFI and FAU, *Microporous and Mesoporous Materials*, **54,** 15-26.

Weir, M. R., Rutinduka, E., Detellier, C., Feng, C. Y., Wang, Q., Matsuura, T. and VanMao, R. L., 2001. Fabrication, characterization and preliminary testing of all-inorganic ultrafiltration membranes composed entirely of a naturally occurring sepiolite clay mineral, *Journal of Membrane Science*, **182**, 41-50.

Weisberg, S. Applied linear regression, John Wiley & Sons, 2005.

Winter, O., 1969. Preliminary economic evaluation of chemical processes at the research level, *Industrial and Engineering Chemistry*, **61**, 45-52.

Wirawan, S. K., Creaser, D., Lindmark, J., Hedlund, J., Bendiyasa, M. and Sediawan, W.B., 2011. H_2/CO_2 Permeation through a Silicalite-1 Composite Membrane, *Journal of Membrane Science*, **375,** 313-322.

Workneh, S. and Shukla, A., 2008. Synthesis of sodaliteoctahydrate zeolite-clay composite membrane and its use in separation of SDS, *Journal of Membrane Science*, **309**, 189-195.

Xu, R., Pang, W., Yu, J., Huo, Q. and Chen, J., 2009. Chemistry of zeolites and related porous materials: synthesis and structure. John Wiley and Sons.

Yan, Y., Davis, M. E. and Gavalas, G. E., 1997. Preparation of Highly Selective Zeolite ZSM-5 Membranes by a Post-Synthetic Coking Treatment, *Journal of Membrane Science*, **123,** 95-103.

Yang, C., Zhang, G., Xu, N. and Shi, J., 1998. Preparation and application in oil-water separation of ZrO_2/α-Al_2O_3 MF membrane, *Journal of Membrane Science,* **142,** 235-243.

Yi, X., Shi, W., Yu, S., Ma, C., Sun, N., Wang, S., Jin, L. and Sun, L., 2011. Optimization of complex conditions by response surface methodology for APAM–oil/water emulsion removal from aqua solutions using nano-sized TiO_2/Al_2O_3 PVDF ultrafiltration membrane, *Journal of Hazardous Materials*, **193**, 37-44.

Yi, X.S., Yu, S.L., Shi, W.X., Wang, S., Sun, N., Jin, L.M. and Ma, C., 2013. Estimation of fouling stages in separation of oil/water emulsion using nano-particles Al_2O_3/TiO_2 modified PVDFUF membranes, *Desalination*, **319**, 38-46.

Yip, V., Arntfield, S. D. and Hydamaka, A.W., 1996. Potential for stainless steel microfiltration processing to reduce effluent from a fluid milk and ice cream processing plant, *Journal of Dairy Science*, **79**, 4, 710-716.

Yoshino, Y., Suzuki, T., Nair, B.N., Taguchi, H. and Itoh, N., 2005. Development of tubular substrates, silica based membranes and membrane modules for hydrogen separation at high temperature, *Journal of Membrane Science*, **267,** 8-17.

Yuen, C. C., Gupta, S. K. and Ray, A. K., 2000. Multi-objective optimization of membrane separation modules using genetic algorithm, *Journal of Membrane Science*, **176**, 177-196.

Zhang, C., Hong, Z., Chen, J., Gu, X., Jin, W. and Xu, N., 2012. Catalytic MFI Zeolite Membranes Supported on α-Al_2O_3 Substrates for m-Xylene Isomerization, *Journal of Membrane Science*, **389,** 451-458.

Zheng, Y., Yu, S., Shuai, S., Zhou, Q., Cheng, Q., Liu, M. and Gao, C., 2013. Color removal and COD reduction of biologically treated textile effluent through submerged filtration using hollow fiber nanofiltration membrane, *Desalination*, **314**, 89-95.

Zhong, J., Sun, X. and Wang, C., 2003. Treatment of oily wastewater produced from refinery processes using flocculation and ceramic membrane filtration, *Separation and Purification Technology,* **32**, 93-98.

Zhu, G., Li, Y., Zhou, H., Liu, J. and Yang, W., 2008. FAU-type Zeolite Membranes Synthesized by Microwave Assisted in Situ Crystallization, *Materials Letters*, **62,** 4357-4359.

Zhu, G., Li, Y., Zhou, H., Liu, J. and Yang, W., 2009. Microwave Synthesis of High Performance FAU-type Zeolite Membranes: Optimization, Characterization and Pervaporation Dehydration of Alcohols, *Journal of Membrane Science,* **337,** 47-54.

Publications

Journals Articles

1. **R. Vinoth Kumar,** Aloke Kumar Ghoshal and G. Pugazhenthi, Elaboration of novel tubular ceramic membrane from inexpensive raw materials by extrusion method and its performance in microfiltration of synthetic oily wastewater treatment, ***Journal of Membrane Science,*** 490 (2015) 92-102.

2. **R. Vinoth Kumar**, I. Ganesh Moorthy and G. Pugazhenthi, Modelling and optimization of critical parameters by hybrid RSM-GA for the separation of BSA using tubular configured MFI-type zeolite microfiltration membrane, ***RSC Advances***, 5 (2015) 87645-87659.

3. **R. Vinoth Kumar,** Lalit Goswami, Kannan Pakshirajan and G. Pugazhenthi, Dairy wastewater treatment using a novel low cost tubular ceramic membrane and membrane fouling mechanism using pore blocking models, ***Journal of Water Process Engineering***, 13 (2016) 168–175.

4. **R. Vinoth Kumar**, P. Monash and G. Pugazhenthi, Treatment of oil-in-water emulsion using tubular ceramic membrane acquired from locally available low cost inorganic precursors, ***Desalination and Water Treatment***, 2016, DOI: 10.1080/19443994.2016.1179221.

5. **R. Vinoth Kumar** and G. Pugazhenthi, Removal of chromium from synthetic wastewater using MFI zeolite membrane supported on inexpensive tubular ceramic substrate, ***Journal of Water Reuse and Desalination***, 2016, DOI: 10.2166/wrd.2016.096.

6. **R. Vinoth Kumar,** I. Ganesh Moorthy and G. Pugazhenthi, Optimization of BSA separation using tubular configured FAU-type zeolite membrane through hybrid Response Surface and bi-objective Genetic Algorithm approach, ***Chemical Engineering Science,*** 2016 (Under Review).

7. **R. Vinoth Kumar,** Ashim Kumar Basumatary and G. Pugazhenthi, Preparation of Faujasite (FAU) zeolite membrane on low cost porous tubular ceramic substrate for removal of chromium from wastewater, ***Journal of Water Process Engineering,*** 2016 (Under Review).

International and National Conferences / Workshops

1. **R. Vinoth Kumar** and G. Pugazhenthi, Optimization of BSA separation using tubular configured FAU-type zeolite membrane through hybrid Response Surface and bi-objective Genetic Algorithm approach, ***14th International Conference on Inorganic Membranes - ICIM 2016,*** 10-13 July, 2016, Georgia Tech Global Learning Center, Atlanta, GA, USA.

2. **R. Vinoth Kumar,** Ashim Kumar Basumatary and G. Pugazhenthi, Preparation of Faujasite (FAU) zeolite membrane on low cost porous tubular ceramic substrate for removal of chromium from wastewater, ***International Conference on Waste Management - RECYCLE 2016,*** 1-2 April 2016, Indian Institute of Technology Guwahati, Assam, India.

3. **R. Vinoth Kumar**, Lalit Goswami, Kannan Pakshirajan, G. Pugazhenthi, Treatment of local dairy industry wastewater using novel low cost tubular ceramic membrane, ***The annual Chemical Engineering symposium - REFLUX 2016,*** 25-27 March 2016, Indian Institute of Technology Guwahati, Assam, India (First Prize in Paper Presentation Competition).

4. **R. Vinoth Kumar** and G. Pugazhenthi, Oily wastewater treatment using tubular configured ceramic membrane elaborated from inexpensive raw materials, ***3rd Indo-German workshop on Advances in Materials, Reaction & Separation Processes***, 23-26 February 2016, Indian Institute of Technology Guwahati, Assam, India.

5. **R. Vinoth Kumar** and G. Pugazhenthi, Hydrothermal synthesis of MFI type zeolite membrane on low cost tubular ceramic substrate for removal of hexavalent chromium, ***International Conference on Environment - ICENV 2015***, 18-19 August 2015, Eastin Hotel, Penang, Malaysia.

6. **R. Vinoth Kumar**, P. Monash and G. Pugazhenthi, Treatment of oil-in-water emulsion using tubular ceramic membrane acquired from locally available low cost inorganic precursors, ***International Conference on Renewable Energy and Sustainable Environment - RESE 2015***, 10-13 August 2015, Dr. Mahalingam College of Engineering and Technology (MCET), Pollachi, Tamil Nadu, India.